REPORT DOCUMENTATION PAGE

Form Approved
OMB No. 0704-0188

1. AGENCY USE ONLY (Leave blank)	2. REPORT DATE	3. REPORT TYPE AND DATES COVERED
	7/11/1995	Final - 1 Aug 1994 - 31 December 1994

4. TITLE AND SUBTITLE

Conference Support - Physics of Estuaries and Coastal Seas

5. FUNDING NUMBERS

N00014-94-1-1055

6. AUTHOR(S)

David G. Aubrey, Principal Investigator

7. PERFORMING ORGANIZATION NAME(S) AND ADDRESS(ES)

Woods Hole Oceanographic Institution
Woods Hole, MA 02543

8. PERFORMING ORGANIZATION REPORT NUMBER

13105500

9. SPONSORING/MONITORING AGENCY NAME(S) AND ADDRESS(ES)

Office of Naval Research
800 North Quincy Street
Arlington, VA 22217

10. SPONSORING/MONITORING AGENCY REPORT NUMBER

11. SUPPLEMENTARY NOTES

12a. DISTRIBUTION/AVAILABILITY STATEMENT

Approved for public release; distribution is unlimited

12b. DISTRIBUTION CODE

13. ABSTRACT *(Maximum 200 words)*

Meeting abstracts (attached abstract book)

14. SUBJECT TERMS

15. NUMBER OF PAGES

16. PRICE CODE

17. SECURITY CLASSIFICATION OF REPORT	18. SECURITY CLASSIFICATION OF THIS PAGE	19. SECURITY CLASSIFICATION OF ABSTRACT	20. LIMITATION OF ABSTRACT
UNCLASSIFIED			

7 th International Biennial Conference on Physics of Estuaries and Coastal Seas:

Buoyancy Effects on Coastal Dynamics

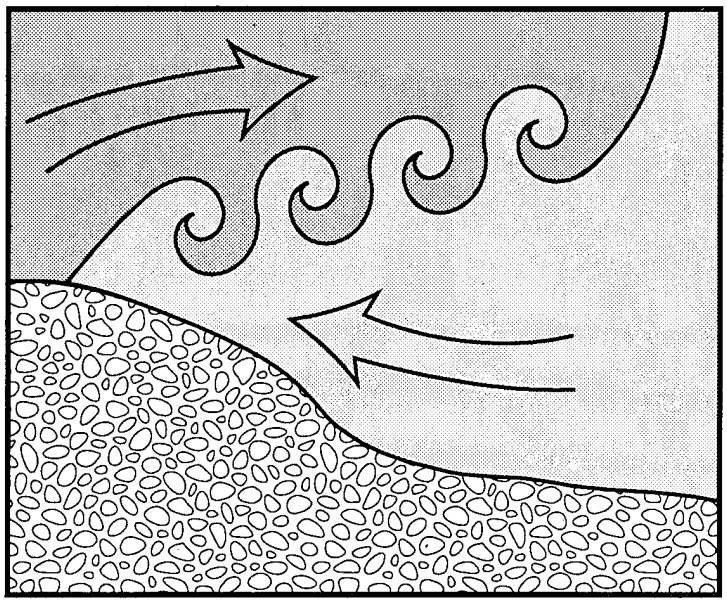

Woods Hole Oceanographic Institution

Redfield Laboratory & MBL Swope Center

28 - 30 November 1994
Woods Hole, MA USA

.....

MEETING ABSTRACTS

Errata

An Airborne and Ground Truth Investigation of a Buoyant Plume in a Stratified English Bay

T.J. Sherwin and P.C. Jonas

"In section 3 paragraph 1 replace 'provided by Southampton University' with 'run by the National Rivers Authority National Centre for Environmental Monitoring and Surveillance' ?

R. Lewis

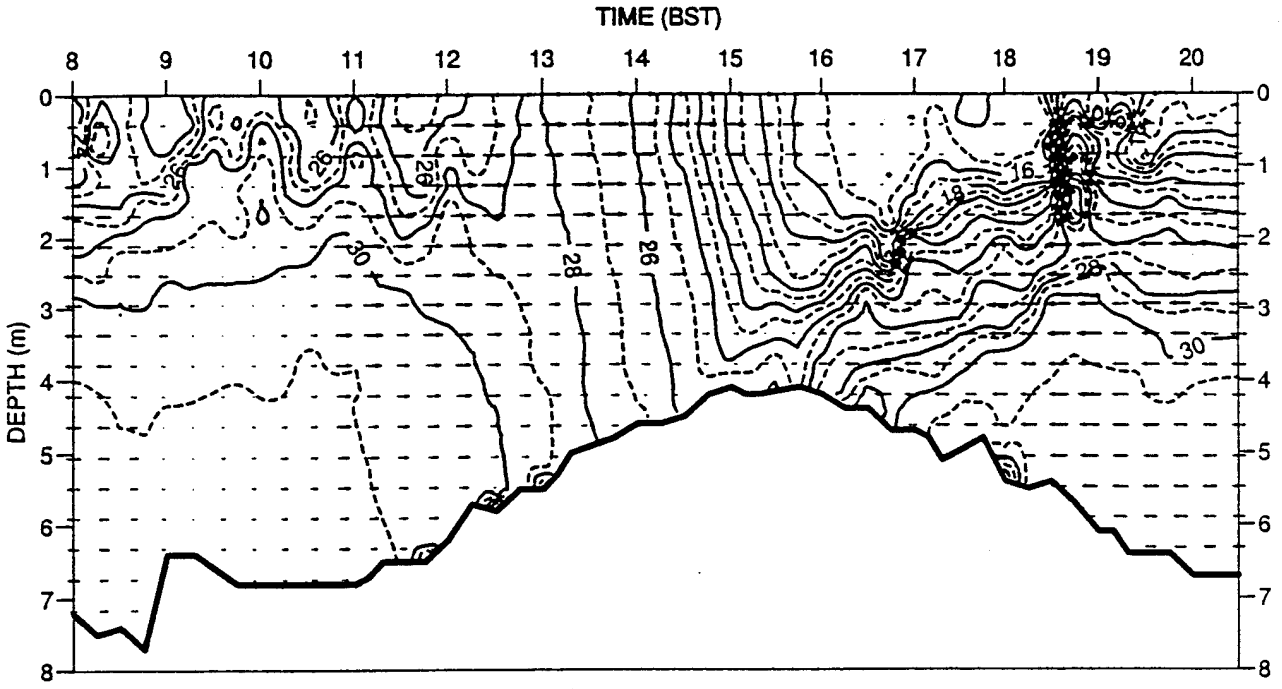

Fig 1 Observed salinity and velocity distributions in the Tees estuary (24/8/93)

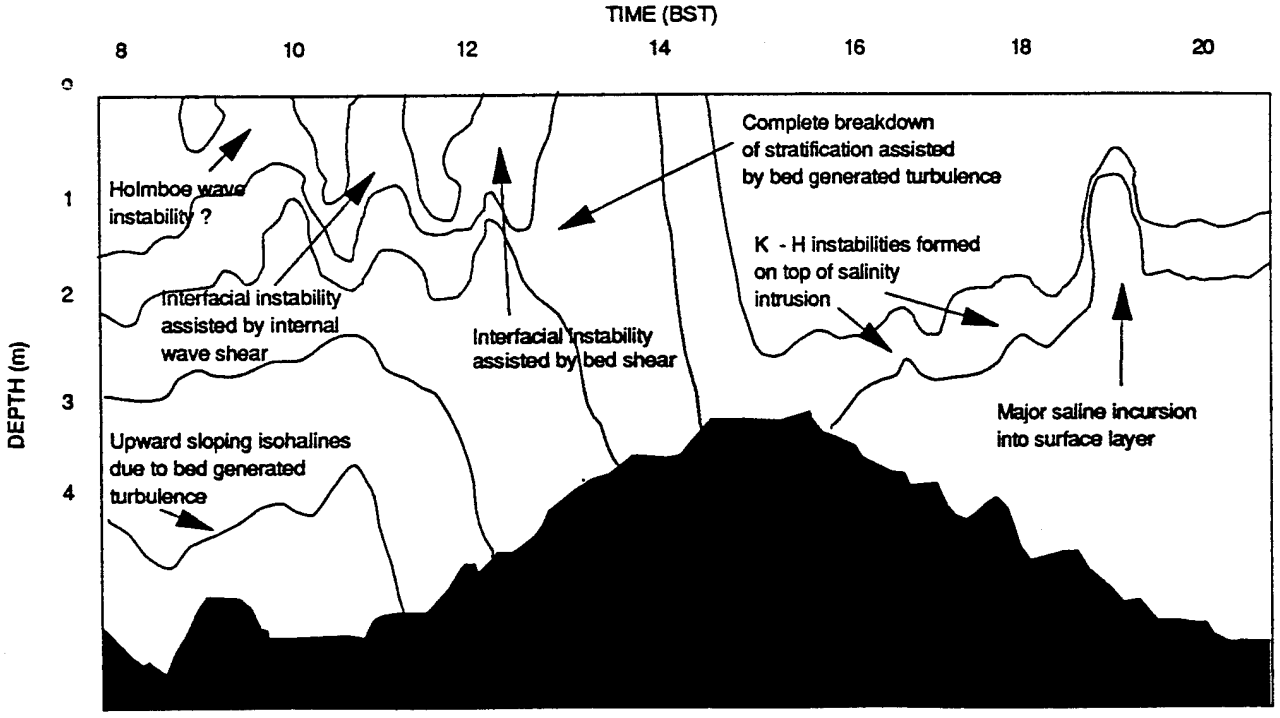

Fig 2 Schematic diagram of salinity variation and postulated causes of mixing

Table of Contents
Speaker Sessions

Session C: Estuarine Dynamics

Effects of Channel Geometry on Gravitational Circulation in Partially-Mixed Estuaries
C. T. Friedrichs and J. M. Hamrick

Tidal Pumping of Salt in a Moderately Stratified Estuary
W. R. Geyer and H. Nepf

Lagrangian Mean Descriptions of Long-Term Estuarine Mass Transport
J. M. Hamrick and Zhaoqing Yang

Effects of Changing Bathymetry on the Dynamics and Ocean Exchange of a Mediterranean Estuary; Tomales Bay California
C. Hearn, S. Smith, J. Largier, J. Plant, J. Rooney and K. Sender

Scalar Transport Calculations from Acoustic Doppler Current Profiler Data
D. J. Kay, D. A. Jay and J. D. Musiak

Seasonal Occurrences of Hypersalinity and Inverse Structures in Low-Inflow "Estuaries"
J. L. Largier and C. J. Hearn

Observations and Modeling of Stratification Episodes and Gravitational Circulation in Northern San Francisco Bay
S.G. Monismith, M. Stacey and J. R. Burau

Study of the Effect of Variation in Vertical Mixing on Estuarine Circulation in Narrow Estuaries Using Theoretical and Numerical Models
K. Park and A. Y. Kuo

Combined Effects of Buoyancy and Tides Upon Longitudinal Dispersion
R. Smith

A Two-Dimensional Baroclinic Model for the Halifax Harbor
K. T. Tee and B. Petrie

Buoyancy Phenomena and Salinity in the Tweed Estuary
R. J. Uncles and J. A. Stephens

Internal Motion in a Stratified Estuary
R. E. Wilson

Session D: Sediment Transport

Characterization of Fine-Grained Sedimentation in Elongated Basins by Settling Velocity/Densimetric Velocity Ratio
P. C.-Po Lin and A. J. Mehta

Effects of Coastal Topography an the Dispersion of Heavy Particles in Weak Tides
C. C. Mei, C. Chian and C. Procaccini

Modeling Fluxes of Suspended Sediments: Development Based on recent Availability of Continuous Measurements of Combined Profiles of Currents and Suspended Sediments
D. Prandle, D. Flatt, D. Hill, S. Jones and P. D. Thorne

The Bottom Boundary Condition for Suspended Sediment Deposition
L. P. Sanford and M. L. Chang

Tidal Variations of Suspended Sediment in the Ems Estuary
J. van de Kreeke and G. C. van Dam

Generation of High Turbidity Layers in the Seto Inland Sea
H. Yasuda, Y. Takasugi and T. Higo

Session E: Shelf Dynamics/Tidal Mixing

Circulation Pattern on the Coastal Zone Offshore Perth, Western Australia: Observations and Numerical Modeling
C. Pattiaratchi

Modeling of the River Run-Off Freshening Effect During Spring Flood on the Northwest Black Sea Shelf
A.I. Kubryakov, E.N. Mikhailova, N.B. Shapiro and V.A. Ivanov

Observations and Modeling of the Black Sea Rim Current
D.G. Aubrey

Bottom Boundary Layer in a Tidal Estuary
R. T. Cheng, J. W. Gartner and R. E. Smith

The Onset and Effect of Intermittent Buoyancy Changes in a Partially Stratified Estuary
R. E. Lewis and J. O. Lewis

The Vertical Structure of Turbulent Dissipation in Shelf Seas
J. H. Simpson, W. Crawford, T. P. Rippeth, A. Campbell and J. Cheok

Table of Contents
Poster Sessions

Session D: Sediment Transport

The Relation Between Hydrodynamics and Suspended Matter Distribution During Periodic Stratification in the Rhine Plume in the North Sea
J.C.A. Joordens, A.J. Souza and A. Visser

The Influence of a Stable Tidal Inlet on the Distributions of Shoreface Grain Sizes Under Low Wave Energy Conditions
J.T. Liu, R.W. Parkinson, P.F. Venanzi and L.-H. Hou

Variation of Sediment Resuspension Characteristics: Experience from the Lower Chesapeake Bay
J.P.-Y. Maa and C.-H. Lee

The Effect of Tidal Asymmetries on the Net Transport of Suspended Sediments in the Ems Dollard Estuary
H. Ridderinkhof

Sediment Transport Studies in River Mouths with the Use of Natural Radioactivity
B. Shteinman

Storm-Induced Sediment Transport in Massachusetts Bay
R.P. Signell, B. Butman and M. Bothner

Session E: Shelf Dynamics/Tidal Mixing

Reinforcement of Gravitational Circulation by Wind
J. Blanton

Simulations of Baroclinic Flow in Dixon Entrance, British Columbia
V.A. Ballantyne, M.G.G. Foreman, W.R. Crawford and K.S. Lee

Seasonal Variation of the Baroclinic Circulation in the Scotia-Maine Region
C.G. Hannah and J.W. Loder

Upwelling on Two Wide Shelves Dominated by Large Lateral Buoyancy Fluxes
A. Munchow

Inlet Control of Tides and Salinity in a Shallow Bay
D.C. Conley

Turbulent Feature on Buoyant Current Toward Inlet in Man-Made Lake
Y. Kitakura and S. Onishi

Interaction Between Mean Water Column Stability and Tidal Shear in the Production of Semi-Diurnal Switching of Stratification in the Rhine ROFI
A.J. Souza and J.H. Simpson

Abstracts for Oral Sessions

INTERACTION BETWEEN TIDALLY DRIVEN EDDY AND STRATIFICATION

R.J. Chant[1], R.E. Wilson[1] and J. Brubaker[2]
[1]State University of New York
Stony Brook, NY
[2]Virginia Institute of Marine Science
School of Marine Science
The College of William and Mary
Gloucester Point, VA 23062

Abstract

Introduction

Rozovski, 1957 showed that a cross stream circulation is induced in a vertically sheared curving flow. The flow is set up by a local imbalance between an inward directed barotropic pressure gradient and outward centrifugal forces. The imbalance arises because centrifugal forces in a sheared flow are depth dependent, while the pressure gradient is depth independent. Typically a vertical gradient in stress divergence is assumed to balance the vertical gradient in centrifugal acceleration.(Kalkwijk and Booij, 1986). Recently Geyer (1993) measured secondary flows around a headland and found them to exceed those predicted by Kalkwijk and Booij. Geyer concluded that the theory underestimates cross stream flows because 1) details in the vertical structure of the streamwise flow are not resolved and 2) secondary flows are intensified by a reduction in vertical mixing.

In the case of tidal flow around a headland an eddy may form down stream of the tip of the headland. Secondary flows associated with the curved flow advects bottom water from off shore towards the eddy. If the water column is stratified secondary circulation increases density in the eddy region. Furthermore, secondary flows associated with the eddy itself may produce upwelling (Garrett and Loucks, 1976) causing isopycnals to dome upward in the center of the eddy.

Recently, we made detailed observations of tidally driven flow around a headland in a highly stratified environment. Our observations indicate that the secondary flow produces a cross channel baroclinic pressure gradient which opposes centrifugal force and tends to reduce secondary flow. After maximum ebb a tidally driven transient eddy evolves down stream of the headland. The secondary flow associated with the larger scale flow around the headland increases salinity in the eddy region. As the eddy spins up during late ebb doming of the density field is observed in the center of the eddy.

In this presentation observations are presented showing the interaction between stratification and tidal flow around a headland. The presentation includes: 2) a description of the field program, 3) description of the transient and residual velocity and density fields 4) a description of the evolution of cross channel density gradients in terms of advective processes, 5) an evaluation of terms in the time dependent cross channel momentum equation

Field Program

The observations were made in the spring of 1993 during an intensive survey of the Hudson River Estuary. The five day survey focused on an 8 km reach of the river and included repeated along channel and cross channel transects. One reason this reach was selected was because of the large changes in channel morphology. A minimum cross section is produced by a headland at the George Washington Bridge. The cross sectional

area changes from 10,000m^2 at this constriction to 16,000m^2 2 km downstream of the headland. Maximum channel depths exceeding 20m occur close to the Manhattan side of the river in the vicinity of the constriction.

The survey was designed to resolve the spatial structure of the intratidal velocity and salinity fields. The instrumentation used included a towed 1.2 MHz narrowband ADCP, an AMS CTD and a 200 kHz echo sounder. The survey was conducted during a period of increasing tidal range. Surface to bottom salinity differences exceeded 20 psu and ebb velocities approached 200 cm/s at the surface. The amplitude of the semidiurnal transport and river discharge were estimated to be approximately 10,000 m^3/sec and 2000 m^3/sec respectively.

Density and Velocity Structure

Cross channel density gradients exhibit significant intratidal variability. Cross channel gradients are strongest during ebb at and down stream of the headland where the halocline slopes upward toward Manhattan. Observations indicate that cross stream density gradients are produced primarily by secondary circulation generated by the curved flow. During ebb cross channel flow is evident primarily off the tip of the headland; with surface and bottom currents tending towards New Jersey and Manhattan respectively. Secondary circulation weakens at 1 km and then reverses 2 km down stream of the headland.

Late in ebb a tidally driven eddy spins up down stream of the headland. The eddy drives dense water on the NY side upstream. Furthermore, isopycnals are seen to dome up in the core of the eddy. As flood commences the domed density field moves upstream with the eddy.

From the repeated transects residual velocity and density fields are estimated and are found to be highly three dimensional. The residual density field exhibits strong cross channel density gradients with isopycnals running obliquely across the channel. Residual currents are composed of a counterclockwise eddy embedded in the longitudinal flow, with velocity vectors veering towards the center of the eddy with depth, opposed to the residual baroclinic forcing. The residual flow pattern represents the sum of gravitationally and tidally induced motion.

Evolution of Cross Channel Density Structure.

The time evolution of the cross channel density gradient is interpreted in terms of a density balance. The interpretation suggests that during early ebb vertical motion associated with secondary flows generate cross channel gradients. As the eddy spins up during late ebb lateral shear acting on the along channel density gradient also generates cross channel gradients. Throughout the ebb cross channel gradients are advected down stream away from the curved flow where they may adjust under the influence of gravity

Momentum Balance

Instantaneous estimates of the cross channel baroclinic pressure gradient and centrifugal accelerations were made. The vertical gradient of these two terms, which appear in a cross stream shear tendency equation, are in near balance. This balance clearly indicates that the tendency for centrifugal forces to produce secondary flows are offset by baroclinicity. Both of these terms exhibit intratidal variability and are significantly larger during ebb. Because of the intratidal asymmetry the vertical structure of terms in the residual momentum equation resembles the ebb tide condition.

References

Garrett, C.J.R. and R.H. Loucks, 1976. Upwelling along the Yarmouth shore of Nova Scotia. *J. Fish. Res. Board of Can,* 33:116-117.

Geyer, W.R., 1993. Three-dimensional tidal flow around headlands, *J. Geophys. Res,* 95:955-966.

Kalwijk, J.P.T. and R. Booij, 1986. Adaptation of secondary flow in near-horizontal flow, *J. Hydraul. Eng.*, 24:19-37,1986.

Rozovski, I.L., 1957. *Flow of water in Bends of Open Channels.* Israel Program for Scientific Translation, Jerusalem,.

CONVERGENCE AND DIVERGENCE OVER TOPOGRAPHIC OBSTACLES IN A STRATIFIED ESTUARY

Jeffery D. Musiak and David A. Jay
Geophysics Program
University of Washington
Seattle WA 98195 USA

Abstract

Flow convergence and divergence play an important role in determining the bathymetry of an estuary. For mobile bed material, persistent convergent mean flow maintains topographic highs and divergence the lows. The investigation of this phenomenon started with two sets of velocity and density data from the Columbia River Estuary. The data were collected from a moving boat equipped with a 1200 kHz, narrow-band Acoustic Doppler Current Profiler (ADCP) and Conductivity-Temperature-Depth-profiler (CTD). An intensive data set was collected near the upstream limits of salinity intrusion 19-24 May 1992 during a spring-neap transition and a period of moderate river discharge. Stations were visited repeatedly on a 3.5 km along channel transect yielding time series ranging in length from 40-112 hr. A 30 hr series was obtained in the lower estuary 8-9 June 1991 during a period of moderate river discharge with spring tides. Both transects contained prominent topographic obstacles and were divided into 150-300 m segments; the along and across channel velocity components and the density were harmonically analyzed in 1 meter depth bins. Sections of the harmonic constituents were plotted. To continue the investigation a harmonic, semi-analytical (-coordinate perturbation model was developed. This model is able to reproduce the features of the flow observed in the ADCP data at residual, tidal and overtide frequencies. Observations from the ADCP data and model results suggest that: 1) there is a zone of residual downstream bottom-flow over a topographic high which is shifted towards the seaward side of the high; 2) near-bed mean stratification increases over the obstacle, even though the total, top to bottom, density difference decreases; 3) the mean horizontal density gradient changes sign over the high. The mean velocity (Figure 1a) and density fields (Figure 1b), show that from station 2 to 12 the stratification and negative mean horizontal density gradient allow a large area of upstream, positive, flow. From station 13 to 20 the density gradient is positive and the mean flow is seaward, at all depths. Upstream of station 20 the density gradient is again negative, and upstream bottom flow is reestablished; 4) there are strong tidal variations in density and stratification near the high. The phases of the velocity and density indicate that changes in the flow must occur at the high first as it is a constriction in the flow; and 5) the overtide amplitudes of the along channel velocity and salinity are elevated near the high indicating that non-linear effects are very significant here.

These observed features can be explained two ways. The first is to consider the flow over an obstacle as having two-layers on flood but as a one-layer, stratified flow on ebb. During the flood seaward of the high, the lower layer is subcritical (the internal Froude number, $G < 1$) because it must thicken to flow over the high; where it is critical ($G = 1$). Landward of the high, the layer thins as it flows down the lee side of the high, near the base the flow is again subcritical ($G < 1$), and thickens. On ebb, the flow landward of the high is strongly sheared; as the flow shoals over the high, vertical mixing increases and the flow becomes more homogenous. Downstream of the high, shear increases as restratification occurs. In this scenario, the flood currents are weakened as the lower layer thickens to go over the high, but augmented as the layer thins going down the

high on the landward side. Very early on the ebb, the stratification is washed out, thus eliminating the possibility of upstream bottom flow on the downstream side of the high.

The second explanation of the observed seaward bottom flow is to consider it an example of internal tidal asymmetry, or residual flow generated by a correlation of vertical shear in the tidal flow and tidal variations in stratification [Jay and Musiak, 1994]. Tidal variability of near-bed salinity is particularly pronounced in the vicinity of the topographic high and exhibits a narrow, sharply defined (in the vertical) maximum 3-5 m above the crest of the high. This is presumably caused by strong vertical excursions of the density field as it encounters the obstacle. All three greater ebbs and two of the three lesser ebbs for which observations are available near the upstream limits of salinity intrusion show a rapid decrease in near-bed salinity caused by intense vertical mixing over and just seaward of the topographic high. This brings about a rapid decrease in density stratification early in the ebb. On the other hand, the phase of the tidal currents and the vertical shear is less strongly perturbed by topography. The sense of the correlation between the tidal shear and stratification just downstream of the obstacle is thus favorable for the generation of seaward bottom-flow by internal asymmetry, whereas it is favorable for upstream bottom flow landward and farther seaward of the high. The result is a decrease in top-to-bottom velocity difference that extends well downstream of the high. The total top-to-bottom velocity difference of >0.85 m s^{-1} at the downstream end of the reach is too large to be accounted for by linear gravitational circulation alone, as is the upstream bottom flow of 0.15 m s^{-1} in the presence of river outflow of ~0.25 m s^{-1}.

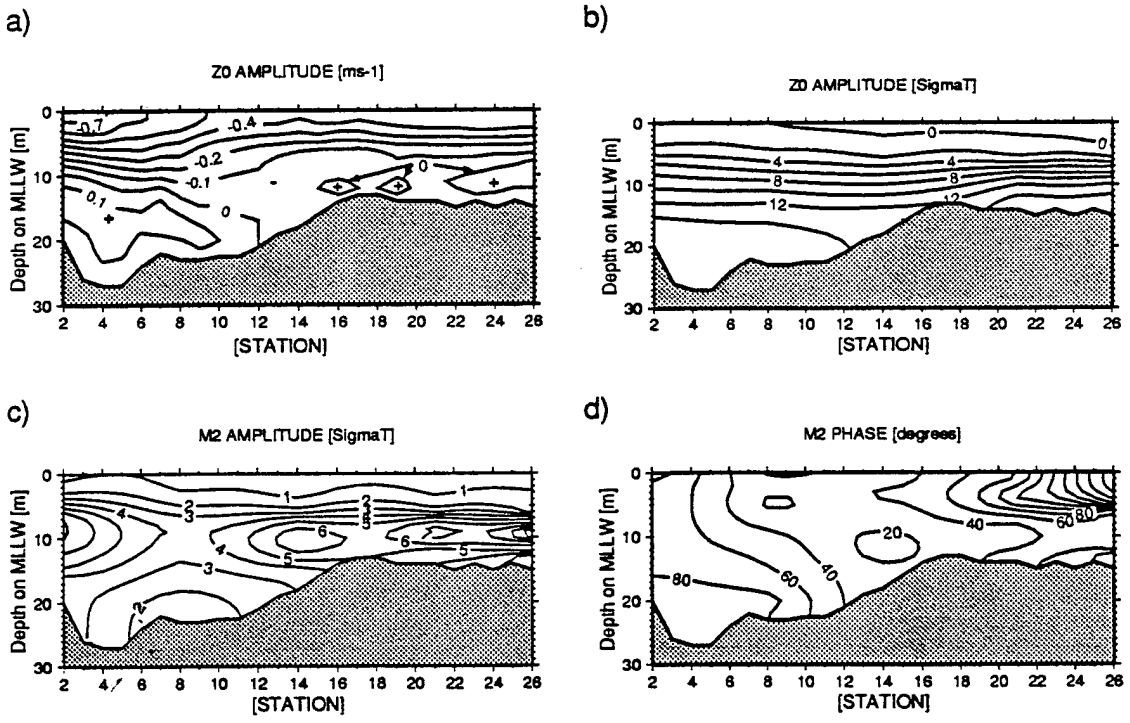

Figure 1. Along-channel transects of harmonic constituents determined by analysis of 40-112 hr time series of ADCP data (26 stations) and CTD data (5 stations) located along a 3.5 km reach of the South Channel of the Columbia River estuary, near the upstream limits of salinity intrusion. (a) Along-channel component of mean or residual velocity, positive flows are landward (to the right). (b) Mean density field expressed in σ_t units. (c) M_2 amplitude of the density field in σ_t units. (d) M_2 phase of density field in degrees.

A harmonic, semi-analytical (-coordinate perturbation model was employed to further analyze the effects of a topographic high on tidal, residual and overtide flows in a stratified estuary (Figure 2a, b, c). The model consists of a vertically-integrated wave propagation model (Jay, 1991) which, together with prescribed Rig and horizontal density gradient fields, drives velocity profile models. Because of the need to include a stratification correction in the model's eddy diffusivity turbulence closure, the profile equations are solved numerically. The model includes along-channel changes in width and depth and tidal flat width. For the present run, the width was taken as constant, the ratio of total width to channel width was 1.7, and bottom depth (Figure 2c) was chosen to imitate the situation near the upstream limits of salinity intrusion as shown in Figure 1. The predicted linear residual, gravitational circulation plus river outflow flow mode shows a top-to-bottom velocity difference of >0.5 m s^{-1} downstream of the hump, which is reduced to ~0.3 m s^{-1} on its landward side. The reversal of the horizontal density gradient seen in Figure 1b and the adverse bed slope cause a major reduction in the shear in this mode over the hump. Similar but smaller effects are seen in internal residual driven by internal asymmetry. There is, moreover an intimate connection between the results for the two

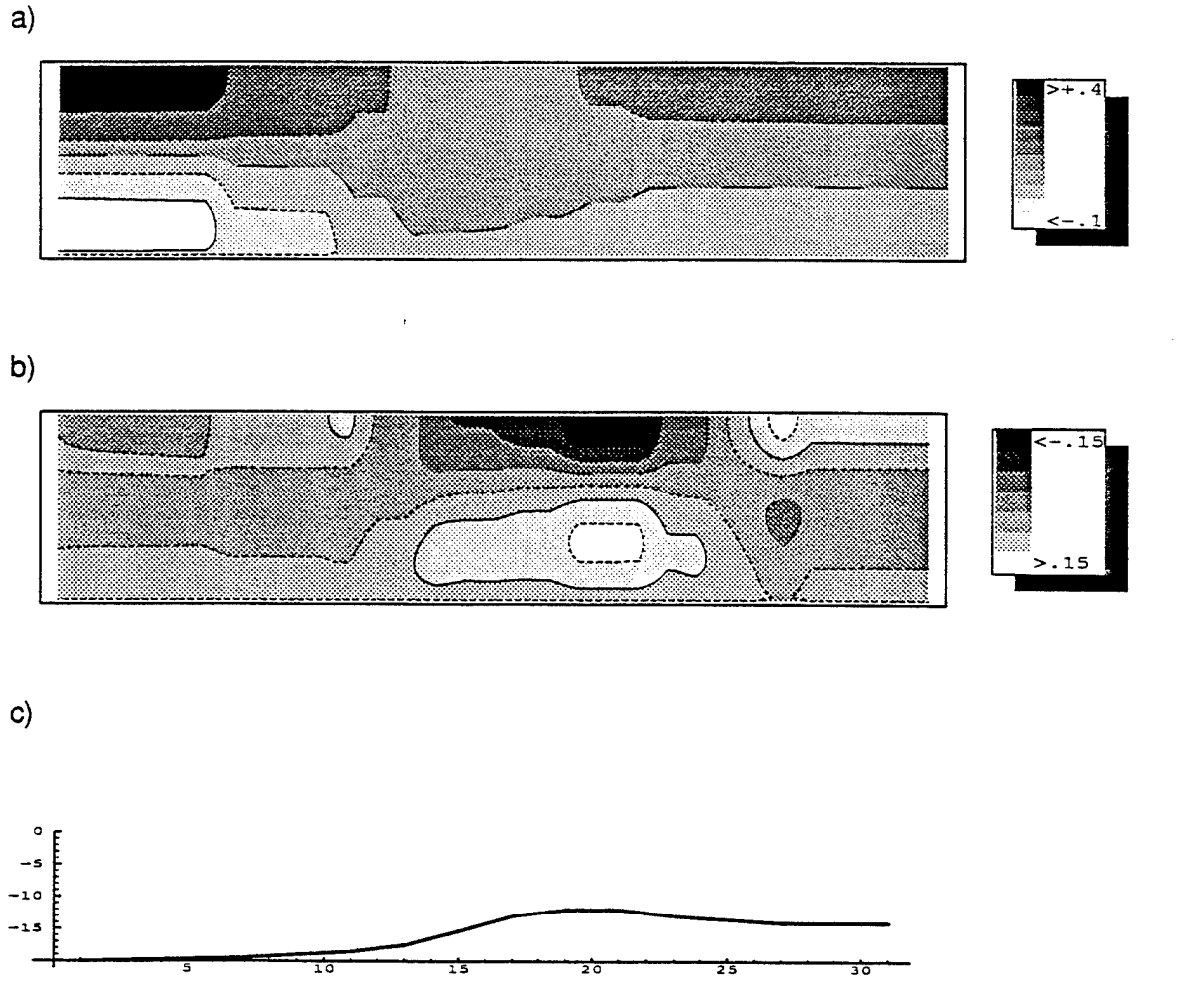

Figure 2. Model predictions of (a) linear residual flow, gravitational circulation plus net outflow, and (b) residual due to internal tidal asymmetry over a topographic high [shown in (c)] in a stratified estuary. Results are presented in (-coordinates and are based on 31 evenly spaced profiles.

modes. Internal asymmetry is the result of tidal shearing of the mean salinity field. This causes tidal changes in stratification and thus in vertical mixing. Reversal of the mean horizontal salinity gradient seaward of the hump alters the phase relationship between the tidal currents and stratification, effectively stalling the residual flow due to internal asymmetry. The only location where internal asymmetry is prominent in this reach is on the landward, downslope side of the high, where the mean horizontal salinity gradient is again favorable. The fact that the horizontal change in M2 salinity phase is only ~60 (rather than 180 (is attributed to the short length of the topographic high, only a few km, relative to the tidal salinity excursion length of ~10-15 km. A more decisive reversal might be seen over a longer topographic obstacle. It is also likely that channel curvature effects, not represented in our model, effect both the density and velocity field in ways that we cannot at present define.

In summary, observations and results from a harmonic, semi-analytical (-coordinate perturbation model suggest that topographic obstacles generate an asymmetric pattern of convergent residual flow on their seaward side and divergent residual flow over their crests, at least during periods of strong stratification. This asymmetric flow patter is caused by the stratification being compressed and raised as the flow encounters an obstacle. The compression and raising of the density field causes the mean horizontal density gradient to reverse, stalling the near bed, upstream residual flow. It seams likely that a more symmetric residual flow pattern must exist at other times (e.g., weakly stratified, low-flow, spring tides) to maintain the long-term stability of these topographic features.

References

Jay, D. A., 1991, Green's Law Revisited: Tidal Long-Wave Propagation in Channels with Strong Topography. *J. Geophys. Research,* 96(C11):20,585-20,598.

Jay, D. A. and J. D. Musiak, 1994. Internal Tidal Asymmetry in Channel Flows: Origins and Consequences. In C. Pattiaratchi (ed.), *Mixing Processes in Estuaries and Coastal Seas,* an *American Geophysical Union Coastal Estuarine Science Monographs*. (in press).

7th International Biennial Conference on the Physics of Estuaries and Shallow Seas, Woods Hole, MA, 28 to 30 November 1994.

THE INFLUENCE OF THE SPRINGS-NEAPS TIDAL CYCLE ON THE POSITION OF SHELF SEA FRONTS.

Jonathan Sharples[1] and John H. Simpson[2]
[1]New Zealand Oceanographic Institute
Greta Point, P.O.Box 14-901,
Kilbirnie, Wellington, New Zealand.
John H. Simpson,
[2]University of Wales School of Ocean Sciences
Menai Bridge, Gwynedd, U.K.

Abstract

Introduction

Shelf sea fronts, separating thermally stratified and vertically mixed regions, are observed to occupy positions that change very little through the months of late spring and summer. For depths typical of fronts found at temperate latitudes (50-100 metres) we have shown (Simpson & Sharples, 1994) that control of the location of a front is dominated by the balance between surface heating and tidal stirring energy inputs, supporting the theory of Simpson & Hunter (1974) that fronts should follow contours of h/u^3, with h the water depth and u the tidal current amplitude. At greater depths, or in places where the tidal currents have a dominant cyclonic component, the simple energy balance argument begins to be affected by boundary-layer limitation of vertical turbulent mixing (e.g. Garrett et al., 1978; Soulsby, 1983; Loder & Greenberg, 1986).

The mean frontal position is observed to change only by approximately 10 to 20 kilometres (Bowers & Simpson, 1987). Most of this movement can be attributed to tidal advection of the front, but a contribution of 2-4 kilometres has been linked to the springs-neaps tidal cycle (Simpson & Bowers, 1979; Simpson, 1981), and postulated as being a consequence of the springs-neaps modulation of the tidal stirring energy (e.g. Pingree et al., 1977). Simpson & Bowers, 1981, showed that the movement of shelf fronts observed by satellite lagged the springs-neaps cycle by approximately 2 days. More recently, Bisagni & Sano, 1993, have presented a detailed analysis of the Georges Bank frontal region observed by Advanced Very High Resolution Radiometer. They showed that there was a significant negative correlation between the variation in sea surface temperature about the seasonal mean, and tidal current speed. A time lag between tidal current and the temperature variation of approximately 3 days was observed; i.e. 3 days after spring tides the surface temperatures reached a minimum below the seasonal mean, and 3 days after neap tides they reached a maximum above the seasonal mean.

Models of Springs-Neaps Frontal Movement

The observed amplitude of the frontal movement over a springs-neaps cycle is considerably less than that predicted by a calculation based on the tidal variation of the h/u^3 parameter. A change in current from springs to neaps by a factor of 2 implies a change in the tidal stirring intensity by a factor of 8, leading to a typical horizontal change in frontal position of approximately 20 km. Simpson & Bowers, 1981, attribute this discrepancy to two inadequacies of the simple energy balance argument:

1) As spring tides approach, the increasing tidal mixing not only has to counteract the surface heating, but must also remove the buoyancy stored since the previous spring tide.
2) Vertical turbulent mixing will be inhibited by the thermocline, effectively reducing the efficiency of tidal mixing on the stratified side of the front.

Simpson & Bowers, 1981, investigated these effects using a 1-dimensional numerical model in which the vertical water column structure was determined by the energetics of wind and tidal mixing, and solar heating. They showed that having to remove the stored buoyancy reduced the predicted frontal movement to approximately half the equilibrium prediction. The extent of the frontal movement predicted by the model was then further reduced towards that typically observed by incorporating a stability-dependent tidal mixing efficiency.

Here we have used a method for modelling a vertical section through a front that we introduced in Simpson & Sharples, 1994. The model uses a level 2 turbulence closure scheme (e.g. Mellor & Yamada, 1982) to control vertical turbulent transport in response to a tidally oscillating sea-surface slope and seasonally varying surface wind stress. Seasonal surface heat flux is included based on a simple bulk parameterisation of solar heating and surface cooling. The model is 1-dimensional in the vertical. A section through a front is generated by running the model over a range of mixing regimes (controlled by altering the amplitude of the tidal slope). Results for each level of mixing from the same time in the annual cycle can then be combined to form a frontal section. Direct integration of the equation of motion, and the use of the closure scheme to control vertical mixing, remove the dependency on energetics arguments as the sole control on water column structure. The model implicitly includes the additional effects of stored buoyancy, turbulence inhibition by stratification, and changes in the boundary layer caused by variations in the tidal current ellipse, the water depth, and latitude. The principle assumption of this modelling approach is that the frontal position is controlled predominantly by local vertical processes; effects due to tidal advection, geostrophic adjustment, and residual circulation are not addressed.

In this work a direct comparison has been made between the turbulence closure model and the energetics-based prescriptive model of Simpson & Bowers (1981, 1984) run under exactly the same boundary conditions.

Results

Both the turbulence closure model and the prescriptive model, the latter without and with stability-dependent mixing efficiencies, were run over 2 annual cycles and a range of mixing conditions from $\log(h/u^3)=1$ to 3. Here h is the water depth (metres) and u^3 ($m^3\ s^{-3}$) is the cube of the depth-mean current speed, averaged over the springs-neaps cycle; this provides a horizontal axis on which to portray the results that remains geographically fixed through time. Results were output during the second annual cycle, having allowed the system to stabilise during the first year. For the initial comparison between the turbulence closure model and the prescriptive model the tidal current ellipse was degenerate, with the S_2 current amplitude being 30% of the M_2 amplitude. For both models the water column depth was fixed at 80 metres, and split into 20 depth cells.

In all cases the position of the front has been defined as the place at which the water column potential energy anomaly was 5 J m^{-3}. Such a value represents only marginal stratification, and was chosen on the basis of its close association with the maximum horizontal temperature gradient in the results from the turbulence closure model. For the prescriptive model without stability inhibition of mixing the extent of frontal movement over the springs-neaps cycle, in units of $\log(h/u^3)$, was 0.35, with a lag of approximately 2 days of the

maximum frontal excursion after neap tides. For the prescriptive model with a stability-dependent tidal mixing efficiency (following Simpson & Bowers, 1981), the movement was reduced to 0.2 and a slightly increased lag of 2-3 days. The same results for the turbulence closure model were 0.26 and a lag between 2 and 3 days.

All three models showed the same asymmetric behaviour of frontal excursion over the springs neaps cycle. The movement towards lower h/u^3, starting 3 days before and finishing 2-3 days after neap tides, was more rapid than the following retreat of the front into the region of higher h/u^3. The highest value of h/u^3 reached by all fronts, typically 3 days after spring tides, corresponds to the position that the front maintains in the absence of any S_2 tidal constituent.

The effect of turbulence limitation by the bottom boundary layer was investigated by running the turbulence closure model with clockwise, degenerate, and anticlockwise tidal current polarisations. The extent of springs-neaps frontal adjustment decreased slightly from clockwise to degenerate current ellipses, with the mid-summer adjustment for the degenerate case being about 92% that of the clockwise case. Frontal movement was negligible when tidal current polaristaion was completely anticlockwise.

Conclusions

Both the prescriptive and the turbulence closure models generate springs-neaps frontal movement similar to that observed, with a 2-3 day lag between the phase of the springs-neaps cycle and the frontal excursion. The turbulence closure model and the prescriptive model with stability-dependent mixing efficiencies produced significantly less frontal movement than the constant efficiency prescriptive model. The lag between frontal movement and the springs-neaps cycle can be understood as the result of two processes. As the front moves to lower h/u^3, due to the drop in tidal currents at neap tides, there is some thermal lag as the solar irradiance stratifies the previously mixed water. Subsequent retreat of the front to higher h/u^3, resulting from stronger mixing around springs tides, is damped by the existing stored buoyancy and also slowed by the inhibition of turbulent mixing by the stratification. Thus the system operates as an oscillator forced by the springs-neaps changes to the h/u^3 parameter, and damped by the influences of thermal inertia, stored buoyancy, and stability-reduced mixing. It is noted that the extent of this lag did not change significantly in the results from the prescriptive model when the stability-dependent mixing efficiency was introduced.

Part of the asymmetry in the curve of frontal movement can be attributed to differences in the damping strengths of the thermal inertia and the inhibition of turbulent mixing by vertical stability. Another influence will be the small change in frontal position caused by the seasonal change in the solar irradiance. In particular the post-solstice seasonal retreat of the front was effective in reducing the springs-neaps response of frontal adjustment in all model runs.

The use of different polarisations of the tidal current ellipse demonstrated the effect of boundary layer limitation of vertical turbulent exchange. The smaller boundary layer associated with fully anticlockwise polarisation reduced the applicability of the h/u^3 criterion resulting not only in the shift of the mean frontal position (Simpson & Sharples, 1994), but also in negligible frontal movement over the springs-neaps cycle.

References

Bisagni, J.J., and M.H. Sano, 1993. Satellite observations of sea surface temperature variability on southern Georges Bank. *Continental Shelf Research,* 13(10):1045-1064.

Bowers, D.G., and J.H. Simpson, 1987. Mean positions of tidal fronts in European shelf seas. *Continental Shelf Research,* 7(1):35-44.

Garrett, C.J.R., J.R. Keeley, and D.A. Greenberg. 1978. Tidal mixing versus thermal stratification in the Bay of Fundy, Maine. *Atmosphere-Ocean,* 16:403-443.

Loder, J.W., and D.A. Greenberg, 1986. Predicted positions of tidal fronts in the Gulf of Maine region. *Continental Shelf Research,* 6:397-414.

Pingree, R.D., P.M. Holligan, and R.N. Head, 1977. Survival of dinoflagellate blooms in the western English Channel. *Nature,* 265:266-269.

Simpson, J.H., 1981. The shelf sea fronts: implications of their existence and behaviour. *Philosophical Transactions of the Royal Society of London,* A302:531-546.

Simpson, J.H., and D.G. Bowers, 1979. Shelf sea fronts' adjustments revealed by satellite I.R. imagery. *Nature,* 280:648-651.

Simpson, J.H., and D.G. Bowers. 1981. Models of stratification and frontal movement in shelf seas. *Deep Sea Research,* 28A:727-738.

Simpson, J.H., and D.G Bowers, 1984. The role of tidal stirring in controlling the seasonal heat cycle in shelf seas. *Annales Geophysicae,* 2(4):411-416.

Simpson, J.H., and J.R. Hunter, 1974. Fronts in the Irish Sea. *Nature,* 250:404-406.

Simpson, J.H., and J. Sharples, 1994. Does the earth's rotation influence the location of shelf sea fronts? *Journal of Geophysical Research,* 99(C2):3315-3319.

Soulsby, R.L., 1983. The bottom boundary layer of the shelf sea. In: *Physical Oceanography of Coastal and Shelf Seas,* B. Johns (ed.), pp 189-266. Elsevier, New York.

Stigebrandt, A., 1988. A note on the locus of a shelf front. *Tellus,* 40A:439-442.

ON EFFECTS OF BUOYANCY ON ESTUARINE CIRCULATION AND SEDIMENT TRANSPORT

Y. Peter Sheng
Coastal & Oceanographic Engineering Department
336 Weil Hall, P.O. Box 116590, University of Florida
Gainesville, Florida 32611-6590

Abstract

Introduction

This paper address the effects of buoyancy on circulation and sediment transport in Tampa Bay (Figure 1), which is a large shallow estuary with an average depth of 4-5 m and a deep (up to 30 m) navigation channel. Exchanges of salt and fresh waters between the coastal ocean and the estuary take place mainly inside the dredged navigation channel, while water column in the shallow region often remains well-mixed. A major oceanographic monitoring program in Tampa Bay was conducted by NOAA in 1990-1992 (NOAA, 1993). Vertical profiles of currents and salinity were measured by ADCP at various locations along the navigation channel. These data form the basis for an examination of the relative importance of wind, tide, and buoyancy in affecting the Tampa Bay circulation. As part of this effort, a three-dimensional curvilinear-grid model (Sheng 1989) has been used to examine the effect of buoyancy on the time-dependent and non-tidal residual circulation in Tampa Bay. In addition to the circulation study, we conducted a field and modeling

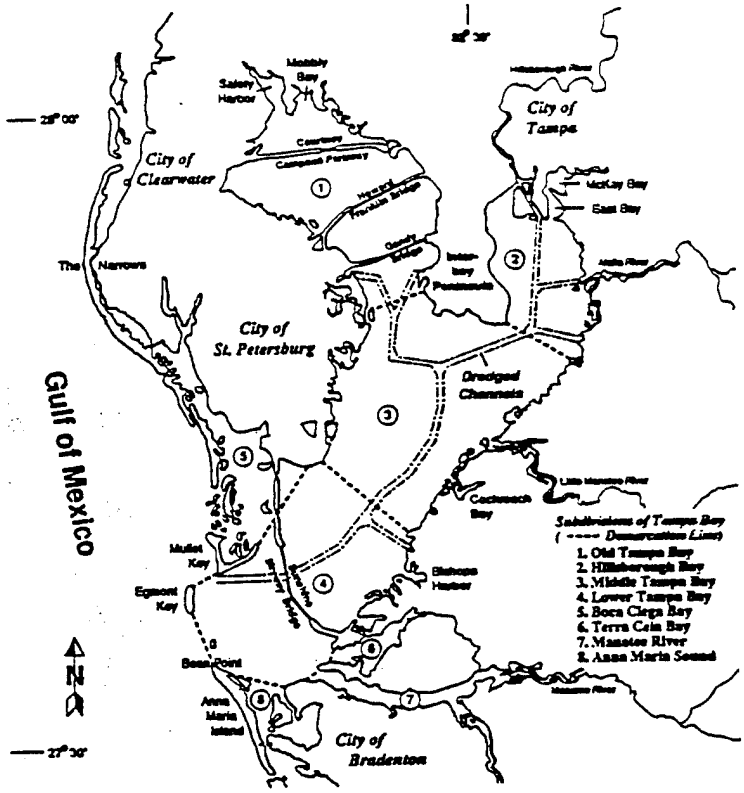

Figure 1. Tampa Bay Map.

study on the resuspension of cohesive sediments in the Hillsborough Bay (see Stations A and B in Figure 2). The potential effect of buoyancy on the resuspension of cohesive sediments and contaminants was investigated. A single-point (i.e., water column) coupled hydrodynamic-sediment-water quality model was used to investigate the role of buoyancy on resuspension dynamics.

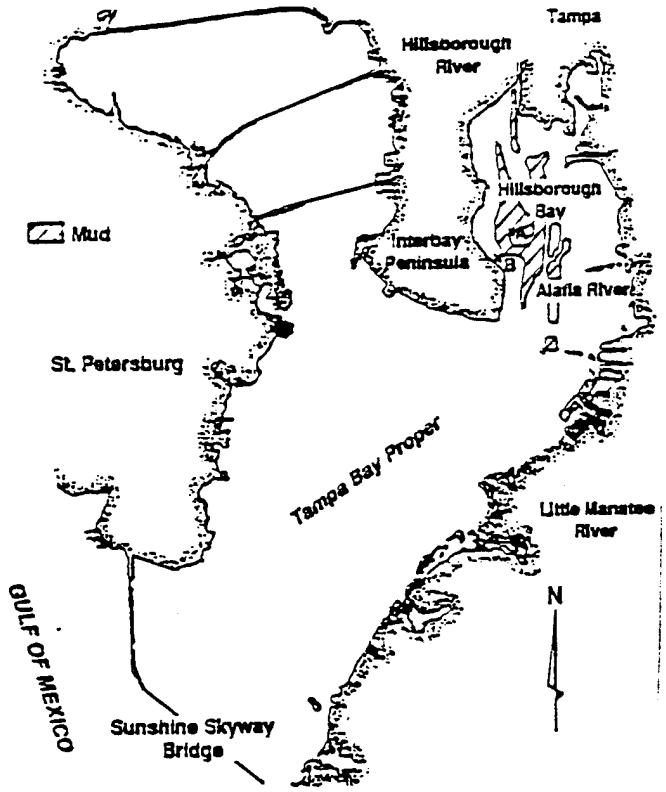

Figure 2. Map of Tampa Bay and Hillsborough Bay.

Methodology

Tampa Bay data used for this study were obtained by NOAA (1993) and University of Florida (Sheng et al. 1993). The NOAA data included vertical profiles of currents and salinity in the deep navigation channels measured with acoustic Doppler current profiler (ADCP). The University of Florida data consist primarily of hydrodynamic and sediment and water quality data measured at fixed platforms in shallow Hillsborough Bay during two storm events. The circulation study uses a 3-D curvilinear-grid hydrodynamic model. The 3-D curvilinear-grid model allows the use of boundary-fitted grid which can fit the detailed geometry of the shorelines and the navigation channel, thus giving much more accurate results than other models which use rectangular or orthogonal grids of similar resolution. The sediment study makes use of a coupled hydrodynamic-sediment-water quality model (Sheng et al. 1993) which describes the dynamics of flow, sediments, and nutrients in the water column and sediment column at any horizontal location. This single-point or water-column model can be used to quantify fully rough turbulent flow as well as transitional flow in the presence of a thin viscous sublayer.

Results

Simulations of baroclinic circulation over 30-day periods are conducted and compared with data in detail. Of particular interest is the residual non-tidal flow driven by the density gradients. For example, Figure 3 shows the 10-day residual near-surface currents and salinity in Tampa Bay subject to forcings of ocean tides and density gradients. The two cases correspond to different combinations of freshwater sources: (a) major rivers only, and (b)major rivers plus watershed flows. The ability of several turbulence models to simulate the measured vertical flow structure is examined in detail.

Resuspension dynamics of sediments during two storm events, one in 1992 and another in 1993, were measured and simulated. Results indicate that the resuspension of sediments were primarily the results of erosion by wave-induced bottom stress. As shown in the data (Figure 4), the tidal and wind-driven currents were too weak to cause sediment erosion. The vertical mixing of sediments in the water column, however, is strongly dependent on the tidal and wind-driven currents. To correctly simulate the vertical mixing, we impose the constraints that simulated currents at the two vertical levels (20% and 80% of depth) must be the same as the measured currents. The horizontal currents and suspended sediment concentration were successfully simulated. Near the bed, suspended sediment concentration could reach vary high values and produce a stable density gradient. This buoyancy effect was investigated by means of the single-point model.

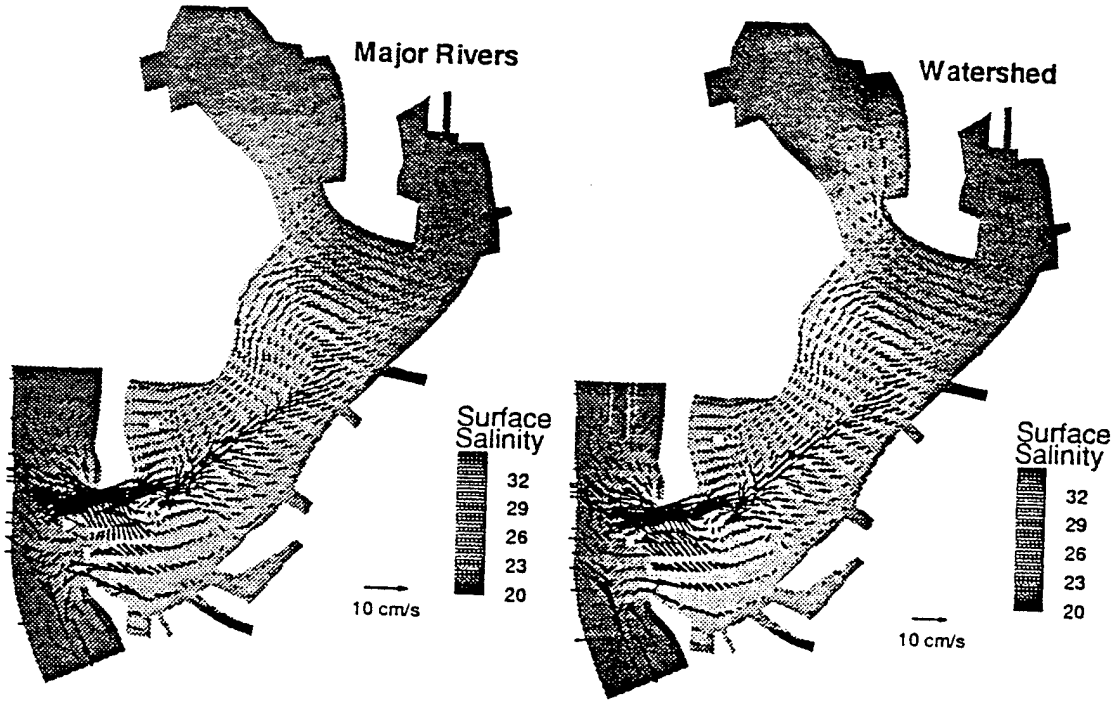

Figure 3. Residual near-surface currents and salinity in Tampa Bay: (a)freshwater from major rivers only, and (b) freshwater from major rivers and watershed.

Acknowledgment

This study was supported by the Florida Sea Grant and the Tampa Bay National Estuary Program.

References

NOAA, 1993. Tampa Bay Oceanography Project: Physical Oceanographic Synthesis, Technical Report.

Sheng, Y.P., X.-J. Chen, and E.A. Yassuda, 1993. Quantifying sediment resuspension flux of nutrients and contaminants in estuaries due to episodic events. Technical Report, Coastal & Oceanographic Engineering Department, University of Florida, Gainesville, Florida.

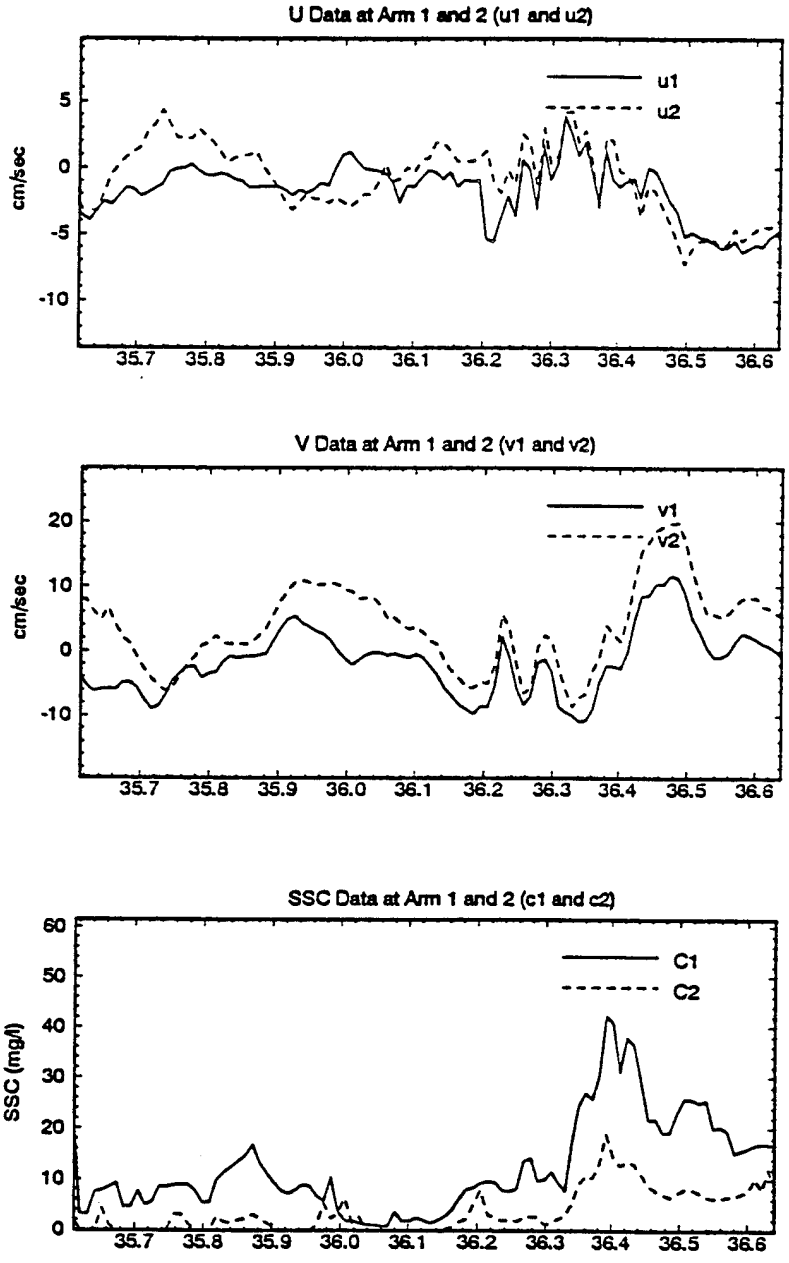

Figure 4. Measured horizontal velocities and suspended sediment concentration at Station A in Hillsborough Bay during Julian day 35.6 to 36.6, 1992.

THE EFFECT OF HYPERPYCNAL WATER ON TIDAL EXCHANGES

Ned P. Smith
Harbor Branch Oceanographic Institution
5600 North U.S. Highway 1
Fort Pierce, Florida 34946, USA

Abstract

Strong hydrographic gradients are common in estuarine and inner shelf waters. They arise most frequently in two ways. First, they appear as a result of the juxtaposition of sea water and fresh water arriving in the form of runoff and groundwater seepage. Alternately, horizontal gradients arise from the different response of deep and shallow water columns to spatially uniform freshwater gains and losses, or to spatially uniform sensible and latent heat fluxes. A relatively shallow water column will show a greater response to a given gain or loss, especially over shorter time scales. Hydrographic time series from tidal channels connecting shelf and estuarine waters clearly demonstrate these hydrographic gradients, as water of different salinity and temperature ebbs and floods past the study site.

A series of field studies conducted in the Bahamas from mid 1990 to mid 1992 included measurements of temperature, salinity and currents in tidal channels connecting Exuma Sound with Great Bahama Bank. Within one tidal excursion seaward of the Exuma Cays, water depths in Exuma Sound are on the order of 300 m; Great Bahama Bank extends for many tens of kilometers in the other direction with water depths on the order of 3.5 m. In terms of air-sea interaction, Great Bahama Bank acts like a large, unbounded evaporation pan, generating hyperpycnal water throughout the year. Freshwater gains are due to rainfall only; there is no river runoff. On average, annual evaporation exceeds precipitation by 175. Seasonal variations in E-P include a winter maximum that is roughly four times the net loss characteristic of midsummer months. The combination of higher net freshwater losses and increased sensible heat fluxes in winter months results in the generation of hyperpycnal water over the bank.

One of the study sites was just inside the entrance to Adderley Channel. The current meter was moored 2 m above the bottom in a water column that averaged 7 m deep. Tidal and low-frequency exchanges were superimposed onto a mean inflow of 220 $m^3 s^{-1}$. M_2 tidal amplitudes at this location are approximately 0.33 m and 0.69 m s^{-1}. An analysis of transport through Adderley Channel revealed large variations in temperature, salinity and density over complete tidal cycles. A one-year time series of density in the form of sigma-t is comprised of a well defined annual cycle, low-frequency variations over time scales on the order of 1-2 weeks and high-frequency fluctuations associated with tidal exchanges. Tidal period deviations from the seasonal and low-frequency nontidal variations occur most commonly in the form of transient "spikes." Sigma-t values increase by one-half to as much as two and a half units (0.5-2.5 kg m^{-3}). Salinity increases by as much as 3‰. Spikes appear through much of the year, but they are most prominent in late winter months and to a lesser extent in mid to late summer.

The relationship between density and along-channel flow in Adderly Channel becomes clear when a plot of density is compared with a plot of along-channel volume transport. Highest densities at the mouth of the channel coincide with slack water after the ebb. Density decreases quickly with the turn of the tide, and for much of the flood half of the tidal cycle, density is low and relatively uniform. The asymmetry of the density plot

over tidal cycles suggests that water entering on the flood tide is not the same water that left on the preceding ebb.

Perturbation analysis of the hydrographic data indicates an export of salt over tidal time scales that opposes the import associated with the annual mean inflow. The presence and absence of salinity spikes, and thus salt transport, is a function of across-shelf wind stress. During periods of strong onshore winds, Exuma Sound water is forced more than one tidal excursion onto Great Bahama Bank. At those times, water ebbing off the bank is the Exuma Sound water that arrived on the preceding flood. At other times, longitudinal mixing entrains high-salinity bank water, and the mixture is hyperpycnal.

This paper extends the earlier work by documenting the movement of hyperpycnal water across the shelf, and by exploring the effects this water has on tidal exchanges at the mouth of the channel. It was hypothesized that hyperpycnal water would cascade down the narrow shelf, and thus not be in position to reenter the tidal channel on the following flood. To measure density currents near the shelf edge, a current meter equipped with a conductivity sensor was moored 0.5 m above the bottom at a second study site, seaward of the mouth of the channel and about 50 m from the top of a nearly vertical wall that constitutes the shelf break. The width of the shelf was approximately 0.5 km. At the shelf study site, water depth was 25 m. High-density water passing this study site was almost certainly lost to intermediate depths in Exuma Sound.

Sigma-t values for an 83-day midsummer time period in 1992 show density spikes superimposed onto a portion of the annual cycle. A general decrease during the first month of the study indicates the last of the spring and early summer warming. Density spikes are less prominent than in Adderley Channel, suggesting that some vertical mixing occurs as hyperpycnal water cascades down the narrow shelf on the ebb tide. Nevertheless, transient spikes are evident, especially early and late in the study. Across-shelf current components recorded during the same time period are decidedly ebb-dominant, as a result of density currents coming out of Adderley Channel forced by the seaward-directed baroclinic pressure gradient. Weak flow toward the entrance to the channel does occur during the flood tide, but the mean landward current speed is -2.4 cm s^{-1}, while the mean seaward speed during the ebb is +5.1 cm s^{-1}. Current meter from Adderley Channel are not available for this time period, but the mean current speed during June, July and August of the 1990-1991 study was approximately -6 cm s^{-1}. Thus it appears that the export of hyperpycnal water as density currents changes a flood-dominant condition in the channel into a locally ebb-dominant condition in near-bottom layers across the narrow shelf.

Salinity recorded in a tidal channel can be used as a natural tracer to estimate percentages of bank and shelf waters in a water sample if the two end points of the mixture are known. If the salinities of homogeneous bank and shelf water are S_b and S_s, respectively, and the salinity in the tidal channel is S_c, then the fraction of the tidal channel sample that originated in Exuma Sound, F_s, is given by

$$F_s = \frac{S_b - S_c}{S_b - S_s}. \qquad (1)$$

While homogeneous Exuma Sound water can be expected within one tidal excursion of the mouth of the tidal channel, hydrographic gradients are common over Great Bahama Bank. Occasionally, however, relatively constant salinity water leaves the bank during much of the latter part of the ebb tide cycle. At such times, this water provides a value for S_b, and one can calculate F_s under flood tide conditions to evaluate the fraction of incoming water that is shelf water. This is given by the ratio of the volume of Exuma

Sound water to the total volume arriving on the flood tide cycle:

$$R_s = \frac{\sum_{m=1}^{n} F_s V_m}{\sum_{m=1}^{n} V_m} \qquad (2)$$

where V_m is the volume of water entering the channel during the m^{th} hour of the flood tide.

Salinity was used as a natural tracer to quantify the percentage of shelf water entering the channel on two successive flood tides. Using (1) to quantify the fraction of sound water in the channel measurements, and using (2) to quantify the percent of sound water entering during the flood tide cycle, results suggest that approximately 95% and 97.5% of the flood tide volume was Exuma Sound water not related to the previous ebb. Fractions of shelf and bank water entering on the flood tide are not easily quantified when bank water and shelf water are gradually blended over the bank within one tidal excursion of the study site. Although salinity can still be used as a natural tracer, one must have a much better picture of the spatial variation of salinity throughout the tidal cycle.

Mean monthly differences between flood and ebb tide densities provide a measure of the likelihood of density currents over the course of a year. During the 1990-1991 study, average ebb densities are between 0.5 and 1.0 kg m^{-3} higher than flood densities. Greatest differences occur from February through April, when shallow bank waters are colder, rainfall is at an annual minimum and when latent heat losses are greatest. It is therefore likely that there is a distinct seasonality in the existence and magnitude of density currents, and thus in the efficiency of tidal exchanges. During fall and winter months, strong shoreward winds force Exuma Sound water onto the bank well beyond one tidal excursion. At those times, tidal exchanges move sound and bank water back and forth through the channel. Hyperpycnal water is not exported into Exuma Sound, and density currents would be infrequent and weak. At other times, with relatively weak shoreward winds, nontidal inflow decreases. Longitudinal diffusion by tidal mixing brings hypersaline conditions to within one tidal excursion of the mouth of the channel. At those times of year, density currents can occur at the end of the ebb tide, bank water will cascade down the narrow shelf, and the following flood tide will involve a higher percentage of sound water.

With the available data, the role played by density currents cannot be separated from the effect that along-shelf currents have in sweeping an ebb tide plume away from the mouth of the tidal channel. Mid-depth current speeds recorded along the shelf just under two kilometers from the study site indicated a mean along-shelf flow of 5.8 cm s^{-1} during the study period. This by itself would increase the efficiency of tidal exchanges. The asymmetry of the near-bottom across-shelf flow, however, is a clear indication that ebbing water is moving seaward, and thus it is not moving back onto Great Bahama Bank through tidal channels that lie to the northwest.

The combination of a net seaward flow in near-bottom layers over the shelf off the mouth of Adderley Channel, combined with the net landward flow through the channel suggests that a strong net inflow must occur in near-surface and intermediate layers over the shelf. Applications of these transport patterns will not be pursued in this paper, but the erosive effects of a seaward near-bottom transport may be significant within the context of sediment transport. Similarly, the landward transport in surface and near-surface layers may be significant within the context of larval transport.

A second effect of a quasi-steady export of hyperpycnal can be postulated, although it lies outside the intended scope of this paper. The nearshore circulation along the western boundary of Exuma Sound is a persistent south-to-north flow. Mid-depth current measurements over a 402-day period of time from late October 1991 through late November 1992 indicate a resultant current speed of just under 6 cm s^{-1}. Shelf circulation cannot been decomposed into thermohaline and wind-driven components, but it is hypothesized that a regular export of hyperpycnal water contribute to the near-shore circulation as well as to the efficiency of tidal exchanges.

TIDAL INTERACTION WITH BUOYANCY-DRIVEN FLOW IN A COASTAL PLAIN ESTUARY

Arnoldo Valle-Levinson[1] and James O'Donnell[2]
[1]Center for Coastal Physical Oceanography,
Crittenton Hall, Old Dominion University, Norfolk VA, 23529
[2]Department of Marine Sciences,
University of Connecticut, Groton, CT 06340)

Abstract

The typical bathymetry of a coastal plain estuary consists of a system of shoals and channels that influence the flow and density fields. Hydrographic observations in coastal plain estuaries with prominent channels show a tendency for front formation along the channels. These fronts have been characterized as shear fronts associated with the differential advection of the estuarine longitudinal density gradient (O'Donnell, 1993). The differential advection is caused by the lateral shear in the barotropic tidal current, which results from differences in the relative importance of bottom friction over the channels and shoals. The amplitude of the current velocity over the channels is typically greater than over the shoals. Examples of shear fronts have been described in the York River (Huzzey and Brubaker, 1988) and in Delaware Bay (Sarabun, 1980). Transverse variations in current speed have also been implicated in the formation of convergence zones related to the deepest parts of channels as observed in the Conway River, North Wales (Nunes and Simpson, 1985). These studies have pointed out the transitional character of these fronts and convergence zones, which occur preferentially during flood stages.

Similar along-channel fronts have been observed with aerial photography in the lower Chesapeake Bay (Nichols et al., 1972). In the same area, strong lateral gradients in intratidal and mean current velocity, associated with abrupt bathymetry changes, have been observed with high resolution acoustic Doppler current profiler measurements (Valle-Levinson et al, 1994a). These measurements also show that the greatest intratidal flow magnitudes, as well as mean inflows, appear over the channels, whereas net outflows develop over the shoals. This flow transverse structure, which agrees with the findings of Wong (1994) in Delaware Bay, might be responsible for the formation of the fronts frequently observed in this area. The purpose of this study is to describe the mechanisms that generate lateral variability both in density and flow fields in systems of abrupt bathymetry changes. This is pursued through a series of simple numerical experiments that illuminate the effects of rotation, bathymetric slope, and tidal forcing on the alteration of the gravitational circulation in an estuary with a channel.

Approach

The numerical model used in this study is modified from that developed by Simons (1974; 1980), as described in Koutitonsky et al. (1987). It uses a C-grid for spatial discretization of the finite difference form of the three-dimensional momentum and continuity equations (Valle-Levinson et al., 1994b). Time integration is performed with a leapfrog scheme. Calculations are carried out in a split mode: external mode for transports, and internal mode for shears. Salt advection is formulated with an antidiffusive scheme (Smolarkiewicz, 1983). Non-linear terms are expressed as in Blumberg and Mellor (1987).

Solutions are computed for several cases for an interval of 3 days (72 h) in a domain consisting of an estuary 15 km wide, 55 km long and 10 m deep with a longitudinally uniform gaussian channel that extends to a depth of 25 m in the middle of the estuary (7.5 km from lateral boundaries). The estuary is open at the seaward and landward boundaries. The horizontal grid size is 500 m and the thickness of each of the 10 levels is 2.5 m. Bottom friction is parameterized with a linear formulation $\tau_b = ru_b$, where r is a friction parameter which equals 8 X 10^{-4} m/s and u_b is the near-bottom velocity vector. Solutions for the flow and salinity fields are examined at three sections across the estuary at distances of 18 km (10 km seaward of the center of the estuary), 28 km (center of the estuary) and 38 km (10 km landward of center of estuary) from the mouth. Areas of transverse flow convergence and of inflows/outflows are compared.

The initial salinity field consists of a vertically uniform longitudinal salinity gradient that varies linearly in the longitudinal direction only. The initial salinity at the landward (seaward) open boundary is 17 (25). The adjustment of this salinity gradient is assessed with and without earth's rotation influences. Then, the effects of the position of the channel across the estuary and the depth of the channel are examined. Finally the effects of tidal forcing of the order of the gravity current speed ($c_g = 0.5[g'H]^{0.5}$, where g' is the reduced gravity), and greater than c_g are explored. For the present estuary and salinity configurations cg ≈ 0.4 m/s.

Surface and bottom salinity fluxes, as well as surface (wind stress) momentum fluxes are set equal to zero. At the open boundaries the momentum transports are normal to the boundaries and are radiated out of the domain using an Orlanski-type condition as described by Miller and Thorpe (1981). Salinity is extrapolated to the boundary for both inflows and outflows through an advective condition similar to the aforementioned condition for momentum (Orlanski-type). Vertical fluxes of momentum and salt are parameterized through time- and space-dependent eddy viscosities and diffusivities. The parameterization is carried out with the Munk-Anderson scheme using neutral values of 5 x 10^{-5} m^2/s.

Results

The first three experiments present cases that have not been forced externally and the last two depict the influence of tidal forcing. The first experiment describes the fluid adjustment to the initial salinity gradient without Earth's rotation influences. After 3 days the flow has reached a quasi-steady state with the baroclinic pressure gradient balancing the bottom stress as in Wong (1994). The intrusion of high salinity fluid is confined to depths below 7 m and becomes more confined to the deep channel as distance from the mouth increases. As a consequence, the inflow associated with this high salinity is of greater magnitude (up to 0.50 m/s) at a distance of 40 km from the mouth than that a distance 20 km from the mouth of the estuary. Similarly, the magnitude of the outflow velocity increases seaward. This behavior is due to the thinning of the low (high) salinity layers with seaward (landward) distance. A cross-estuary structure is apparent only in the flow field as the strongest inflow is found in the channel.

The second experiment illustrates the effects of the Earth's rotation on the gravitational flow over an estuary with a channel. After 3 days of adjustment, a well-defined lateral structure in the flow and salinity fields becomes evident. Close to the mouth the salinity and flow fields are not greatly affected by the channel in the estuary (Figure 1). High-salinity inflow is weak and occupies most of the cross-section, whereas low-salinity outflow is strong and restricted to a near-surface distance of approximately one internal radius of deformation ($R_d = 2c_g/f \approx 8$ km) from the coast. The separation between the zero isotach and the right boundary decreases with depth and becomes zero before reaching

bottom so that the outflow is detached from the bottom. The lateral flow structure shows strong downwelling and convergence associated with the large shear of the longitudinal flow. Further landward, the outflow weakens and appears over both the left and right boundaries of the channel. Inflow is concentrated over the deep channel and extends to the surface. Its magnitude increases landward as the high salinity fluid becomes restricted to the channel. The lateral flow, or secondary circulation, in the upper 10 m constitutes a clockwise gyre in the vertical plane that is limited to the left by the boundary and to the right by the zero isotach. Another clockwise gyre occurs inside the channel associated with the core of maximum-magnitude inflow. The area of strongest convergence of near-surface lateral flow occurs over the channel. In a separate calculation, a channel with a depth of 17 m induces weaker flows with lower inflow salinities than the case with the deeper (25 m) channel.

The third experiment demonstrates the influence of the position of the channel on the gravitational flow and density fields. When the channel is near the right boundary (for an observer looking seaward in the northern hemisphere) the inflow region appears mainly over the channel. As in the other experiments with rotation, inflow reaches the surface over this area and favors strong lateral shears in the areas of maximum bathymetry gradient. Weak inflow also develops near the bottom in the vicinity of the left wall as a consequence of rotational effects. This weak inflow disappears as the distance from the mouth increases. Outflow is restricted to an area less than 2 km (much smaller than R_d) near the right wall and with approximately the same width along the estuary. This is due to the presence of the channel, which guides the inflow. Outflow also develops to the left of the estuary and, far from the mouth (38 km), can reach to the bottom in the region between the left wall and the channel. The secondary circulation is similar to previous experiments with the development of two clockwise gyres and greatest surface convergence over the channel than elsewhere across the estuary.

The fourth experiment examines the interaction of tidal flows of the order of c_g with the buoyancy flows produced by the initial salinity gradient. The ratio of surface elevation to water depth, which establishes the magnitude of the nonlinearly induced residual circulation, is 0.03, i.e. small relative to the tidal current amplitude. Intratidal behavior shows that the transverse structure of salinity is similar to that of previous experiments throughout the tidal cycle in a cross-section located in the middle between the open boundaries. High salinity fluid is confined to the deep channel and the lowest salinity is restricted to the right wall as described in the unforced case. Local variations of salinity depict fluctuations of less than 2 with maxima (minima) on flood (ebb). Isohalines migrate vertically with upward motions during flood and downward during ebb periods. The flow field displays well-established transverse structures. During early flood, outflow occurs over the shoals and inflow over the channel from the bottom to the surface. The core of maximum inflow migrates upward from the channel to the surface as the tidal forcing increases in strength. The greatest lateral gradients in the longitudinal flow develop over the regions of strongest bathymetry gradient. The lateral gradients on the right are greater than those on the left due to the persistent outflow on the right shoal. Even during maximum flood, near-surface outflow is present near the right wall owing to Earth's rotation effects. The weak barotropic forcing of this experiment is unable to counteract the effects of the longitudinal baroclinic pressure gradient in that region of the estuary. During ebb, the magnitude of the outflows is always greatest near the surface and decreases with depth. In the channel it is close to zero except during slack periods when inflow is present. The lateral flow structure shows that the zone of surface flow convergence migrates from the abrupt bathymetry change on the right (during early flood) to the middle of the channel (end of flood, early ebb) and back to the right (end of ebb). The strongest convergence occurs over the channel at the end of flood-beginning of ebb. This is the time of the tidal cycle when the longitudinal flow is the weakest and the transverse baroclinic pressure

gradient the strongest. This pressure gradient arises from high salinity over the channel and low salinity over the right shoal at this tidal stage. This is also the time of the tidal cycle when aggregation of material should develop, which is consistent with the findings of Nunes and Simpson (1985). Mean fields after one tidal cycle show that weak forcing does not appreciably alter the unforced distributions of salinity, longitudinal flow and transverse flow.

The fifth experiment shows the interaction of tidal forcing greater than c_g with the gravitational flow. The ratio of surface elevation to water depth is 0.05. Intratidal fields depict the effects of tidally-induced vertical mixing on the salinity fields. The vertical structure of salinity is relatively uniform compared to the weak forcing case. Relatively low (high) salinity appears over the shoals (channel) throughout the tidal cycle. This transverse structure agrees with that described by Huzzey (1988) in the narrower York river during flood tides. It does not agree with her observations during ebb periods thus suggesting that the width of the channel and the magnitude of the tidal forcing are also important in determining the transverse density field. In this case, strongest flood flows occur over the channel, but in contrast to Huzzey (1988) and Huzzey and Brubaker (1988) strongest ebb flows do not develop over the middle of the channel. They appear 1 km to the right (only for 2 hours) and are not high enough to reverse the transverse salinity gradient established during flood periods. Tidal forcing is strong enough, however, to counteract the effects of the baroclinic pressure gradient over the right wall during flood and over the channel during ebb. The lateral flow shows persistent convergence in the middle of the channel at every tidal stage but strongest at end of flood-early ebb. This lateral flow now exhibits a pair of counter-rotating gyres, which resemble the axial convergence pattern described by Nunes and Simpson (1985) in a well-mixed estuary. Mean fields after one tidal cycle show greater flow convergence and weaker longitudinal flows than the weak forcing and unforced cases. This is due to the increased transverse salinity gradients produced by enhanced tidally induced vertical mixing, which is reflected by the presence of vertically uniform low (high) salinity fluid over the shoals (channel). Thus, the position, strength, and pattern of transverse flows and front-generating convergences in estuaries are a function of the estuary width, the tidal forcing, the water column stratification and the bathymetry.

References

Blumberg, A.F., and G.L. Mellor, 1987. A description of a three-dimensional coastal ocean circulation model, in Three Dimensional Coastal Ocean Models. *Coastal Estuarine Sci. Ser.*, vol. 4, N.S. Heaps (ed.), pp. 1-16, *AGU*, Washington, D.C.

Huzzey, L.M., 1988. The lateral density distribution in a partially mixed estuary. *Estuarine, Coastal and Shelf Science,* 9:351-358.

Huzzey, L.M. and J.M. Brubaker. The formation of longitudinal fronts in a coastal plain estuary. *Journal of Geophysical Research,* 93(C2):1329-1334.

Nichols, M., M. Kelly, G. Thompson, and L. Castiglione, 1972. Sequential photography for coastal oceanography. SRAMSOE Rep. 95, VIMS, Gloucester Point.

Nunes, R.A. and J.H. Simpson, 1985. Axial convergence in a well-mixed estuary. *Estuarine, Coastal and Shelf Science,* 20:637-649.

O'Donnell, J., 1993. Surface fronts in estuaries: a review. *Estuaries,* 16(1):12-39.

Simons, T.J., 1974. Verification of numerical models of Lake Ontario, 1, Circulation in spring and early summer. *J. Phys. Oceanogr.*, 4:507-523.

Simons, T.J., 1980. Circulation models of lakes and inland seas. *Can. Bull. Fish. Aquat. Sci.*, 203, 146 pp.

Smolarkiewicz, P.K., 1983. A simple positive definite advection scheme with small implicit diffusion. *Mon. Weather Rev.*, 111:479-486.

Sarabun, C.C., 1980. Structure and formation of Delaware bay fronts. Ph.D. Dissertation. The University of Delaware, Newark, Delaware, 229 p.

Valle-Levinson, A., K.M. Lwiza, and B.D. Connolly., 1994a. Flow lateral structure in the lower Chesapeake Bay. *EOS, Transactions AGU*, Supplement, 75(16).

Valle-Levinson, A., G. Wheless, and J.M. Klinck., 1994b. Baroclinic exchange in the lower Chesapeake Bay. Submitted to *Continental Shelf Research.*

Wong, K.-C., 1994. On the nature of transverse variability in a coastal plain estuary. *J. Geophys. Res.*, 99(C7):14,209-14,222.

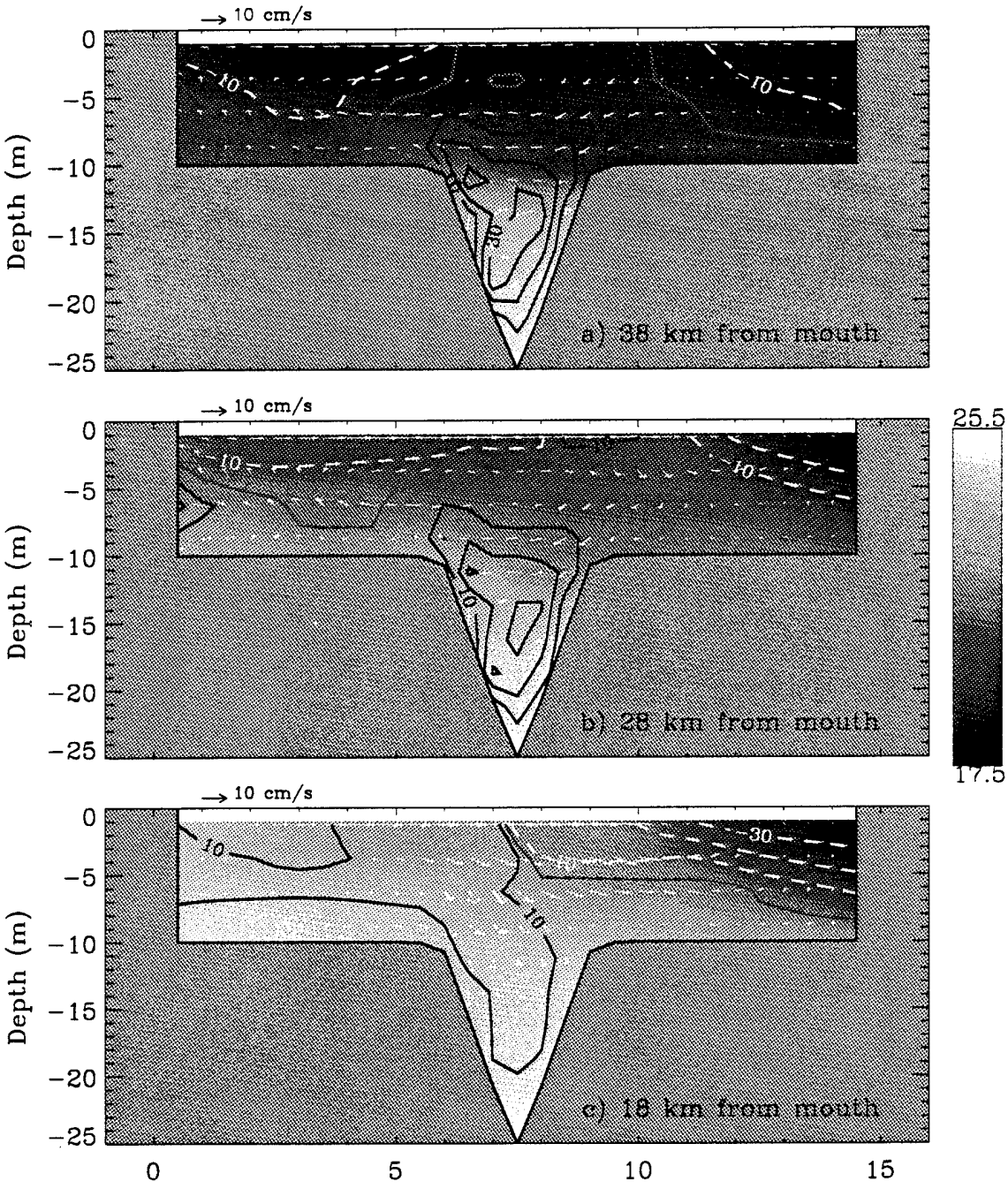

Figure 1. Fields of salinity (shaded), longitudinal flow magnitude (contour), and lateral flow (vectors) for experiment 2 at a) 38 km, b) 28 km, and c) 18 km from mouth of estuary. Positive (negative) contour values indicate longitudinal flows into (out of) the estuary. Contour interval is 10 cm/s. Figure is looking seaward.

CONVERGENCE, DIVERGENCE AND VERTICAL VELOCITY AROUND COASTAL FRONTS

Tetsuo Yanagi
Department of Civil and Ocean Engineering
Ehime University
Matsuyama 790, Japan

Abstract

The field observations were carried out at the south-western part of the Kii Channel by R.V. *Tansei-Maru* of the Ocean Research Institute, University of Tokyo, on 25 and 26 January 1993. The vertical profiles of water temperature, salinity, dissolved oxygen, beam-transmittance (wave length of 492 nm with the light pass of 1 m) and *in vivo* fluorescence were observed with use of the OCTOPUS system at 14 stations during 13:30 through 16:25 on 25 January, 1993. The distance between successive observation stations is about 500 m. The horizontal distributions of water temperature at surface (4 m depth) and velocity at the depth of 5 m, 25 m and 40 m were observed continuously along the observation line from A to B with use of a thermistor and an ADCP (Furuno Electric, CI-30), respectively, from 15:43 to 17:59 on 26 January. Water temperature and velocity were measured at 1 minute intervals, which corresponds to a 150 m interval for R.V. *Tansei-Maru* steaming at about 5 kt.

The thermohaline front between cooler coastal water and warmer offshore water, runs in a northeast to southwest direction in the southern part of the Kii Channel. Due to cooling through the sea surface in winter, water in the southern part of the channel with moderate salinity becomes the heaviest and sinks there. The colder coastal water cannot become heavy enough to sink due to the fresh water inflow from land. Oceanic saline water also cannot become heavy enough to sink because of the mixing with warm Kuroshio water. The thermohaline front exists here from late autumn to early spring with short-term variation of the period of 10 to 15 days.

The horizontal gradients of water temperature and salinity up to 3.5°C km^{-1} and 0.8 psu km^{-1}, respectively, are observed in the surface layer. On the other hand, the density gradient does not exist across the transition zone as seen in water temperature and salinity distributions. A slight vertical density gradient is observed in the surface layer of warm offshore water. Turbidity is high in the colder coastal water and low in the warmer oceanic water. Chl.*a* is high in the surface layer of colder coastal water and low in the surface layer of warmer oceanic water and in the bottom layer. Dissolved oxygen is super-saturated at the transition zone and is high in the colder coastal water. The super-saturation of dissolved oxygen in the surface layer of the transition zone is likely to be the result of photosynthesis by phytoplankton accumulated at the transition zone. It appears that the surface water converges at the transition zone sinks there and diverges like a skirt in the lower layer. Such distribution patterns have been observed at a thermohaline front at the mouth of Tokyo Bay.

The averaged southeastward current is predominant at all observation points. We assume that little alteration in vertical and horizontal frontal structure took place in a general southeastward barotropic flow field during our observation period of 2 hours 16 minutes. Hence we shift the position of the observation points along the A-B line to the position at the beginning of our field observation, that is, at 15:43 on 26 January 1993; each

observation point was moved to upstream direction by the distance calculated by multiplying the vertically averaged velocity at each point with the time difference between 15:43 and the observation time. Temperature values are objectively interpolated at each grid (0.1,N x 0.1,E, that is, 154 m eastward x 185 m northward mesh size) with use of a hyperbolic function from the observed data along the A - B line. The maximum horizontal gradient of water temperature is 3.5°C km^{-1}.

The horizontal distributions of anomaly velocity at each depth from the vertically averaged velocity are also objectively interpolated in the same manner as water temperature. The colder coastal water and warmer oceanic water in the surface layer flow along the frontal zone counterclockwise at the speed of about 15 cm s^{-1}. The surface water around the transition zone nearly stagnates. On the other hand, the colder coastal water and warmer oceanic water at the depth of 40 m flow clockwise along the transition zone. The flow pattern is consistent with what is expected from the conservation law of potential vorticity; i.e., the converging and shrinking water column in the surface layer gets the positive vorticity (counterclockwise rotation) and diverging and expanding water column in the lower layer the negative vorticity (clockwise rotation).

The horizontal distributions of convergence and divergence Q, defined by Eq. (1), at each depth are calculated as.

$$Q = \frac{\partial u}{\partial x} + \partial \frac{\partial v}{\partial y} \tag{1}$$

Here u denotes the eastward velocity and v the northward velocity. The surface convergence with the value of -2.0 x 10^{-4} s^{-1} is seen just at the transition zone of water temperature and the large divergence of 2.0 x 10^{-4} s^{-1} is seen at the depth of 40 m just below the surface convergence zone. The surface divergence zone exists next to the convergence zone in the northern part of this observation area. The observed divergence or convergence is one-order of magnitude larger than those observed in the coastal sea or open ocean except at the frontal region.

The vertical velocity is estimated on the basis of the continuity equation and the Q. It is assumed that the vertical velocity W at the sea surface is 0 and the Q between the surface and 5 m depth is equal to that at the depth of 5 m. It is shown as,

$$Q|_{z=5m} = -Q|_{z=5m} \; x \; 500cm \tag{2}$$

Vertical velocities at the depth of 25 m and 40 m are estimated in the same manner and shown as,

$$W|_{z=25m} = -\frac{1}{2}\left(Q|_{z=5m} + Q|_{z=25m}\right) x \; 2000cm + W|_{z=5m} \tag{3}$$

$$W|_{z=40m} = -\frac{1}{2}\left(Q|_{z=25m} + Q|_{z=40m}\right) x \; 1500cm + W|_{z=25m} \tag{4}$$

From the estimated horizontal distributions of vertical velocity at each depth, the flow structure around the thermohaline front can be delineated. The surface coastal water and the surface oceanic water are advected counterclockwise to the thermohaline front at the speed of about 15 cm s^{-1}. The downward velocity of 0.1 cm s^{-1} is seen at the surface convergence zone. The maximum downward current of 0.25 cm s^{-1} appears at 25 m depth just below the surface convergence zone. Interestingly, an upward current coexists with the downward current at the depth of 25 m. This indicates the existence of strong vertical mixing at a middle layer of the thermohaline front. Below the mid-depth mixing layer, the mixed water diverges clockwise to both sides of the front with the speed of about 15 cm s^{-1}. This estimation of vertical velocity, although just a snapshot at the frontal region, is the first case where the directly observed current data were utilized to reconstruct a three-dimensional flow field around a coastal front. The magnitude of vertical velocity obtained here is about twice as that estimated theoretically for the front driven by the cabbeling effect, and nearly the same as that estimated by diagnostic model calculation using the observed density distribution data at a thermohaline front.

The detailed flow structure around a tidal front in Hiuchi-Nada, Seto Inland Sea is also discussed in the presentation.

MESOSCALE VARIABILITY GENERATED BY AN UNSTABLE BUOYANCY-DRIVEN COASTAL CURRENT WITH APPLICATION TO THE ALASKA COASTAL CURRENT

J. A. Barth
College of Oceanic & Atmospheric Sciences,
Oregon State University,
Corvallis, OR 97331-5503;

Abstract

In order to understand the origin and dynamics of the considerable mesoscale variability observed in association with buoyancy-driven coastal currents, the stability of these jets is studied using both a linear instability analysis based on the full primitive equations applied to a continuously stratified fluid and a three-dimensional, time-dependent, fine-resolution primitive equation model. Understanding eddy and filament formation processes is crucial for quantifying the cross-shelf flux of fresh water and biogeochemical and anthropogenic material. It is demonstrated how "mushroom-shaped" patterns in surface salinity, for example as observed in satellite visible-band imagery of near-surface sediment carried by the freshwater input that drives the Alaska Coastal Current, can be formed through mesoscale activity generated by an unstable coastal current. Through conservation of potential vorticity, significant (up to 20 m d^{-1}) vertical velocities are associated with the meandering coastal current. Thus, mesoscale meander and eddy formation via baroclinic instability represents a likely mechanism for the transport of nutrients into the euphotic zone over the southern Alaskan continental shelf (Royer, personal communication, 1994).

This study focuses on the Alaska Coastal Current (ACC) as a prototype for a buoyancy-driven coastal current. The ACC is driven by fresh-water runoff (local precipitation and glacier melt) all along the coastal region of the northeastern Gulf of Alaska and flows westward as an energetic (speeds in excess of 1 m s^{-1}), highly sheared jet (Royer, 1981; Johnson et al., 1988). The transport and vertical structure of the ACC varies seasonally (strongest and deepest in the autumn during peak runoff) and in response to variations in alongshore wind stress. There exists observational evidence for considerable mesoscale activity associated with the ACC, for example, the identification of multiple meanders and dipole eddies in a visible-band satellite image (Ahlnäs et al., 1987) and time-varying eddy energy in current meter records from over the Alaskan shelf (Johnson et al., 1988). Variations in the structure and intensity of mesoscale activity are apparent between regions of the ACC, making it a natural laboratory for investigating the influence of topography (shelf width and slope; alongshore variations in the coastline and/or bottom topography) on the stability of the freshwater-driven current. Finally, the southern Alaskan shelf and the Gulf of Alaska are biologically rich regions and have been and continue to be impacted by human activity (Royer et al., 1990).

Studies aimed at understanding the processes responsible for mesoscale variability associated with the ACC follow two approaches. First, a linear instability analysis using the full primitive equations applied to a continuously stratified fluid which may overlie sloping bottom topography (Barth, 1994) is applied to observed salinity (density controlling) and velocity sections from the ACC (Johnson et al., 1988). To obtain the basic state, a velocity distribution is selected based on observations and since the mean flow is in geostrophic balance, the thermal wind equation is integrated across the jet to obtain the salinity (density) distribution. The eigenvalue problem yields two distinct modes

of instability. One mode represents a modified form of traditional baroclinic instability whose fastest-growing wave (e-folding in 1.8 days) occurs at 63 km with a slow phase speed (10 cm s^{-1}) in the direction of the mean flow. This mode extends into the water column in roughly the same manner as the basic state current. A second, rapidly growing mode, captured only by using the full primitive equations, is an ageostrophic, frontal instability (Barth, 1994). The frontal mode propagates rapidly (50 cm s^{-1}) and has a growth rate that increases with wavenumber so that at a wavelength of 36 km, the wave e-folds in 1.3 days. The frontal mode is trapped closely to the surface front and is growing by converting energy from the available potential energy of the mean flow via a baroclinic instability mechanism. The frontal instability is not a result of horizontal shear instability as might be expected at these short wavelengths. The growth rate of these small-scale instabilities can be attenuated by horizontal friction and in order to include this mode of variability in a time-dependent numerical model, there must be sufficient resolution to allow the coefficient of horizontal friction (e.g., Laplacian or biharmonic) to be kept small.

The second approach is to model the ACC using a three-dimensional, time-dependent, fine-resolution primitive equation numerical model. The Haidvogel et al. (1991) semi-spectral primitive equation model (SPEM), which employs orthogonal curvilinear coordinates in the horizontal and a bottom-following (sigma) coordinate in the vertical, is used with horizontal resolution of 1-2.5 km in a regional scale domain (several hundred kilometers on a side) and with 15 vertical polynomials over 150 m of water resulting in vertical grid spacings of 2 to 16 m. As mentioned above, this fine-resolution allows both the horizontal friction and vertical diffusion coefficients to be kept small. Convective adjustment to retain gravitational stability is applied, if necessary, at every time step. The system's evolution is studied using both an initial-value problem and a buoyancy forced problem.

In the first series of experiments, the model is initialized with the same salinity (density) and velocity fields observed in the ACC near 149W as used in the linear stability analysis. The fields are assumed to be constant in the alongshore direction, except that a small (10%) white-noise perturbation is added at t=0 to hasten the development of the instability. The model geometry, a 200 x 200 km periodic channel, is chosen to represent the roughly flat-bottomed, straight-coastline shelf of the ACC region near 149°W. The numerical model is stepped forward for 30 days with a 5 minute time step. The vertical diffusion coefficient is $\kappa = 5 \times 10^{-4}$ m^2 s^{-1} and the horizontal biharmonic friction coefficient is $\upsilon_4 = 5 \times 10^7$ m^4 s^{-1}. The time evolution of the surface salinity and velocity fields indicates that for $t < 18$ days, there is some indication of rapid growth of the short-wavelength frontal instability, but by day 18 the nonlinear evolution has favored the long-wavelength ($\lambda = 63$ km) baroclinic instability predicted by the linear instability analysis. At t=18 days, the instability has just begun to form finite-amplitude meanders in the coastal current. Consistent with the conservation of potential vorticity, there is upwelling (downwelling) where the meandering fluid parcels enter regions of anticyclonic (cyclonic) relative vorticity. By day 25, the large-amplitude meanders have broken backwards with respect to the basic state current, trapping cyclonic regions of high-salinity offshore water in their troughs. There still exists a more-or-less continuous meandering coastal jet which has been amplified ($u > 1$ m s^{-1}) next to the coastal wall where it has been squeezed by the meanders. On day 25, anticyclonic eddies of fresh water have begun to break off the wave crests. By day 28, several detached anticyclonic, fresh-water eddies exist offshore of a roughly straight coastal jet inshore. The evolution has elements readily identifiable with mesoscale features (jet meanders; detached cyclonic and anticyclonic eddies) evident in maps of dynamic height from the central ACC region (Johnson et al., 1988).

In the second series of experiments, the same periodic channel geometry is used but the model is initialized in a state of rest with uniform water of density anomaly $\sigma_t = 25$ kg m^{-3} (corresponding to S=31.787 using a linear equation-of-state relating σ_t and S as determined from observations presented in Johnson et al., 1988). Starting at t=0, the model is forced by a line source of freshwater along the coastal wall using a flux value (3×10^{-2} m^2 s^{-1} per m of coastline) in line with values reported from a hydrology model of the south coast of Alaska (Royer, 1981). The model is stepped forward with a 10 minute time step and the vertical diffusion coefficient is $\kappa = 5 \times 10^{-4}$ m^2 s^{-1} and the horizontal Laplacian friction coefficient is $\upsilon = 50$ m^2 s^{-1}. By day 20 of the model simulation, a coastal current is well established with a maximum speed of 0.4 m s^{-1} and a low-salinity wedge next to the coast. The mean flow over the shelf is estuarine in character, modified by earth's rotation. By day 30, meanders form via baroclinic instability and their properties (wavelength ~ 40 km; e-folding time ~ 1 day; phase speed ~ 0.05 m s^{-1}) are in excellent agreement with predictions from a linear instability analysis of the model density and velocity fields on day 25. As the simulation continues, the unstable meanders propagate in the downstream direction and their crests begin to break backward with respect to the mean flow. The backward-breaking waves continue to grow, enclosing saline, cyclonic eddies in their troughs and breaking off fresh, anticyclones from their crests. The offshore anticyclones propagate in the upstream direction and interact with the backward breaking meanders immediately upstream to pull off low salinity water thus forming distinctive "mushroom-shaped" surface patterns. The same pattern in the surface expression of the unstable coastal jet is evident in a satellite visible-band image from the ACC (Ahlnäs et al., 1987). The results here demonstrate that these dipole or "mushroom-like" patterns can result from a finite-amplitude, eddy--meander interaction. This is a different mechanism than the evolution of an "isolated momentum patch" into an eddy dipole and subsequent mushroom-shaped tracer field (Mied et al., 1991).

Finally, although the above results demonstrate that considerable alongshore variability and subsequent cross-shore flux via eddy and filament formation can occur in the absence of coastline variations, results from a buoyancy-forced experiment with a coastal promontory show enhanced mesoscale activity in the vicinity of and downstream of the cape (Figure 1). In this model run (flat-bottom, periodic channel 300 km long and 150 km wide), finite-amplitude meanders growing via baroclinic instability appear sooner near the cape than in the straight-walled regions where the baroclinically unstable waves form a train of uniformly spaced waves. Again, through conservation of potential vorticity, significant vertical velocities (up to 20 m per day) are associated with the baroclinically unstable coastal jet.

References

Ahlnäs, K., T. C. Royer, and T. H. George, 1987. Multiple dipole eddies in the Alaska Coastal Current detected with Landsat thematic mapper data. *J. Geophys. Res.*, 92:13041-13047.

Barth, J.A., 1994. Short-wavelength instabilities on coastal jets and fronts. *J. Geophys. Res.*, 99:16,095-16115.

Haidvogel, D. B., J. L. Wilkin and R. Young, 1991. A semi-spectral primitive equation ocean circulation model using vertical sigma and orthogonal curvilinear horizontal coordinates. *J. Comput. Phys.*, 94:151-185.

Johnson, W. R., T. C. Royer, and J. L. Luick, 1988. On the seasonal variability of the Alaska Coastal Current. *J. Geophys. Res.*, 93:12423-12437.

Mied, R. P., J. C. McWilliams and G. J. Lindemann, 1991. The generation and evolution of mushroom-like vortices. *J. Phys. Oceanogr.*, 21:489-510.

Royer, T. C., 1981. Baroclinic transport in the Gulf of Alaska: Part II. A fresh water driven coastal current. *J. Mar. Res.*, 39:251-266.

Royer, T. C., J. A. Vermersch, T. J. Weingartner, H. J. Niebauer, and R. D. Muench, 1990. Ocean circulation influencing the Exxon Valdez oil spill. *Oceanography,* 3:3-10.

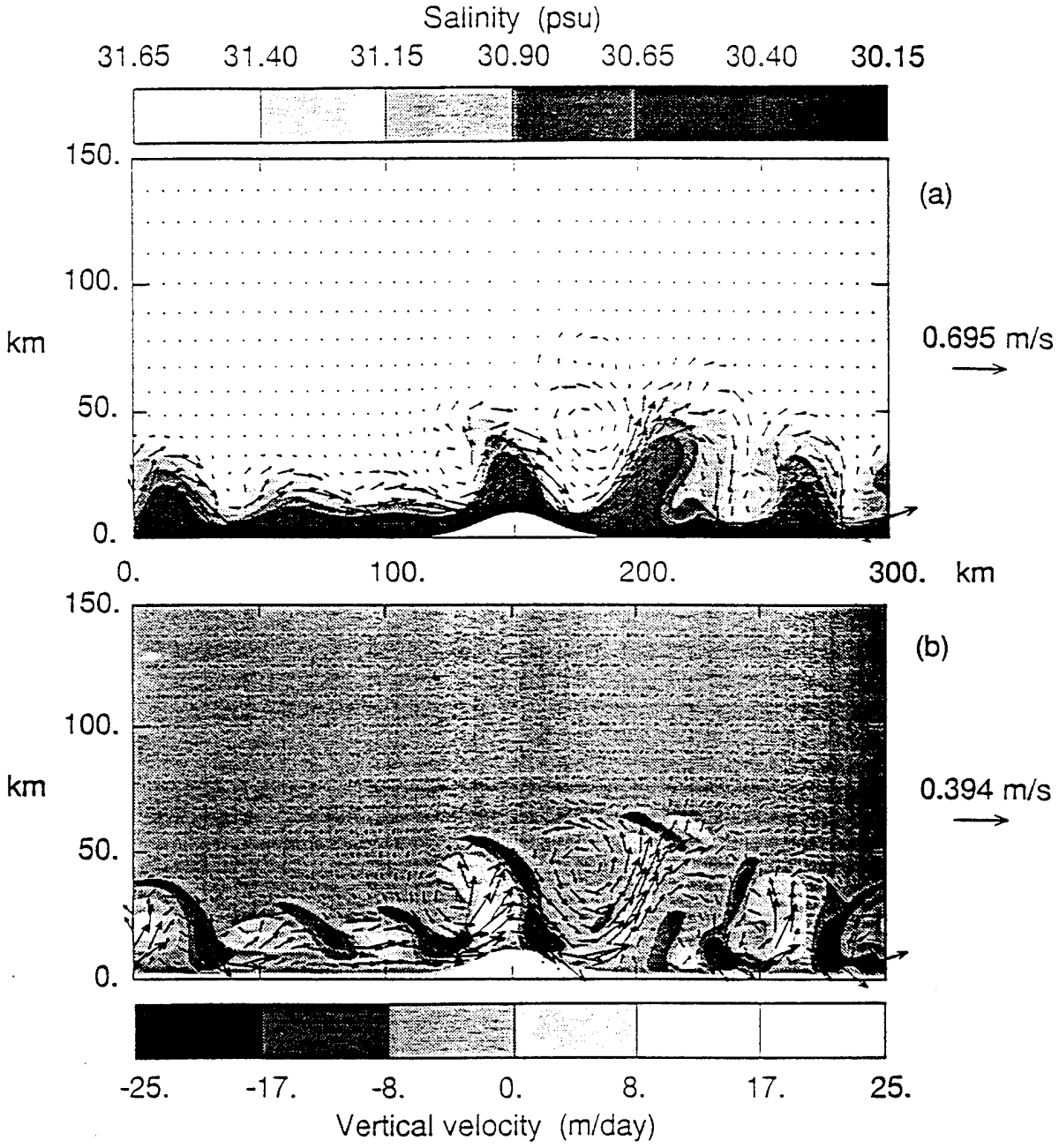

Figure 1. Buoyancy-forced coastal current on day 23 in the presence of a coastal promontory. (a) Surface salinity and velocity. (b) Horizontal velocity vectors and vertical velocities (shaded) at 25 m. Enhanced mesoscale activity is found downstream and near the cape and includes backward-breaking baroclinically unstable waves and cyclonic eddies that pull fresh water off the adjacent wave crests (e.g., near 175 km). Vertical velocities associated with this vigorous mesoscale activity are large, reaching values of 20 m per day.

THE INFLUENCE OF BUOYANCY ON THE DYNAMICS OF WELL-MIXED ESTUARIES

J. Dronkers
Institute for Marine and Atmospheric Research Utrecht
Netherlands Centre for Coastal Research.

Abstract

Topographical effects play a dominant role in large scale mixing and flushing of coastal plain estuaries. Retention zones and lateral shear in the longitudinal tidal velocity field together with transverse secundary currents produce strong dispersion which may account for the average salinity intrusion in the estuary and the flushing of released substances. It is shown that transverse mixing is enhanced by buoyancy effects. This is primarily due to the reduction of vertical momentum exchange, causing a substantial increase of transverse secundary currents generated by topographic effects. Current measurements in the Volkerak estuary reveal transverse secondary currents in the bends of the meandering main channel which are significantly larger than one might expect in homogeneous flow conditions. These measurements are analyzed and the implications for longitudinal dispersion are discussed. Finally the influence of buoyancy on estuarine morphodynamics is considered. Some evidence is presented for an eroding effect on tidal flats.

Introduction

Many large estuarine systems, especially those existing in temperate regions, possess a complex morphological structure which is generated by the interaction of tidal currents with topography. This is the case, in particular, for coastal plain estuaries, which are characterized by a flood delta with numerous shoals and tidal flats, and a branched, winding channel system. Examples are Chesapeake Bay, San Francisco Bay, Gulf of St. Lawrence, Wadden Sea, Baie d'Arcachon, Thames, Severn, Bahia Bianca, Pearl River and many others. These estuaries receive a fresh water input which may be considerable, but which is yet much less than the tidal discharge through the estuarine inlet. The major part of the estuary can be described as "well mixed": the salinity difference over the vertical is on the same order of magnitude or smaller than the salinity difference over the channel width, and there is no sharp interface between fluid layers.

Still buoyancy effects are present and play a significant role in the hydrodynamic behaviour of these estuaries, as will be discussed in this paper. In the sixties it was recognized, in particular owing to the work of Pritchard (1967), that mixing processes prevent the establishment of a stationary salt wedge and maintain a density gradient along the channel axis. This longitudinal density gradient induces a depth dependent pressure gradient which cannot be balanced by landward water level set up and therefore drives a circulation with landward velocity in the lower part of the vertical and seaward velocity in the upper part. This so-called estuarine circulation may possess a 3-dimensional character as a result of density differences between the deeper channel and the shallower channel banks (Fischer 1972, Smith 1980). In estuaries without pronounced topographical structure, such as a flood delta, estuarine circulation is the major secondary current pattern. It strongly influences salt intrusion, dispersion and flushing of contaminants and the residual transport of suspended sediments.

In the well-mixed estuaries described earlier the situation is different. Secondary currents are due not only to horizontal density gradients, but also to the interaction of tidal currents with topography. The larger scale of estuarine circulation with respect to topographical eddies would enhance its role in large scale dispersion and residual transport, but this is counteracted by tidal mixing. As shown by Fischer (1972), if the time scale for vertical mixing is short with respect to the tidal period then the longitudinal dispersion resulting from the vertical estuarine circulation is strongly reduced. This is confirmed by measurements in well mixed estuaries, by decomposition of the residual salt transport into different components (Fischer et al. 1979, Dronkers & Van de Kreeke 1986). Horizontal shear and horizontal circulation due to the interaction of tidal currents with topography are the dominant mechanisms for longitudinal dispersion.

Neglecting buoyancy effects is too strong a simplification, however. The reason is that buoyancy affects the hydrodynamics in still another way, which is the damping of turbulent water motions. This effect has been studied since a long time already. It means that the diffusion of momentum through the water column is reduced. Figure 1 shows the ratio of vertical momentum diffusion coefficients ε and $\varepsilon_{neutral}$ for buoyant and neutral fluids as a function of the local Richardson number

$$Ri = -\frac{g}{\rho}\frac{\partial \rho / \partial z}{(\partial u / \partial z)^2}$$

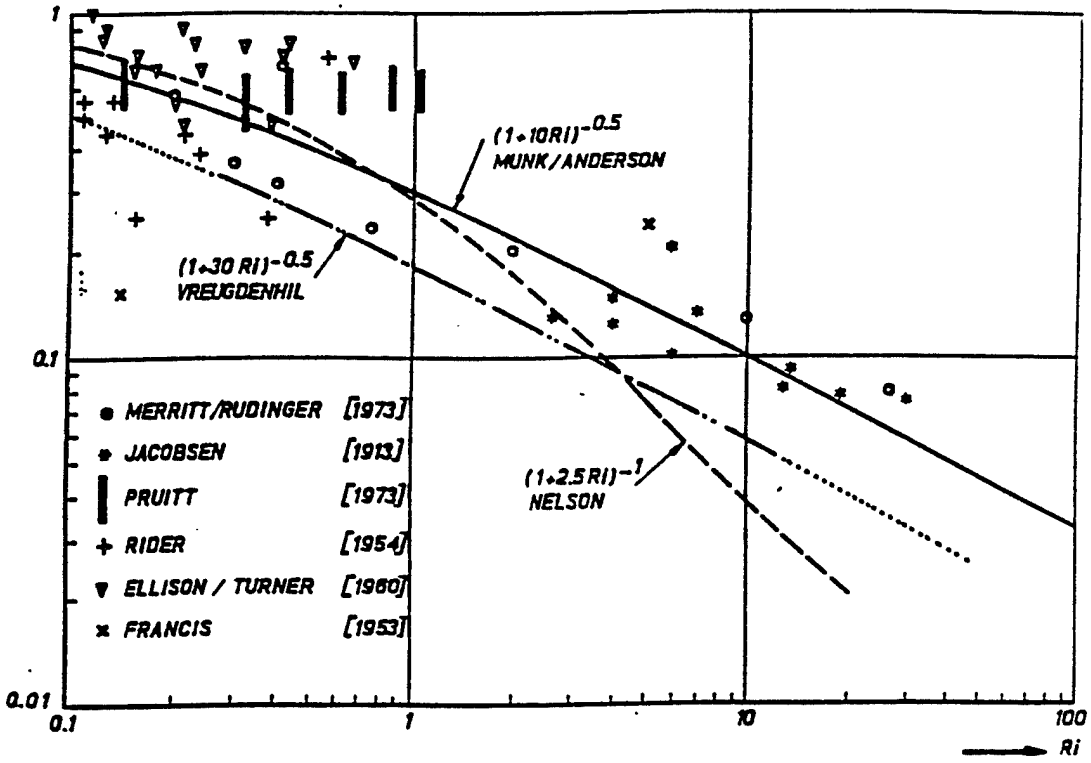

Figure. 1. Damping of the turbulent vertical diffusion of momentum by buoyancy. Ratio of the diffusion coefficients for buoyant and neutral flows obtained from different experiments and models (Karelse et al., 1974).

For well mixed fluids one may expect Ri « 1, as Ri represents the ratio of buoyant potential energy and kinetic energy potentially available for mixing. An increase in the vertical density gradient reduces the vertical momentum diffusion coefficient. From recent experiments (Uittenbogaard, 1994) it appears that the damping of turbulent diffusion with increasing Ri-number is much stronger than indicated by the well known Munk-Anderson relation. As a consequence, there is less cohesion between the water motions in the upper and lower parts of the vertical in a well mixed buoyant flow than in a similar neutral flow. In other words, small scale dissipative fluid motions are suppressed, while large scale organized fluid motions are enhanced.

The foregoing is illustrated by the occurrence of large internal waves in the well mixed Volkerak estuary, during periods of strong tidal currents. Figure 2 shows the time variation of the salinity and the horizontal current velocity at a fixed depth of a vertical in the central part of the estuary, measured during the last stage of ebb flow. The buoyancy frequency $N = \left(-(g/\rho)\partial\rho/\partial z\right)^{1/2}$ ranges between 1/30 and 1/20 s^{-1}, while the velocity shear is in the order of 1/15-1/20 s^{-1}, the corresponding Richardson number being Ri = 0.5-1. The internal wave character follows from the regularity of the signal and the strong phase correlation between salinity and current velocity. The magnitude of the salinity variation corresponds to a vertical water motion of about 1 meter, which is nearly 10% of the water depth. The internal wave phenomenon cannot represent an upstream traveling internal wave as the internal wave speed does not exceed the ebb current velocity. Probably it represents a lateral internal seiche, as the internal wave period (8 minutes) coincides well with the resonance period of a lateral surface oscillation (Dyer 1982).

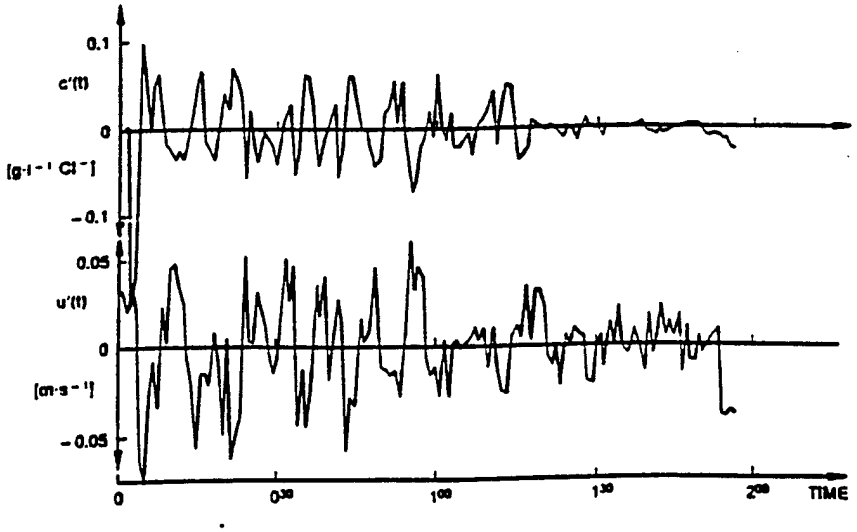

Figure 2. Fluctuations in current velocity (m/s) and salt concentration (g/l Cl-) at a fixed station 7m above the bottom after high-pass filtering. Location: in the middle of the tidal channel halfway between sections 6 and 8. Tidal phase: last three hours of ebb current.

In this paper the secundary currents measured in the Volkerak estuary (part of the Rhine-Meuse-Scheldt delta) will be discussed. Particular attention will be given to secundary currents resulting from the interaction of tidal currents with topography. It will be shown that these secundary currents are strongly enhanced by the influence of buoyancy, due to the damping of turbulent diffusion of momentum and the reduction of internal friction. This phenomenon has been described earlier by Dyer (1989) and by Geyer & Signell (1993) in comparable tidal environments. These secundary currents contribute to the transverse mixing in the estuary. Transverse mixing, in turn, is important for the

longitudinal dispersion by transverse shear. In this indirect way buoyancy affects longitudinal dispersion; in well mixed flood plain estuaries this mechanism can be more important than estuarine circulation. Secundary currents also affect the estuarine morphology, in particular, the shape of channel cross-sections, the channel curvature and the distribution of channels and tidal flats. Some consideration is given to morphological characteristics which could be attributed to the influence of buoyancy effects on secundary currents.

OBSERVATIONS OF NEAR-SURFACE CURRENTS AND HYDROGRAPHY IN THE CONNECTICUT RIVER PLUME WITH THE SCUD ARRAY.

James O'Donnell and David Cohen
Department of Marine Sciences,
The University of Connecticut,
Groton, CT 06340

Abstract

It has been well established that the Connecticut River forms a large plume in the vicinity of its mouth during periods of high river discharge. The plume is bounded on the offshore side by a distinct front at which the water color and turbidity changes rapidly and foam and detritus accumulate. Though there have been many observations of similar fronts throughout the world, the details of the density and velocity structure in the vicinity of the front, and the propagation velocity of the front have not been adequately resolved.

We have constructed a ship mounted array of instruments (SCUD) to measure the near surface currents and density distribution in plumes and fronts. SCUD provides current velocity components at four levels, conductivity and temperature at five levels in the upper 2.5 m which, in combination with ship heading, velocity and position obtained using differential mode GPS, allow the estimation of velocity components with an uncertainty of approximately 0.05 m/s with a horizontal resolution of 5 m.

In the spring of 1994, two pairs of 200 m across-front SCUD transects separated by half an hour were obtained during the late ebb in Long Island Sound. During this period the front advanced to the west at 0.07 (±.005) m/s into an eastward tidal current of 1.4 (±.05) m/s. A salinity jump of 10 PSU over 10 m was observed on crossing the front. In concert, the front-normal velocity component changed by 0.4 (±.05) m/s over 10 m and the front parallel component increased by a similar amount on scale of 20 m. During this period the plume thinned and the average buoyancy decreased. The implication of these observations for theories of river plume fronts will be discussed.

Introduction

There have been numerous reports of near surface fronts in the coastal ocean. They are often made clearly visible from ships by discontinuities in water color and turbidity and a line of foam and detritus. Examples are described in O'Donnell (1993). Systematic observation of the hydrography and flow field in the vicinity of fronts is difficult because the structures are transient, shallow and in motion. Garvine and Monk (1974) made the first observations of the density field in the vicinity of the front of the Connecticut River plume. They found the front associated with the foam line to be less than 100 m in width and to separate waters differing in salinity by 10 PSU. They estimated the order of magnitude of the frontal propagation velocity to be 1 m/s and the particle velocity relative to the front to be 10 cm/s. No commercially available systems are capable of observing the structure of these strongly sheared near surface flows though Simpson and Turrell (1986) built a rigid array of current meters similar in concept to that described here, and several towed profilers have been developed.

The Surface Current and Density (SCUD) Array

To observe the structure and velocity fields at the front of the Connecticut River plume, we have constructed an array of instruments that are mounted in front of the bow of the RV *Libinia*, a small (9 m) workboat. A schematic of the arrangement of the instruments is shown in Figure 1a. The vertical mast is 6 m of schedule-80 Aluminum pipe of approximately 8 cm inner diameter. This mast fits into a cylindrical sleeve of the same material which is welded to a crosspiece. The depth of the mast in the water can be adjusted by moving it through the sleeve. The crosspiece slots into an H-shaped deck frame of 8 cm Aluminum 90° angle stock which is bolted to the deck of the RV *Libinia*. We estimate that the structure would withstand the drag associated with a 5 m/s relative flow in calm water, but since this would exceed the dynamic range, and the mechanical strength, of the current meters, we restrict the ship speed to between 1 and 2 m/s. A sea trial in 50 cm waves demonstrated the mount to be an effective instrument platform in calm conditions.

Four Marsh-McBirney model 511 two axis electromagnetic current meters were mounted on the array approximately 50 cm in front of the mast as shown in Figure 1a. The current meters are powered individually by battery packs and provide analog displays of the current speed past the sensor. The time constants of the sensors are adjustable and the fastest, 1 second, has been employed. The dynamic range is also optional and ±2 m/s is used since the ship motion contributes to the flow past the sensor. The signal voltage of the instruments are passed to a data acquisition system, described in detail below, where it is digitized, converted to m/s and stored on magnetic disk. The operation of the current meters in this configuration has been tested in the field and the performance found to be acceptable.

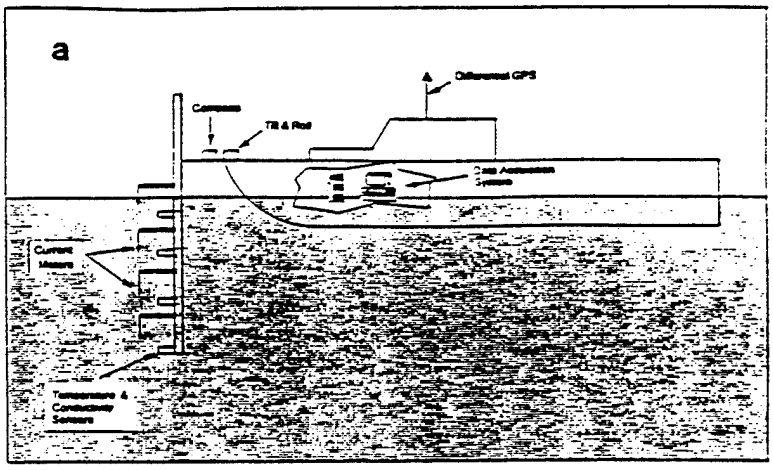

Figure 1a. Schematic of the SCUD array.

Conductivity is measured with Falmouth Scientific C-T sensors: an induction conductivity sensor and a highly stable thermistor in a molded package and a circuit board that controls the instruments. The circuit boards are mounted in 10 cm diameter PVC pipe junctions and attached to the array mast with aluminum clamps in an orientation that maximizes the flow through the conductivity sensor. The nominal accuracy of the C-T sensors are 0.025 Siemens/m and 0.05 °C. The time constant of the conductivity sensor is short, 0.1 s, but the thermal inertia of the coil and molding make the temperature time constant 100 s. Since this mismatch is too large for frontal studies, we added a fast

response (2 s time constant) matched thermistor pair manufactured by Betatherm to our package. The thermistors are incorporated in the simple voltage divider so that the output to input voltage ratio, E_o/E_I, is proportional to temperature. A stable voltage regulator (LM-317L) is used to ensure E_I=1.25 V which keeps power dissipation in an acceptable range. Both E_I and E_0 are connected to a multiplexer (HC4051) so that the stability of the regulator can be monitored without additional connectors and cables. The accuracy of the temperature measurements are determined by the precision of the analog-digital conversion of the voltage E_o as will be discussed below.

To obtain the spatial and temporal structure of the flow velocity relative to the front from the velocity measured by the current meters, the ship position, speed, course and heading must be measured and recorded. In much of the north-east, the Coast Guard operates VHF transmitters that broadcast corrections to GPS positions to mitigate the effect of the errors introduced by "selective availability". SCUD is equipped with a Magnavox MX200 GPS receiver and a MX50-R differential correction receiver. Tests with this system have shown that 1 minute averages of positions at 0.5 Hz provides positions with an uncertainty that varies between 2.5 and 8.0 m and is dependent on the geometric configuration of the satellites which is indicated by the HDOP parameter. The ship heading is obtained from a KVH C100 flux-gate compass and forwarded to the MX200 though the NMEA port so that it is logged on microcomputer together with the other parameters. Since the pitch and roll motion must also be monitored, a Spectron dual axis tilt sensor is mounted on the SCUD array. This instrument provides two analog voltages proportional to the tilt angles with a time constant of 1 s and an accuracy of about 5 degrees.

With four dual axis current meters, five conductivity and temperature sensors, and a dual axis tilt and roll sensor, there are a total of twenty two analog channels to be recorded in addition to the serial data from the navigation system. The FSI circuit board and the thermistor circuit are controlled by two logic lines so that the a single cable provides both temperature and conductivity measurements from the FSI board, and a second line the input and output voltage from the thermistor circuit. The control and logging system is based on the popular Kiethley-Metrabyte DAS-1600G2 analog-digital converter board with an EXP16 expansion card in a 486SX microcomputer. These provide two software programmable voltage sources that are used to control the instruments, and 31 analog inputs with 12 bit A-D conversion that can sample at 50 kHz. The range of the A-D conversion and the gain of the input amplifiers are software selectable. The control and acquisition program is written in QuickBasic and the data rate is controlled by the two second cycle of the delivery of positions from the GPS system to the serial port of the PC. Once the navigation data is received, all the voltages that provide temperature are sampled five times, averaged and logged. The conductivity voltages are then switched to the A-D input. The current meter outputs are then logged which takes enough time to allow the amplifiers to equilibrate and the conductivities are then sampled and logged in the same manner as the temperatures.

With sampling at 0.5 Hz and a cruising speed of 1 m/s, this system can resolve horizontal spatial scales of 2 m. The vertical separation of the current meters and conductivity-temperature sensors is ~0.5 m with the top sensor just below the water level. The accuracy of the conductivity and temperature sensors provides density estimates with an uncertainty of 0.05 PPT. Though this not equivalent to standards provided by commercial CTD systems, it is certainly adequate to advance the observation of the structure of plume fronts. The navigation system can provide over-ground ship velocity estimates on a 30 s average with an uncertainty of 0.05 m/s, which is about twice that of the current meters and adequate to resolve the convergence at the front.

In addition to the observation of the motion field in the vicinity of the front, the translational velocity of the front is required to relate the observations to theoretical predictions. In the observations reported here, the SCUD measurements are complemented by a sequence of front position observations that were acquired by a small, fast boat (the RV *Caprella*) equipped with differential GPS navigation and an underway surface conductivity and temperature observation system.

Observations of the Front of the Connecticut River Plume

During the latter half of the ebb tide on April 5, 1994, the front of the Connecticut River plume was observed by the RV *Caprella* at the positions shown in Figure 1b. The x and + symbols indicate locations at which the RV *Caprella* crossed the front while surveying the surface salinity and temperature. The solid lines show the track of the RV *Caprella* as it cruised rapidly (5 m/s) along the front without instruments in the water. Since the surveys required approximately 45 minutes, whereas tracing the location of the front could be accomplished in 10 minutes, the latter are much closer to being synoptic. The separation of the front positions can be used to calculate the frontal propagation speed in the direction locally normal to the front. Near the breakwaters the front speed is 4.8 cm/s to the west but, further from shore, it veers to the southwest and increases to 19.1 cm/s.

The four straight lines that cross the front in Figure 1b show tracks along which the SCUD array made observations. A cross-section of density (sigma-T) is shown in Figure 1c. The position of the foam line is coincident with the transition from the cold, salty water of Long Island Sound to the warmer, fresher, stratified water of the plume. The largest horizontal gradients appear at the front and are small elsewhere. The transition from LIS to plume water appears to take place over less than 5 m, a smaller scale than suggested by Garvine and Monk (1974). The salinity and temperature sections suggest that there is considerable sinking of fluid at the front; the water overshoots the equilibrium level and rises again behind the front.

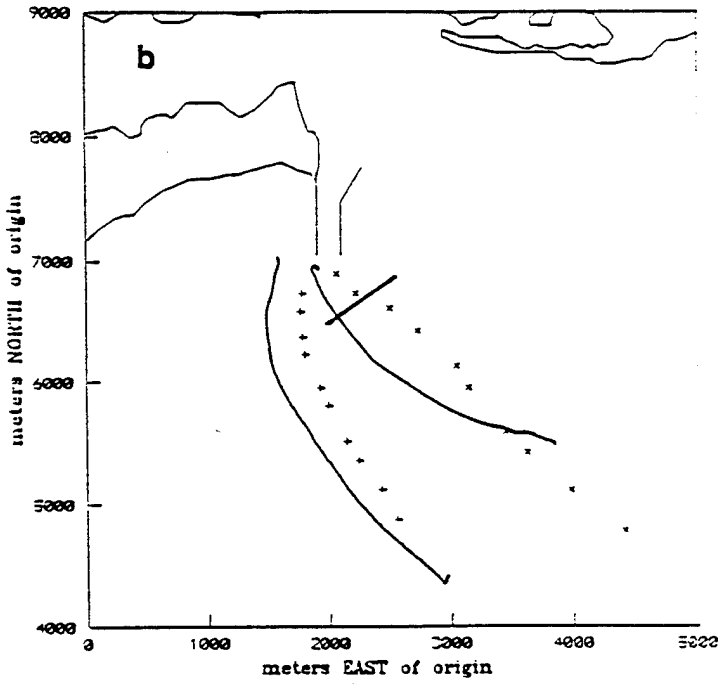

Figure 1b. A sequence of front positions at the mouth of the Connecticut River.

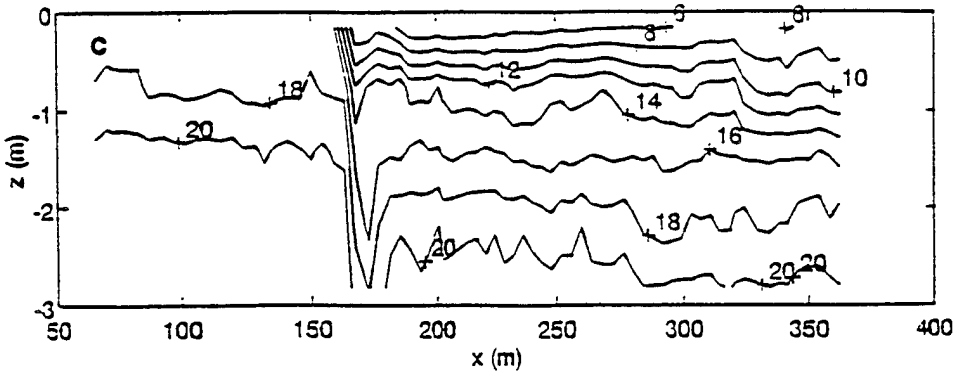

Figure 1c. Across front vertical cross-sections of density.

A vertical cross-section of the along track (which is approximately the front normal) component of velocity in the along track direction is shown in Figure 1d with the position of the surface foam line the zero of the horizontal coordinate. The structure of the flow is complex but some expected features are revealed. In particular, the strong convergence at the front line (the source of the foam accumulation) is evident. An abrupt decrease (increase in negative) in the along front component on the plume side of the front is also observed though not shown here. Comparison of the observations to theories is more easily accomplished in the frame of reference that moves with, and is locally normal and parallel to, the front. In this coordinates the flow is clearly towards the front throughout the plume at the two upper levels (0.6m and 1.3m). A region of divergence appears 50 m to the right of the front which is associated with strong across-front shear in the along front velocity. Though this feature has not been observed previously, it is consistent with the predictions of the models of Garvine (1982) and O'Donnell (1990).

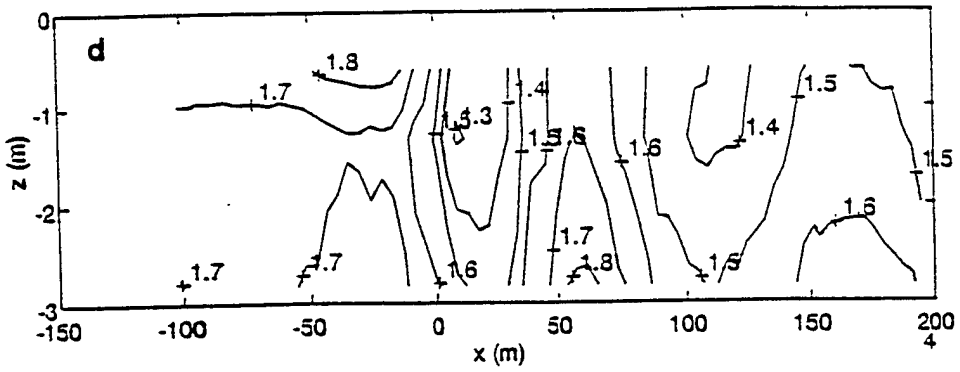

Figure 1d. Across front velocity component.

Conclusions and Discussion

The near surface hydrographic and current fields in the vicinity of a river plume front can be resolved by the SCUD array and, in combination with another ship to observe the front location and motion, can provide a valuable description of the small scale structure. The preliminary observations described here show that the hydrographic structure of the plume front has much in common with that reported by Garvine and Monk (1974). The

horizontal gradients are much larger than they reported however and the horizontal length scale is less than 5m. The velocity field shows strong convergence at the front of order .05 s^{-1}. Since the front appear locally straight, this must result in rapid downwelling with a velocity of order 10cm/s at 2 m below the surface. Future work will address the effect of the angle between the crossflow and the front line on the structure and dynamics of the front.

References

Garvine, R.W. and J.D. Monk, 1974. Frontal structure of a river plume. *J. Geophys. Res.*, 79:2251-2259.

Garvine, R.W., 1982. A steady state model of buoyant surface plumes in coastal waters. *Tellus*, 34:293-306.

O'Donnell, J., 1988. A numerical technique to incorporate frontal boundaries in layer models of ocean dynamics. *J. Phys. Oceanography*, 18:1584-1600.

O'Donnell, J., 1993. Surface fronts in estuaries. *Estuaries*, 16:12-39.

Simpson, J. H. and W.R. Turrell, 1986. Convergent fronts in the circulation of tidal estuaries. 139-152. In D.D. Wolfe (ed.), *Estuarine Variability*, Academic Press, Orlando, Florida.

SHEAR DISPERSION IN A WIND AND DENSITY DRIVEN PLUME

Andre W. Visser
IMAU, Utrecht University
Utrecht, the Netherlands

Abstract

The lateral spreading induced by shear dispersion for a river plume is examined. In the absence of wind, the self-induced shear associated with the cross plume density structure promotes a lateral spreading which may be characterized by a horizontal diffusivity proportional to the square of the cross plume density gradient. Examining the time scales for this process indicates that the width of the plume goes as $t^{1/7}$ where t is the "age" of the plume water. With wind it appears that under normal circumstances for the Rhine plume, wind induced circulation will dominate shear dispersion and suggest a much more rapid ($t^{1/2}$) spreading rate. However, there are two effects which tend to moderate the wind efficiency in inducing lateral spreading, namely (a) convective overturn since wind induced circulation may promote unstable water column conditions, and (b) wind mixing which increases vertical mixing rates thus reducing effective horizontal diffusivity.

Introduction

The dynamics of ROFI's; regions of freshwater influence, have received considerable attention over recent years. A question of some interest to these studies is how large do these regions get. It remains a remarkable fact that river plumes remain as distinct as they do. Despite the highly energetic and turbulent environments in which they are often found, river plumes maintain their integrity, remain coastally trapped, and contribute to local dynamic conditions over long distances from the river mouth.

One feature of ROFI's which is noteworthy here is the preponderance of vertically sheared horizontal flow. These appear not only in the low frequency currents, but also at tidal frequencies. This observation suggests that shear dispersion, the combined effects of vertical mixing with horizontal shears may prove to be a dominant factor contributing to the lateral dispersion (and hence dimensions) of a ROFI.

The principal of shear dispersion (*cf.* Bowden 1965) proceeds on the premise that the processes controlling the advection / diffusion of density (indeed any passive tracer) proceed o two distinct time scales. In particular, there is a fast time scale associated with vertical mixing given by (H^2/K_z) where H is the water column depth and K_z is the vertical diffusivity. A typical value for the Rhine ROFI along the Netherlands coast is of the order of hours to a few days (Van Alphen *et al.* 1987). Compared to this is a slower time scale over which period the large scale horizontal distribution varies. Following the arguments of Bowden 1965 and others, the effective horizontal diffusion coefficient for a plume dominated by a gradient in the y (cross shore) direction, may be written as:

$$K_H^* = -\frac{H^2}{K_z}\int_{-1}^{0}\left\{\int_z^0 v'dz\right\}^2 dz \qquad (1)$$

where $v'(z)$ is the vertically dependent component of the cross shore velocity.

Assuming that vertical mixing (both diffusivity K_z and eddy viscosity N_z) are vertically uniform, it is relatively straight forward to determine the vertical velocity structure (u', v') for a density plume under the influence of surface wind stress, $\tau(0) = (\tau_x, \tau_y)$, and linear bottom stress parameterized as $\tau(-1) = k\mathbf{u}(-1)$. Substituting the form of this solution into Eq(1) gives:

$$K_H^* = \frac{2H^2}{fK_zN_z}\left\{\left[\tau_x - \frac{gN_z}{f\rho_0}\frac{\partial\overline{\rho}}{\partial y}\right]^2 A_1 + \tau_y\left[\tau_x - \frac{gN_z}{f\rho_0}\frac{\partial\overline{\rho}}{\partial y}\right]A_2 + \left[\tau_y\right]^2 A_3\right\} \qquad (2)$$

where $A_{1,2,3}$ functions dependent on the Ekman number E, and $R = k/(fH)$ the ratio of the bottom spin down frequency, and the Coriolis frequency. This is similar in form as the expression found by Stommel and Leetma 1972 in investigating large scale circulation in continental shelf seas. A few points might be noted directly from Eq(2).

- Effective horizontal diffusivity becomes increasingly significant for weak vertical mixing.
- In the absence of wind, the density flux is proportional to the cube of the density gradient.
- For the Rhine ROFI, the effect of wind becomes comparable to that of density driven circulation for wind speeds in excess of 10 m/s, i.e. a moderately strong but not unusual wind for this area.

Lateral Spreading Rate

Suppose we have a low density plume which is coastally trapped, with lateral (off shore) dimension Y, and with a uniform cross shore density gradient given by $\overline{\rho}(y) = \rho_c + y\{\rho_o - \rho_c\}/Y$ where ρ_c is the density at the coast and ρ_o is the density of ocean (North sea) water. This density gradient will drive an "estuarine" circulation cell associated with density plumes; *i.e.* with surface water flowing seaward and bottom water flowing landward. This sheared flow interacting with rapid vertical mixing produces a landward flux of sea water. In the absence of wind stress, according to Eq (10), this flux is proportional to the cube of the density gradient, *i.e.*

$$\overline{F}_y \propto \frac{(\rho_o - \rho_c)^3}{Y^3} \qquad (3)$$

Assuming there are no low density sources and sinks along the coast, and moving along shore with the mean velocity $\overline{u} \propto \overline{\rho}_y$, then total density deficit within the moving cross section must be constant. That is

$$(\rho_o + \rho_c(t)) \cdot Y(t) = \text{constant} = R$$

Thus a coast ward flux of dense water, equivalent to a seaward propagation of the outer plume boundary may be written as:

$$\overline{F}_y = \rho_o \frac{dY}{dt} \propto \frac{R^3}{Y^6} \text{ that is } \frac{d}{dt}\left(Y^7\right) = \text{constant or } \quad Y(t) \propto t^{1/7}$$

This is a very slow spreading rate, at least quantitatively in agreement with observations.

Convective Overturn

With a strong south west wind blowing along the Netherlands coast, the surface Ekman transport has an onshore component and an off shore counter current at depth. This shear under commonly found conditions will drive salty North sea water over fresher Rhine water. Clearly this will produce an unstable situation which is susceptible to convective overturn. Effectively this increases the rate of vertical exchange. The criterion when this occurs may be written as:

$$\tau_x = \frac{\rho_{\text{air}}}{\rho_0} C_D |\mathbf{w}| w_x > \frac{g N_z}{f \rho_0} \frac{\partial \overline{\rho}}{\partial y}$$

i.e. when a destablizing shear associated with a positive wind stress overwhelms the stabilizing shear associated with the density adjustment. Relatively simple considerations of time scales allows us to write the increase in vertical exchange due to convective overturn as:

$$K_z^* = K_z + K_z^{\text{conv}} \approx K_z + \left\{ \frac{H^3}{K_z} \frac{g}{\overline{\rho}} \frac{\partial \overline{\rho}}{\partial y} \frac{2\tau_x}{f} \right\}^{1/2}$$

Wind Mixing

A wind blowing over the surface of the ocean imparts turbulent kinetic energy a percentage of which may promote vertical exchange. The rate at which a wind with velocity $\mathbf{w} = (w_x, w_y)$ does work on the water column is

$$K_z^{\text{wind}} \propto \frac{\partial \Gamma}{\partial t} = \tau \bullet \mathbf{w} = \frac{\rho_{\text{air}}}{\rho_0} C_D |\mathbf{w}| \mathbf{w} \bullet \mathbf{w}$$

That is, if we consider only an along shore (x) directed wind, then $K_z^{\text{wind}} \propto w_x^3$. A similar expression may be written for vertical eddy viscosity, *i.e.* $N_z^{\text{wind}} \propto w_x^3$, or as is often used, define the Prandlt Number $P_t = K_z / N_z$. Effective vertical diffusion coefficients taking wind mixing into account may therefore be written as:

$$K_z^* = K_z \left\{ 1 + \gamma_1 w_x^3 \right\} \text{ and } N_z^* = K_z \left\{ 1 + \gamma_1 w_x^3 \right\} / P_t$$

Substituting these expressions into the effective horizontal diffusivity (Eq. 2), gives a wind mixing / advection contribution of the form:

$$K_H^* = \frac{2H^2}{f K_z^2} \frac{\rho_a}{\rho_0} C_D P_t A_3 \left\{ \frac{|w_x| w_x}{1 + \gamma_1 |w_x|^3} - \xi \right\}^2$$

In other words, there is an optimum value of the wind speed for which lateral dispersion of salt (or any tracer). Below this wind speed, (reversible) advection dominates, and above this wind speed, vigorous vertical mixing tends to arrest lateral dispersion.

References

Bowden, K.F., 1965. Horizontal mixing in the sea due to a shearing current. *J. Fluid Mech.*, 21:83-95.

Stommel, H. and A. Leetmaa, 1972. Circulation on the continental shelf. *Proc. Nat. Acad. Sci. USA*, 69:3380-3384.

EFFECTS OF CHANNEL GEOMETRY ON GRAVITATIONAL CIRCULATION IN PARTIALLY-MIXED ESTUARIES

Carl T. Friedrichs and John M. Hamrick
College of William and Mary, School of Marine Science
Virginia Institute of Marine Science
Gloucester Point, VA 23062-1346

Abstract

The most widely quoted analytic solution for gravitational estuarine circulation (Hansen and Rattray, 1965) assumes the estuary channel to be prismatic with a rectangular cross-section. To motivate their discussion, Hansen and Rattray (1965) cite observations of tidally-averaged salinity and velocity along and within the Lower Delaware and James Rivers. Yet these two estuaries exhibit strong across-channel variation in depth, strong along-channel variation in width, and moderate along-channel variation in depth. The purpose of the present discussion is to investigate the impact of such variations in depth and width on the classical description of estuarine circulation.

Transverse and vertical circulation can be considered together in a straightforward manner if one assumes the tidally-averaged momentum balance to be between the along-channel pressure gradient and the vertical shear stress associated with gravitational circulation. (For consistency, contributions to the balance by acceleration and transverse shear stress should be no larger than δ^2, where δ is the fresh water velocity relative to the magnitude of the gravitational circulation.) By decomposing the pressure gradient into barotropic and baroclinic components, and differentiating the momentum balance with respect to z, the momentum balance can then be re-expressed as

$$g\,a\frac{\partial S}{\partial x} = A_z\frac{\partial^3 u}{\partial z^3}, \qquad (1)$$

where g is the acceleration of gravity, S is salinity, a is the coefficient of saline expansion, A_z is vertical turbulent viscosity, u is along-channel velocity, and x and z are positive seaward and downward, respectively.

If one then assumes that $\partial S/\partial x$ is independent of z (to $O(\delta^2)$), (1) can be integrated easily with respect to z, such that $u = 0$ at $z = h$, $\partial u/\partial z = 0$ at $z = 0$, and $\iint u\,dy\,dz = Q_f$, where Q_f is fresh-water discharge. Solutions to (1) for triangular cross-sections have been derived previously assuming either constant A_z (Hamrick, 1979; Wong 1994) or A_z proportional to h (Fischer, 1972). Here we consider the trapezoidal cross-section illustrated in Figure 1 (assuming A_z independent of y and z), which was also considered by Hamrick (1979). For $y/B \le \sigma$, (1) then integrates to

$$u = u_g\left\{10(\tilde{z}^3 - \tilde{y}^3) - 9\left(\frac{5-4\sigma}{4-3\sigma}\right)(\tilde{z}^2 - \tilde{y}^2)\right\} - 3u_f\left(\frac{2-\sigma}{4-3\sigma}\right)(\tilde{z}^2 - \tilde{y}^2), \qquad (2)$$

where $\tilde{z} = z/H$, $\tilde{y} = y/B$, $u_g = (agH^3/60A_z)(\partial S/\partial x)$, and u_f is given by averaging Q_f over the cross-section. For $\tilde{y} > \sigma$, u is obtained from (2) simply by letting $\tilde{y} = \sigma$.

For $\sigma = 0$ and $\tilde{y} = 1$, (2) reduces to the classical solution of Hansen and Rattray (1965); for $\sigma = 1$ and $u_f = 0$, (2) reduces to solution published recently by Wong (1994). Figures 2 and 3 compare results calculated from (2) to observations of velocity obtained at a nearly triangular cross-section of the James River (Kuo et al., 1990). The solution reproduces the observed tilting of the zero velocity contour up toward the northeastern side of estuary, an effect which had previously been attributed largely to geostrophy.

In solving for the salinity distribution, we assume cross-sectional variation in salinity to be $O(\delta)$ relative to along-channel variation and consider longitudinal salt transport to be due only to the density driven circulation. Then the only terms which remain in the $O(\delta)$ salt balance for (a) laterally-mixed or (b) vertically-mixed estuaries are

$$b\,\bar{u}\frac{\partial S}{\partial x} = \frac{\partial}{\partial z}\left\{b\,K_z\frac{\partial S}{\partial z}\right\}, \quad \text{or} \quad h\,\bar{u}\frac{\partial S}{\partial x} = \frac{\partial}{\partial y}\left\{h\,K_y\frac{\partial S}{\partial y}\right\}, \tag{3a,b}$$

where $\bar{u}$ is either (a) laterally- or (b) vertically-averaged velocity. Boundary conditions are $\partial S/\partial z = 0$ at $z = 0$ and $z = h$ for (a), and $\partial S/\partial y = 0$ at $y = 0$ and $y = b$ for (b).

Since the zero-order solution for salinity is independent of y and z, the right-hand-side of (3a) and (3b) vanish at lowest order, and the left-hand side must be at most $O(\delta)$. The major advantage of this scaling is that the $O(\delta)$ solution to (3) need only consider the first term on the r.h.s. of (2). If an alternative scaling is chosen which includes u_f in (3), then one must prescribe the form of K_x in order to complete the salt balance. For example, Hansen and Rattray (1965) required $\partial K_x/\partial x = u_f$, an assumption which is not physically-based and which inhibits insight into the relationship between freshwater discharge and the length of the salt water intrusion.

Application of boundary conditions to (3) is greatly simplified if one assumes $\sigma = 1$ or $\sigma = 0$ in the laterally- or vertically-mixed case, respectively. Then solutions to (3) become (with K_y and K_z constant in y and z)

$$\text{laterally-mixed:} \quad S = \overline{S} + \frac{u_g H^2}{48\,K_z}\frac{d\overline{S}}{dx}\left(24\tilde{z}^5 - 45\tilde{z}^4 + 30\tilde{z}^2 - 5\right), \tag{4a}$$

$$\text{vertically-mixed:} \quad S = \overline{S} + \frac{u_g B^2}{40\,K_y}\frac{d\overline{S}}{dx}\left(-12\tilde{y}^5 + 15\tilde{y}^4 - 1\right), \tag{4b}$$

where $\overline{S}$ is cross-sectionally averaged salinity.

The solution for $\overline{S}$ is obtained by (i) inserting (2) and (4) into the cross-sectionally integrated salt balance, $\iint u\,S\,dy\,dz = 0$, and (ii) integrating in x. The only terms which contribute to $\iint u\,S\,dy\,dz$ at $O(\delta)$ are the second term in (2) times the first term in (4) and the first term in (2) times the second term in (4). Integration over the cross-section then gives

$$\text{laterally-mixed:} \quad u_f\,\overline{S} = \frac{95}{2016}\frac{H^2\,u_g^2}{K_z}\frac{d\overline{S}}{dx} = \text{"}K_x\text{"}\,\frac{d\overline{S}}{dx}, \tag{5a}$$

$$\text{vertically-mixed:} \quad u_f\,\overline{S} = \frac{1}{80}\frac{B^2\,u_g^2}{K_y}\frac{d\overline{S}}{dx} = \text{"}K_x\text{"}\,\frac{d\overline{S}}{dx}, \tag{5b}$$

where "K_x" is the effective 1-D longitudinal dispersion coefficient due entirely to the gravitational circulation. Since u_g is proportional to $d\bar{S}/dx$, (5) also indicates that $d\bar{S}/dx \sim u_f^{1/3}$, i.e., the density gradient is relatively insensitive to the freshwater discharge.

If we let $S = 0$ at $x = 0$, and assume Q_f to be constant in x, then (5) integrates to

laterally-mixed:
$$\bar{S} = \frac{150\, Q_f^{1/2}}{a\, g} \left\{ \int_0^x \frac{A_z^{2/3} K_z^{1/3}}{B^{1/3} H^3}\, dx \right\}^{3/2}, \qquad (6a)$$

vertically-mixed:
$$\bar{S} = \frac{207\, Q_f^{1/2}}{a\, g} \left\{ \int_0^x \frac{A_z^{2/3} K_y^{1/3}}{B\, H^{7/3}}\, dx \right\}^{3/2}, \qquad (6b)$$

where we have reinserted the definitions for u_f and u_g into (6). Equation (6) illustrates the strong sensitivity of the longitudinal salinity distribution to along-channel variations in width and depth, as well as to longitudinal variation in vertical and lateral mixing. In our presentation we will further examine the implications of (6) with regards to observed salinity distributions along real estuaries such as the Chesapeake Bay tributaries and the Delaware Bay.

References

Fischer, H. B., 1972. Mass transport mechanisms in partially stratified estuaries. *Journal of Fluid Mechanics,* 53:671-687.

Hamrick, J. M., 1979. Salinity intrusion and gravitational circulation in partially stratified estuaries. Ph.D., University of California, Berkeley, 451 pp.

Hansen, D. V., and M. Rattray, 1965. Gravitational circulation in straits and estuaries. *Journal of Marine Research,* 23:104-122.

Kuo, A. Y., J. M. Hamrick and G. M. Sisson, 1990. Persistence of residual currents in the James River Estuary and its implications to mass transport. In: R. T. Cheng (ed.), *Residual Currents and Long-term Transport. Coastal and Estuarine Studies,* Vol. 38, Springer-Verlag, New York, p. 389-401.

Wong, K.-C., 1994. On the nature of transverse variability in a coastal plain estuary. *Journal of Geophysical Research,* 99:14,209-14,222.

TIDAL PUMPING OF SALT IN A MODERATELY STRATIFIED ESTUARY

Rocky Geyer and Heidi Nepf
Woods Hole Oceanographic Inst.
Woods Hole, MA 02543

Abstract

Observations during different discharge conditions in the Hudson River estuary indicate large variations in the magnitude of tidal pumping, i.e., correlation between tidal variations in salinity and velocity. Tidal pumping is strongest during periods of high river discharge and strong stratification, providing more than 50% of the upstream salt flux. During low and moderate discharge conditions, tidal pumping of salt is small or even counter-gradient, i.e., seaward. The tidal pumping during high discharge conditions is caused by the propagation of a gravity current during the flood, which results in an elevated pycnocline and higher salinities during the flood than the ebb, during which the salinity intrusion collapses due do divergence of the near-bottom flow. The gravity current appears to result from frontogenesis during the latter portion of the ebb. This process is inhibited by more vigorous vertical mixing during low discharge conditions.

Introduction

The seaward advection of salt in estuaries due to the river outflow is balanced in the mean by landward fluxes due to spatial and temporal correlation of velocity and salinity. Among the various contributors to the upstream flux, the major terms are generally the estuarine circulation, i.e., the vertical variations of tidally averaged velocity and salinity, and tidal pumping, i.e., temporal correlations of velocity and salinity (Uncles et al., 1985, Lewis and Lewis, 1983). Tidal pumping has long been recognized to be an important mechanism for horizontal exchange, and a number of physical mechanisms have been described to explain tidal pumping in various flow regimes. Stommel and Farmer (1952) invoked flow separation to explain tidal pumping at the mouths of estuaries; Schijf and Schonfeld (1953) and Okubo (1973) developed the concept of "tidal trapping", wherein transverse variations of tidal phase lead to net salt transport. Fischer et al., (1979) developed a theory for oscillatory shear dispersion, indicating that it may be an important contributor to tidal pumping in some instances. Jay (1991) showed that for straight, narrow estuaries, the barotropic tidal pumping is exactly equal to the product of the Stokes velocity and the vertically averaged salinity, and that by mass conservation constraints it has a negligible influence on the net salt flux. However Jay noted that an internal tidal oscillation could contribute to the net salt flux in highly stratified estuaries.

Observations in the Hudson River estuary indicate that tidal pumping occurs as a result of the correlation of fluctuations in interface elevation and horizontal tidal velocity. It can be regarded as the Stokes transport associated with internal tidal fluctuations, although the observed fluctuations do not appear to be freely propagating internal tidal waves but instead are associated with propagation of a salinity front. This type of tidal pumping was only observed during high discharge conditions; in fact during low discharge conditions, tidal pumping became weak or even counter-gradient, i.e., seaward (Hunkins, 1981).

The lower Hudson River estuary (adjacent to Manhattan Island, New York) is moderately stratified, with a vertical salinity difference that varies from 2--3 psu during low

discharge conditions to more than 10 psu during high discharge. It maintains a strong longitudinal salinity gradient during both low and high discharge conditions, ranging from 0.4--1 psu/km. Tidal currents are approximately 100 cm/s, and non-tidal, estuarine velocities are 20--30 cm/s. Hunkins (1981) analyzed the salt balance during low runoff conditions and found that estuarine circulation was the dominant contributor to the upstream salt flux, with tidal pumping actually producing a counter-gradient, i.e., seaward, salt flux. In this paper the analysis of new observations from the Hudson confirm Hunkins result that tidal pumping is not an important contributor to upstream salt flux during low discharge conditions. However, observations during high discharge conditions indicate that tidal pumping becomes a major term in the salt balance, exceeding the magnitude of the estuarine circulation. The tidal pumping results from fluctuations in interface elevation that are correlated with the horizontal tidal velocity, leading to net upstream salt transport.

Methods

Measurements of water properties and currents were obtained during tidal-cycle surveys in the lower Hudson estuary during low discharge conditions in August, 1992 and high discharge conditions in April--May, 1993. A 1.2 mHz shipboard acoustic Doppler current profiler provided the velocity data, and an Ocean Sensors CTD provided temperature, salinity and light transmission data. Measurements were obtained at 5 cross-channel locations at hourly intervals through the tidal cycle. Several tidal-cycle surveys at different locations were performed during each of the measurement periods. These measurements provided the basis for estimates of the various components of salt flux.

Results

During the August 1992 survey, there was significant salt stratification, roughly 8 psu difference between surface and bottom waters. Tidal currents were at moderate spring conditions, with near-surface speeds of 100 cm/s. Tidally averaged currents showed a pronounced estuarine circulation, with velocity differences of up to 50 cm/s between the surface outflow and bottom inflow. Tidal variations in salinity of up to 5 psu resulted from advection of the longitudinal salinity gradient. However, the magnitude of tidal pumping was small; it was close to zero in one section and weakly counter-gradient, i.e., seaward, at the other section.

During the April 1993 survey, the stratification was stronger than the 1992 period, with roughly 12 psu difference between surface and bottom waters. Tidal currents increased from intermediate to strong spring conditions during the observation period, with near-surface tidal current speeds of up to 140 cm/s. Estuarine shears were similar to the 1992 observations (Δu=50 cm/s) at the beginning of the observations, but the non-tidal velocity difference decreased to 25 cm/s during strongest spring tide conditions. Tidal salinity variations of up to 10 psu resulted from the advection of the salinity gradient. In these observations, in contrast to the 1992 data, tidal pumping was found to be quite pronounced. Salt flux associated with tidal pumping was 2--3 times the magnitude of the salt flux due to estuarine circulation.

The large magnitude of tidal pumping during the 1993 observations resulted from an asymmetric variation in salinity between the ebb and flood phases of the tide. The salinity in the mid-water column began to decrease early in the ebb phase of the tide, and through much of the ebb the outflowing water had low salinity. Early in the flood, there was an abrupt increase in salinity, causing the mid-depth inflow to have significantly higher salinity than the ebb. This asymmetry of salinity variations cannot be explained solely by horizontal advection, because that would lead to quadrature between the salinity and

velocity and no net flux. Nor can lateral advection explain the variations, based on observations of the transverse salinity structure. Rather, the salinity variations are the result of vertical advective motions. There is a slow downward motion during the early ebb causing a reduction in salinity, and a pronounced upward motion of as much as 4 m/hour during the early flood. The upward motion during the flood makes the dominant contribution to the tidal pumping.

The vertical motion of the pycnocline during the flood appears to be associated with the landward propagation of a salinity front. The front develops during the latter portion of the ebb and in the seaward most reach of the estuary. It propagates landward during the flood as a gravity current, similar to the observations of Geyer and Farmer (1989), although it propagates into brackish rather than fresh water. The front does not simply retreat during the ebb. Rather it slowly collapses and disperses, due to the strong shears and vertical mixing that occur during the ebb.

The mechanism of frontogenesis is still under investigation. It appears to be associated with a near-bottom convergence in the seaward portion of the estuary during the latter portion of the ebb. It only occurs during periods of strong stratification; presumably tide-induced mixing inhibits frontogenesis during periods of weaker stratification.

References

Fischer, H.B., E.J. List, R.C.Y. Kho, J. Imberger and N.H. Brooks, 1979. Mixing in Inland and Coastal Waters. Academic Press, New York. 483 pp.

Hunkins, Kenneth, 1981. Salt dispersion in the Hudson Estuary. *J. of Phys. Oceanogr.*, 11:729-738.

Jay, D. A., 1991. Estuarine salt conservation: a Lagrangian approach. *Estuarine, Coastal and Shelf Science,* 32:547-565.

Lewis, R.E. and J.O. Lewis, 1983. The principal factors contributing to the flux of salt in a narrow, partially stratified estuary. *Estuarine, Coastal and Mar. Sci.,* 16:599-626.

Okubo, A., 1973. Effects of shoreline irregularities on streamwise dispersion in estuaries and other embayments. *Netherlands J. of Sea Res.,* 6:213--224.

Schijf, J.B. and J.C. Schonfeld, 1953. Theoretical considerations on the motion of salt and fresh water. *Proc. Minn. Intl. Hydr. Con.,* 5th Cong. I.A.H.R., p. 321-333.

Stommel, H. and H.G. Farmer, 1952. On the nature of estuarine circulation, Part I. Reference no. 52-88, Woods Hole Oceanographic Inst., Woods Hole, MA.

Uncles, R. J. Elliott, R. C. A. and S. A. Weston, 1985, Dispersion of salt and suspended sediment in a partly mixed estuary. *Estuaries,* 8:256-269.

Lagrangian Mean Descriptions of Long-Term Estuarine Mass Transport

John M. Hamrick and Zhaoqing Yang
School of Marine Science
The College of William and Mary
Gloucester Point, VA 23062

Theoretical descriptions of long-term mass transport in estuaries are of interest in both basic and applied research. The quest for basic understanding of long-term transport in estuaries has motivated theoretical efforts to describe mean circulation and transport (Hamrick, 1990). Mean circulation and mass transport descriptions have also provided computationally efficient formulations for long-terms simulations of water quality and nutrient cycling (Cerco and Cole, 1993). The rapidly advancing capabilities of estuarine hydrodynamic and transport models might lead to the assessment that descriptions of mean circulation and transport are no longer essential. However, there are two primary arguments against such an assessment. Since numerical models produce vast amounts of information, analysis methodologies capable of extracting realistic and concise information regarding long-term dynamics and transport are desirable for interpretation of model results. Although long-term intratidal simulation of water quality and nutrient cycling is becoming a reality, it remains computationally intensive (Hamrick, 1994) and requires resources that are not widely available. Thus models based on mean transport fields remain of interest.

The purpose of this paper is to present a number of methodologies for describing long-term estuarine transport, using Lagrangian mean transport equations, which provide both theoretical insight and tools for the analysis of numerical model results. The terminology Lagrangian mean is adopted, because the transport equations to be considered can be derived in the context of Andrews and McIntyre's (1978) generalized Lagrangian mean (GLM) theory of wave-mean flow interaction. The first, most general, description to be presented is a nonlinear Lagrangian mean mass transport equation obtained by direct application of the fully nonlinear GLM theory. This is followed by the derivation of a second weakly nonlinear Lagrangian mean transport equation. Technical difficulties arising in the actual application of the GLM transport equation and limitations of the weakly nonlinear Lagrangian mean transport equations lead to a third approach for the determination of the Lagrangian mean transport field. The third approach involves the variational inversion of an ad hoc mean mass transport equation, whose form is suggested by GLM and weakly nonlinear transport equations. The oral presentation and full paper will present results from preliminary applications of these approaches to an idealized estuary, the James River, Virginia and the Chesapeake Bay.

To define the problem of deriving a mean transport equation, consider the intratidal advective transport equation for a material c, which in curvilinear-orthogonal horizontal and stretched vertical coordinates is

$$\partial_t(mhc) + \partial_i\left(mhm_i^{-1}u_i c\right) = mhs \qquad (1)$$

where m_i is the scale factor in coordinate direction i (i = 1,3), $m = m_1 m_2 m_3$, h is the total depth, and s represents sources and sinks, including turbulent diffusion. The corresponding continuity equation is obtained by setting c and s to unity and zero, respectively. The stretched coordinate vertical velocity, w or u_3, is related to the physical vertical velocity, w^*, by

$$hw = hu_3 = w^* - z\left(\partial_t z_s^* + m_\alpha^{-1} u_\alpha \partial_\alpha z_s^*\right) - (1-z) m_\alpha^{-1} u_\alpha \partial_\alpha z_b^* \tag{2}$$

where * denotes physical variables, the subscripts b and s denote the bottom bed and free surface, respectively, and α = 1,2. If the concentration and velocity fields are decomposed into temporal Eulerian averages and deviations or disturbances, $\phi = \langle\phi\rangle + \phi'$, the traditional Eulerian mean of (1) is

$$\partial_t\left(m\langle h\rangle\langle c\rangle\right) + \partial_i\left(m\langle h\rangle\frac{\langle u_i\rangle}{m_i}\langle c\rangle\right) = -\partial_i\left(m\left(\left\langle h\frac{u_i}{m_i}c\right\rangle - \langle h\rangle\frac{\langle u_i\rangle}{m_i}\langle c\rangle\right)\right) + m\langle hs\rangle \tag{3}$$

Previous efforts to derive temporal mean mass transport equations from (3) involve representation of the right side as enhanced advection and diffusion of the mean concentration field. The enhanced advection field, corresponding to a first order approximation of the Stokes drift, and the diffusion coefficients are expressed in terms of correlations of the original disturbance velocity field (Feng, *et. al.*, 1986; Hamrick, 1990). The success of such efforts has been based on weak nonlinearity of the disturbance velocity field associated with tidal and atmospheric forced long wave motions. Hamrick (1994) has shown that in an estuarine system such as the Chesapeake Bay, where the magnitude of the tidal forcing and large scale flow response is consistent with the weakly nonlinear approximation, local nonlinearites in the flow field, associated primarily with strong topographic variability, may locally invalidate the weakly nonlinear approximation.

The generalized Lagrangian mean theory allows an exact Lagrangian mean transport equation to be formulated for cases of finite amplitude mean flows and disturbances. The GLM transport equation corresponding to (1) is

$$\partial_t\left(J(mh)^\xi\{c\}\right) + \partial_i\left(J(mh)^\xi\left\{m_i^{-1}u_i\right\}\{c\}\right) = J(mh)^\xi\{s\} \tag{4}$$

with the GLM continuity equation obtained by setting c and s to unity and zero, respectively. The GLM variables and the Jacobian are defined by

$$\{\phi\} = \left\langle\phi^\xi\right\rangle \tag{5}$$

$$\phi^\xi = \phi\left(x_j + \xi_j\left(x_j,t\right),t\right) \tag{6}$$

$$J = \det\left[\delta_{ij} + \partial_j\xi_i\right] \tag{7}$$

where ξ_i, the zero Eulerian mean disturbance displacement vector associated with point x_i, is the solution of

$$\partial_t\left(J(mh)^{\xi}\xi_i\right)+\partial_j\left(J(mh)^{\xi}\left\{m_j^{-1}u_j\right\}\xi_i\right)=J(mh)^{\xi}\left(u_i^{\xi}-\left\{u_i\right\}\right) \tag{8}$$

Equations (5&6) define the generalized Lagrangian mean of a quantity, interpreted as an Eulerian field variable at x_i, as the Eulerian mean along a displacement trajectory given by the solution of equation (8). Comparison of the GLM transport equation (4) and the Eulerian mean (3) reveals the simplicity and elegance of the GLM formulation, which has no disturbance correlation terms. This simplicity is however deceptive until the highly nonlinear nature of the transport equation (8) for the disturbance displacement vector is considered. The solution of (8) poses formidable technical difficulties, due to both its nonlinear form and the selection of initial conditions such that the zero Eulerian mean constraint is satisfied. A promising technique for solving (8) and obtaining GLM advection fields will be presented in the oral presentation and the full paper.

Approximate Lagrangian mean transport equations for the Eulerian mean concentration distribution can be derived directly from (4-8) using Taylor series expansions for weakly nonlinear flows. An approximate equation, representing an extension beyond previous results, is

$$\partial_t(m\langle h\rangle\langle c\rangle)+\partial_i\left(\left(mm_i^{-1}\langle hu_i\rangle+\partial_j L_{ij}\right)\langle c\rangle\right)=\partial_i\left(m\left(m_i m_j\langle h\rangle\right)^{-1}\delta_{i3}\langle K_v\rangle\partial_j\langle c\rangle\right) \tag{9}$$

$$L_{ij}=L_{ij}^{(0)}+L_{ij}^{(1)}=m\langle h\rangle\left\langle\partial_t\xi_i^{(0)}\left(\xi_j^{(0)}+\xi_j^{(1)}\right)\right\rangle \tag{10}$$

$$\partial_t\xi_i^{(0)}=m_i^{-1}u_i' \tag{11}$$

$$\begin{aligned}\partial_t\left(m\langle h\rangle\xi_i^{(1)}\right)+\partial_j\left(\left(mm_j^{-1}\langle hu_j\rangle+\partial_k L_{jk}^{(0)}\right)\xi_i^{(0)}\right)=m\langle h\rangle\left(m_i^{-1}\langle u_i\rangle+\xi_j^{(0)}\partial_j\left(\partial_t\xi_i^{(0)}\right)\right)\\ -\left(mm_i^{-1}\langle hu_i\rangle+\partial_j L_{ij}^{(0)}\right)\end{aligned} \tag{12}$$

Advection in (9) includes the Eulerian mean transport, $\langle hu_i\rangle$, and an approximation of the Stokes drift in terms of the antisymmetric tensor L_{ij}, whose three unique components define a vector potential. The diffusion term in (9) represents only the mean vertical turbulent diffusion. If L_{ij} is evaluated using only the first term in (10), (9) reduces to the weakly nonlinear transport equation presented by Hamrick (1990, 1994). The inclusion of the second term in (10) and the solution of (12) extends the weakly nonlinear transport equation in a manner consistent with GLM theory.

The extended weakly nonlinear Lagrangian mean transport equation suggest a third approach for determining an effective Lagrangian mean transport field. Since the form of Eulerian mean transport contribution to the Lagrangian mean will be unchanged as the dynamics become moderately nonlinear, it is reasonable to assume the increased nonlinear effects will appear in the portion of the Lagrangian mean represented by L_{ij} or the equivalent vector potential. Thus, an ad hoc Lagrangian mean transport equation of the form

$$\begin{aligned}\partial_t(m\langle h\rangle\chi)+\partial_x\left(\left(mm_x^{-1}\langle hu\rangle+\partial_y A_z-\partial_z A_y\right)\chi\right)+\partial_y\left(\left(mm_y^{-1}\langle hv\rangle+\partial_z A_x-\partial_x A_z\right)\chi\right)\\ +\partial_z\left(\left(mm_z^{-1}\langle hw\rangle+\partial_x A_y-\partial_y A_x\right)\chi\right)-\partial_z\left(m\left(m_z^2\langle h\rangle\right)^{-1}\gamma_v^2\partial_z\chi\right)=\Gamma(\chi)=0\end{aligned} \tag{13}$$

is proposed, where $\boldsymbol{A}$ is a vector potential and γ_v is the square root of the vertical turbulent diffusion coefficient. The components of $\boldsymbol{A}$ and γ_v can be determined by minimizing the squared difference between χ, predicted by (12) and $\langle c \rangle$ provided by a numerical model (Thacker and Long, 1988; Hamrick, 1994). Formally, this is accomplished by minimizing a Lagrange function

$$\Lambda = \frac{1}{2}\int_\tau \int_V \left(\langle c \rangle - \chi\right)^2 dV d\tau + \int_\tau \int_V \lambda \Gamma(\chi) dV d\tau \tag{14}$$

with respect to the Lagrange multiplier, λ, and χ, A_x, A_y, A_z, and γ_v. Minimization with respect to λ recovers (13), while minimization of with respect to χ, yields the backward in time adjoint transport equation

$$\begin{aligned} &\partial_t\left(m\langle h\rangle\lambda\right) + \partial_x\left(\left(mm_x^{-1}\langle hu\rangle + \partial_y A_z - \partial_z A_y\right)\lambda\right) + \partial_y\left(\left(mm_y^{-1}\langle hv\rangle + \partial_z A_x - \partial_x A_z\right)\lambda\right) \\ &+\partial_z\left(\left(mm_z^{-1}\langle hw\rangle + \partial_x A_y - \partial_y A_x\right)\lambda\right) + \partial_z\left(m\left(m_z^2\langle h\rangle\right)^{-1}\gamma_v^2\partial_z\lambda\right) + \left(\langle c\rangle - \chi\right) = 0 \end{aligned} \tag{15}$$

for λ, which is forced by the misfit between $\langle c \rangle$ and χ. Minimization with respect to the components of $\boldsymbol{A}$ and γ_v yields

$$\begin{aligned} &\nabla_{A_x}\Lambda = -\left(\partial_y\left(\chi\partial_z\lambda\right) - \partial_z\left(\chi\partial_y\lambda\right)\right) : \nabla_{A_y}\Lambda = -\left(\partial_z\left(\chi\partial_x\lambda\right) - \partial_x\left(\chi\partial_z\lambda\right)\right) \\ &\nabla_{A_z}\Lambda = -\left(\partial_x\left(\chi\partial_y\lambda\right) - \partial_y\left(\chi\partial_x\lambda\right)\right) : \nabla_{\gamma_v}\Lambda = -2\gamma_v\partial_z\left(m\left(m_z^2\langle h\rangle\right)^{-1}\lambda\partial_z\chi\right) \end{aligned} \tag{16}$$

the gradients of the Lagrange function. The inverse procedure then involves: a forward integration of (13); evaluation of Λ using only the first term on the right of (14); a backward integration of (15); evaluation of the gradients using (16); the application of a quasi-Newton minimization to update $\boldsymbol{A}$ and γ_v; and repetition of the preceeding sequence until Λ is sufficiently small. Initial estimates of $\boldsymbol{A}$ and γ_v can be provided by the results of the weakly nonlinear analysis or by particle tracking trajectories as described by Hamrick (1994).

References

Andrews, D. G., and M. E. McIntyre, 1978: An exact theory for of nonlinear waves on a Lagrangian flow. *J. Fluid Mech.*, **89**, 609-646.

Cerco, C. F., and T. M. Cole, 1993: Three-dimensional eutrophication model of Chesapeake Bay. *Journal of Environmental Engineering*, **119**, 1006-1025.

Feng, S., R. T. Cheng, and P. Xi, 1986a: On tide-induced residual current and residual transport: Part 1, Lagrangian Residual Current. *Water Resour. Res.*, **22**, 1623-1634.

Hamrick, J. M., 1990: The dynamics of long-term mass transport in estuaries. *Residual Circulation and Long-Term Transport in Estuaries and Shallow Bays*, In: R. T. Cheng, ed., Springer-Verlag, 17-33.

Hamrick, J. M., 1994: Linking hydrodynamic and biogeochemcial transport models for estuarine and coastal waters. *Estuarine and Coastal Modeling, Proceedings of the 3rd International Conference*, M. L. Spaulding *et al*, Eds., American Society of Civil Engineers, New York, 591-608.

Thacker, W. C., and R. B. Long, 1988: Fitting dynamics to data. *J. Geophys. Res.*, **93**, 1227-1240.

EFFECTS OF CHANGING BATHYMETRY ON THE DYNAMICS AND OCEAN EXCHANGE OF A MEDITERRANEAN ESTUARY; TOMALES BAY, CALIFORNIA.

Clifford Hearn[1], Stephen Smith[2], John Largier[3], Joshua Plant[2], John Rooney[2], and Karen Sender[4]

[1]Department of Geography and Oceanography, University College, University of New South Wales, ADFA, Canberra 2600, Australia.

[2]Department of Oceanography, University of Hawaii, Honolulu, Hawaii 96822.

[3]Scrips Institution of Oceanography, University of California at San Diego, La Jolla, California 92093.

[4]School of Ocean and Earth Science and Technology, University of Hawaii, Honolulu, Hawaii 96822.

Abstract

This paper considers the ways in which anthropogenic modifications to the environment of estuaries on coasts with mediterranean climates influence their buoyancy dynamics, circulation and ocean exchange. Detailed consideration is given to Tomales Bay, California (Smith et al, 1991) which is presently a study site within NSF's "Land-Margin Ecosystems Research" (LMER) program designed to study the role of estuaries in the exchange of material between the land and coastal ocean (LMER Coordinating Committee, 1992).

Tomales Bay (figures 1 and 2) is situated on the west coast of California just to the north of San Francisco Bay. It lies directly along the San Andreas Fault which results in the extremely unidirectional form of the estuary seen in the figure. The estuary is some 23 km long and 1500 m wide.

The flushing of Tomales Bay (outside of direct riverflow events) appears to be primarily due to tidal and buoyancy effects (arising from river flow, and in summer, net evaporation and heating). The central theme of this paper concerns likely long term changes in the estuarine dynamics which are produced by bathymetric modifications to the basin. These are caused by changes in sedimentation resulting from human usage of land and water resources. The resultant alterations in the estuarine circulation, and ocean exchange, affect the transport of nutrients, pollutants and suspended terrestrial sediments.

The paper also considers the affects of changing buoyancy fluxes produced by human modification of the amount, and temporal distribution, of freshwater inflow to the estuary (through the construction of reservoirs in the catchment); Tomales Bay presently receives a controlled summer release of reservoir water (which exceeds the expected natural seasonal rainfall).

The upper (and usually very shallow) parts of mediterranean estuaries may exhibit marginal to strong hypersalinity in late summer due to net evaporation; salinities at the head of Tomales Bay exceed those at the mouth by 1 to 2 parts per thousand (figure 3). This hypersalinity affects the ocean flushing with important implications for annual and long term geochemical balances. The summer negative buoyancy input produces convective processes which are affected by the long term changes of the topography of the upper estuary and tidal processes.

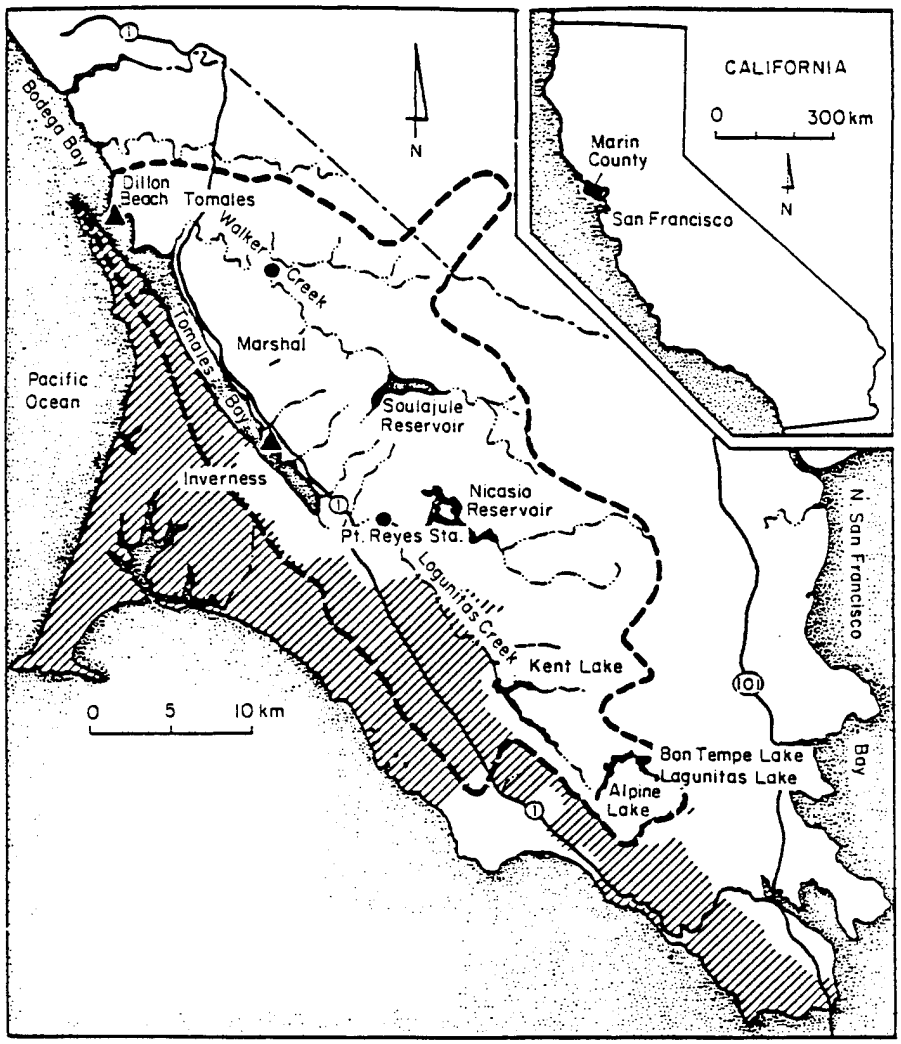

Figure 1. Map of the Tomales Bay watershed. Important landmarks on the map include six water catchment reservoirs, two weather stations, and two stream gauges. Towns in the watershed are Pt. Reyes Sta., Inverness, Marshall, Tomales and Dillon Beach. State Highway no. 1 is the major highway through the watershed. ● Stream gauge; ▲ weather station; ——— watershed boundary; ▨ parkland.

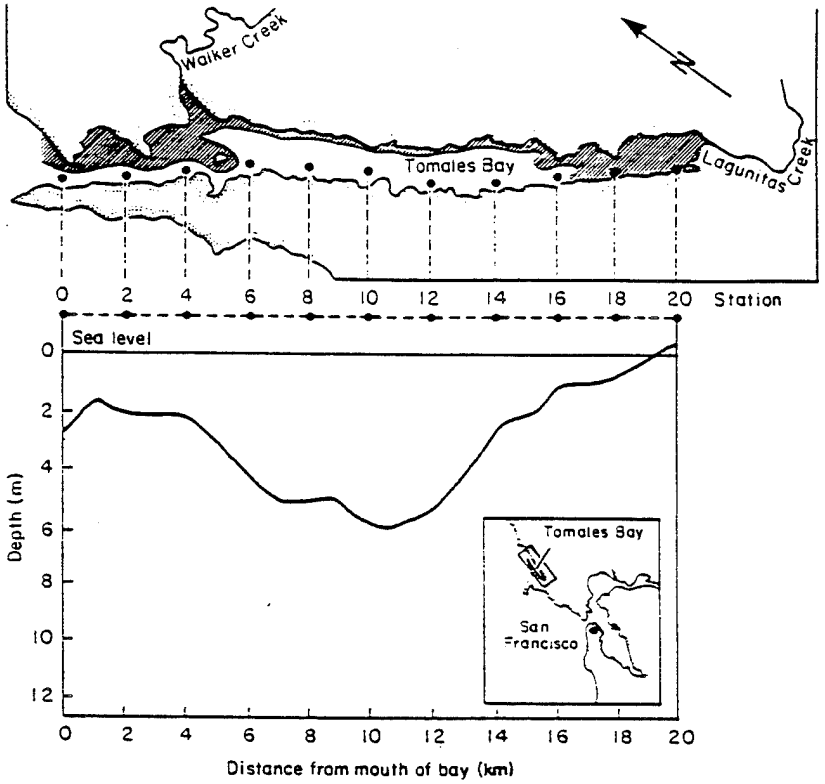

Figure 2. Tomales Bay sampling stations. The bay between stations 0 and 8 is designated the Outer Bay. The remainder is designated the Inner Bay. Routine sampling excluded station 20. Shaded areas are shoals < 2 m deep. The depth profile is sectionally averaged; a channel near the western shore breaches the sill at the ocean end of the bay.

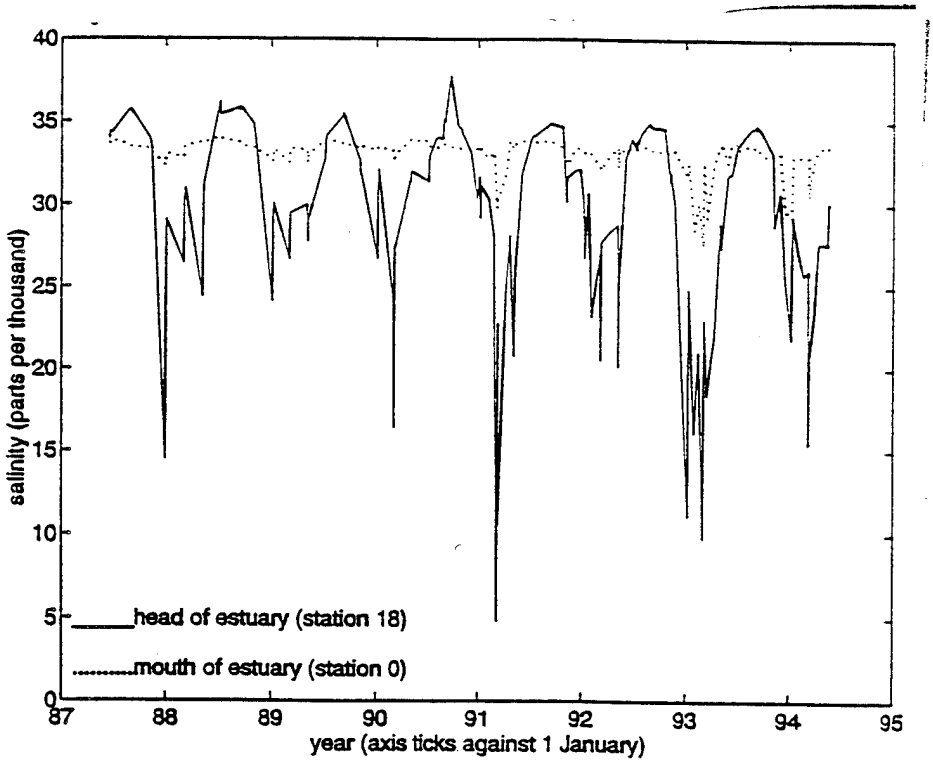

Figure 3. Time series of salinities at mouth and head (stations 0 and 18 in Figure 2).

The analysis of the paper is based on both simple mathematical, and numerical, one dimensional models and a fully three dimensional numerical model (called SPECIES). Tomales Bay is ideal for testing such one-dimensional models in view of its shape; the models use various forms for the diffusion coefficient inorder to represent baroclinic and tidal mixing. They use widths and depths derived from the bathymetry files and are fully tidal including the effects of drying.

All the numerical models follow the physical and chemical parameters of the estuary through the annual cycles of wet winters and dry summers. The model inputs involve annual time series of riverflow and meteorological data. The specimen years 1990 and 1991 (the first having a dry, and the second a wet, winter) are selected for detailed analysis of the estuarine dynamics. The models use salinity, temperature, and tidal, boundary conditions based on data collected at the mouth of the estuary (station 0 in figure 2).

Two major creeks empty into Tomales Bay (figure 2); one at the head of the estuary (Lagunitas Creek) and the other some 5 km from the mouth (Walker Creek). Sediment from Lagunitas Creek has shoaled the upper reaches of the basin where there is a shallow region about 5 km long. There is also a shallow bank, which extends from the entry point of Walker Creek to the ocean mouth, with a deep channel on the other side of the basin with depths down to 20 m (figure 2). Therefore, the bathymetry of the estuary consists of an inner basin (with depths down to 7 m), of width about 1500 m and length 10 to 15 km, which has a very shallow bank at its head and is connected to the ocean through a deep channel (of width 300m, length 6km, and depths to 20 m) which shoals to 2 m close to the mouth.

Bathymetry surveys of Tomales Bay date from 1861 and represent a full record of anthropogenic changes in the estuary; during this time there has been 1 to 2 m of net shoaling (locally more) due to increased erosion in the watershed. The model simulations use bathymetry files for 1861, 1931, 1957, and 1994 with riverflow, and meteorological, data for the two specimen (dry and wet) years mentioned above. The model results are compared with field data for these specimen years and then analysed from the perspective of the effect of changing bathymetry on the estuarine dynamics and buoyancy balance.

Some generalisations are attempted regarding the influence of long term changes in estuarine topography and depth on the summer and winter buoyancy dynamics of mediterranean estuaries, with specific results from Tomales Bay, and illustrations drawn from other estuaries. Local water authorities can release reservoir water directly into rivers in summer and this raises the possibility of some management of the seasonal flushing of mediterranean estuaries given an adequate understanding of the role of the summer buoyancy balance in their ocean exchange.

References

LMER Coordinating Committee, 1992. Understanding Changes in Coastal Environments: The LMER Program. *Eos Transactions*, (American Geophysical Union), 73:481 and 484-85.

Smith S V, Hollibaugh J T, Dollar S J, and Vink S, 1991. Tomales Bay Metabolism: C-N-P Stoichiometry and Ecosystem Heterotrophy at the Land-Sea Interface. *Estuarine, Coastal and Shelf Science*, 33:223-257.

SCALAR TRANSPORT CALCULATIONS FROM ACOUSTIC DOPPLER CURRENT PROFILER DATA

David J. Kay, David A. Jay and Jeffrey D. Musiak
University of Washington
Seattle, WA 98195 USA

Abstract

Urgent management questions posed by extensive alteration of coastal systems require measurement, understanding and prediction of nutrient, carbon and total suspended matter transports. Any ability to predict long-term changes in fluxes must be based on knowledge of flux mechanisms and their role in and response to changes in estuarine circulation. This bring a renewed urgency to the topic of scalar flux calculation. Attempts during the last three decades to directly measure estuarine scalar fluxes have encountered three primary problems: a) net scalar transport is typically a small, statistically insignificant difference between much larger flood and ebb fluxes; b) available instrumentation has not provided spatial resolution of the velocity field (and in some cases, of scalar variability) sufficient to remedy this statistical difficulty; and c) scalar transport is variable in three dimensions, while theoretical models used to understand estuarine circulation and transport are two dimensional.

We report here salt transport calculations based on conductivity-temperature-depth (CTD) profiles and velocity measurements obtained in the Columbia River estuary with a boat-mounted, 1.2 mHz narrow-band, acoustic Doppler current profiler (ADCP). The use of a boat-mounted ADCP offers many advantages over other techniques in measuring estuarine velocity fields (e.g. it allows for 1 meter spatial resolution in the vertical and horizontal resolution of O(100m) or less). But one weakness of ADCP technology for these calculations must be recognized from the outset. That is the inability to sample the bottom 15% of the velocity profiles (2-3 meters in our case). To remedy this problem a method was developed to extrapolate the velocity profiles to the bed by integrating the momentum balance from the bed to the free surface using an eddy-diffusivity turbulence closure with a stratification correction. Using measured velocities in the top 85% and velocities in the bottom 15% obtained from the integrated momentum balance, calculations were carried out to evaluate the ADCP as a remedy to the first two of the above difficulties in determining estuarine scalar fluxes.

Data Collection

CTD and ADCP observations were made on each of two cross sections for 25-35 hours (35 hours at Clatsop Spit, where the calculations shown below are carried out), with four CTD stations on each of the cross sections. The CTD stations were sampled roughly once per hour with the ADCP running continuously during the sampling periods. Each section was then divided into 4 boxes of (250-300 m) for purposes of averaging the velocity. The resultant velocity and salinity records were then subjected to harmonic analysis, giving mean-flow and amplitude/phase of the first eight tidal species for each meter depth bin in the vertical. These data were then used as input for both the momentum balance and the salt transport calculations.

Velocity Profile

To estimate the velocities in the bottom 15% of the flow and as part of an analysis of the estuarine momentum balance, a method was developed to calculate a complete velocity profile by integrating the momentum balance using an eddy-diffusivity turbulence closure with a stratification correction. The bed stress T_b was chosen to minimize the discrepancy between observations and the calculated profile. The technique involves integrating the momentum balance from the bed to the free surface and subtracting this from the momentum balance integrated from a point z in the flow to the free surface. From this the velocity gradient is formulated as a function of the bed-stress, vertical integrals of acceleration and the horizontal density gradient, and the eddy-viscosity with stratification correction.

$$\frac{du}{dz} = \frac{1}{km}\left[\frac{(\xi - z)}{H}\int_{z_0}^{\xi}\frac{du}{dt}dz - \int_{z}^{\xi}\frac{du}{dt}dz' + \frac{g}{\rho_0}\frac{(\xi - z)}{H}\int_{z_0}^{\xi}\int_{z''}^{\xi}\frac{d\rho}{dx}dz'\,dz'' - \frac{g}{\rho_0}\int_{z}^{\xi}\int_{z'}^{\xi}\frac{d\rho}{dx}dz'\,dz'' + \frac{(\xi - z)}{H}T_b\right] \qquad (1)$$

Where z is position in the vertical, x is position in the along estuary direction, (ρ is density, K_m is the eddy diffusivity, and z_o is the roughness length. The friction velocity u_* appears in the expression for the eddy-viscosity and in the bedstress ($T_b=u_*^2$). A 'calculated' velocity profile (with parts of terms evaluated from data) is determined by integrating this expression from the bed for a given u_*. The procedure is then iterated to find a u_* that optimizes the fit between the observed velocity profile and the 'calculated' profile in the middle part of the profile where velocity data is good. This differencing approach allows the elimination of the unknown surface slope term in the momentum balance. But it requires a zeroth order estimate of the acceleration and the eddy-diffusivity in the bottom 15%. The acceleration is taken down to the bottom as a power law, allowing for continuity of both the acceleration and its gradient at our first good data point 3 meters off the bed. The Richardson number is also taken down as a power law, allowing for an estimate of the stratification correction and, therefore, K_m. The K_m stratification correction used is essentially identical to that of Lehfeldt and Bloss (1988), except that it includes a viscosity cutoff of .15 for large Richardson number, to include the effects of Kelvin Helmholtz instabilities.

The approach worked reasonably well at times of peak current (figure 1) but was not entirely satisfactory during periods of weak currents for two reasons: a) errors in determining the acceleration sometimes dominated the calculation when bed-stress was small; and b) the eddy diffusivity turbulence closure employed probably did not represent very well the interfacial mixing that controls the velocity profile at these times. A velocity record and profiles are shown below (figure 1).

Fluxes

As mentioned earlier, a major difficulty with approaches to measuring scalar fluxes in the past was that the net flux was a small difference between much larger ebb and flood fluxes. To attempt to eliminate this statistical difficulty, an approach is taken in calculating the net transfer that distinguishes between the river flow and the Stokes drift and uses the equivalence of the Stokes transport of the mean scalar field and the tidal transport of tidal variations in the mean field (Jay 1991). This approach allows for the elimination of terms in the flux equation that should cancel each other. The resulting expression, explicitly including lateral and vertical variations, is as follows:

$$\int \overline{UC}\,d\overline{A} = -\overline{Q}^{R}\left\langle\{\overline{C}\}\right\rangle + \overline{A}\left(\left\langle\{\overline{U_v}\}\{\overline{C_v}\}\right\rangle + \sum_{j=1}^{n}\overline{\left\langle\{U_{jv}\}\{C_{jv}\}\right\rangle}\right.$$

$$\left. + \left\langle\{\overline{U_{vb}C_{vb}}\}\right\rangle + \sum_{j=1}^{n}\overline{\left\langle\{U_{jvb}C_{jbv}\}\right\rangle} + \left\{\left\langle\overline{U_b}\right\rangle\left\langle\overline{C_b}\right\rangle\right\} + \sum_{j=1}^{n}\left\{\overline{\left\langle U_{jb}\right\rangle\left\langle C_{jb}\right\rangle}\right\}\right) \qquad (2)$$

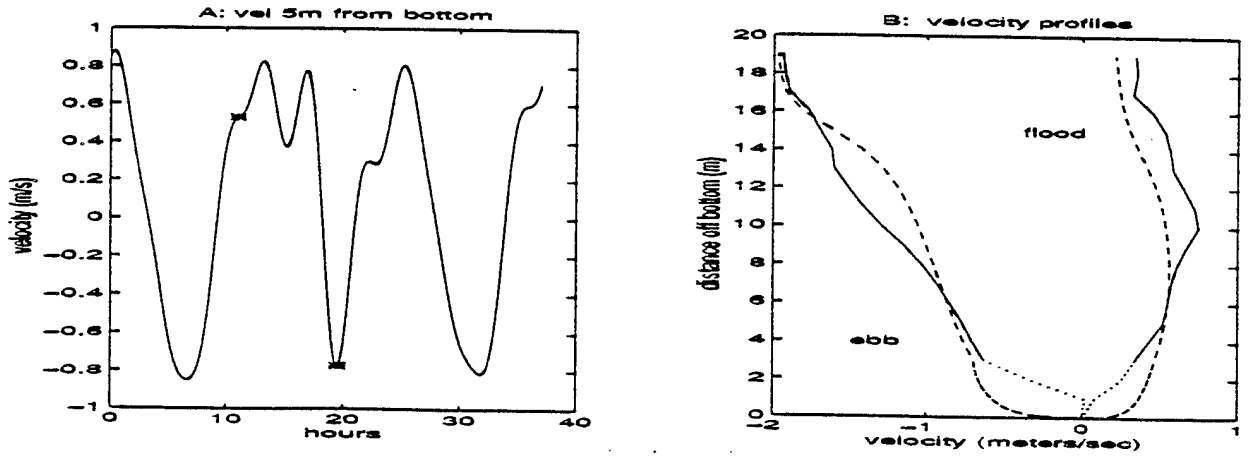

Figure 1. A: Velocity record of point 5 meters off the bed at the northern part of the Clatsop Spit cross-section at the mouth of the Columbia River. The data was collected for 34 hours starting at 2300 hrs PST, 8/27/91. B: Velocity profiles during flood (hour 11) and ebb (hour 19.5) portions of the sampling period (marked on figure 1a). The dashed (--) line is the fit resulting from the momentum balance calculation; the solid (l) line is the data; and the portion of the profile measurement that is subject to interference from the bottom signal is dotted (:). Optimum fits were at a u(of 4.9 cm/s for the ebb profile and 3.0 cm/s for the flood profile.

Where for velocities $\langle v_j\rangle = \{\langle v_j\rangle\} + \langle v_{jb}\rangle$ and $v_{jb} = \{v_j\} + v_{jv}$, and similarly for scalars C. Subscript b denotes a deviation from a lateral average, and subscript v indicates a difference from a vertical average. Summation is over tidal species; { } signifies a lateral average, <> signifies a vertical average, and residual flux terms, indicated by overbars, are left separate for clarity.

Direct comparison of net salt transfer with outward river-flow flux was made for the Clatsop Spit cross section. In this case the landward flux nearly balanced Q_R ,<{S}>, where Q_R is riverflow, <{S}> is tidal-averaged salinity, and <{ }> indicates a sectional average. Net outward salt transfer was found to be 23% of Q_R <{S}>. Contributions to the net salt transfer involving lateral variability in the flow were found to be significant contribute over 30% of the total inward tidal salt transfer (Figure 2). Clearly, three dimensional effects of topography and bottom friction must be considered in measurements of scalar balances even when barotropic and baroclinic forcing are two dimensional.

The dotted line in Figure 2a, which is the zero frequency component, illustrates a circulation pattern characterized by lower than average salinity water flowing outward in the southern portion of the entrance (where the dredged navigation channel is located) and high salinity water flowing inward in the northern portion. The M_2 curve show either below average salinity flowing inward or above average salinity flowing outward at both ends of the cross section; in either case there is a net inward flux at the M_2 frequency. Figure 2b shows the lateral variations in the correlations of the differences from the vertical means of

the velocity and salinity. As can be seen from the scales of the vertical axes, the contribution to the balance of terms of the type $\langle U_{vb}S_{vb}\rangle$ is an order of magnitude greater than the contribution of terms of the type $\langle U_b\rangle\langle S_b\rangle$.

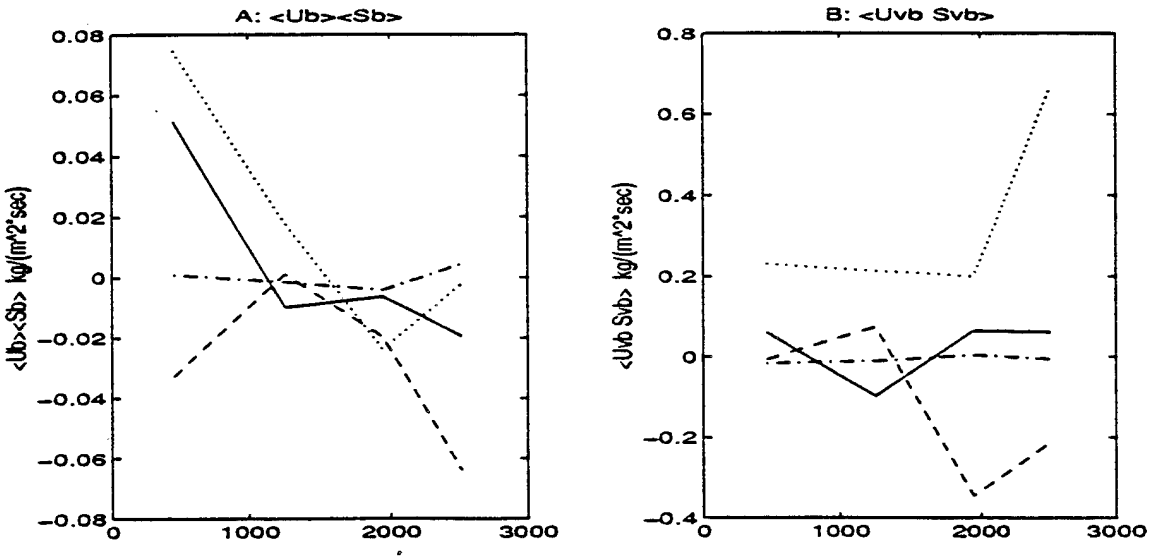

Figure 2. A: Lateral variability in $\langle U_{jb}\rangle\langle S_{jb}\rangle$, the correlation between the vertical averages of the differences in U and S from their lateral averages. B. Lateral variability in $\langle U_{jvb}S_{jvb}\rangle$, the vertical average of the correlation between the differences in Uv and Sv from their lateral averages. Dotted (:) is Z0 curve, solid (l) is K1 curve, dashed (-) is M_2 curve, and dash-dot (-.-) is M_4 curve.

There are several factors that contribute to the 23% difference between the outflow Q_R [S] and the sum of the inward salt fluxes. There may actually have been a net outward salt flux. Tidal records show that the data was taken for a period just following a spring tide. During this period the mean salt quantity upstream of the transect is usually decreasing, resulting in a net outflow over a 24 hour period. Other factors may contribute as errors. First, these measurements occurred right after a 9% decrease in riverflow due to upstream reservoir manipulation. Also, four CTD stations are inadequate to characterize horizontal salinity gradients in a stratified estuary. Furthermore, as mentioned earlier, current ADCP technology does not allow for measurements close to the bed. Finally, very shallow areas near shore that were not measured probably had a net outward transport of low salinity water (i.e. a landward salt flux). Failure to measure these areas also probably causes a underestimation of the lateral variability contribution to the landward salt flux.

These results demonstrate that a) the use of the equivalence of the Stokes transport of the mean scalar field and the tidal transport of the tidal variations in the mean field is a helpful analytical result for transport calculations, and b) successful wide coverage of the velocity field obtainable with a boat-mounted ADCP, allowing for reliable velocity measurements over entire estuarine cross-sections, can be very helpful in determining transport processes in estuaries.

The equivalence of the Stoke transport of the mean field and the tidal transport of tidal variations in the mean field is the result of the application of Generalized Lagrangian Mean (GLM) theory (Andrews and McIntyre 1978) to estuarine dynamics (Jay 1991). A much greater discrepancy was found when not utilizing the result from GLM, embedded in

eq. (2). It appears that the use of the GLM relationship eliminates terms involving the difference in large ebb and flood fluxes, and thereby reduces errors. The narrow-band ADCP and CTD profiler used in this study made possible the wide coverage necessary for meaningful transport measurements. Use of a broad-band ADCP, however, would improve velocity resolution and a towed CTD would improve salinity resolution, thereby improving the accuracy of flux measurements.

References

Andrews D. G. and M. E. McIntyre. 1978. An exact theory of non-linear waves on a Lagrangian-mean flow. *Journal of Fluid Mechanics,* 89:609-646.

Jay, D. A.. 1991. Estuarine salt conservation: a Lagrangian approach. *Estuarine, Coastal and Shelf Science,* 32:547-565.

Lehfeldt, R. and S. Bloss. 1988. Algebraic turbulence model for stratified flows. In *Physical Processes in Estuaries,* J. Dronkers and W. van Leussen (eds.), p. 278-291, Springer-Verlag, New York.

Abstract submitted for presentation at the 7th International Biennial Conference on Physics of Estuaries and Coastal Seas (PECS 7), 28-30 November 1994, Woods Hole, MA.

SEASONAL OCCURRENCE OF HYPERSALINITY AND INVERSE STRUCTURES IN LOW-INFLOW "ESTUARIES"

John L. Largier
Scripps Institution of Oceanography
and
Clifford J. Hearn
Australian Defence Force Academy

The study of estuarine hydrodynamics has been dominated by a focus on the defining feature of estuaries: freshwater inflow. Unfortunately, this has led to a lack of study of low-inflow "estuaries". Perhaps better described as semi-enclosed bays, these low-inflow systems are not only common in drier climates (eg. Laguna Madre, TX). From an initial survey of regions with a temperate mediterranean climate, it would appear that the seasonal occurrence of this type of estuary/bay is characteristic of the mediterranean climate region. In support of this assertion, we present field data from a variety of systems in the Californias (Mexico and USA), in western Australia and in southern Africa.

In these systems, the buoyancy fluxes are dominated by air-water exchange. Although the heat (buoyancy) gain in a shallow system can be large during summer, the concommitant mass efflux through evaporation leads to a counteracting buoyancy loss. Thus, in spite of large thermohaline signals, the resultant buoyancy flux is often too weak to bring about vertical stratification and buoyancy-driven exchange in the presence of strong tidal stirring typical of shallow basins. Through a simple box model, we investigate the seasonal cycles of temperature, salinity and density as they are forced by surface heat and mass fluxes in the presence of tidal stirring and diffusive exchange with an ambient oceanic basin.

In a one-dimensional model of a tidally flushed low-inflow system, the rate at which water is exchanged with the ambient ocean is primarily a function of distance from the mouth of the estuary/bay. In low-inflow (summer) mediterranean basins, one can identify four regimes: a marine regime in the outer bay (extending roughly one tidal excursion), a thermal regime, a hypersaline regime and an estuarine regime (where salinities are depressed owing to freshwater inflow). The separation of thermal and hypersaline regimes is due to the increase of residence time with distance from the mouth. On entering the basin, cool oceanic water gains heat (and buoyancy) rapidly, within the first several days, whereas salinity increases slowly (buoyancy loss), but persistently. The longer a given basin, and the greater the residence time at the back of the basin, the longer the hypersaline regime and the greater the maximum salinity attained.

Through simple scale criteria (which compare surface buoyancy fluxes with basin morphometry, freshwater inflow, tidal stirring and ocean water type), we discuss the essential differences in a variety of systems of different size, from different climates and/or with different tidal forcing. While we discuss the potential for buoyancy-driven exchange due to inverse density gradients, a more complete discussion of buoyancy dynamics in a specific system (Tomales Bay, CA) is presented in a companion paper at this conference (Hearn, et al.).

Observations and Modeling of Stratification Episodes and Gravitational Circulation in Northern San Francisco Bay

S. G. Monismith, M. Stacey and J.R. Burau[1]
Environmental Fluid Mechanics Laboratory, Stanford University, Stanford, CA. 94305-4020

Using field observations and 1D (vertical) modeling, we discuss the dynamical basis of periodic (strain induced) stratification in Northern San Francisco Bay. The primary field data we present, which was collected by the USGS California District Office, consists of top and bottom salinity measurements and vertical velocity profiles made with a 1.2 MHZ upward looking ADCP. All data were collected in the western end of Carquinez Strait, a relatively narrow and deep reach of Northern San Francisco Bay (Gartner unpub.). The salinity data (fig 1) show several episodes of sustained stratification that were tied to tidal conditions and freshwater inflow to San Francisco Bay.

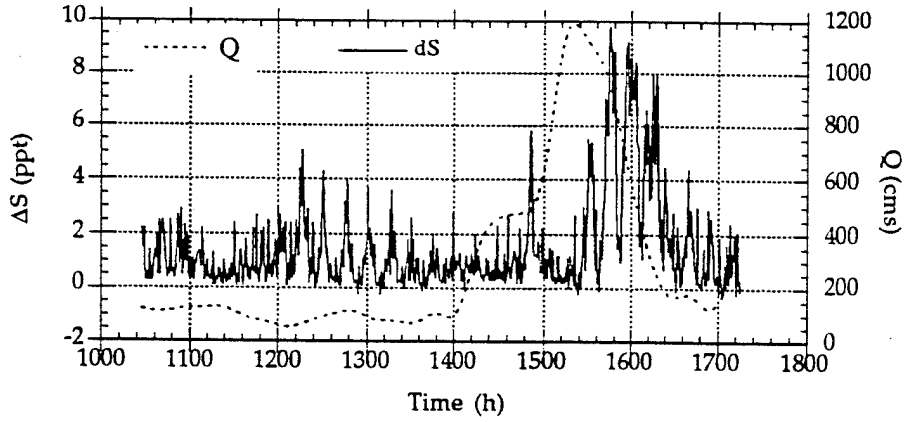

Figure 1: Salinity stratification and river flow Feb-March 1991

Using principal components analysis (PCA), we extracted from the ADCP data for this period two modes of motion (shapes given in fig 2), the first of which represents a stratification-altered barotropic tide that has approximately 98% of the total variance, the other which we take to be unsteady gravitational circulation and which accounts for most of the remaining variance. Both modes exhibit cross channel flows, giving a slight curvature-induced net flow across the channel (Geyer 1993). As shown in figure 3, plots of the amplitudes of pc1 and

---

[1]Also: USGS, Water Resources Division, 2800 Cottage Way, Sacramento, Ca. 95825

pc2 as functions of time, the baroclinic flow varies tidally as well as subtidally. The tidal timescale variability in the baroclinic flow appears to result from the time-variable stratification. When the water column is unstratified, velocities are nearly in-phase through the entire depth; when the water column is stratified, primarily during the ebb, bottom friction only acts of the lower portion of the water column, allowing the upper part of the water column to accelerate nearly unimpeded by bottom friction (Monismith and Fong 1994). Thus ebb-flood asymmetries in tidal currents that lead to gravitational circulation (Jay 1991) naturally arise through ebb-flood variations in stratification.

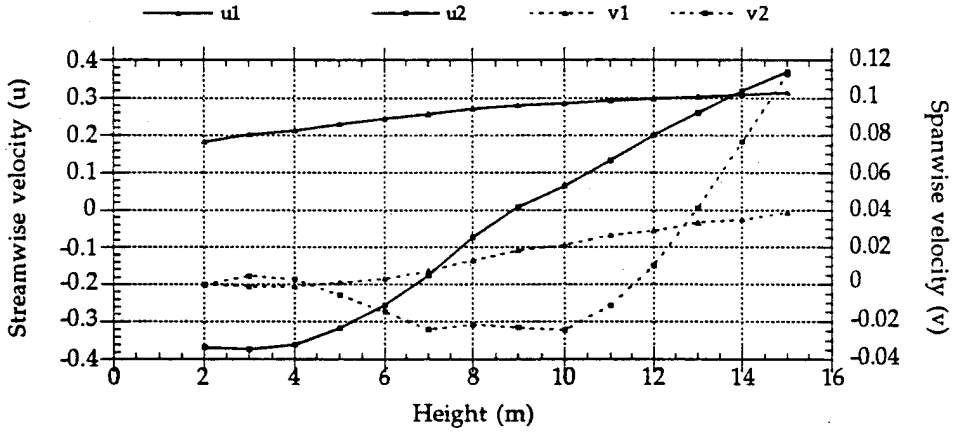

Figure 2: Shapes of first two principal components deduced from ADCP data

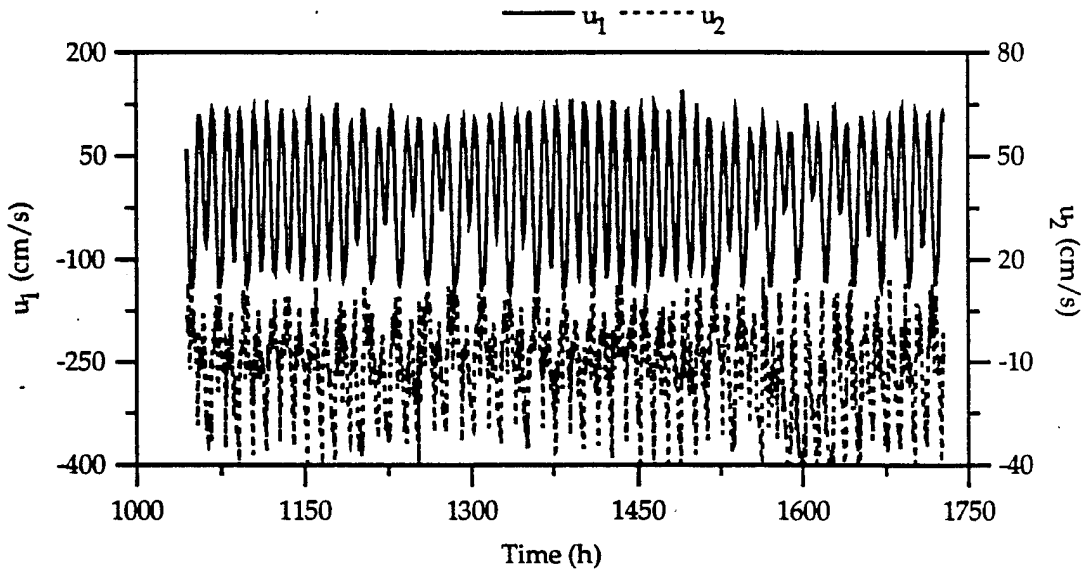

Figure 3: Time series of streamwise components of PC1 and PC2. Magnitude of velocity at 15m induced by each mode. Positive velocities are landward.

The subtidal variation of the gravitational circulation mode is strongly linked to the subtidal variation in stratification. When stratification persists (c. 1500 h), strong (O (20 cm/s)) baroclinically driven subtidal currents develop.

In our model of this flow, currents are driven by a specified tidal barotropic pressure gradient and a constant baroclinic pressure gradient associated with a specified longitudinal salinity gradient. Vertical mixing of momentum and salt are modelled with the Mellor-Yamada level 2.5 closure including a stratification-based lengthscale limit (Blumberg et al 1992). The salinity field also changes in response to sheared advection of the longitudinal gradient. Lastly, a constant pressure gradient proportional to the depth-averaged baroclinic pressure gradient must be specified.

Depending on the constant of proportionality and the tidal pressure gradient, flows resulting in fresh, ocean or two-layer water columns. The latter case arises when the depth-averaged flow is set to zero. The nature of the resulting stratification depends on the parameter $Ri_x = \beta\, g\, \Gamma\, H^2\, U_{max}^{-2}$, where β is the saline expansivity, Γ is the longitudional salinity gradient, H is the fluid depth, and U_{max} is the velocity that would be induced by the specified tidal pressure gradient in the absence of friction. When Ri_x is greater than its critical value, the stratification "runs away" to produce a water column that is half ocean and half fresh water. Additionally, upstream salt fluxes due to shear-stratification correlations dramatically increase. In contrast, when Ri_x is subcritical, tidal mixing is sufficient to produce periodic stratification via Strain Induced Periodic Stratification (Simpson et al 1990).

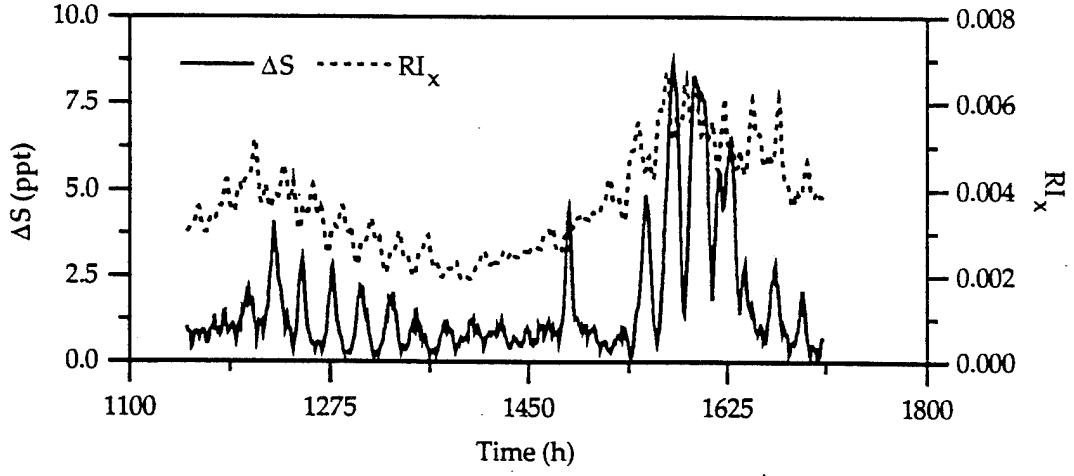

Figure 4: Ri_x and ΔS during Feb-Mar 1991

This behavior is illustrated in figure 4, where we have calculated Ri_x and DS using lowpass filtered (30h) values of U and ΔS. Our interpretation of these

observations is that twice during the period of interest the estuary passed through the critical condition of $Ri_x \approx 0.004$, and stratification began to intensify; when Ri_x dropped again, the stratification weakened again. However, the observed critical value is considerably smaller (roughly a factor of 10) than what we calculate, which may be due to lateral flow variations. Firstly, the stratification is likely to be weaker on the side of the channel where the salinity measurements were made, and, secondly, lateral variations in salinity could lead to enhanced transverse circulation. In this case, vertical mixing over the shoals could be communicated to the deeper channel.

In summary, as seen in the field and in modeling, the unsteadiness of the gravitational circulation modes extracted by PCA is connected intimately to the dynamics of the stratification; it is relatively weak when the water column is well-mixed and strengthens as the water column stratifies during each tidal cycle. When Ri_x becomes supercritical, strong stratification and strong baroclinic flows develop, further intensifying stratification.

Acknowledgements
This work has been partially supported by the EPA San Francisco Estuary Project and by NSF through grant CTS 8958314. We are grateful for continuing support from the the USGS Water Resources Division, California District. We also would like to thank Jeff Gartner, Rick Oltman, Ralph Cheng, Alan Blumberg and Jeff Koseff for their help and advice.

References

Blumberg, A.F., B. Galperin, and D.J. O'Connor, Modeling vertical structure of open channel flows, *J. Hyd. Eng., 118(H8)*, 119-1134, 1992.

Geyer, W. R., Three dimensional tidal flow around headlands, *J. Geophys. Res., 98(*, 955-966, 1993.

Jay, D. A., Internal asymetry and anharmocity in estuarine flows, in *Tidal Hydrodynamics*, ed. B.B. Parker, pp. 521-543, Wiley Interscience, New York, 1991.

Monismith, S.G. and D.A. Fong, A simple model of mixing in stratified tidal flows, submitted to J. Geophys Res (Oceans)

Simpson, J.H., J. Brown, J. Matthews, and G. Allen, Tidal straining, density currents and stirring in the control of estuarine stratification, *Estuaries, 13*, 125-132, 1990.

Simpson, J.H. and J. Sharples , Dynamically-active models in the prediction of estuarine stratification, in *Dynamics and exchanges in estuaries and the coastal zone*, ed. D. Prandle, 101-113, Springer Verlag, New York, 1991.

STUDY OF THE EFFECT OF VARIATION IN VERTICAL MIXING ON ESTUARINE CIRCULATION IN NARROW ESTUARIES USING THEORETICAL AND NUMERICAL MODELS

Kyeong Park and Albert Y. Kuo
Virginia Institute of Marine Sciences, School of Marine Science
The College of William and Mary
Gloucester Point, VA 23062

Abstract

In estuaries, the long-term, large scale transport and distribution of waterborne materials are primarily determined by residual circulation. In narrow estuaries where the flow and salinity distributions are essentially two dimensional in the longitudinal (x) and vertical (z) directions, residual circulation consists of three modes: barotropic flow due to freshwater discharge, baroclinic flow induced by longitudinal density gradient, and wind-induced flow due to wind stress. Positive and negative feedback loops exist among vertical mixing, longitudinal salinity gradient ($\partial s/\partial x$), vertical stratification ($\partial s/\partial z$) and residual circulation (Fig. 1): i.e., the estuarine circulation and the salinity distribution are a coupled problem with positive and negative feedback loops.

This paper addresses the effect of variation in vertical mixing on residual circulation in narrow estuaries excluding wind-induced mode. As vertical mixing varies, it has two opposing effects on estuarine circulation. One is a direct effect, in which increased vertical mixing weakens circulation by enhancing vertical momentum exchange (arrow C in Fig. 1). The other is an indirect effect, in which increased vertical mixing modifies the salinity distribution, strengthens $\partial s/\partial x$, and results in stronger circulation (arrows E and F in Fig. 1). The importance of the latter indirect effect, which involves the response of mass (salinity) distribution, depends on the time scale of the adjustment of salinity distribution relative to that of variation in vertical mixing. The theoretical models of residual circulation in narrow estuaries (Hansen & Rattray, 1965; Prandle, 1985) are analyzed to quantify the relative importance of these two opposing processes.

Although the above theoretical models have been derived by imposing a known density (salinity) distribution, the models are revisited with the inter-dependency of the circulation and the salinity distribution (Fig. 1) in mind. From these theoretical models, two dimensionless ratios, γ and γ_P, which indicate the fractional change in $\partial s/\partial x$ relative to that in vertical mixing as the vertical mixing varies, are identified:

$$\gamma = \frac{\left[\frac{\partial S}{\partial x}\right]_S}{\left[\frac{\partial S}{\partial x}\right]_N} \cdot \left[\frac{(A_z)_S}{(A_z)_N}\right]^{-1} \qquad \gamma_P = \frac{\left[\frac{\partial S}{\partial x}\right]_S}{\left[\frac{\partial S}{\partial x}\right]_N} \cdot \left[\frac{(U_1)_S}{(U_1)_N}\right]^{-1}$$

where S is tidal mean salinity, A_z is vertical turbulent viscosity and U_t is tidal current amplitude. The subscript "S" designates the variables during high vertical mixing (e.g., spring tide) and the subscript "N" designates those during low vertical mixing (e.g., neap tide). These ratios dictate the relative importance of the

two opposing processes on residual circulation as the vertical mixing varies. If γ (or γ_P) > 1, then the indirect effect of increased $\partial s/\partial x$ overcomes the direct effect of increased vertical mixing, and residual circulation increases as the vertical mixing increases. If γ (or γ_P) < 1, then the effect of increased vertical mixing overcomes that of $\partial s/\partial x$, and residual circulation decreases as the vertical mixing increases.

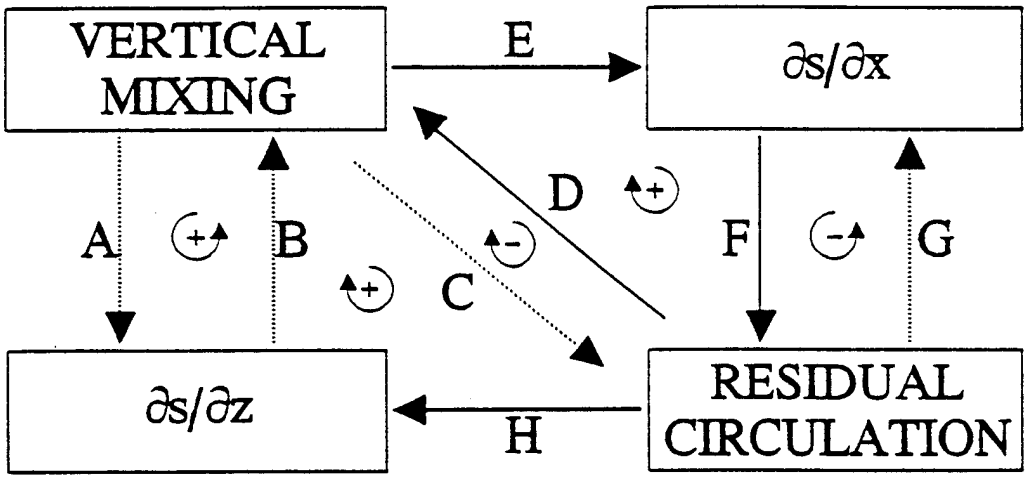

Figure 1. A schematic diagram showing interactions among vertical mixing, longitudinal salinity gradient, vertical stratification and residual circulation. A straight line with an arrow indicates direct effect of one parameter on the other: solid line indicates positive effect and dashed line indicates negative effect, i.e., increase in one parameter decreases the other. An open circle with an arrow indicates a positive (+) or a negative (-) feedback loop.

The three parameters, $\partial s/\partial x$, A_Z and U_t, in terms of which the ratios, γ and γ_P, are expressed, are either difficult (even impossible) or too expensive to measure over an entire estuary. Hence, the vertical two-dimensional hydrodynamic model described in Park & Kuo (1994) is applied to the Rappahannock Estuary, a western shore tributary of Chesapeake Bay, to estimate these parameters. The objectives of this model application are to examine the behavior of the ratios, γ and γ_P, and to study the dominant process(es) in determining the effect of variation in vertical mixing on residual circulation.

The residual circulation and salinity distribution calculated by the numerical model are well explained using the processes illustrated in Fig. 1. Comparison of model calculated residual circulations between spring and neap tides confirms the role of the ratios, γ and γ_P, as indicators of variation in residual circulation. The model results indicate that the variation in residual circulation as the vertical mixing varies is determined by the time scale of variation in vertical mixing relative to the response time of longitudinal salinity distribution. In the Rappahannock Estuary, the fortnightly spring-neap cycle is short compared to the response time of the longitudinal salinity distribution, which is on the order of months. Hence, from neap tide to spring tide, the effect of increase in $\partial s/\partial x$ (arrows E and F in Fig. 1) is not as important as that of increase in vertical mixing (arrow C in Fig. 1), which results in a decrease in residual circulation during spring tide. The model results also show that the boundary conditions on salinity at the river mouth and freshwater discharge at the fall line can modify $\partial s/\partial x$ and overcome the direct effect of vertical mixing on residual circulation.

References

Hansen, D.V. and Rattray, M., Jr. 1965. Gravitational circulation in straits and estuaries. *Journal of Marine Research,* 23(2): 104-122.

Park, K. and Kuo, A.Y. 1994. Numerical modeling of advective and diffusive transport in tidal Rappahannock Estuary, Virginia, pp. 461-474. In: M.L. Spaulding, K.W. Bedford, A.F. Blumberg, R.T. Cheng & J.C. Swanson (eds.), *Proceedings of the Third International Conference on Estuarine and Coastal Modeling, ASCE.*

Prandle, D. 1985. On salinity regimes and the vertical structure of residual flows in narrow tidal estuaries. *Estuarine, Coastal and Shelf Science,* 20(5): 615-635.

COMBINED EFFECTS OF BUOYANCY AND TIDES UPON LONGITUDINAL DISPERSION

Ronald Smith
Mathematical Sciences
Loughborough University of Technology
Loughborough LE11 3TU, UK

Abstract

This paper focuses upon the fluid mechanics of how buoyancy modifies the mixing process and the velocity profile in partially mixed estuaries. In a similar way to the shear augmented Taylor dispersion of solutes, there is a shear-augmented "Taylor viscosity" across the estuary for the longitudinal tidal current. Also, there is transverse advection of longitudinal momentum which results in different velocity profiles between ebb and flood. As a consequence, the longitudinal dispersion of salinity or of other solutes exhibits different dilution rates between ebb and flood.

Introduction

Along the minor estuaries in the UK the summer drought of 1976 was aggravated by salinity penetration many tens of kilometres upstream. Farmers who traditionally could rely on extracting fresh water for irrigation from what they regarded as rivers far from the sea, found that they were damaging their crops with brine. By contrast, along the major estuaries such as the Humber and the Thames, the salinity penetration was not very different from any other summer.

The salinity distribution along a partially mixed estuary can be explained as a balance between the flushing out to sea by the fresh water run-off and the diffusion-like spreading upstream of the salt. In a drought the fresh water run-off is greatly reduced. So, if the longitudinal spreading remained unchanged, the salt (and the salinity gradient) would penetrate further upstream. For small estuaries the effective longitudinal diffusivity can increase as the fresh water run-off decreases, giving exaggerated salinity penetration (Smith, 1977). However, in large estuaries both theory (Fischer, 1972, Smith, 1980) and observation (Williams & West, 1974, Uncles & Radford, 1980) concur that as the fresh water run-off decreases, so does the effective longitudinal diffusivity. Hence, the low vulnerability of large estuaries to salinity penetration.

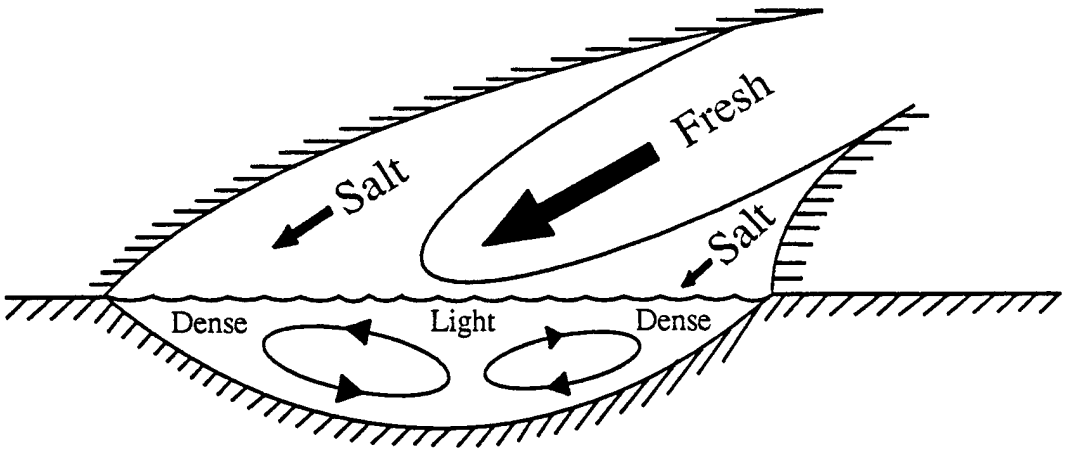

Figure 1a: During the ebb tide the faster flow near the centre of the estuary carries lighter fresh water further seawards and results in density differences across the estuary.

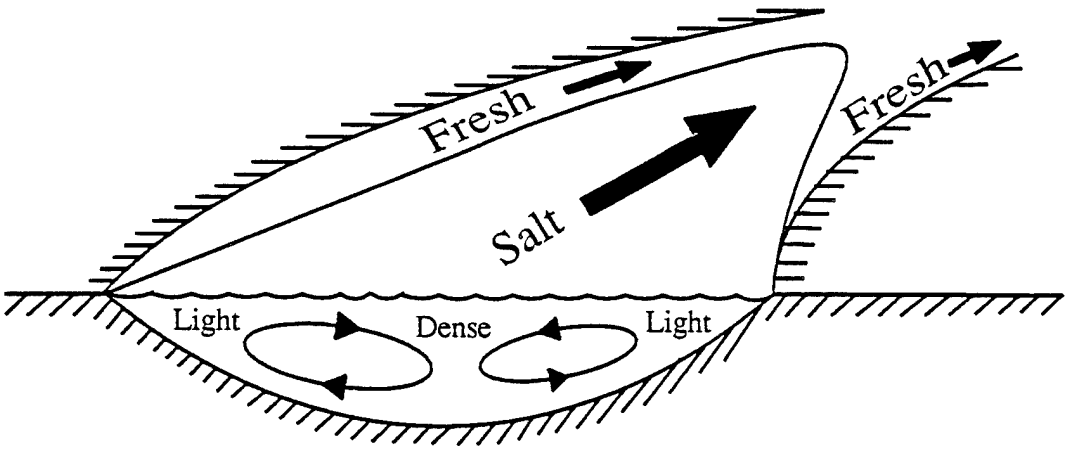

Figure 1b: During the flood tide the density tends to be greater in the centre than at the sides. This drives a density-driven circulation.

The key ingredient that makes the longitudinal spreading depend upon the run-off is the fact that the transverse flow and the resulting transverse mixing process in a well-mixed estuary is affected by the salinity, as illustrated in figures 1a,b.

An easy way to confirm the existence of the transverse flow is to observe the movement of surface debris or of scum-lines (Nunes & Simpson, 1985). On the ebb, flotsam tends to be carried towards the banks as suggested in figure 1a. While during flood tide flotsam tends to accumulate towards the middle of the estuary as suggested in figure 1b. Detailed measurements of the flow and salinity structure are presented by Guymer & West (1991).

Shear Dispersion Mechanism

The way that non-uniform flows dramatically effect the rate of spreading was first explained by Townsend (1951)in a paper communicated to the Royal Society of London by G I Taylor. Figure 2 gives a graphical version of the way that both shear and diffusion are involved in the transverse dilution process.

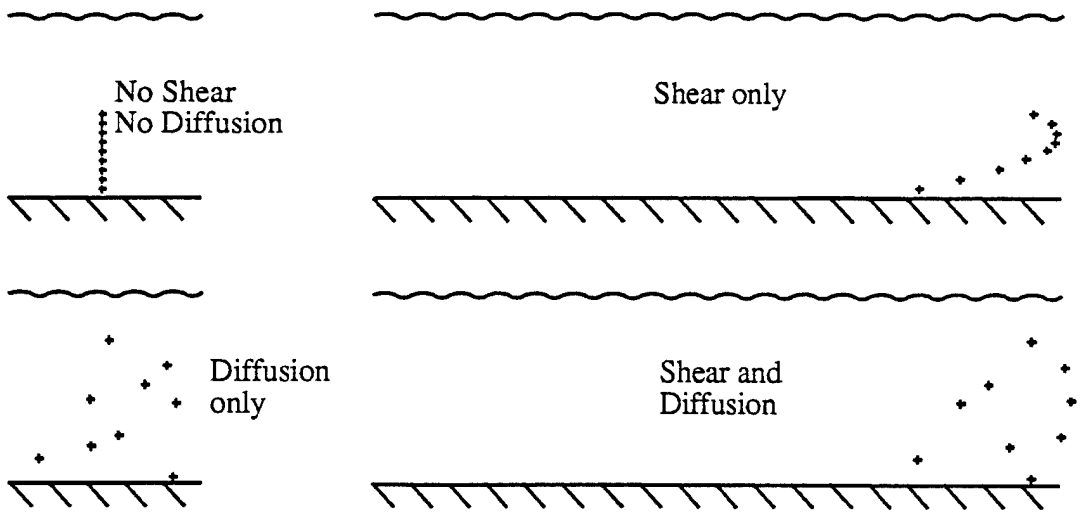

Figure 2: The process of shear dispersion in the density-driven circulation across an estuary.

If there were neither shear nor diffusion then salt or any other tracer would merely be transported along with the mean flow. A line of small circles and crosses would remain exactly in line. If instead there were shear but no diffusion, then the line of circles and crosses would become increasingly sheared out into a curve whose shape revealed the shape of the velocity profile. Hence, in the upper right-hand part of figure 2 we infer that the velocity profile is to the left at the (wavy) free surface, to the right deeper down and reduces to zero at the (hatched) bed. At any level within the flow there is zero horizontal spread. It is only by vertically averaging that there is the false illusion of spread which increases linearly with time. When there is diffusion, but no shear, the line of circles and crosses gradually become spread out both vertically and horizontally. The horizontal size increases as the square-root of time (horizontal variance increases linearly with time). Finally, when there is both shear and diffusion the distribution of circles and crosses (or any solute) exhibits some of the features of the pure shear and of the pure diffusion. In the lower right-hand part of figure 2 we see that near the (wavy) free surface the centroid of the particles is displaced to the left, whilst lower down the centroid becomes displaced to the right. Some of the horizontal spread is inherited from the diffusion (for example a few of the crosses are slightly ahead of where they could have reached by advection alone). Importantly, the vertical migration of the particles combined with the shear gives rise to a considerably augmented horizontal variance.

Townsend (1951) showed that, away from boundaries, as time increases the shear contribution to the variance eventually dominates the diffusive contribution. Initially, the shear dispersion is proportional to the square of the local shear. Hence the much greater horizontal spread of the circles than of the crosses in figure 2.

Taylor Dispersion Coefficient Across a Shallow Estuary

Eventually the vertical diffusion the circles and crosses, would smooth out any differences in the rate of dispersion at different levels. G I Taylor (1953) showed that beyond this time scale of mixing across the flow, the shear dispersion process becomes diffusive in character. The shear dispersion can then be characterized by the increase in the effective diffusivity along the flow: the Taylor (or shear) dispersion coefficient. Taylor (1953) calculated the shear dispersion coefficient for laminar pipe flow and verified his results experimentally. What makes G I Taylor's work so important is that the method of calculation is readily adapted to other flows or to encompass additional physics.

For a shallow partially mixed estuary of total depth $(h+\zeta)$, with a cross-flow velocity profile $\mathrm{v}(x,y,z,t)$ and vertical diffusivity $\kappa_3(x,y,z,t)$ the eventual Taylor dispersion coefficient $D_2(x,y,t)$ across the estuary is given by the double integral :

$$D_2 = \frac{1}{(h+\zeta)} \int_{-h}^{\zeta} \frac{1}{\kappa_3} \left[\int_{-h}^{z} (\mathrm{v} - \|\mathrm{v}\|) \mathrm{d}z' \right]^2 \mathrm{d}z \quad , \tag{3.1}$$

$$\text{with} \quad \|\mathrm{v}\| = \frac{1}{(h+\zeta)} \int_{-h}^{\zeta} \mathrm{v}\, \mathrm{d}z \quad . \tag{3.2}$$

Hence, the stronger the buoyancy-driven transverse flow $\mathrm{v}(x,y,z,t)$ the greater the effective mixing across the estuary. (The co-ordinate system (x,y,z) is assumed to be aligned along, across and vertically with respect to the long shallow estuary.)

The shallowness of the water is required to ensure that the vertical mixing occurs more rapidly than any reversal of the tidal flow. The formula (3.1) exhibits

several standard features of shear dispersion coefficients. There is inverse dependence upon the mixing κ_3 and quadratic dependence upon the velocity shear $(v-\|v\|)$.

Taylor Viscosity Across a Shallow Estuary

An important recent development has been the recognition that the longitudinal velocity distribution is itself subject to shear dispersion (Scott, 1994, Svendsen & Putrevu, 1994). If we envisage the circles and crosses in figure 2 as being parcels of fluid, then as they are advected and diffused the parcels of fluid carry longitudinal momentum from one part of the estuary cross-section to another. The combined effect of shear and diffusion is to give lateral mixing (effective viscosity). Since the physical mechanism is akin to that of Taylor dispersion, the description "Taylor viscosity" will be used.

Provided that the vertical diffusivity $\kappa_3(x,y,z,t)$ is replaced by the vertical eddy viscosity $\nu_{13}(x,y,z,t)$, the no-slip boundary condition for the velocity at the bed is the counterpart to a solute which is perfectly absorbed at the bed (Smith, 1986). The normalized shape $\Phi(x,y,z,t)$ of the velocity profile with zero driving force is the lowest eigenmode of the equation:

$$\partial_z(\nu_{13}\partial_z\Phi)+\mu\Phi=0 \ , \text{ with } \|\Phi^2\|=1 \ , \qquad (4.1a,b).$$

$$\text{where } \nu_{13}\partial_z\Phi=0 \text{ on } z=\zeta \text{ and } \Phi=0 \text{ on } z=-h \ , \qquad (4.1d,e)$$

The eigenvalue $\mu(x,y,t)$ is related to the local drag at the bed and would be the time decay rate if the longitudinal motion were unforced.

The equation satisfied by the longitudinal velocity $u_0(x,y,t)=\|u\Phi\|$ is the Φ-component of the longitudinal momentum equation (in conservation form):

$$\begin{aligned}&\partial_t\{(h+\zeta)u_0\}+\partial_x\{(h+\zeta)\|\Phi^3\|u_0^2\}+\partial_y\{(h+\zeta)\|v\Phi^2\|u_0\}-f\|v\Phi^2\| \\ &=-g(h+\zeta)\|\Phi\|\partial_x\zeta-\mu(h+\zeta)u_0+\partial_y\{(h+\zeta)(\|\nu_{12}\Phi^2\|+N_{12})\partial_y u_0\}\end{aligned} \qquad (4.2)$$

For a solute the Coriolis and gravitational forcing terms would be absent (Smith, 1986). The omission of the Φ,Φ^2 and Φ^3 factors was of little consequence in the specific examples considered by Svendsen & Putrevu (1994) but are vital in the following discussion.

The non uniform vertical distribution Φ (zero at the bed, maximum at the free surface) implies that for longitudinal momentum the effective transverse advection is the weighted velocity $\|v\Phi^2\|$. Even if there is no net flow $\|v\|$ across an estuary, there can be transverse advection of longitudinal momentum. In particular, during ebb tide (figure 1a) longitudinal momentum is carried towards the shoreline, implying flattened longitudinal velocity profiles $u_0(y,t)$. While during flood (figure 1b), the transverse circulation and advection of longitudinal momentum are reversed, implying steepened longitudinal velocity profiles Such tidal asymmetries are noted by West & Mangat (1986) and by Scott (1994).

The transverse Taylor viscosity $N_{12}(x,y,t)$ for the longitudinal velocity $u_0(x,y,t)$ is given by a weighted version of equation (3.1) :

$$N_{12} = \frac{1}{(h+\zeta)} \int_{-h}^{\zeta} \frac{1}{\nu_{13}\Phi^2} \left[\int_{-h}^{z} \left(v - \left\| v\Phi^2 \right\| \right) \Phi^2 dz' \right]^2 dz \ . \tag{4.3}$$

During both ebb and flood the Taylor viscosity N_{12} augments the weighted average eddy viscosity $\left\| \nu_{12}\Phi^2 \right\|$ in smoothing-out transverse gradients of the longitudinal velocity.

A TWO-DIMENSIONAL BAROCLINIC MODEL FOR THE HALIFAX HARBOR

Kim T. Tee and Brian Petrie
Physical and Chemical Science Branch
Department of Fisheries and Oceans
Bedford Institute of Oceanography
Dartmouth, N. S., Canada. B2Y 4A2

Abstract

For over 200 years raw sewage has been dumped into Halifax Harbor resulting in the building of deposits of material and metals in the sediment and dissolved metals in the water. The concentration of these variables is sensitive to the mean circulation of the harbor. Halifax Harbor is an estuary, i.e., a semi-enclosed body of water whose properties and circulation are influenced by freshwater runoff from the land. The circulation in such an estuary would feature outflow towards the shelf in the upper layer and inflow towards the head of the Harbor with mixing between the 2 layers. The upper layer salinity would increase as the water moved towards the shelf because of the mixing with the deeper, saltier waters. By similar reasoning, the deeper waters would freshen as they moved from the shelf towards the head of the estuary. However, the input of the raw sewage along the harbor and a wind forcing may change this simple feature of the salinity variation. The objective of this paper is to simulate the mean circulation of the Halifax Harbor using a 2-D (horizontal and depth) model.

The equations of the model are:

$$(uB)_t + (uuB)_x + (uwB)_z + Bg\zeta_x + Bg/\rho\left(\int_{z'}^{0}\rho dz'\right)_x - \left(BAu_x\right)_x - \left(BNu_z\right)_z + \lambda uB_z = 0 \qquad (1)$$

$$\left[\int_{-h}^{0}(uB)dz\right]_x = 0 \qquad (2)$$

$$(SB)_t + (SuB)_x + (SwB)_z - \left(BkS_x\right)_x - \left(BMS_z\right)_z = 0 \qquad (3)$$

$$(uB)_x + (wB)_z = 0 \qquad (4)$$

$$\rho = \rho_0(1+\beta S) \qquad (5)$$

where (1) is the momentum equation for u, (2) the continuity equation, (3) the salt conservation equation for S, (4) the equation for calculated w, and (5) the equation of state with coefficient $\beta = 7.5 \times 10^{-4}$ per ppt (part per thousand). The notations in the equation are: x,z are Cartesian Co-ordinates where x is positive seaward from the head of the estuary, and z is positive upward from the surface. u,w are velocity components in the x and z directions. A,N are the horizontal and vertical eddy viscosity. K,M are the horizontal and vertical eddy diffusivity. B is the width of the estuary, which is a function of x and z. ζ is the surface elevation. The variables t and s are time and salinity. The parameters g, h, λ, ρ, and ρ_0 are respectively the gravity, depth, linear friction coefficient, density of the

sea water, and density of the freshwater. As for the eddy viscosity and diffusivity, the vertical components are depth dependent (functions of the Richardson number), and the horizontal components are constant. The subscript t, x and z are denoted as differentiating with respect to time, along-channel distance, and depth.

The above equation are written in the finite difference form and solved using the boundary condition of rigid lid and no salt flux on surface, zero normal velocity and no salt flux on coastal wall, and slip boundary condition at the bottom ($Nu_z=\lambda u_b$). At the head of the estuary, we specify the volume transport of the river runoff, and set S=0 (fresh water) at all depths. At the surface, the climatological wind velocity of Shearwater near Halifax in winter is applied. At the side wall, the sewage outflow at surface with zero salinity are specified. There are two components of sewage outflow: the point source at certain locations and the distributed source at all locations. the grid spacing is constant for the x-direction, and variable in the z-direction. The numerical formulation of the government equations, similar to Bryan's three dimensional ocean circulation model, has been shown to conserve energy, mass and salt.

The numerical model was run with time step of 100 sec until the solution reach a steady state (several months). This requires 50000-100000 iterations. The results show a two layer circulation with outflow in the top layer and inflow in the lower layer. This computed current shows the characteristic flow pattern of the estuarine circulation of a partial mixed estuary. The salinity in the upper layer increase toward the oceanic boundary. However, there is a slight decrease of salinity toward the ocean at 5-10 m layer. In the deep layer (over 15 m), the salinity along the Harbor varies only slightly.

The observations include a CTD measurement by F. Jordan of the Bedford Institute of Oceanography in the winter of 1970 (November 1970 to April 1971). The measurement involved six sections: three sections in the Bedford Basin (sections F, G and H), one section in Halifax narrow (section E) and two sections in the outer Harbor (sections C and D). The average salinity at section C is used as the specified salinity in the lower layer at the oceanic boundary.

The current meter measurements were taken near the boundary between the Bedford Basin and Halifax Narrow. The results indicated a two layer flow with outflow in the top layer and inflow in the lower layer.

By chosen a reasonable coefficients, the computed velocity and salinity are compared with the measurements. The result shows that most of the observed salinity and velocity can be reproduced except the decrease of observed surface salinity toward the ocean in the Bedford Basin. The reason for such disagreement is under investigation.

Also included in the study is a series of numerical experiments to examine the sensitivity of the numerical model to various parameters including the horizontal and vertical eddy viscosity and diffusivity, the wind stress, the shape of the cross section, and the sewage outflow. It was found that the runoff from the Sackville River at the head of the Harbor is the major contributor. The estuarine circulation is enhanced by wind forcing, but reduced by sewage outflow. The wind effect is most significant near the surface (within 2 m). The sensitivity of the model result to the shape of the Halifax section, and to the horizontal and vertical eddy viscosity and diffusivity will be described.

BUOYANCY PHENOMENA AND SALINITY IN THE TWEED ESTUARY

R. J. Uncles and J. A. Stephens
Plymouth Marine Laboratory
Prospect Place, The Hoe
Plymouth PL1 3DH, U.K.

Abstract

Results are presented from a two week field programme in the Tweed Estuary. Maximum values of the Estuarine Richardson Number, Ri_E, occurred during neap tides and minimum values during spring tides. Estimated values of Ri_E varied between 0.3 and 2.3, indicating partially mixed to strongly stratified conditions, depending on tidal state and freshwater inflow. These relatively large values of Ri_E were consistent both with strong salinity stratification and large salt fluxes due to vertical shear transport. The salinity intrusion was a strong function of spring-neap tidal state and a weaker function of freshwater inflow. The estimated salinity intrusion varied from about 4.7 to 7.6km during the fieldwork period. The strong dependence on tidal range followed from the comparable lengths of the tidal excursion and salinity intrusion. Long excursion lengths were also partly responsible for the short residence (or flushing) times and their strong dependence on spring-neap tidal state. For typical summer freshwater inflows of 40 m^3 s^{-1}, the estimated residence times varied from one tide at large spring tides (removal on one ebb) to two tides (removal over two ebbs) at neap tides. A complex pattern of frontal systems was observed throughout the estuary. A tidal intrusion front sometimes occurred at the constricted mouth. The seaward reaches of the estuary were particularly complex. Large areas of high salinity waters abutted waters of much lower salinity with the formation of distinct frontal systems. Longitudinal foam lines, associated with axial convergences, sometimes occurred in the seaward reaches and further into the estuary.

Introduction

In this report we present results from a two week field programme in the Tweed Estuary during 14-29 September 1993. The mouth of the Tweed is located at Berwick-upon-Tweed (Berwick). The River Tweed and its tributaries drain a sparsely populated, mainly agricultural area on the eastern borders of England and Scotland. The river is categorized as of the highest quality in the British national river classification. It is particularly important as a fishery for trout and salmon.

The Tweed is a fairly steeply rising and shallow estuary. Anecdotal evidence places the tidal limit about 13km from the mouth. The width at the tidal limit is about 100m and the width near the old Berwick Bridge, at 2km from the mouth, is about 300m. Further down-estuary, the width increases to about 600m in the vicinity of the harbour. The width at the mouth is confined between the pier and a sand spit, which is exposed at low water. The width there is about 50m at low water. Depths at high water are typically a few metres in the upper estuary and several metres in the lower estuary. The estuary can be strongly stratified with respect to salinity and buoyancy effects are then very important.

Observations

Longitudinal transects were undertaken throughout the saline reaches of the Tweed. Vertical profiles of salinity, temperature and suspended particulate matter concentrations (SPM) were obtained from surface to bed at between 7 to 18 stations (depending on tidal state) along a deep-channel transect.

Two near-bed instrument packages ('rigs') were deployed during the survey. Salinity, temperature, pressure and SPM concentrations at 0.25m above the bed were recorded. The Bridges rig was deployed between the rail bridge and the new road bridge (2.3km from the mouth) during 17 to 29 September. The Toddies Shiel rig (4.7km from the mouth) was deployed during 18 to 29 September.

Profiling measurements of longitudinal currents, salinity, temperature and SPM concentrations were made between surface and bed at two stations on three occasions during the field work. An anchor station was worked for 7h on 28 September near the Toddies Shiel rig, covering the duration of saline intrusion there. Anchor stations for periods of 10.5h and 3.5h were worked near the Bridges rig on 23 and 26 September, respectively.

Results

The root-mean-square (RMS) surface elevations at the Bridges rig, 2.3km from the mouth, varied between approximately 1.6m and 0.8m during the deployment. The RMS surface elevations at the Toddies Shiel rig, 4.7km from the mouth, varied between approximately 1.0m and 0.5m. Therefore, a considerable up-estuary reduction in tidal amplitude occurred over the 2.4km between rigs. The up-estuary reduction in RMS elevations was accompanied by a reduction in RMS current speeds at 0.25m above the bed. RMS current speeds at the Bridges rig varied between 0.43 and 0.22 m s^{-1} and those for the Toddies Shiel rig varied between 0.30 and 0.18 m s^{-1}.

The longitudinal and vertical salinity distributions within the Tweed depended strongly on tidal range and freshwater inflow. The tendency for the Tweed to be partially mixed on the late flood at spring tides was illustrated on 20 September, when the high-water level at North Shields was 5.0m (mean springs) and the freshwater inflow to the Tweed was 34 m^3 s^{-1} (typical summer inflow). The tendency for stratified conditions at neap tides was illustrated on 25 September, when the high-water level at North Shields was only 4.0m (approximately mean neaps) and the inflow was 33 m^3 s^{-1}, nearly the same as that on 20 September.

Observed salt intrusions during the longitudinal transects compared reasonably well with those estimated from tidal excursions of the salt wedge 'nose' deduced from rig data. Where rig and transect time-series did not overlap, intrusions estimated from transect data compared well with those computed from a multiple regression, which was based on rig data. Overall, agreement was very satisfactory.

Residence times (freshwater flushing times) of the Tweed were estimated from measured freshwater volumes within the estuary. These were computed as functions of distance between the mouth and the assumed tidal limit (13km from the mouth). Volumes were computed from salinity data measured during the longitudinal transect of maximum salt intrusion, close to the time of high-water. Dividing these volumes by the freshwater inflow to the estuary, averaged over the tidal cycle leading up to each surveyed high-water, provided an estimate of the residence times at various locations along the estuary.

An investigation of frontal features in the seaward reaches of the Tweed was undertaken during the afternoon flood on 21 September. A tidal intrusion front first appeared in the mouth region at 2.3h after low-water. The buoyant surface waters of the coastal ebb plume were forced back towards the mouth of the estuary. The front was located at the constricted mouth and was slightly convex towards the sea by 2.7h after low-water. Within 10min, the surface front was slightly concave. By 2.7h before high-water the surface plume was 'V' shaped with the 'V' pointing inwards. The surface salinity within the 'V' was approximately 34ppt, whereas that immediately outside it was approximately 15ppt. By 2.4h before high-water the 'V' had progressed slightly further into the estuary with one frontal arm 'tied' to the end of the sand spit and the other moving inwards and along the harbour pier wall. At this time a foam line was apparent, moving away from the 'V' of the intrusion front and following the curvature of the deep channel.

A series of photographs was taken of the outer Tweed from an elevated site on the southern shore. The series commenced at 2.2h before high-water and ended 1h before high-water. A complex pattern of foam-highlighted fronts was observed, with some consistent features which were reproduced throughout the period. These features were generated by the interaction of tide, topography and buoyancy.

A surface transect was worked over a 15min. period centered on 0.9h before high-water. A self-recording salinometer was strapped to the side of an inflatable which was then steered between navigation points. The salinometer recorded surface salinity at 6s intervals. Surface salinity was a complex function of time during the transect. If the time-axis is also viewed as a distance-axis, then two spatially separated frontal systems are evident from the record which also had clear visual manifestations.

Conclusions

(1) Maximum values of the Estuarine Richardson number, Ri_E, occurred during neap tides and minimum values during spring tides. The importance of tidal state arose from the dependence of tidal mixing power on the cube of current speed. Estimated values of Ri_E varied between 0.3 and 2.3, indicating partially mixed to strongly stratified conditions, depending on tidal state and freshwater inflow. These relatively large values of Ri_E were consistent both with the strong stratification and the large salt fluxes which arose from vertical shear transport in the Tweed.

(2) Estimates of the Layer-Richardson Number, Ri_L, suggested that tidal mixing had a non-negligible influence on the halocline thickness and its vertical position for most of the tidal cycle. Only for relatively short periods (1-2h) over high-water slack and, under very stratified conditions, immediately following the intrusion of the salt wedge 'nose', was mixing ineffective.

(3) Low values (<0.25) of the gradient Richardson Number, Ri, were generally observed close to the bed on the flood, suggestive of tidal mixing there, and higher (>0.5) values in the halocline, indicating stability there. A velocity maximum occurred within the halocline during early flood. Turbulence reduction in the interior of the halocline probably occurred in the Tweed when stratification was strong.

(4) Wave-like spatial oscillations of the halocline occurred on the ebb. The oscillation troughs were situated above deep holes located just down-estuary of the rail and old road bridges. There was an indication that the constricted flow between the bridges arches resulted in enhanced mixing of near surface waters and a thickening of the halocline. It is also possible that these wave-like structures in the isohalines were stationary, near-critical

internal lee waves, triggered by the deep holes.

(5) Trapping of high salinity waters occurred on the ebb in the Tweed when bottom mixed waters, located beneath the halocline and unable to mix further upwards, were isolated within a deep hole or deeper section of bed by the falling halocline. When the salt wedge moved further down-estuary, the 'trapped' water was subjected to strongly ebbing, overlying fresh-water, and was subsequently entrained and flushed.

(6) Maximum salt intrusion occurred after local high-water. At high-water the near-bed currents were slow, but still flooding, and often remained slack for some time into the falling tide. Slack-water at the surface occurred before high-water. The time lag between start of surface ebb and near-bed ebb was 1-2h. This lag was a result of buoyancy-driven currents. These currents were enhanced because of the very weak vertical mixing which occurred in the halocline and upper layer over the high-water slack period.

(7) The salinity intrusion was a strong function of spring-neap tidal state and a weaker function of freshwater inflow. The estimated salinity intrusion varied from about 4.7 to 7.6km during the fieldwork period. The strong dependence on tidal range followed from the comparable lengths of the tidal excursion and salinity intrusion.

(8) Long excursion lengths were also partly responsible for the short residence (or flushing) times and their strong dependence on spring-neap tidal state. For typical summer freshwater inflows of 40 $m^3 s^{-1}$, the residence times estimated from a regression formula varied from one tide at large spring tides (removal on one ebb) to two tides (removal over two ebbs) at neap tides. Computed residence times were shorter for typical winter inflows of 140 $m^3 s^{-1}$ but, physically, flushing still required one to two ebbs, depending on tidal state.

(9) A complex pattern of frontal systems was observed throughout the estuary. A tidal intrusion front sometimes occurred at the constricted mouth. An inflow Froude number criterion, when applied to the constricted mouth, appeared to control the timing and shape of the 'plunge' line. The seaward reaches of the estuary were particularly complex. Large areas of high salinity waters abutted waters of much lower salinity with the formation of distinct frontal systems. These systems were largely controlled by the bathymetry of the region, especially the shoal morphology. Longitudinal foam lines emanated from the mouth and were associated with ridges of high salinity surface waters. Either side of these high salinity ridges were less saline surface waters. Similar longitudinal foam lines, associated with axial convergences, sometimes occurred further into the estuary. Here, lateral salinity gradients were generated by two mechanisms: tidal straining of the longitudinal salinity gradient and sideways displacement of low salinity waters which had earlier occupied the deep channel during the late ebb and early flood.

INTERNAL MOTION IN A STRATIFIED ESTUARY

Robert E. Wilson
Marine Sciences Research Center
State University of New York
Stony Brook, NY 11794-5000

Abstract

Introduction

During the period 04/28/93 to 05/05/93 intensive observations were conducted within a 10 km reach of the lower Hudson River Estuary to obtain a description of the intratidal variations in velocity and salinity under high river flow conditions. During the period spanned by the experiment, the barotropic tide was accelerating from neap to spring conditions. One specific objective was to obtain sufficient data to evaluate terms in both the longitudinal and lateral momentum balance on ebb and flood.

Cruise strategy involved repeated longitudinal sections and repeated adjacent lateral sections. The instruments used were a 1200 kHz narrowband ADCP on a towed surface sled, an AMS CTD and a 200 kHz echosounder. A GPS was used for navigation. Data from repeated transects were used to construct time series which could subsequently be analyzed by least squares methods. The time required to complete one transect was short enough so that it could be considered quasi-synoptic.

This reach exhibits large fractional changes in both depth and channel cross sectional area. This morphology produces large along channel accelerations in the barotropic current. During neap tide conditions, salinity structure on ebb is characterized by a broadened halocline region and very large amplitude excursions of the halocline. The transition from ebb to flood at a particular station was typically associated with the passage of a weak bottom salt front. As the salt front passes the halocline is elevated and sharpened. During maximum flood, along channel halocline slopes were much reduced from those encountered during ebb.

Analyses

The analyses described in this paper relate to an evaluation of terms contributing to the instantaneous longitudinal momentum balance over the length of the reach on both ebb and flood. They relate also to the change in the nature of this balance from neap to spring tide conditions.

More specifically, the longitudinal baroclinic pressure gradient at points within the reach was estimated from data at adjacent channel CTD stations. ADCP ensembles having times corresponding (with given tolerance) to those of the adjacent CTD casts were used to estimate directly that contribution to the inertial acceleration which depends on along channel gradients in velocity. The remaining contribution depending on the vertical velocity and on shear required estimation of the vertical velocity. For this purpose, two methods of estimating vertical velocity were compared: the first depending on a laterally integrated continuity equation, the second on the assumption that isohalines corresponded to streamlines. Data from adjacent lateral transects afforded a check of these methods.

Results

Evaluation of the baroclinic pressure gradient emphasizes that during neap tide conditions it is dominated by the halocline slope, especially on ebb. The sign of the baroclinic pressure gradient depends almost exclusively on the sign of the halocline slope. Even during flood, when the magnitude of the halocline slope and the amplitude of its along channel variations are appreciably reduced from those encountered during ebb, the halocline slope is still the major contribution to the baroclinic pressure gradient. In particular it exceeds the contribution from the along channel density gradient within the lower layer.

Comparison of the vertical structure of the baroclinic pressure gradient with that of the total inertial accelerations (including the contribution depending on vertical velocity and shear) emphasizes that during maximum ebb under neap tide conditions the momentum balance is nearly inertial. Details in the structure of the baroclinic pressure gradient are also found in the vertical structure of the inertial accelerations. That contribution to the inertial accelerations which depends on vertical advection is comparable that depending on horizontal advection. comparisons indicate that the contribution of stress divergence to the momentum balance is very small during ebb. Richardson numbers were estimated from the 1 m ADCP data and from the CTD data subject to the same window as the ADCP data. During ebb under neap tide conditions the magnitude of these estimates typically did not fall below 0.5.

During maximum flood, comparison of the vertical structure of pressure gradient and inertial accelerations indicates that an inertial balance is maintained within the upper water column, and that there is some contribution to stress divergence within the lower water column.

Discussion and Implications

The behavior of a continuously stratified fluid in which the momentum balance is inertial has been investigated by Long (1953,1955). His results suggest that the flow is defined in terms of an internal Froude number F

$$F = U/ND$$

where U is the depth mean flow, N is the Vaisala frequency and D is the depth. Long predicts that a critical value for the internal Froude number is $1/\Pi$. As the Froude number approaches $1/\Pi$ turbulence and mixing within the interior of the water column is generated by the steepening and breaking of long internal waves resulting in hydraulic jumps.

Estimates of internal Froude numbers from ADCP and CTD data emphasize that during ebb under neap tide conditions the values fall below $1/\Pi$. For a fixed stratification found during ebb under neap tide conditions, the Froude number does exceed $1/\Pi$ as the barotropic currents accelerates into spring tide conditions.

Long term moorings within this reach emphasize that during neap tide conditions Froude numbers during ebb are below $1/\Pi$ and that they exceed $1/\Pi$ at precisely the time of the neap to spring transition in stratification.

The fact that the momentum balance is basically inertial, and the observed dependence of flow behavior on internal Froude number indicate that internal hydraulic jumps are important mechanisms for turbulence generation and mixing. Partch and Smith

(1978) reached these same conclusions in connection with mixing processes in the Duwamish. They concluded that intense mixing events were associated neither with turbulence generated by bottom friction or by interfacial shear. They did, however, coincide with conditions of nearly critical flow on ebb which would lead to the formation of localized hydraulic jumps.

References

Long , R.R. 1953. Some aspects of the flow of stratified fluids. I: A theoretical investigation. *Tellus,* 5:43-58.

_____ 1955. Some aspects of the flow of stratified fluids. III: Continuous density gradients. *Tellus,* 7:341-357.

Partch, E.N. and J.D. Smith, 1978. Time dependent mixing in a salt wedge estuary. *ECMS,* 6:3-19.

CHARACTERIZATION OF FINE-GRAINED SEDIMENTATION IN ELONGATED BASINS BY THE SETTLING VELOCITY/DENSIMETRIC VELOCITY RATIO

Paul C. -P. Lin[1] and Ashish J. Mehta[2]
[1]Coastal Technology Corporation
Coral Gables, FL 33143
[2]Coastal and Oceanographic Engineering Department
University of Florida
Gainsville, FL 32611

Abstract

Suspended fine-grained sediment can enter coastal basins via tidal advection and as a turbid current. The latter mechanism can be particularly important in microtidal environments where turbidity is often generated and transported episodically. Thus, for example, commonly occurring elongated basins such as docks and residential canals are susceptible to infilling patterns characteristic of turbidity-driven sediment transport. In order to elucidate the basics of this problem, front behavior, flow circulation and sedimentation associated with moderate concentration turbidity currents propagating along a shallow horizontal channel were investigated. Fine-grained sediments of wide ranging properties were used to generate the turbid suspension. Results on the general characteristics of front motion, induced flow patterns, suspension profiles and the pattern of sedimentation indicated that important features characterizing the behavior of decelerating turbidity currents are contingent upon the ratio of particle settling velocity to the densimetric velocity, referred to here as the relative settling velocity, and on the densimetric Reynolds number. The speed of the turbid front and mean concentration below the interface showed exponential-type decrease with distance, with corresponding trends in sediment deposition and particle sorting with distance. The significance of the relative settling velocity as a transport governing parameter is briefly explored, and an expression for the rate of sediment intrusion is developed.

Introduction and Background

Turbidity-induced density currents are driven by an excess gravity force due to the presence of sediment-laden water relative to the ambient sediment-free water. Such currents can be erosional or depositional depending on the initial consolidation history of the deposit. In this study, the decelerating and depositional type turbidity current resulting from settling of initially suspended fine sediment has been experimentally examined.

To generate a continuous turbidity current, a T-shaped plexiglass flume, schematically depicted in Figure 1, was designed. It consisted of a long side channel of 14.7m length and 0.1m width orthogonally connected to the main channel. The height of the channel was 0.2m. The side channel was filled with sediment-free water and separated from the turbulent sediment-laden flow in the main channel by a gate. Turbidity current was produced by lifting the gate to allow the sediment-laden water to move into the side channel. Sediment concentration and flow conditions in the main channel were maintained practically constant throughout each test, so as to allow the turbidity current to propagate into the side channel with a constant supply of sediment at the entrance.

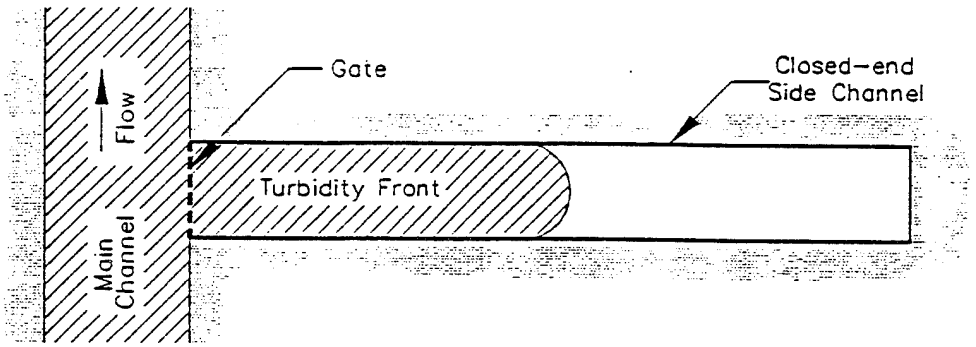

PLAN VIEW

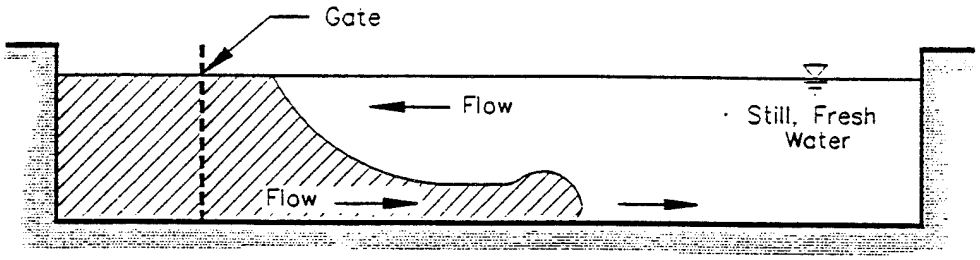

LONGITUDINAL SECTION

Figure 1. Experimental investigation of Turbidity current.

A total of eleven tests were performed. Characteristic test governing parameters included sediment type, mean water depth, concentration maintained at the entrance, the corresponding settling velocity and the densimetric Reynolds number. Seven tests were carried out with kaolinite as the sediment, three using a flyash, and a single test using a natural mud.

Results

The variation of the turbid front velocity with distance in five tests is presented in Figure 2. In those tests, the relative settling velocity and the densimetric Reynolds number ranged from 0.0023 to 0.0172 and 1260 to 3830, respectively. In all cases the front velocity decreased exponentially with distance as the turbid front propagated forward. This decrease resulted from settling of the suspended material and boundary friction inherent in the experiments. The rate of decrease was generally found to vary directly with the relative settling velocity but inversely with the densimetric Reynolds number. For instance, the greatest decrease of front velocity with distance was found in test 9, which had the highest relative settling velocity and the smallest densimetric Reynolds number.

The sub-layer turbidity current generated a stratified counter flow with clearwater outflow in the upper layer. At steady state, the horizontal velocity profile showed a decrease of the velocity in both layers with distance. The vertical concentration distribution was relatively uniform within the turbidity current, and a maximum gradient was observed at about mid-depth. A small amount of fine sediment was usually entrained into the upper layer due to diffusive mixing across the interface. At steady state a sediment wedge

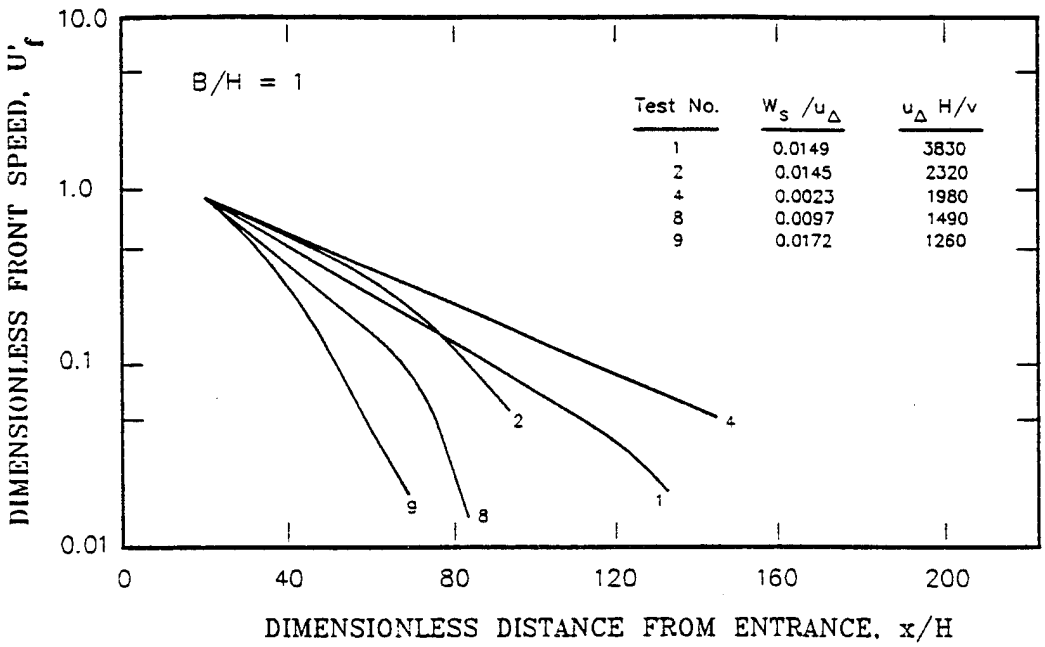

Figure 2. Variation of dimensionless front speed with dimensionless distance (W_S: Particle Settling Veloicty; u_Δ: Densimetric Velocity; v: Kinematic Viscosity).

developed as the finest particles in the front settled onto the channel bottom. The steady state longitudinal distribution of mean concentration below the interface from three test results was evaluated. The relative settling velocity in these tests varied from 0.0023 to 0.0149. The mean concentration below the interface in each test showed an exponential-type decrease with distance. The rate of decrease increased with increasing relative settling velocity.

Similar trends as above were also found in the resulting sedimentation pattern along the channel. In four kaolinite tests, the variation of the deposition rate with distance is shown in Figure 3. The rate of sediment deposition was also strongly dependent on the relative settling velocity. In test 4 having a relative settling velocity of 0.0149, the deposition rate at 5m distance from the entrance was approximately five percent of that at the entrance. However, in tests 3 and 4 having the relative settling velocities of 0.0023 to 0.0033, respectively, the deposition rate at the same location increased to thirty-five percent of that at the entrance. Particle sorting observed along the channel. The deposited particle size in general was found to decrease with distance. Sorting became more prominent as the relative settling velocity increased.

At steady state, the sediment influx through the lower layer at the entrance per unit area can be calculated as the product of the depth-averaged concentration and the velocity at the entrance. In the tests, the particle velocity at the entrance was found to be proportional to the initial front velocity, which equals one half of the densimetric velocity. Hence, the steady state sediment flux into the channel can be expressed as:

$$S = U_1 C_1 = \alpha \left[\frac{gH}{\rho_w} \left(1 - \frac{1}{G_s} \right) \right]^{1/2} C_1^{3/2}$$

Where U_1, C_1 are the depth-averaged velocity and concentration at the entrance, respectively; g is gravity acceleration; H is water depth; ρ_w is density of water; G_s is the

specific gravity of sediment and α is a constant. The sediment flux in eight tests was calculated using the measured deposition rate of sediment and plotted in Figure 4 against the calculated flux.

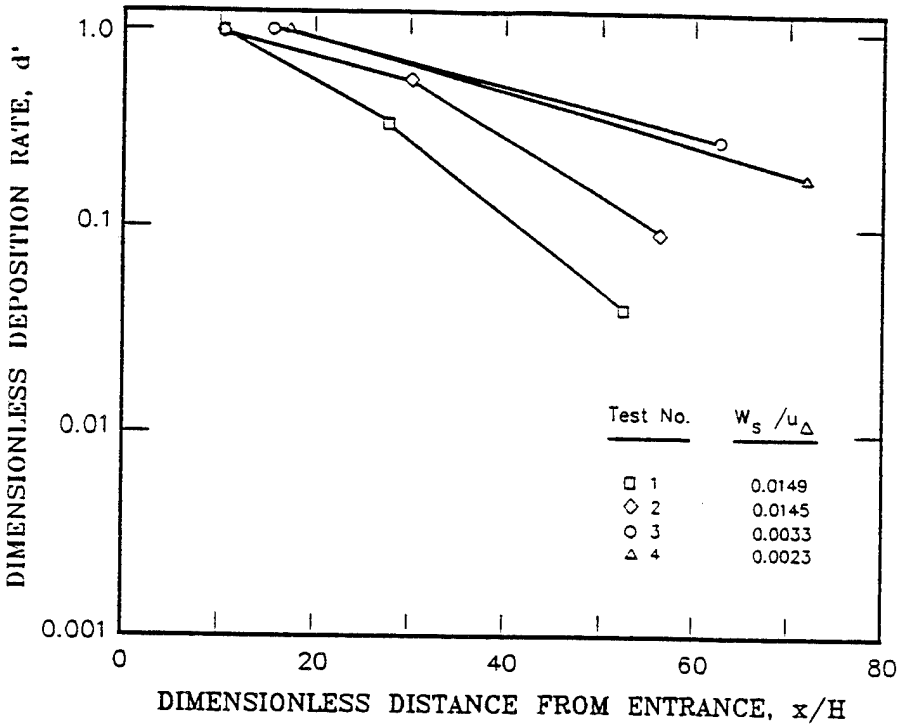

Figure 3. Variation of dimensionless deposition rate with dimensionless distance for Kaolinite tests (W_S: Particle Settling Velocity; u_Δ: Densimetric Velocity).

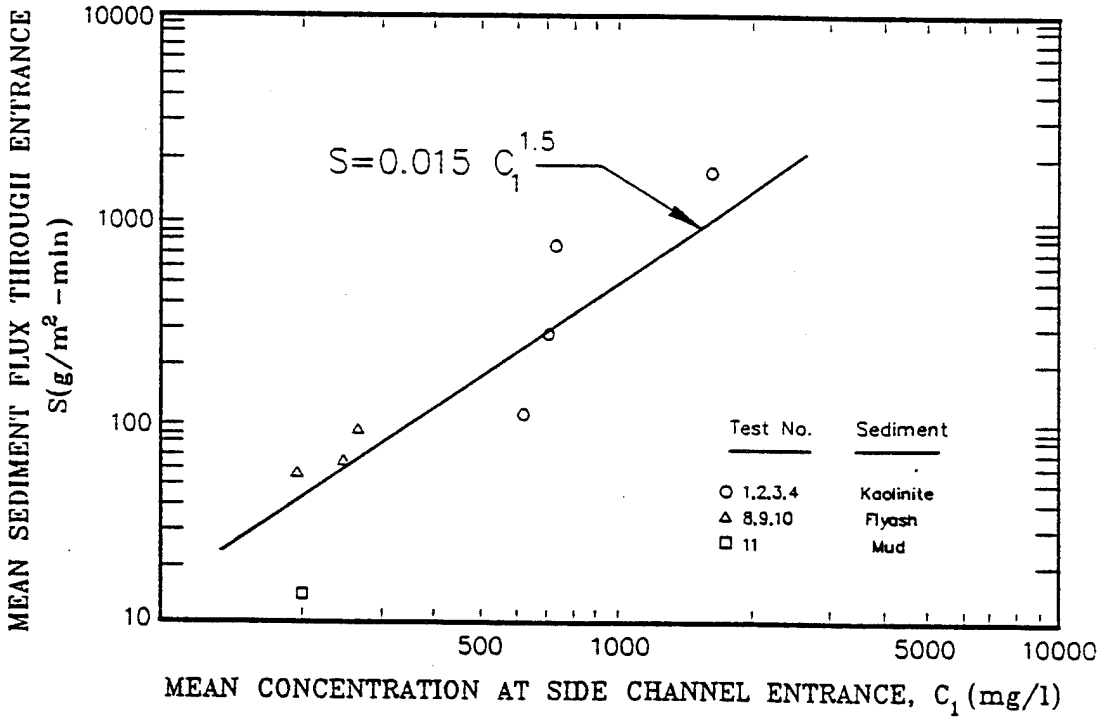

Figure 4. Mean sediment flux into the channel through entrance vs. mean concentration at entrance.

Table 1: Summary of Basic Test Parameters

Test No.	Sediment	Water Depth (cm)	Concentration at entrance (mg/L)	Settling Velocity (cm/sec)	Densimetric Reynolds No.
1	Kaolinite	10.3	1,657	0.048	3,830
2	Kaolinite	9.6	748	0.030	2,320
3	Kaolinite	10.6	724	0.007	2,630
4	Kaolinite	9.3	628	0.004	1,980
5	Kaolinite	10.0	895	0.007	2,450
6	Kaolinite	10.3	1,005	0.008	2,520
7	Kaolinite	10.5	1,093	0.009	2,740
8	Flash	10.5	250	0.012	1,490
9	Flash	10.2	193	0.019	1,260
10	Flash	9.4	269	0.026	1,300
11	Mud	10.3	202	0.002	1,100

EFFECTS OF COASTAL TOPOGRAPHY ON THE DISPERSION OF HEAVY PARTICLES IN WEAK TIDES

Chiang C. Mei, Chimin Chian & Carlo Procaccini
R.M. Parsons Laboratory
Department of Civil and Environmental Engineering
Massachusetts Institute of Technology
Cambridge, MA 02139

Abstract

Mixing of substances in coastal and oceanic waters has been an area of intensive study for decades due, in part, to its environmental importance. The dispersal behavior of a suspension consisting of particles with finite fall velocities is of interest because of its relevance to coastal waste disposal, coastal morphology and the ecological processes of larvae birth and growth.

Dispersion of a neutrally buoyant cloud in a horizontally uniform, oscillatory current has been studied by a number of authors (e.g., Bowden, 1965; Holly & Harleman, 1965; Okubo, 1967; Fukuoka, 1974). For the dispersion of heavy particles, Yasuda (1989) gave a theory also for an oscillating, horizontally uniform current with a Stokes boundary layer. The effective dispersivity at the final stationary stage was found to depend on the fall velocity of the particles. Carter & Okubo (1965) investigated a straight channel flow with linear variation of velocity in the two transverse directions and obtained solutions for the concentration distribution of a neutrally buoyant cloud. Although some important physical features are revealed by these works, they are applicable only when the cloud size and the distance of advection are much smaller than the horizontal scale of the mean flow. If one is interested in the long-time fate of a particulate cloud with a size comparable to the length scale of a estuary, a nearby island or a peninsula, the uniform-tide theories cannot be satisfactory.

For the mixing and flushing of tidal embayments in the Dutch Wadden Sea, Zimmerman (1976, 1977) found that the large diffusivity (100-1000 m^2/s) is attributable to horizontal mixing in a spatially varying flow. Since then a number of papers have addressed the effect of horizontal variation of bathymetry or topography on advection and dispersion.

There have been two approaches to model mixing in nonuniform tides. One is to compute the depth-averaged flow first. Then the trajectories (or Stokes drift) of a large number of marked fluid particles are computed numerically as a Euler-Lagrange problem (Zimmerman, 1986). If the computed time history is sufficiently long the particle paths of this Stokes drift become chaotic. Effective diffusivity is then calculated from the variance of the particle separation. Using this approach Awaji et al. (1980) and Awaji (1982) studied the tidal mixing in an idealized strait. Signell & Geyer (1990) studied a similar problem for a headland which is small compared to the tidal excursion length so that separation eddies are a dominant feature. The second approach, taken by Young et al. (1982) is Eulerian. They examined an idealized flow field with simple dependence on depth and horizontal coordinates, and sinusoidal dependence in time. The three dimensional convective diffusion problem was solved to enable the calculation of the effective horizontal diffusivity.

In this paper we wish to extend the Eulerian approach to dispersion in tidal flows affected strongly by nonuniformities due to coastal topography. The analysis is analogous to our companion paper (Mei & Chian, 1994) on the dispersion of heavy particles in a bottom boundary layer generated by gravity waves. Under the assumptions to be specified, we take advantage of two features of the phenomenon: (i) the existence of two vastly different time scales (time for vertical diffusion across the seabed boundary layer, and time for horizontal diffusion across the topographical length), and (ii) the problem is periodic on the shorter (micro) time scale which is just the tidal period. These features enable us to employ the perturbation method of multiple scales (method of homogenization) for deriving the effective equation governing the horizontal convection and dispersion of the particle concentration. Both the dispersivities and convection velocities will be derived for general flow patterns with significant spatial variations produced by the interaction of tides with lateral boundaries.

Other main assumptions are as follows. The topographical length scale is assumed to be much smaller than the tidal excursion length (e.g., an island of O(10-100 km) diameter and tidal excursion of O(1-10 km)), so that flow separation is not important. Let h denote the sea depth, r_o the horizontal size of the coastal topography, A the typical tide amplitude, ω the tidal frequency, and $U \sim \frac{A}{h}\sqrt{gh}$ the typical horizontal flow velocity. Just above the sea bed, an oscillatory Ekman boundary layer of the thickness $\delta = O\left(\sqrt{\upsilon / \omega}\right)$ is expected to develop, where υ denoted the eddy viscosity. The various scales involved in this problem are assumed to satisfy the following constraints:

$$\varepsilon \equiv \frac{U}{\omega r_o} << 1, \quad \frac{\delta}{h} << 1, \quad \frac{h}{r_o} << 1, \quad kr_o << 1$$

They mean, respectively, that the tidal excursion is small compared to the island size, the Ekman layer is totally submerged near the sea bottom beneath the inviscid zone, the sea is shallow, and the topographical length scale is small relative to the tidal wave length.

General expressions of shear-induced dispersivities and convection velocity are derived in terms of the ambient flow field. The horizontal flow nonuniformity is found to have pronounced effects on the distributions of the dispersion tensor as well as the convection velocity in the horizontal plane. Two numerical examples will be given for the tidal dispersion near a coastal topography: one for an isolated island in an open sea, and the other for an offshore island at a finite distance from a coast. The dispersion of a cloud of suspended particles will be examined as a function of the island size, the cloud size and the initial location of the cloud.

References

Awaji, T., Imasato, N. and Kunishi, H., 1980. Tidal exchange through a strait: A numerical experiment using a simple model basin. *J. Phys. Oceanogr.*, 10:1499-1508.

Awaji, T., 1982. Water mixing in a tidal current and the effect of turbulence on tidal exchange through a strait. *J. Physical Oceanography*, 12:501-514.

Bowden, K.F., 1965. Horizontal mixing in the sea due to a shearing current. *J. Fluid Mech.*, 21:83-95.

Carter, H. H. and Okubo, A., 1965. A study of the physical processes of movement and dispersion in the Cape Kennedy area. Chesapeake Bay Inst., Johns Hopkins Univ., Rep. Ref. 65-2, 150 pp.

Fukuoka, S., 1974. A laboratory study on longitudinal dispersion in alternating shear flows. *Res. Bull., No. 112,* Dept. of Eng., James Cook Univ. of North Queensland, Australia.

Holly, E.R. and Harleman, D.R.F., 1965. Dispersion of pollutants in estuary type flows. MIT Hydrogen. Lab. Rep. No. 74, 202 pp.

Mei, C. C. and Chian, C., 1993. Dispersion of small suspended particles in a wave boundary layer. submitted for publication.

Okubo, A., 1967. The effect of shear in an oscillatory current on horizontal diffusion from an instantaneous source. *Int. J. Oceanol. Limnol.,* 1:194-204.

Signell, R.P. and Geyer, W.R., 1991. Transient Eddy Formation Around Headlands. *J. Geophysical Research,* 96(C2):2561-2575.

Yasuda, H., 1989. Longitudinal dispersion of suspended particles in oscillatory currents. *J. Marine Res.,* 47:153-168.

Young, W.R, Rhines, P.B., and Garrett, C.J.R. Shear-flow dispersion, internal waves and horizontal mixing in the ocean. *J. Physical Oceanography,* 12:515-527.

Zimmerman, J.T.F., 1976. Mixing and flushing of tidal embayments in the western Dutch Wadden Sea. Part I: Distribution of salinity and calculation of mixing time scales. *Netherlands Journal of Sea Research,* 10(2):149-191.

Zimmerman, J.T.F., 1977. Dispersion by tide-induced residual current vortices. In: Hydrodynamics in Estuaries and Fjords. *Elsevier Oceanography Series,* 23, Nihoul, J.C.J. (ed.), Elsevier, Amsterdam.

MODELLING FLUXES OF SUSPENDED SEDIMENTS: DEVELOPMENT BASED ON RECENT AVAILABILITY OF CONTINUOUS MEASUREMENTS OF COMBINED PROFILES OF CURRENTS AND SUSPENDED SEDIMENTS

David Prandle, David Flatt, David Hill, Sarah Jones* and Peter D. Thorne*
Proudman Oceanographic Laboratory, Birkenhead, U.K.
*Marine Science Laboratories, Bangor, U.K.

Abstract

Background

Traditionally, measurement and modelling of suspended particulate matter (SPM) has focused on problems of net erosion/accretion in estuaries and the immediate coastal region. More recently, awareness of large scale pollution problems has extended interest to predicting suspended sediment concentrations in Shelf Seas. Such concentrations can modulate biological production in two conflicting ways, one by occluding light penetration and one by conveying adsorbed nutrients into photic surface layers. The large-scale transport of fine particles is also important in determining the distribution of associated adsorbed contaminants.

Modelling

While modelling of tide, wind and density-driven flows in shelf seas is well established, extension to include transport of SPM is at a developmental stage. The random-walk modelling technique is intrinsically analogous to particle movement, and this has been extensively used in shelf sea simulations (Sundermann 1994). However, simulation using a dispersion algorithm based on a fixed-grid scheme is equally valid. Irrespective of the modelling technique, the major difficulties are: (i) the specification of sinks and sources and (ii) ensuring adequate temporal and spatial resolution of both sediments and their transporting currents (or alternatively appropriate averaging. Specification of sources involves not only conventional stress-erosion formulae but also availability of bed sediments. The sink or loss rate is dependent on settling velocity ω_s and vertical eddy diffusivity E and, thereby, interactively the vertical SPM profile.

Measurements

Simulated values of sediment concentrations, and net fluxes vary wildly according to the specification of the stress-erosion formula; ω_s , E, subtle details of flow and turbulence and the many complications of near-bed dynamical-sedimentological processes.

Thus, in the present study, the modelling focuses on reproducing actual observed SPM concentrations. Moreover, the early model development is facilitated by selecting observational data from tidally-dominated regions. This enables direct comparison of specific facets of the observational time-series, namely (i) the predominant semi-diurnal component, (ii) asymmetry in (i), (iii) spring-neap amplitude, phase and supply-limited variability.

Instrumentation

Early measurements made use of optical transmissometers, both moored and from a continuously-profiled CTD probe (Jones et al 1994). More recently ABS (acoustic backscatter) probes have been used both for single-point monitoring but also as part of an ADCP (Acoustic Doppler Current Profiler) vertical profiling instrument. Recent comparisons between ABS and profiling transmissometer results are shown in figure 1(a) and (b). Deployments have been made in the Dover Strait with SPM of typically 5mg ℓ^{-1} and in the Mersey Estuary with SPM exceeding 500mg ℓ^{-1}. The high correlation found over such a diversity of regimes illustrates the capacity of the ABS system to measure vertical SPM profiles.

Calibration

Interpretation of transmissometers, ABS or OBS (optical backscatter) measurements is complicated by the unknown and often time-varying particle-size spectrum (or more appropriately the settling velocity spectrum). Use of multi-wave length signals with reflective/scattering properties sensitive to particle size can provide some insight. Likewise, in-situ laser reflectance techniques are being developed to determine particle size. However, here we report progress towards the goal of self-calibrating the observed time series using the information available as the basis for implying the particle size-spectra involved. Two characteristics of SPM time-series can be used, first the vertical variability and second the spring-neap variability.

Vertical Profiles of SPM

For the case of a constant (in time and over depth) vertical eddy diffusivity coefficient E, it can be shown that

(i) For $E > 10\ \omega_s\ D$, particles are near-uniformly distributed through the vertical. (D water depth)

Whereas

(ii) For $E < 0.1\ \omega_s\ D$, particles do not reach the surface.

Simulations indicate that the power n in the approximation

$$C(z) = Co\ z^n$$

(where C(z) is the instantaneous concentration at fractional height z, Co at the bed) is a particularly robust indicator of the value of ω_s in any tidally-dominated regime.

Spring-Neap Cycle of SPM

The relative predominance of the mean SPM concentration: the spring-neap cycle: semi-diurnal component can be directly related to the statistically-averaged settling times. Moreover the phase-lag between the erosional currents and the observed SPM time-series serves as an additional indicator. Figure 2 derived from a simplified modelling simulation highlights the above characteristics.

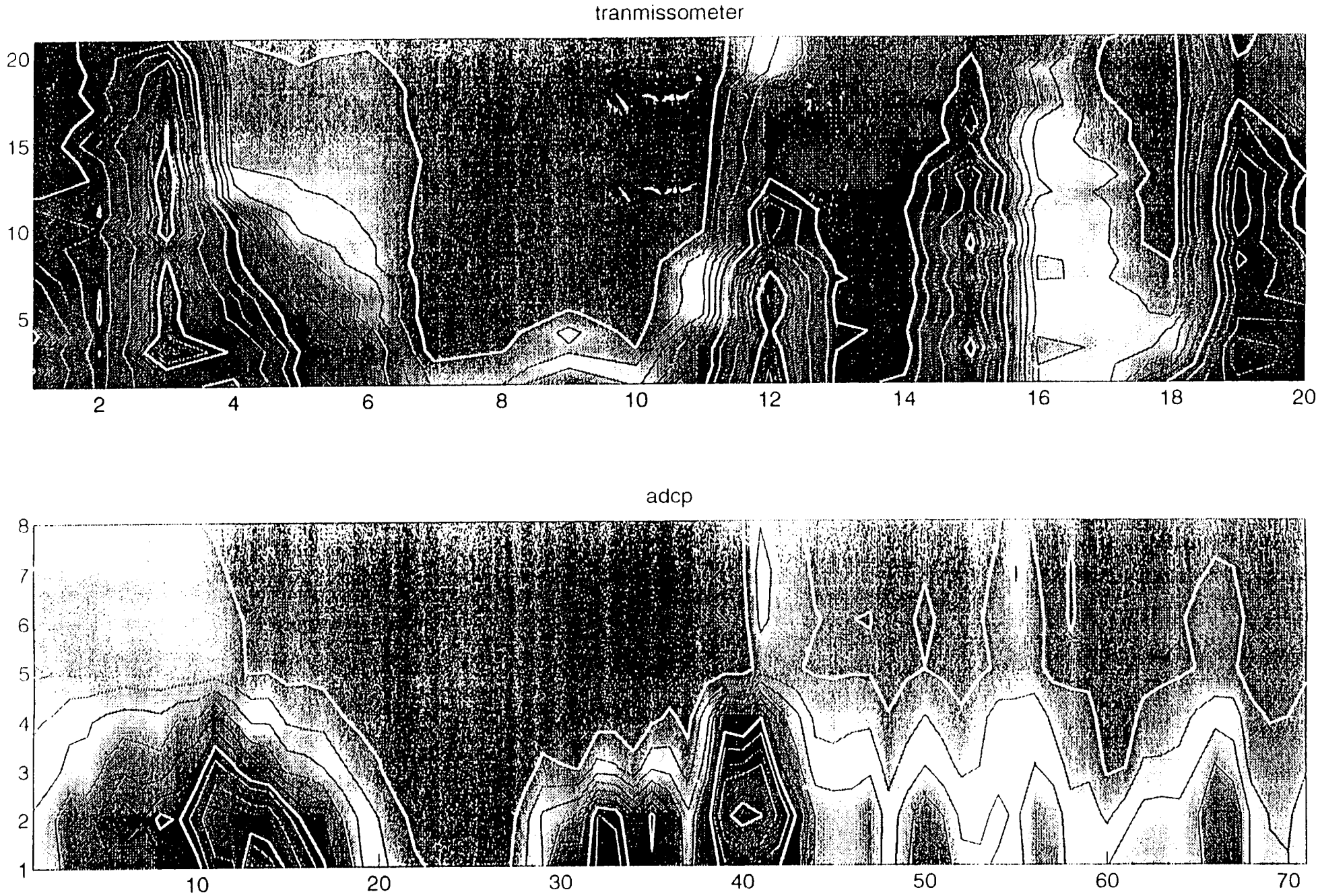

Figure 1. Synoptic vertical profiles of suspended particulate matter over 20 hours in the Mersey Estuary.

(a) top, profiling transmissometer; (b) bottom, ABS

E VERTICAL EDDY DIFFUSIVITY; D DEPTH; W_S SETTLING VELOCITY

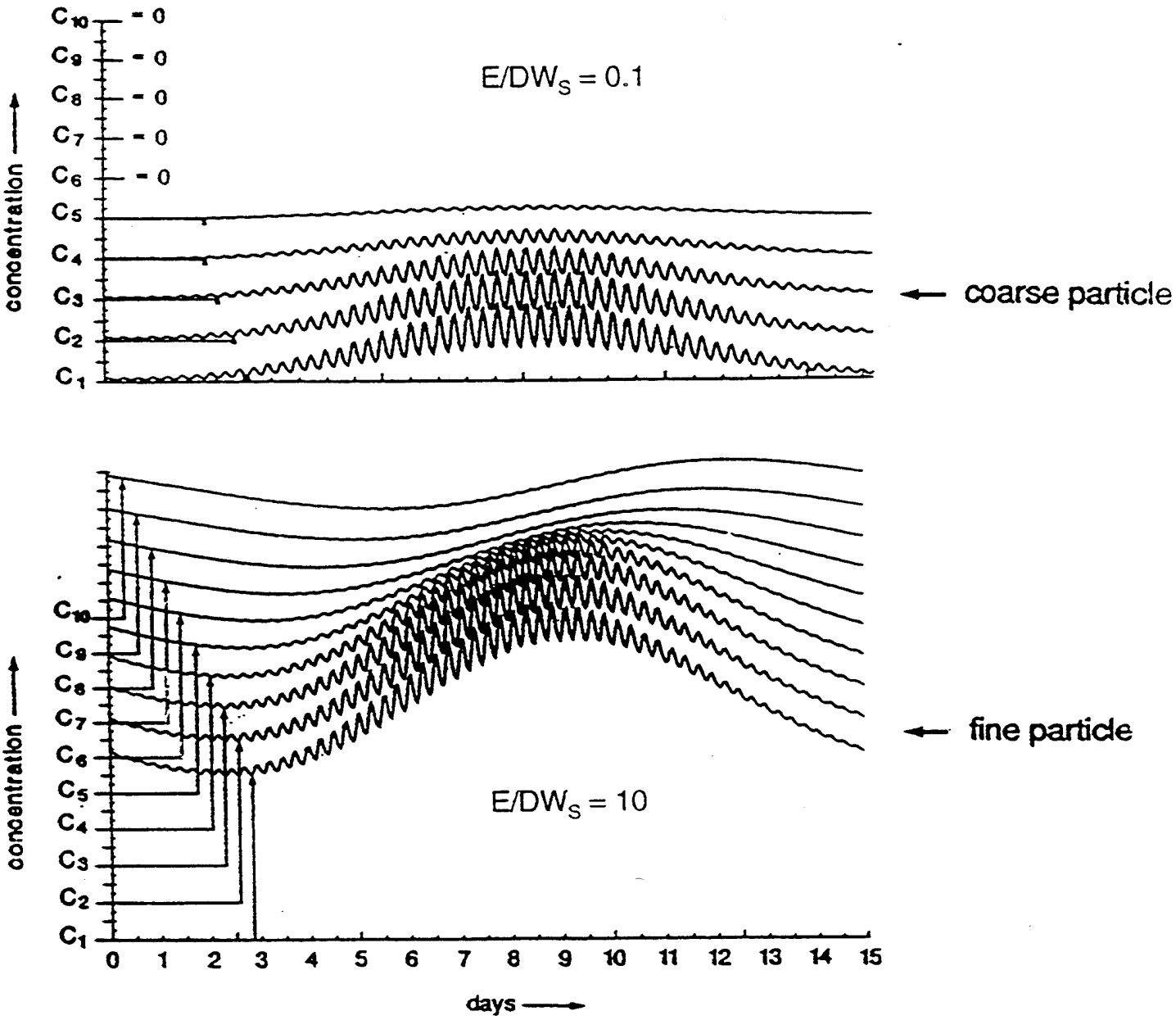

Computed suspended sediment concentrations

GENERAL RESULTS :

$E/DW_S < 0.1$ PARTICLES DO NOT REACH SURFACE

$E/DW_S > 10$ PARTICLES WELL MIXED VERTICALLY

Figure 2. Model simulation of concentrations at fractional heights, C_1 0.5 to C_{10} 0.95 over a neap-spring-neap tidal cycle.

THE BOTTOM BOUNDARY CONDITION FOR SUSPENDED SEDIMENT DEPOSITION

L.P. Sanford and M.-L. Chang
Horn Point Environmental Laboratory
P.O. Box 775
Cambridge, MD 21613

Abstract

Assumptions about suspended sediment deposition mechanisms at the sediment-water interface have important consequences for understanding and modeling suspended sediment transport. Rates of deposition, total suspended sediment loads, vertical distributions of suspended sediment near the bed, and particle exchanges across the sediment-water interface are all affected. Sanford and Halka (1993, Mar. Geol., 114, 37-57) explored the concept and usage of a critical stress for deposition. The present paper continues by examining the influence of the deposition height, which is the height at which sediment concentration is evaluated to determine deposition rates due to gravitational settling. This problem is similar to determination of the reference height a in noncohesive sediment transport theory. A slightly modified version of a shallow water boundary layer and vertical particle transport model (Gross et al. 1992, JMR, 50, 611-642) was used to examine this question for the case of tidally modulated resuspension and deposition. Different model scenarios were compared to tidal resuspension-deposition data from Chesapeake Bay.

The results indicate that modeled suspended sediment concentrations are very sensitive to specification of a deposition height for moderate to high Rouse numbers. Numerical solutions depend on the discretization scheme if the lowest grid cell is taken as the reference, with total suspended sediment load decreasing for finer grid sizes all other things remaining constant. Following a suggestion of Gross et al. (1992), two ideas were tested for an effective deposition concentration determined by the turbulent flow conditions rather than an arbitrarily chosen reference height. A scaling representing a balance between an outer boundary layer intermittence time scale and the sediment fall velocity seems to give reasonable results in comparison to the data, and should be given further consideration.

TIDAL VARIATIONS OF SUSPENDED SEDIMENT IN THE EMS ESTUARY

J.van de Kreeke[1] and G.C. van Dam[2]
[1]Rosenstiel School of Marine and Atmospheric Science
University of Miami
Miami, USA
[2]National Institute for Coastal and Marine Management
Ministry of Transport, The Netherlands

Abstract

The Ems estuary, situated along the Dutch-German border, is part of the Wadden Sea. Its morphology is characterized by a main channel bordered by tidal flats. Channel widths and depths are typically 3000 m and 10 m, respectively. The water motion is dominated by the tide. The principal water level constituent is M_2 followed by S_2. Amplitudes of M_2 and S_2 in the study area, located in the seaward part of the estuary, are 1.33 m and 0.21 m, respectively. Tidal current amplitudes are on the order of 1 m/s. River discharges are relatively small, resulting in well-mixed conditions and negligible density currents in the study area.

Observations of silt concentrations in a station located in the main channel at a water depth of 6 m were carried out during the period April 18 - December 6, 1990 and March 14 - October 11, 1991. Here silt is defined as the anorganic fraction of the sediment that has a diameter smaller than 53μm. Silt concentrations were derived using data of Mex-3 turbidity meters located at bottom +0.25 m, bottom +0.75 m, bottom +1.75 m and bottom + 3.30 m. Concentrations are averaged values over a 10 minute interval. To aid in the interpretation of the silt concentrations, in the same station current velocity, salinity, water level and wave climate were observed.

In addition to longterm variations, the observations exhibit a consistent pattern of tidal variations in the silt concentrations. As an example, for the sensor at bottom +0.75 m and a period of little wind and wave action, tidal variations in silt concentration during spring tide conditions are presented in Fig.1. The 10 min. values are smoothed using a one hour sliding average. In the same figure the 10 min. values of the current speed at the turbidity sensor are plotted.

Focusing attention on the current speed, starting at L(ow) W(ater) S(lack) (= 0 hr), the current speed rapidly increases, reaching a maximum of 0.75 m/s at LWS + 1.5 hr. After that, currents gradually decrease to zero at LWS + 6 hrs, corresponding to H(igh) W(ater) S(lack). The ensuing ebb tidal currents reach a maximum of 0.5 m/s at HWS + 1.5 hrs and have decreased to zero at HWS + 6.5 hrs. Tidal currents exhibit considerable asymmetry.

Referring to Fig.1, silt concentrations during flood increase from 75 mg/l at LWS to a level of 200 mg/l at LWS +1.5 hr corresponding to maximum flood. Between LWS +1.5 hr and LWS +5 hr, the general trend is a slight increase in concentration. Superimposed on this trend are fluctuations with peaks at LWS + 1 hr, LWS +3 hr and LWS +5 hr corresponding to a period of approximately 2 hours. Most likely these fluctuations are associated with meandering of the main channel flow and settling as a result

of the decreasing current speed and possibly flocculation. Between LWS +5 hr and LWS +6 hr (=HWS), there is a rapid decrease in concentration to a level of 50-75 mg/l. Comparison of the concentrations of the four sensors showed that between LWS +1 hr and LWS +4 hr, the vertical distribution of silt is relatively uniform. During the first and last part of the flood, distinct gradients in concentration exist. During ebb, silt concentrations rapidly increase to a maximum at approximately one half hour past maximum ebb. Between HWS +1.5 hr and HWS +4.5 hr, concentrations decrease at a relatively moderate rate, followed by more rapid decrease between HWS +4.5 hr and HWS +6 hr. Minimum concentrations at LWS are at the 80 mg/l level. The 2 hour period fluctuations observed during flood are virtually absent during ebb. On the average, concentrations during ebb are higher than during flood. At all times during ebb there is a strong vertical gradient in the concentrations. The sediment that remains in the water column at times of slack water is considered wash load that never settles.

The objective of this study is to delineate the processes that are responsible for the observed tidal variations in silt concentration.

To attain the objectives a Lagrangian approach is followed. Observed silt concentrations pertain to the continuous series of water columns passing by the measuring station. Therefore the observed silt concentrations depend on the time history of the silt concentrations in the individual water columns. These water columns have different origins (here selected as the position at times of the preceding slack water) and travel along different paths. To trace the paths of the water columns, use is made of a 2-D vertically integrated hydrodynamics model. The results of the calculations show that water columns originate in widely different areas of the estuary.

It is postulated that during its travel from the origin to the measuring station, the concentration distribution in a water column is governed by the 1-D advection-diffusion equation in vertical direction. To account for flocculation, the fall velocity, w, in this equation can vary with time. The diffusion coefficient, K_z, is assumed to increase with increasing values of the tidal velocity. Based on the results of " 13-hour measurements", it is shown that at all times, including times of slack water, there are large spatial variations in silt concentrations. The "13-hour measurements" were carried out in six vertical profiles located in the same cross-section as the measuring station. Therefore the initial, i.e. at the origin, amount of silt in a water column and its distribution will differ from one water column to the other. In addition to the initial amount of sediment, at any given time the total amount of sediment in the water column depends on the amount of sediment that has been eroded and deposited. When silt is available in the bottom sediment, erosion occurs when the tidal velocity is larger than the critical velocity of erosion, u_e, and similarly deposition takes place when the tidal velocity is smaller than the critical velocity of deposition, u_d. Information on the tidal velocity of the water column along its path is available as part of the trajectory calculations. Information on silt concentrations in the bottom sediment was obtained from a geographic information system of the estuary.

Taking values of w(t), K_z (t), u_e, u_d and the erosion rate coefficient within an accepted range of values, the time history of concentration variations in the different water columns passing by the measuring station is calculated. From this information the concentration variations at the measuring station are derived and compared with observed concentrations. The advection-diffusion equation for each water column is solved using a particle technique. The sediment is represented by a discrete number of particles. In the calculations the maximum number of particles in a water column is 10,000, the exact number depending on the amount of sediment in the water column. Particles are given discrete downward displacements to account for the fall velocity and are given random

vertical displacements to account for the mixing. If necessary, depending on the comparison between calculated and observed concentrations, adjustments will be made in the values of the pertinent parameters. Based on these results the validity of the advection-erosion-deposition model in describing the tidal variations in silt concentrations will be judged.

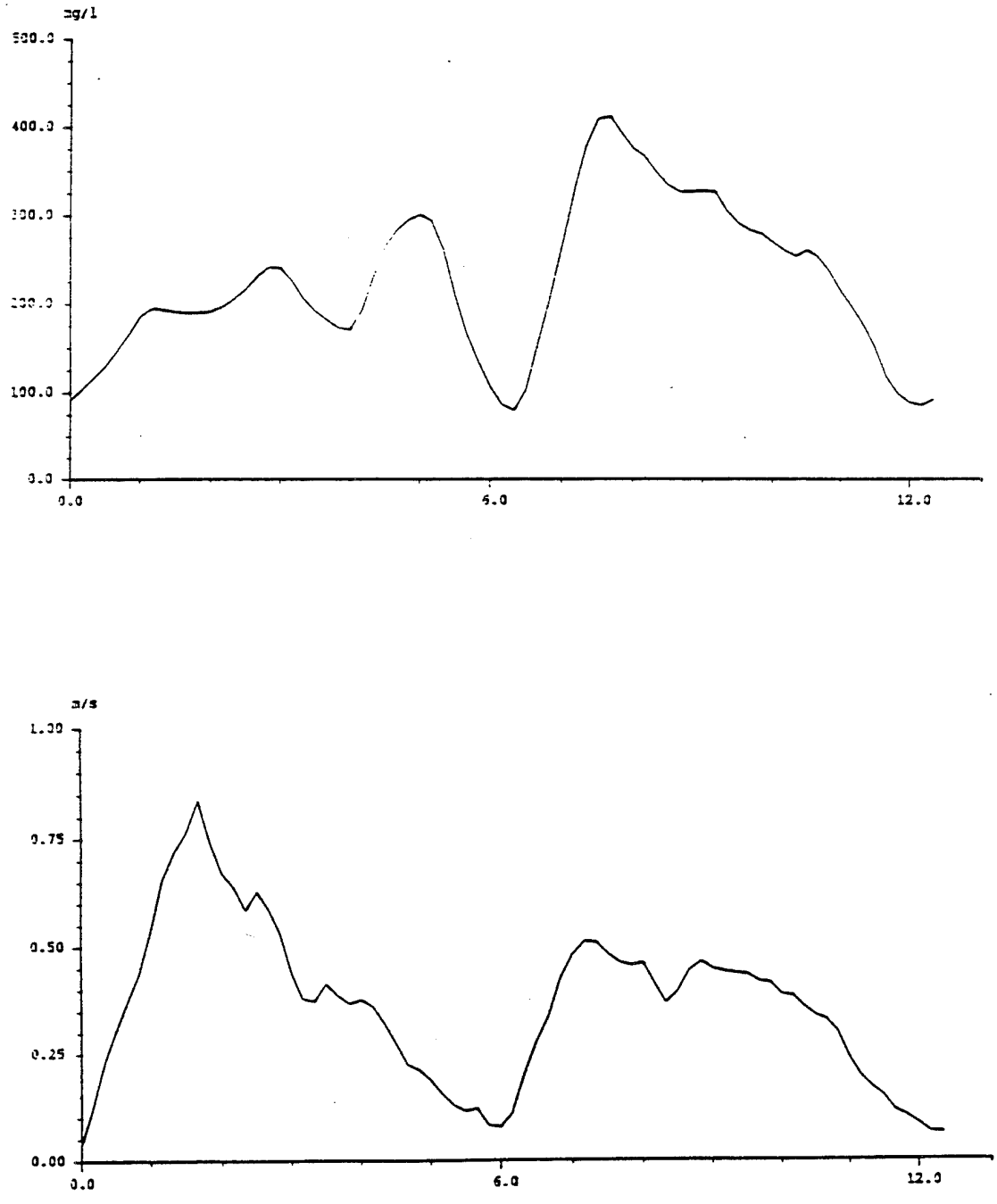

Figure 1. Silt concentrations and current speed at bottom +0,75 m. Time in hours, LWS = o.hr.

GENERATION OF HIGH TURBIDITY LAYERS IN THE SETO INLAND SEA

Hidekazu Yasuda, Yoshio Takasugi and Takehiko Higo
Chugoku National Industrial Research Institute
2-2-2 Hiro-Suehiro, Kure, Japan 737-01

Abstract

Introduction

In the benthic boundary layer, currents behave complicatedly with shear and suspended particles are sometimes distributed at high concentration. Therefore this layer plays an important role in the mass transport process in enclosed waters although it is rather thin in the whole depth. In order to understand the behavior of suspended particles and the sedimentation process in coastal waters and lakes, we developed a new instrument to measure the vertical profiles of the current and the turbidity simultaneously in the benthic boundary layer. By the field observation in Lake Biwa and the Seto Inland Sea using this instrument, we have got a new understanding on the generation of the high turbidity in the bottom layer. In this study, we'll show the result of the observation and its consideration in the Seto Inland Sea

Current-Shear Meter

A new instrument developed in this work consists of four flux sensors with the current and the turbidity sensors (Fig. 1). The current is measured by the electro-magnetic method and the turbidity by the infrared back-scattering method. A thermistor is attached to and an inclinometer is included by the data chamber. This instrument, the weight and the length of which are respectively about 37 *kg* (25 *kg* in the water) and 2.6 *m*, can be moored with ease even from a small boat. Since it can stand on the floor using an anchor and floats like Fig. 1, it gets the reasonable data of the vertical profile in the bottom layer as time series although many of the other instruments to measure the bottom current generates disturbance around itself by its structure. It can be prevented from inclination by strong currents using larger floats and a heavier anchor. Data can be got basically every 50 cm in the bottom layer. It can be lengthened by one meter using junctions prepared for connection of each sensor.

The shortest time-interval for measurement by this instrument is 0.5 seconds in the continuous mode and the bursting mode is also available in the case of long term measurement.

We have named this new instrument "the current-shear meter".

Field Observations in Hiuchinada of the Seto Inland Sea

Hiuchinada in the Seto Inland Sea

Hiuchinada is an enclosed sea located in the middle of the Seto Inland Sea. Figure 2 shows the distribution of the grain size on the floor of this sea. Residual currents flows along the east and west coasts in the sea as arrows in the figure. Figure 3 is the vertical section along the dashed line in Fig 2. The grain size near the west coast is rather finer than that near the

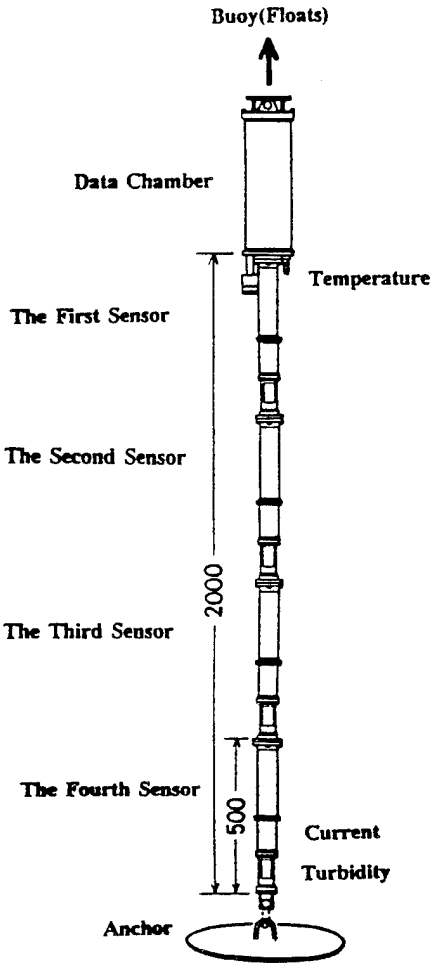

Fig. 1. The current-shear meter.

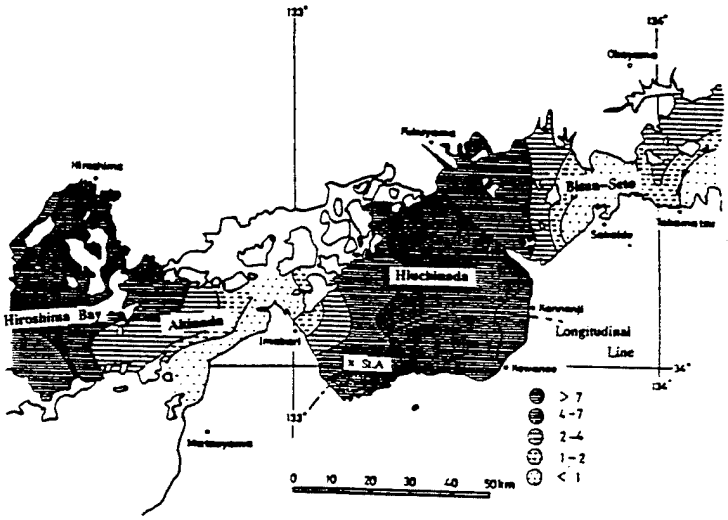

Fig. 2. Mdϕ of the basin floor in Hiuchinada, located in the middle area of the Seto Inland Sea.

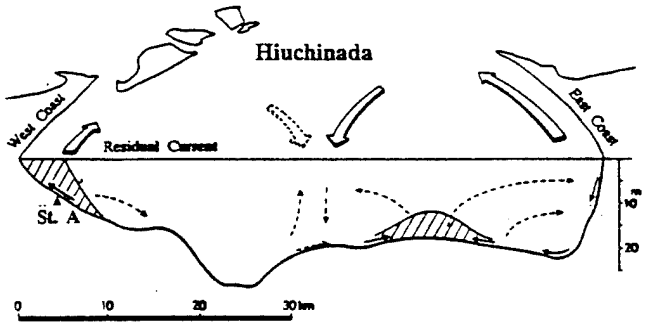

Fig. 3. The longitudinal section of the basin floor of Hiuchinada.

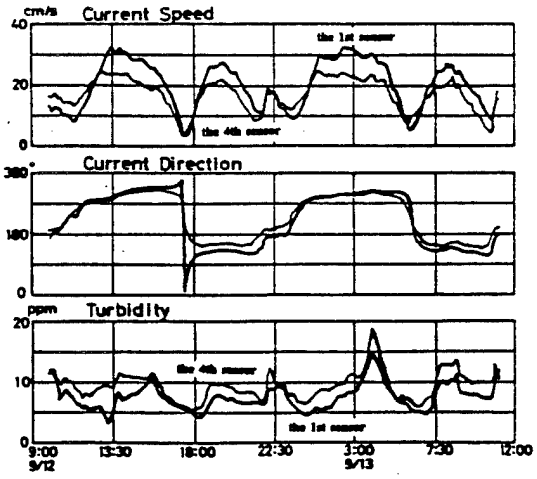

Fig. 4. Variations with time of the current speed, its direction and the turbidity got from the first and the fourth sensors of the current-shear meter.

east coast and the west area is shallower than the east area near the coast of this sea. The south-west area of this sea is considered to be under the accumulating circumstances. Incidentally the roughness of the grain size around the straits, north-west side in this sea, has been recognized to be caused by the strong tidal current.

The outline of the tidal current in this sea has been known by lots of field-observations carried out so far. In the present study, we'll mainly show the result obtained on the spring tide(from Sept. 12 to 13, 1992) at St. A where the mean depth was around 13 m. Instruments used here were an electro-magnetic current meter for the upper layer and ADCP for the vertical profile in the whole depth besides the current-shear meter for the bottom layer.

Vertical profile of the tidal current

Measuring levels are 0.5, 1.0, 1.5 and 2.0 meters upward from the basin floor obtained through the current-shear meter, every one meter from 2 *m* to 10 *m* through ADCP and 2 *m* from the sea surface through the ordinary current meter. The maximum of the current is about 40 cm/sec near the sea surface.

Seeing the harmonically analyzed result of ADCP, the phase of M_2-component leads gradually with approach to the bottom though the amplitude is fairly uniform in the vertical. The speed of the residual component is also uniform, while the direction is deflected counter-clockwise toward the bottom. Since the current value at each level is smoothed by averaging spatially around the level, the profiles are not fluctuated so much in the vertical.

Figure 4 is the variations with time of the current speed, its direction and the turbidity got from the first and fourth sensors of the current-shear meter. Figure 5 shows the vertical profiles of the elements of the tidal current ellipse, obtained from the ordinary current meter and the current-shear meter.

These figures prove that the amplitude of the M_2-current gets smaller and the phase leads more with approach to the floor and that the orientation of the residual current, that is along the coastline in the upper layer, deflects counter-clockwise near the floor although the speed does not vary so much. The residual current obtained here has a component toward the coast in the bottom layer by such deflection. The deflection of the residual current direction suggests the Coriolis effect in the bottom layer, that is, the formation of the Ekman layer.

Variations of turbidity

Figure 6 shows the variations with time of the vertical profile of turbidity obtained from the current-shear meter. The unit of numerical values in the figure is *ppm* corresponding to the concentration of kaoline. The shadow shows high turbidity, more than 8 ppm. The dot above the abscissa indicates the peak time of the current at the lowest level. This figure represents that the peak of turbidity lags behind the current peak, and further the lag of turbidity peak gets larger slightly with the height from the floor.

In order to reveal the phase of the current and the turbidity, we analyzed them harmonically. Figure 7 shows the amplitude and the phase lag of the M_4-component and the average on the current speed and the turbidity. Seeing the figure, the averaged turbidity is larger with approaching to the floor and the phase of the turbidity lags behind that of the current by about 60 degrees, corresponding to one hour.

The reason for the delay of the turbidity peak will be suggested by considering not only the current speed but also the degree of turbulence. We have drawn the variation with time of turbulence degree, defined here as the standard deviation of the 30 second-averaged current from the 30 minute-averaged one. It reveals that the turbulence gets larger after the peak of the current. It is suggested from these that the high turbidity is induced not so much by the current as by the turbulence.

Concluding Remarks

The component of the floor at this station is known to consist of fine clay, the Md ϕ value of which is nearly six, by field observations carried out so far. The turbidity peak is observed not at the period of current maximum but at the decelerating period of current. It has been suggested that suspended particles are stirred up by turbulence of tidal currents and transported toward the coast by the deflected bottom current. These means this area would be under the accumulating circumstances.

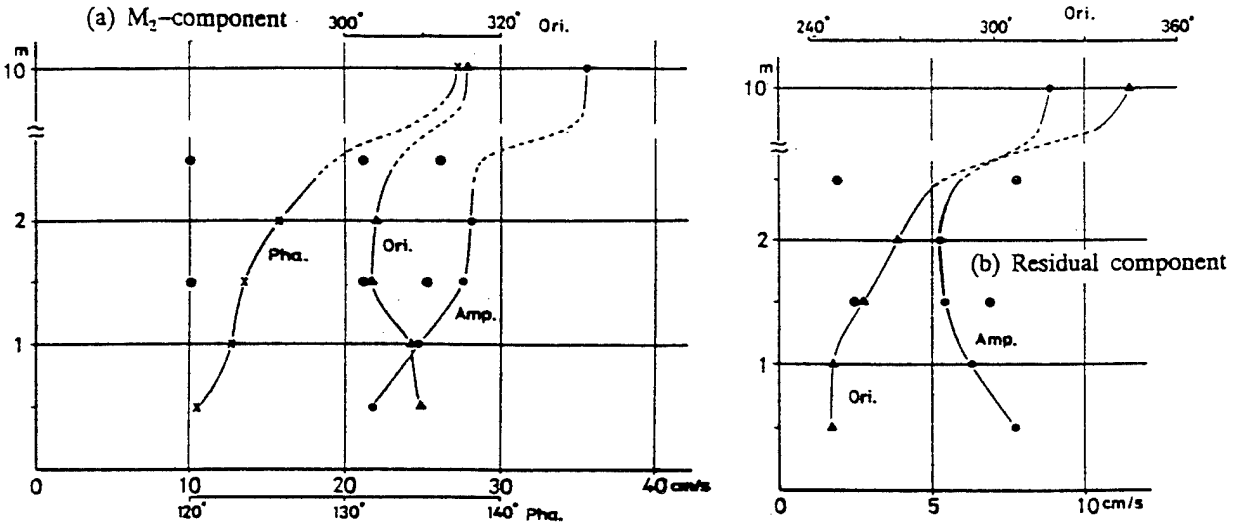

Fig. 5. Vertical profiles of the elements of the tidal current ellipse.

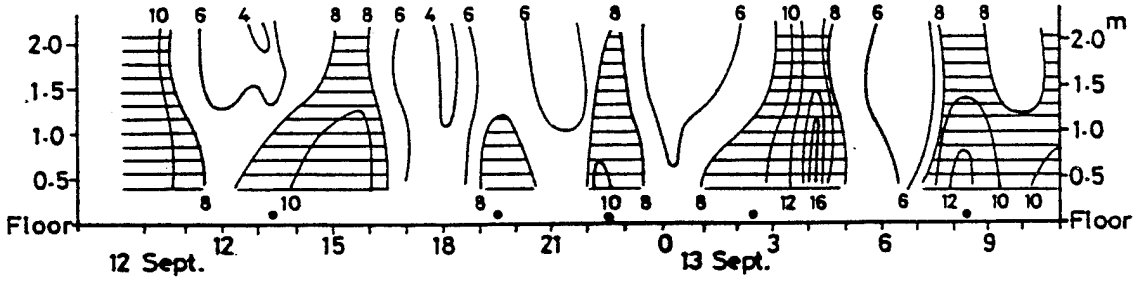

Fig. 6. Variations with time of the vertical profile of the turbidity near the floor.

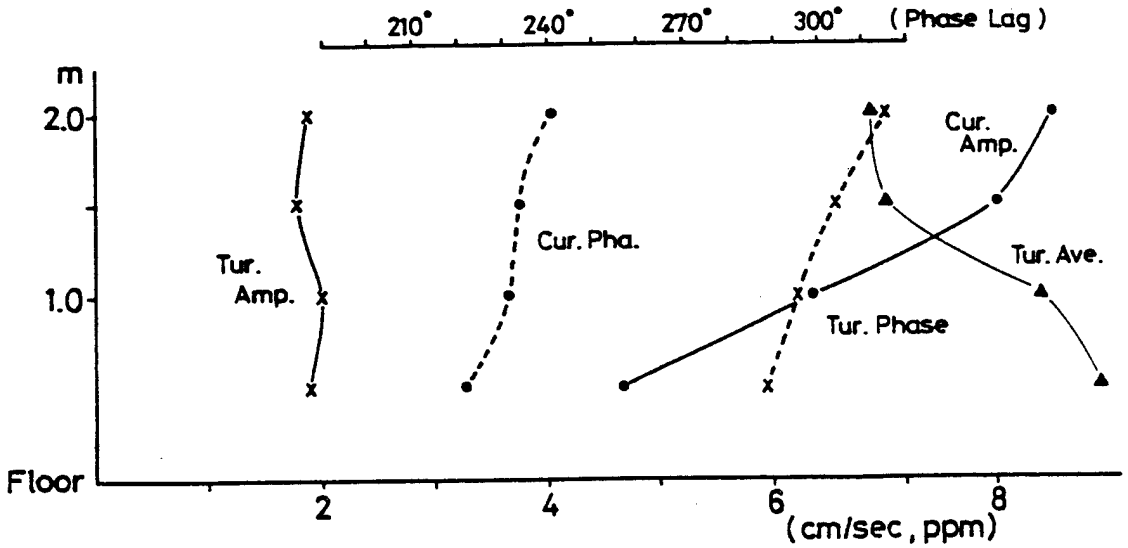

Fig. 7. Vertical profiles of the M_4-component and the residue by the harmonic analysis of the current speed and the turbidity.

CIRCULATION PATTERNS ON THE COASTAL ZONE OFFSHORE PERTH, WESTERN AUSTRALIA: OBSERVATIONS AND NUMERICAL MODELING

Charitha Pattiaratchi
Department of Environmental Engineering, Centre for Water Research,
The University of Western Australia, Nedlands

Abstract

Introduction

Dynamic processes on the continental shelf play an important role for the seaward transport and dilution of pollutants introduced at the shoreline through outfalls, submarine groundwater and/or river discharges. These pollutants have a potential to cause deleterious, and in some cases irreversible, effects on the environment such the promotion of algal blooms, loss of seagrass and other benthic communities, contamination of fisheries and risks to human health. It is generally accepted that a finite amount of a pollutant may be discharged into the ocean without having significant effects on the system. This is dependent on the total load of contaminants it delivers to the system, and the capacity of that system to assimilate those contaminants which is influenced by a number of factors including water circulation patterns under various conditions and exchange with open ocean waters. Hence, the initial stage to determine this assimilative capacity is to understand the processes which influence hydrodynamics in a particular area which may be undertaken through numerical modelling and field investigations. The dynamics of the coastal zone offshore Perth, Western Australia, are presented in this paper.

Study area and Observations

Topography

The major physical feature of the nearshore waters along the West Australian coastline is a limestone reef system which is approximately 700 km long and extends from 33°S to 28°S. It consists of irregular lines of outcropping limestone generally parallel to the coastline. The formation of this reef system has been attributed to the rise in sea level during last transgression approximately 6000-8000 years BP. The seaward edge of this reef line is located near the 20 m contour which varies between distances of 3 to 10 km of the shoreline. Within the present study area, the presence of the reef system forms a topographic barrier for the exchange of the nearshore waters with those offshore. Offshore of the reef system the continental shelf is uniform except for the presence of Rottnest Island, Direction Bank and the start of the Perth Canyon. Rottnest Island is located almost at the centre of the present study area and provides an obstruction to the shore-parallel currents. Near the coast, the reef system is present and therefore the water which is traveling from south to north has to travel past the western tip of the Island. Direction Bank is an elongated shoal located to the north of Rottnest Island. The Perth Canyon begins at the western tip of Rottnest Island and extends offshore up to a depth of 2000 m. However, the offshore boundary of the study area is located at a depth 165 m.

Barotropic effects: tides and winds

Along the West Australian continental shelf, the water levels are subject to oscillations ranging from periods of seconds to days. They include, in addition to locally generated wind and swell waves, infra-gravity waves and seiches which have periods ranging from 0.5 to 10 minutes and continental shelf waves with periods of the order of several days. All of these motions have an influence on the water circulation and mixing on the continental shelf and the adjacent ocean.

The tides along the West Australian coastline is small due an amphidromic point located offshore of Cape Naturaliste and the tides are mainly diurnal with a maximum tidal range of 0.6 m. The main tidal constituents are the diurnal O_1 and K_1 constituents which have amplitudes of 0.16 m and 0.12 m respectively at the Fremantle Boat Harbour. In contrast, the semi-diurnal M_2 and S_2 constituents have amplitudes of 0.056 m and 0.050 m respectively. Harmonic analysis of tidal data from Ocean Reef harbour indicate that the diurnal O_1 and K1 constituents have amplitudes of 0.12 m and 0.18 m respectively and the semi-diurnal M_2 and S_2 constituents have amplitudes of 0.052 m and 0.042 m. Harmonic analysis of current data obtained from the continental shelf has shown that the tidal currents in the region are negligible. The main tidal constituents O_1 and K_1 have amplitudes of 0.016 ms^{-1} and 0.013 ms^{-1} respectively whilst the amplitudes of the M_2 and S_2 constituents are < 0.005 ms^{-1}. Hence, the tidal currents within the study area are negligible and are of the order of 0.02 ms^{-1}.

As the tidal influence is small, the major driving force of the currents is wind stress acting on the sea surface. The prevailing winds have a strong northerly component during the summer months whilst during winter, the winds are variable with strong north-westerly winds veering to south-westerly are common. During the summer months the sea breeze system, termed the 'Fremantle Doctor', plays a dominant role with speeds frequently exceeding 15 ms^{-1} with a mean of 7 ms^{-1}.

Regression analyses between wind and current vectors indicate that there is a high correlation between the wind field and currents. In particular, during the summer months, when the wind speeds are high and are predominantly from the south, up to 60% of the variance in the current field may be explained by the wind field and when wind speeds exceed 3 - 5 ms^{-1} then the winds dominate the flow dynamics in the nearshore waters where the water depths are < 10 m. During the summer months there is a consistent northward flow of water except during short periods when there are reversals in the wind direction and the currents respond to these changes in wind direction almost instantaneously. During the winter months, the currents correlate well with the wind field except there are instances when the currents flow opposite to the direction of the wind. During these periods there appear to be a correlation between the sea level and current field.

Another important feature in the regression analyses between winds and measured currents is that in shallow water, for wind stress components > 0.01 Nm^{-2} the response of the currents is constant and there is no linear dependence between the wind stress and currents. i.e., there is an upper limit on the currents generated by the wind field in this region.

Baroclinic effects: Leeuwin Current, Air-Sea Exchange, Swan River

The basin scale thermo-haline circulation in the Indian Ocean sets up a meridional pressure gradient along the west Australian coast which is the driving force of the Leeuwin Current which is a shallow (< 300 m), narrow band (< 100 km wide) of relatively warm, lower

salinity, nutrient depleted water of tropical origin that flows poleward from Exmouth to Cape Leeuwin and onto the Great Australian Bight (Cresswell and Golding, 1980; Church et al., 1989; Smith et al., 1991). Studies undertaken over the past decade have demonstrated that the pressure gradient overwhelms the opposing equatorward wind stress (Thompson, 1984; 1987; Godfrey and Ridgway, 1985; Weaver and Middleton, 1989; Pattiaratchi and Buchan, 1991). The Current exhibits a seasonal behaviour which reflects the changes in the local wind stress and the pressure gradient. During the summer months the LC is weakest as it accelerates into the maximum equatorward wind stress and is located more offshore whereas during the winter months the LC, located towards the coast, is strongest as the stress applied by the equatorward wind stress is weaker and the pressure gradient is also higher (Godfrey and Ridgway, 1985). The pressure gradient has a mean of 1.75×10^{-7}.

The meanders of the Leeuwin Current were monitored from satellite imagery in 1993 and during a period of 16 days the current was observed to meander across the continental shelf. The current meter data collected at deep water and shallow water locations indicated that the effects of the Leeuwin Current meanders on the continental shelf has a negligible effect in controlling the nearshore circulation patterns.

Another important baroclinic forcing mechanism is the air-sea exchanges of heat. Heat fluxes, estimated using bulk formulae, indicate large diurnal variations in heat fluxes, especially during the summer months where the surface receives a net heat flux of the order of 800 Wm-2 during day and looses of the order of 400 Wm^{-2} during the night. Hence, strong heating and cooling in the day-night cycle is expected.

The input of freshwater into the study area is mainly from the Swan River and to a lesser extent through submarine groundwater. During the summer months the river discharge is negligible whilst maximum river discharge occurs during the winter months.

From above summary of processes observed on the shelf, we would expect that the dynamics on the continental shelf would be controlled by mainly by wind with the steric pressure gradient providing an additional force. To investigate the balance between these phenomena we shall use a 3-D hydrodynamic model developed for the area.

Numerical Modelling

The three dimensional primitive equation model, based upon a semi-implicit numerical scheme, is described by Backhaus (1985) and Stronach et al. (1993). The model uses fixed permeable interfaces between layers and the equations of continuity and momentum are vertically integrated over a depth range of h, corresponding to a computational model layer of the same thickness. The distribution of pressure is assumed to be hydrostatic and the Boussinesq approximation is invoked.

The model uses a finite-difference scheme with the variables distributed on a Arakawa C grid (Arakawa and Lamb, 1977). The solution technique is described in Backhaus (1985) and Stronach et al. (1993). The model treats both external and internal modes implicitly and is independent of the stringent stability criteria valid for explicit schemes. In contrast to the most commonly applied explicit shelf sea models, this scheme is much faster and allows the inclusion of deep ocean regions without being limited by stability considerations for the free surface.

The vertical eddy viscosity (Av) is specified according to Kochergin (1987) where Av is a function of the velocity gradient and stratification between the layers. The

horizontal eddy viscosity (AH) is set to a constant value of 1 m^2s^{-1}. At the sea bed a quadratic bottom stress law is specified with a constant drag coefficient of 0.0025. The steric pressure gradient is included as an additional term in the equations of motion in the y-(north-south) direction. The mean steric pressure gradient along the West Australian continental shelf is 1.75×10^{-7} (Smith et al., 1991). This corresponds to a 3.5 cm change in sea level over 200 km. In the model domain, which is 50 km, a pressure gradient equivalent to a 2.5 cm change in sea level is used.

The topography was the area was obtained using the digital survey data. The simulations presented here are from a model with a horizontal resolution of 250 m with 2 vertical layers. The time step in the model is 60 s. An Orlanski radiation boundary condition is applied at the open boundaries. Numerical tests using different boundary conditions indicated that the main study area is insensitive to the specification of the open boundary condition.

The model described above was used to simulate the behaviour of the coastal waters under different wind patterns. These included: (a) wind speed and direction data recorded at coastal stations over a one year period; this enabled the comparison of the model with measured data in barotropic mode; (b) baroclinic mode with specification of surface heat fluxes; and, (c) inclusion of Swan River discharges.

Comparison between predicted and measured currents indicate that during the summer months there is a very good correlation between the predicted currents and measurements. However, during the winter months, when the winds are variable the correlation is poor. This could be attributed to the fact that the action of wind is not the primary driving force during the winter months. Specification of the observed sea level at the open boundaries reproduced the observed sea level but the did not improve the correlation between the model predictions and observations. Inclusion of the baroclinic effects, slightly increased the correlation between the model predictions and observations.

The model has been used to examine the flushing times of a nearshore lagoon area on the assumption that the water within a given volume is completely exchanged when the time (and line) integrals of the influxes (or effluxes) at the boundaries equals its volume. Results of this analysis indicates that the flushing time of the lagoon ranges from < 1 day to > 8 days depending on the wind regime. As wind stress on the sea surface is the major driving force of the currents there is a clear relationship between the wind climate and the flushing time of the lagoon.

References

Arakawa, A. and Lamb, V.R., 1977. Computational design of the basic dynamical processes of the UCLA general circulation model. *Methods Comput. Phys.*, 16:173-263.

Backhaus, J., 1985. A 3 Dimensional model for the simulation of shelf sea dynamics. *Dt. Hydrogr. Z.*, 38:165-187.

Backhaus, J., Crean, P.B. and Lee, D.K., 1987. On the application of a three-dimensional numerical model to the waters between Vancouver Island and the main land coast of British Columbia and Washington State. In: Heaps, N.M. (ed.), Three dimensional coastal ocean models, *Coastal and Estaurine Sciences Vol 4, American Geophysical Union,* 149-176.

Church, J.A., Cresswell, G.R. and Godfrey, J.S., 1989. The Leeuwin current. In: Neshyba, S., Mooers, C.N.K. Smith, R.L. and Barber, R.T. (eds.). Poleward flow along eastern ocean boundaries. *Lecture notes on Coastal and Estuarine studies 34*. Springer-Verlag, 230-252.

Cresswell, G. and Golding, T.J., 1980. Observations of a south-flowing current in the southeastern Indian Ocean. *Deep Sea Res.*, 27:449-466.

Kochergin, V.P., 1987. Three-dimensional prognostic models. In: Heaps, N.M. (ed.) Three dimensional coastal ocean models, *Coastal and Estaurine Sciences Vol 4, American Geophysical Union,* 149-176.

Godfrey, J.S. and Ridgway, K.R., 1985. The large-scale environment of the poleward-flowing Leeuwin current, Western Australia: Longshore steric height gradients, wind stresses and geostrophic flow. *J. Physical Oceanogr.*, 15:481-495.

Pattiaratchi, C.B. and Buchan, S., 1991. Implications of long-term climate change for the Leeuwin Current. *Proc. Royal Soc of WA,* 74:133-140.

Pearce, A. F. and Church, J. A., 1992. A coastal heat and salt budget using seasonal temperature and salinity data off Perth, Western Australia. (Submitted to *Continental Shelf Research*).

Smith, R.L., Huyer, A., Godfrey, S. and Church, J., 1991. The Leeuwin Current off western Australia, 1986-1987. *J. Phys. Oceanogr.*, 21:323-345.

Steedman and Associates, 1981. Cape Peron wastewater ocean outlet effluent dispersion studies. Unpublished Report prepared for Binnie and Partners.

Stronach, J.A., Backhaus, J., Murty, T.S., 1993. An update on the numerical simulation of oceanographic processes in the waters between Vancouver island and the mainland: The GF8 model. *Oceanogr. Mar. Biol. Annu. Rev.*, 31:1-87.

Thompson, R.O.R.Y., 1984. Observations of the Leeuwin Current off Western Australia. *J. Phys. Oceanogr.*, 14:624-628.

Thompson, R.O.R.Y., 1987. Continental-shelf scale model of the Leeuwin Current. *J. Marine Res.*, 45:813-827.

Weaver, A.J. and Middleton J.H., 1989. On the dynamics of the Leeuwin Current. *J. Phys. Oceanogr.*, 19:626-648.

MODELING OF THE RIVER RUN-OFF FRESHENING EFFECT DURING SPRING FLOOD ON THE NORTHWEST BLACK SEA SHELF

A.I. Kubryakov, E.N. Mikhailova, N.B. Shapiro, V.A. Ivanov
Marine Hydrophysical Institute
Sevastopol, 2, St. Kapitanskaya,
Crimea,335000 Ukraine

Abstract

One of the salient features of the northwest Black Sea hydrodynamics is a large river run-off. Salinity has been observed to play a distinctly major role in the formation of three-dimensional circulation and the intensification of horizontal and vertical density field inhomogeneities.

The present work focuses on the study of the river run-off freshening effect during spring flood upon the stratification and water circulation in the north-west part of the Black Sea with assistance of numerical modelling techniques. Calculations involve a multilevel model based on the primitive hydrodynamic equation system using a rigid-lid approximation and simple turbulence parameterization. The area located to the north of 44°N and to the west 34°E was divided into boxes of 5° of latitude by 2.5° of longitude, that is, 6.105 x 4.615 km. Vertically, the maximal number of depth level was 8, with the horizontal current velocity, temperature, and salinity components being calculated at the following levels: 0.5; 1.5; 6.5; 13.5; 26.5; 43.5; 76.5; and 12.35 m. Vertical velocity was determined at midpoints between these depths. Thickness of lowest boxes is equal to the difference between the real depth of the sea and the depth of the last but one box's lower boundary. The largest depth of the sea was 2000 m, and the minimal one, being 7 m, was in the coastal zone. The initial system of differential equations was approximated by the difference analogues using a conservative scheme with the dosed schematic viscosity, which had a transportation capability on shifted grids both in the horizontal (grid B) and vertical. The scheme is two-layered over time and implicit, when vertical diffusion, viscosity, advection, near-bottom friction, and Coriolis acceleration are calculated.

An essential point for the given problem is to prescribe boundary condition at the lateral surface, viz., at the coastline contour, at the open boundary adjoining the central basin, and finally, at the river mouths. At the sea surface and bottom, zero heat and salt fluxes are specified. At the solid lateral boundary the no-slip conditions and the absence of heat/salt fluxes is imposed. At the open fluid boundary adjacent to the main part of the sea, we adopted the free flow conditions for the velocity and specified temperature and salinity for the external sea that may be "imported" into the shelf waters. We suppose that however despite the fluvial dynamic effect's river discharge upon the integrated circulation being fairly modest, its contribution to circulation in the upper layers may prove to be appreciable. Therefore, the effect of river discharge is taken into account here through specifying distributed or point-like sources of water with the given temperature, salinity and velocities. Basically, the river run-off in the northwest Black Sea is constituted by three major rivers, namely, the Danube, the Dniepr, and the Dniestr. Although the Yuzhny Bug-river together with the Ingul-river carry by far smaller amount water into the sea, their rates of flow, too, have been considered in the calculations. The contributions from other

rivers and streams is negligible compared with the rivers mentioned above. Vertically, the total discharge was distributed by two boxes, i.e., within a 4 m - that layer.

The following respective velocities had been adopted for the Danube, Dniestr, Dniepr, Yuzhny Bug and Ingul flows: 10; 7; 15; and 2 cm/s, corresponding to the rates of flow of 27750; 1480; 8325 and 488.4 cubm/s. The overstated values of the rates of flow allow to simulate springtime flood.

Initially the velocities were assumed to be zero, and temperature and salinity throughout the area were prescribed equal to 8°C and 18 psu, respectively, thus imitating the homogeneous state of waters at the end of winter, achieved through convective mixing. Water temperature in the sea and rivers was assumed identical - by virtue of the adopted boundary conditions, it remained invariably at 8°C - thus making it unnecessary to allow for the effect of temperature upon the three-dimensional circulation structure. River water salinity is assumed to be zero and salinity at the external border of the test area equal to 18 psu.

Analysis of salinity distribution reveals that over 30 days, the freshened waters front on the Black Sea surface had shifted away from the Danube estuary by 100 km. By estimating the specific range over which the front may travel over 30 days by virtue of turbulent diffusion we deduce that the upper layer freshening occurs, basically, due to horizontal advection. Highly-freshened waters are, naturally, to be found near the rivers estuaries. The 16 psu isohaline limits approximately half of the sea surface freshened area. In the layers below 20 m, the smallest salinity has proved to be 16 psu, at most. The vertical transect along 45°N shows that the weakly-freshened zone, with S = 16 to 18 psu, constitutes up to 60 - 70 percent of the freshened area. During the initial 10 days, the freshened area's boundary, denoted by the 17 psu isohaline, along the zonal transect across the Danube estuary, which is the most powerful source of freshwater, is saliently steplike (the upper and lower layer's thicknesses are 20 and 15 m, respectively). Within each layer, the front was virtually vertical. During time, the step thicknesses successively increase and by the end of the term (t = 30 days) attain 35 and 20 m, respectively. In each layer, the front remains practically vertical, that is, the upper layer flows related to the river discharge bring down the upper layer's salinity, where by a strong gradient is generated. It should be appropriately noted that each layer being discussed comprises several calculational boxes. With the vertical diffusion coefficient adopted characteristic thickness of the mixing layer is estimated as less than 20 m, i.e., the new salinity structure is largely sustained through vertical advection.

The distribution of integral streamfunction shows that in the two upper layers that receive most of the fluvial water, southward flows dominate throughout the calculation. Starting from the third layer, circulation becomes reminiscent of a gyre, with the predominantly cyclonic sense of rotation. Across the open southern border, saline seawater is flowing into the study area all along the latter's length and outflows in the form of a jet stream near the western shore. To deeper circulation intensity attenuates. As has been demonstrated by the barotropic model, this cyclonic circulation occurs due to the bottom relief.

After about 10 days, an anticyclonic eddy starts to evolve in the subsurface layers of the Danube estuarine area. Getting stronger, the eddy forces the cyclonic flow's northern boundary toward the open sea, this showing off in the integrated circulation distribution. On day 15, the anticyclonic eddy is readily visualized in the integral

streamfunction field. On day 30, the eddy's spatial scale attains 70 km. In the upper layers, receiving fluvial waters, anticyclonic vorticity in the Danube estuarine area also intensifies. In situ data confirm that an anticyclonic eddy occurs in the western part of the northwestern Black Sea shelf area. Such an eddy can be readily seen in the satellite image obtained at the time of spring flooding.

Analysis of the circulation's vertical structure reveals the following. The freshening area is constituted by two distinctly pronounced zones. Near the external border, an upwelling of water occurs, whereas in the estuarine area the water is downwelling. Thus, the entire freshening area is occupied by a single vertical circulation cell.

The process of freshened water propagation may be presented in the following way. Fresh water is coming into the sea from the river, propagating over the surface and veering to the right under the effect of the Coriolis force. Vertical circulation, generated thereby, facilitates a descending of freshwater near the external border of the freshening area and an ascending of relatively salty water in the near-estuarine area, thus contributing to their intense mixing. Stratification transformation due to the freshening leads to an occurrence of an anticyclonic gyre in the vicinity of the Danube estuary, where this effect seems to be strongest . For this the influx of saline waters across the southern open border of the basin, caused by the bottom topography, intensifies.

Also both evolution of the anticyclonic eddy after cessation of the river run-off and influence of wind stress were studied.

The effects discussed above are instrumental for identification of the mechanisms behind the aeration of deep shelf layers and the circulation generation in the northwestern part of the Black Sea.

The work has been accomplished in the framework of the SHELF RESOURCES project with the financial support of the State Committee for Science and Technology of the Ukraine.

BOTTOM BOUNDARY LAYER IN A TIDAL ESTUARY

Ralph T. Cheng, Jeffrey W. Gartner, and Richard E. Smith
Water Resource Division
U. S. Geological Survey
Menlo Park, California 94025

Abstract

Advances in current measuring technology such as used in an Acoustic Doppler Current Profiler (ADCP) have made it possible to determine time-series of three dimensional (3-D) tidal currents in estuaries for an extended period of time. This type of time-series data has been proven to be extremely valuable for improving understanding of estuarine hydrodynamics and transport processes at both tidal and residual time-scales.

However, there are two areas that velocity data are extremely difficult to obtain; namely velocity measurements in the near surface layer and in the bottom boundary layer near water-sediment interface. Unfortunately, these data gaps constrain further understanding the estuarine hydrodynamics. When the water column is stratified (a typical estuarine condition), the dynamics of the surface layer is often de-coupled from the rest of the water column. Without data from the near surface layer, it is hard to define the mixing processes in partially mixed and stratified estuaries. Of course, detailed flow structure in the bottom boundary layer directly affects the balance of momentum, and controls processes associated with sediment erosion, deposition, and transport. Without the velocity data from the bottom boundary layer, it is nearly impossible to quantify the sediment dynamics. This paper addresses one of these two problem areas. The velocity in the bottom boundary layer was measured by a Broad-Band Acoustic Doppler Current Profiler (BB-ADCP). Ancillary data were also taken to assess parameters controlling sediment dynamics in a well-mixed estuary.

A 1200 KHz BB-ADCP was deployed in South San Francisco Bay (South Bay) to measure the detailed velocity distribution within the first 1.5 meter of the water column from the sediment-water interface. South Bay is a nearly well mixed tidal embayment where tidal propagation can be approximated by standing waves, Cheng et al., (1993). The BB-ADCP was mounted on a bottom platform 2 meters above bed, with four transducers pointing downward at an angle 20 from the vertical. Operating in "mode-5" and averaging 5 pings per ensemble (sampling rate), the BB-ADCP was able to determine velocities with a vertical resolution of 5 cm and a standard error of about 0.67 cm/sec, (Rogers, 1993). In this configuration, non-intrusive velocity measurements were made every two-minutes for the first 1.5 meter from bed. The first meaningful velocity measurement was estimated to be as close as 7 cm from the sediment-water interface. Concurrently, ancillary data were collected in the channel of South Bay for two weeks in November 1993. These data included an in-situ upward looking narrow band ADCP (NB-ADCP) for velocity measurements out-side of the bottom boundary layer, a recording Conductivity Temperature and Depth (CTD) for measuring tides, temperature and conductivity, and two Optical Back-Scattering sensors (OBS) for measuring turbidity. The OBS observations were converted to suspended sediment concentration (SSC) by regression against limited water samples. Additionally, OBS measurements were taken at a near-by bridge piling (San Mateo Bridge).

The apparent bottom shear stress, $t_b/\rho = (u^*)^{**}2$, or equivalently, the friction velocity u^*, and the bottom roughness coefficient, z_o, are estimated from time-series of bottom boundary layer velocity data. Each measured velocity profile consists of 32 velocity observations in the vertical. u^* and z_o are estimated by a least-squares regression fitting to the fully developed turbulent boundary layer velocity profile (logarithmic velocity profile, Schlichting, 1962). Reasonable estimates of u^* and z_o have been obtained for periods centered around maximum ebb and maximum flood when the tidal currents were reasonably steady. During transition periods, from ebb to flood or flood to ebb, owing to acceleration or deceleration of tidal currents, the bottom turbulent boundary layer no longer obeys the law of wall. Thus, the estimates of u^* and z_o during transitions determined by fitting to logarithmic profiles are clearly erroneous.

To account for the acceleration or deceleration of tidal currents, two methods are proposed. Following Soulsby and Dyer (1981), a correction term for accelerating or decelerating flows is introduced in the velocity profile, with which more reasonable estimates of u^* and z_o have been obtained. Cacchione et al. (1994) also use this approach for analyzing bottom velocity data from Amazon River Delta. The second approach assumes that the turbulent eddy mixing coefficient remains constant near bed; a mean eddy mixing coefficient is obtained from data representing periods of steady flow. Furthermore, it is assumed that the same eddy mixing coefficient can be used also for transition periods. Using the measured velocity profile and the mean eddy mixing coefficient, the apparent bottom shear stress equals the eddy coefficient times the vertical velocity gradient. While there is no direct measurement of the bottom shear stress available, it is difficult to conclude which method gives a better estimate of u^*.

The second objective of the bottom boundary layer study is to define the relations between hydrodynamics, erosion and deposition of sediments at the sediment-water interface, and transport of suspended sediments. Besides hydrodynamic data, long-term (weeks) SSC data are difficult to obtain. Typically, the SSC are determined indirectly by measuring optical back-scattering intensities that are converted to physical units by regression against limited water samples (ground truth data). Time-series of SSC are extremely hard to determine because the water samples used for regression are difficult to obtain and the OBS sensors (optical lens) are susceptible to marine growth. Errors from marine growth (blockage of light path) produce significant uncertainties in the values of SSC determined by this method. Potentially, acoustic backscattering signals (ABS) can be used to determine suspended sediment concentration by establishing a similar regression relation with ground truth data, (Thevenot and Kraus, 1993). Marine growth can also affect the performance of acoustic measurements. However, the acoustic transducers of ADCP are much less sensitive to marine growth than optical devices.

At deployment site (~15 m at mean lower low water), there were five independent concurrent measurements that can be used for determination of SSC. Two time-series of OBS measurements were taken from the same bottom platform used to mount the downward looking BB-ADCP. Time-series of acoustic backscattering signals are available from both the NB-ADCP (upward looking) and the BB-ADCP (downward looking). Water samples were taken immediately after deployment and immediately before recovery of the BB-ADCP. Furthermore, OBS time-series and water samples were taken from the piling of San Mateo Bridge less than 1 km away from the ADCP deployments.

The ABS signals from the NB-ADCP and the BB-ADCP are similar, but the BB-ADCP gives higher resolution. Thus, only the correlations between the ABS from BB-ADCP and OBS are sought. For a short period up to about 30 hours, this correlation is close to linear (SSC was in the range of 50-150 mg/l). Departure from linearity develops for records covering longer than about 30 hours, probably, owing to a significant OBS

signal drift (possible instrument baseline drift). The OBS time-series at San Mateo Bridge and the OBS time-series at ADCP platform are coherent with some normal scattering of data. These analyses suggest that ABS can be used equally well (and in some sense better than) OBS measurements for SSC. Some uncertainties remain, and they are caused by insufficient "ground truth" data. Although there were OBS signal drifts, linear correlation between ABS and OBS for short periods suggests that a time series of SSC could be inferred from the time-series of ABS. The SSC time-series obtained from ABS is well correlated with the SSC time-series deduced from OBS measurements at San Mateo Bridge for up to 7 to 10 days. Because of the water depth and meteorological conditions during deployment, there was no evidence that the SSC was related to wind waves.

Valuable insights and useful hydrodynamic boundary layer data were obtained and analyzed in this study. Further studies will consider the bottom boundary layer and sediment dynamics in shallow water where wind-waves will be an important factor controlling the bottom stress, erosion and deposition of sediments.

References

Cacchione, D. A., D. E. Drake, R. W. Kayen, R. W. Sterberg, G. C. Kineke and G. B. Tate, 1994. Measurements in the Bottom Boundary layer on the Amazon Subaqueous Delta. to appear in *Marine Geology*.

Cheng, R. T., V. Casulli, and J. W. Gartner, 1993. Tidal, Residual, and Intertidal Mudflat (TRIM) Model and it's Applications to San Francisco Bay, California. *Estuarine, Coastal and Shelf Science*, 36:235-280.

Rogers, J., R D Instrument, 1994. Personal communication.

Schlichting, H., 1962. Boundary Layer Theory. (6th Edition), McGraw-Hill, 744 pp.

Soulsby, R. L., and K. R. Dyer, 1981. The form of the near-bed velocity profile in a tidally accelerating flow. *Journal of Geophysical Research*, 86(C9):8067-8074.

Thevenot, M. M., and N. C. Kraus, 1993. Comparison of acoustic and optical measurements of suspended material in the Chesapeake Estuary. *J. of Marine Environmental Engineering*, 1(1):65-79.

THE ONSET AND EFFECT OF INTERMITTENT BUOYANCY CHANGES IN A PARTIALLY STRATIFIED ESTUARY

Roy E Lewis and Jonathan O Lewis
Brixham Environmental Laboratory
Zeneca Ltd.
Brixham, Devon, UK, TQ5 8BA

Abstract

Introduction

Echo-sounder observations in the Tees estuary, which is a partially stratified system, have shown that appreciable changes in density structure can occur during a tidal period (New et al. 1986). These changes have been associated with the advection of mixed water though the estuary and with abrupt mixing events arising from local instabilities. Observations of velocity, salinity and temperature at anchored stations along the estuary axis have revealed how different salt flux components contribute to the salt balance (Lewis and Lewis, 1983), and how the internal shear stress varies during a tide (Lewis and Lewis, 1987). However, these measurements have generally been taken at discrete one metre intervals which means that it has taken about 20 minutes to profile the full depth. As significant changes in density structure are produced by mixing events on this timescale, such observations are of limited value in determining the causes and effects of mixing.

Instrument packages have been specifically developed for investigating detailed changes in estuary structure. These have revealed highly time dependent mixing during the tidal period (Partch and Smith, 1978), and indicated that shears resulting from the internal wave field make a significant contribution to the active mixing (Geyer and Smith, 1987).

To gain more insight into mixing processes in the Tees estuary, a sampling device was developed which measured velocity and density over the full depth of the water column at a fixed position. Preliminary results obtained with this instrument revealed instances in which conditions rapidly changed from stratified to mixed at the measuring point.

Field Investigation

The profiling device deployed in the Tees estuary consisted of an electromagnetic flowmeter (Valeport Series 800) and a CTD (Valeport Series 600 MK2) attached to a trolley. A beam was set vertically in the bed of the estuary alongside an anchored vessel, and the trolley was attached to this beam so that it could be lowered and raised at any required speed. In this way velocity profiles could be obtained over the full water depth without any significant disturbance by the beam or the vessel which logged the results. Profiles were obtained at 15 minute intervals over the full 12.5 hour period of the semi-diurnal tidal cycle on two successive days (Fig 1).

Mixing Mechanisms During a Tide

In examining data from a single fixed position there is always an element of doubt as to whether the structural changes have occurred locally or whether they represent the simple advection of water past the measuring point from a remote location where a mixing event

has happened. This explanation has been suggested for the appearance of mixed zones in the Tees (New et al., 1987). However, simple advection is unlikely on the ebb because shearing flow is nearly always present and would tend to stratify even an initially well mixed patch as it is carried downstream.

To date mixing in stratified or partially stratified estuaries has been ascribed to three principal causes - bed generated turbulence, interfacial turbulence due to breaking or arrested internal waves, and interfacial turbulence produced by shear instabilities. Bed generated turbulence is typified by erosion of the pycnocline from below and is usually the dominant factor in mixing in shallow estuaries. A prerequisite for wave generated mixing is that interfacial waves with sufficient energy be present in the system, and this in turn depends on a the degree of stratification and the form of the estuary topography. Shear instabilities of the Kelvin-Helmholtz (K-H) type are believed to be particularly important and, as the name implies, they require strong shear across a density interface; such shears may be assisted by shear due to internal waves.

The flow can be characterized by bulk and gradient Richardson numbers so that together with direct and echo-sounder observations of the way the pycnocline alters, it is possible to infer which mechanisms might be responsible for the changes in salinity distribution illustrated in Fig 1. Fig 2 shows schematically the various changes in salinity structure over a tidal period and summarizes the possible explanations for the observed features.

At the start of the ebb tide turbulence generated by bed friction mixes saline water near the bottom higher up into the water column, resulting in the characteristic upward slope of the isohalines and a sharpening of the pycnocline.

The mixing at 10.00 appeared to be triggered at about 09.45 when the bulk Richardson number (Ri_B) was 21.0. Gradient Richardson numbers (Ri) at 09.45 were about 2.0 in the upper 0.5 m of the water column and appreciably higher at greater depth. Such conditions indicate that the mixing was not due to a K-H instability, but it could have resulted from the cusp formations produced by Holmboe waves (Turner, 1973:p 106).

The next mixing event was triggered at about 10.30 when Ri_B was 1.2 and the minimum Ri value of about 1.0 was measured at 1.1 m, which lay within the pycnocline. The flow conditions favor the formation of K-H instabilities which could produce an overturning which carries saline water up the sea surface. The occurrence of K-H instabilities depends on there being sufficient shear across the density interface. As the flow was still just subcritical, the influence of bed drag on interfacial shear may have been limited (Geyer and Farmer, 1989), but internal waves could have provided additional shear.

The mixing event triggered at 11.30 occurred when Ri_B was about 0.2, implying that the flow conditions were supercritical. Gradient Richardson numbers down to a depth of about 2 m were above 3.0 at this time, but reduced to less than 1.0 just below this depth. The strengthened shear across the density interface in the supercritical flow would promote K-H shear instabilities, even in the absence of shears due to internal waves.

The 11.30 mixing event appeared to be complete by about 12.15 as the depth of the pycnocline started to increase. However, by 12.30 the isohalines in the near surface waters had moved upwards and the deeper isohalines became steeply directed downwards to the bed, apparently due to the vertical transport of salt and the seaward advection of the saline intrusion. At 12.30 Ri_B was approximately 0.1, meaning that the flow was distinctly

supercritical and shear across any density interface would be greatly enhanced by bottom friction. This appears to have permitted shear instabilities to continue, thus destroying the stability of the upper layer and allowing bed generated turbulence to complete the process of homogenization.

Very different processes occurred on the flooding tide. The intrusion of saline water near the bottom resulted in a very marked pycnocline. The low Ri values which were measured early on the flood tide implied that Kelvin-Helmholtz instabilities could have formed on the saline intrusion, leading to small prominences on the density interface as have been observed in laboratory experiments (Simpson, 1987).

Nearly 3 hours into the flood tide, a large upward movement of salt occurred over a distance of about 1 km. The incursion appeared to resemble the large billows which have been occasionally observed to form on the backs of saline intrusions in laboratory investigations (Simpson, 1987:p 151). As the flow had become interfacially supercritical, the event could have had its origin in an internal hydraulic jump but more evidence is needed to substantiate such an argument.

References

Geyer, W.R. and J.D. Smith, 1987. Shear instability in a highly stratified estuary. *J. Phys. Ocean,* 17(10):1668-1679.

Geyer, W.R. and D.M. Farmer, 1989. Tide-induced variation of the dynamics of a salt wedge estuary. *J. Phys. Ocean,* 19(8):1060-1072.

Lewis, R.E. and J.O. Lewis, 1983. The principal factors contributing to the flux of salt in a narrow, partially stratified estuary. *Estuarine, Coastal and Shelf Science,* 16:599-626.

Lewis, R.E. and J.O. Lewis, 1987. Shear stress variations in an estuary. *Estuarine, Coastal and Shelf Science,* 25:621-635.

New, A.L., K.R. Dyer and R.E. Lewis, 1986. Predictions of the generation and propagation of internal waves and mixing in a partially stratified estuary. *Estuarine, Coastal and Shelf Science,* 22:199-214.

New, A.L., K.R. Dyer and R.E. Lewis, 1987. Internal waves and intense mixing periods in a partially stratified estuary. *Estuarine, Coastal and Shelf Science,* 24:15-33.

Partch, E.N. and J.D. Smith, 1978. Time dependent mixing in a salt wedge estuary. *Estuarine, Coastal and Shelf Science,* 6:3-19.

Simpson, J.E., 1987. Gravity Currents: In the Environment and the Laboratory. Ellis Horwood, Chichester.

Turner, J.S., 1973. Buoyancy Effects in Fluids. Cambridge University Press, Cambridge.

THE VERTICAL STRUCTURE OF TURBULENT DISSIPATION IN SHELF SEAS

*J.H. Simpson, W. Crawford**, *T.P. Rippeth, A. Campbell and J. Cheok*
University of Wales, Bangor
School of Ocean Sciences,
Menai Bridge, Gwynedd, LL59 5EY
*Institute of Ocean Sciences,
Sidney, B.C.

Abstract

Introduction

A central part of the current agenda in Physical Oceanography of shelf seas is to understand the interactions of the processes which control vertical structure and the diffusion of properties through the water column. First order accounts of the evolution of the density structure have been given in terms of "prescriptive models" which are based on energy arguments and simplified assumptions about the efficiency of mixing processes (e.g. Simpson and Bowers, 1984) and, for the case of freshwater buoyancy input, on prescribed forms of the velocity structure (e.g., Simpson, Sharples and Rippeth, 1991). Such models do not deal with the dynamics of tidal and density driven flow explicitly but rely on combining separate analytical solutions for each component of the flow.

To achieve a more fundamental description of the processes involved and allow for the non-linear interaction between them, it is necessary to solve the dynamical equations for appropriate forcing by the tides (specified as components of the surface slope) and surface windstress. To complete the solution and allow for the vital (two way) interaction between vertical fluxes and water column stratification, the solution must be completed by an appropriate closure scheme, several of which are currently being used (e.g., Lutyen et al.) Most of these schemes involve the explicit representation of the turbulent kinetic energy and its dissipation function ε through which energy is converted into heat. It would seem that an important test of these schemes should be their ability to describe the depth dependence and time evolution of these turbulent parameters.

In this contribution, we report on the first set of observations of turbulent dissipation in the water column in the European shelf seas using the FLY profiler which allows measurements to made to within a few centimetres of the bottom boundary. Observations over full tidal cycles were obtained in March and July 1993 in conditions of (i) near vertical homogeneity, with and without surface heating, and (ii) strong thermal stratification. The observations were made in parallel with measurements from conventional moored current meters and a profiling CTD/transmissometer system with calibration of the latter by gravimetric samples to provide estimates of seston distributions.

Lutyen, P.J., E. Deleersnijder, J. Ozer and K.G. Ruddick. Presentation of a family of turbulence closure models of stratified shallow water flows and application to the Rhine outflow region. (submitted to *Oceanologica Acta*).

Simpson, J.H., J. Sharples and T.P. Rippeth (1991). A prescriptive model of stratification induced by freshwater run-off. *Estuarine, Coastal and Shelf Science,* 33:23-35.

Simpson, J.H., and D.G. Bowers, 1984. The role of tidal stirring in controlling the seasonal heat cycle in shelf seas. *Annales Geophysicae,* 2:411-416

A 1-d Model of Vertical Structure and Flow

The flow properties, both mean and turbulent are to be compared with hindcasts of the flow made using a point models of the dynamics and vertical diffusion with different closure schemes. Initially we shall use the 1-d dynamics model (Simpson and Sharples 1992) with a Mellor-Yamada level 2 closure scheme which is arguably the simplest type of scheme needed in order represent the interaction of flow and stratification. The model solves the dynamical equations for forcing by surface slopes, horizontal density gradients and surface windstress. The eddy viscosity N_z and diffusivity K_z are determined by:

$$N_z = S_M l q; \qquad K_z = S_H l q \tag{1}$$

where S_M and S_H are stability functions of the local gradient Richardson number and l is a prescribed lengthscale.

The evolution of the turbulent kinetic energy $q^2/2$ is described by the equation:

$$\frac{\partial}{\partial t}\left(\frac{q^2}{2}\right) - \frac{\partial}{\partial z}\left(K_q \frac{\partial}{\partial z}\left(\frac{q^2}{q}\right)\right) = N_z\left[\left(\frac{\partial u}{\partial z}\right)^2\right] + K_z\left(\frac{g}{\rho}\frac{\partial \rho}{\partial z}\right) - \frac{q^3}{B_1 l} \tag{2}$$

We shall utilize two versions of the model. In the simplest (MY level 2), we neglect the time derivative and vertical diffusion terms on the LHS and assume a local equilibrium between shear and buoyancy production of turbulent K.E. and dissipation. In the second version (MY2.1) we shall retain the LHS and hence allow for the influence of turbulence diffusing upwards into the flow from the main generation zones near the bottom boundary.

For each of the observational periods and locations, we have run the model with forcing tidal slopes from a 2-d model and the observed winds and surface heat exchange. An example of the simulation of the variation of the ε profile at one of the well-mixed sites in the northern Irish sea over two tidal cycles is shown in fig 1.

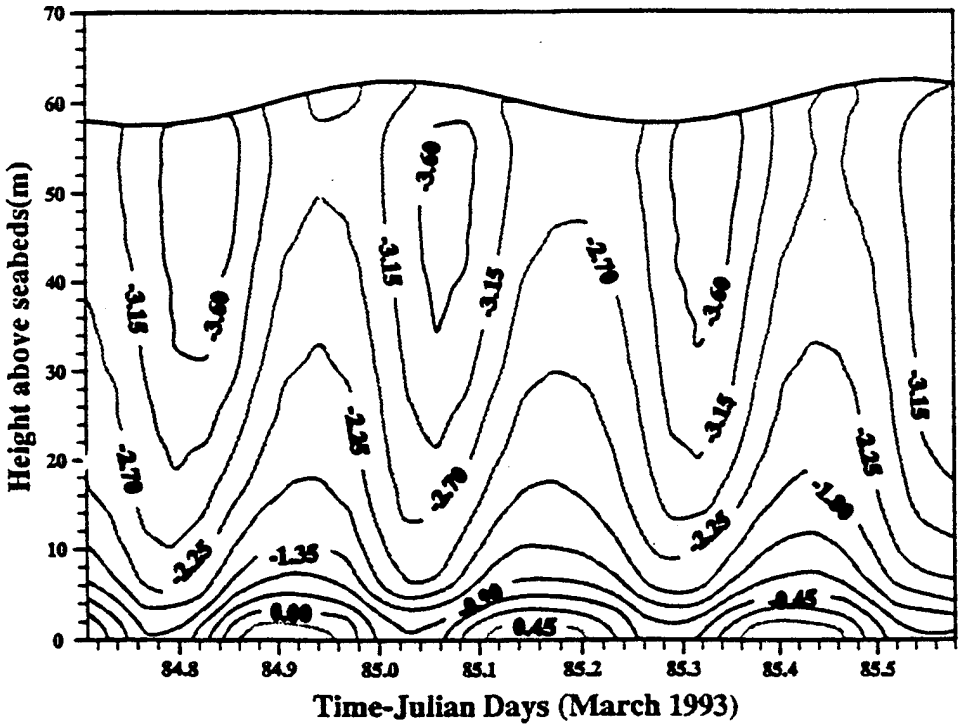

Figure 1. Variation of log E (Wm^{-3}) over a 25 hour cycle from MY2.1 model at IS1 in the northern Irish Sea.

Measurement of turbulent Dissipation

The FLY profiler (Dewey, et al., 1987) falls freely at a speed of 70-80 cm/s and measures components of the horizontal velocity via a piezo-electric sensor which detects the force exerted on a small aerofoil probe by the transverse flow. This force, which is proportional to the horizontal velocity, is differentiated to give the vertical shear on scales down to ~1.5cm. Estimates of dissipation are derived from the mean square shear are obtained from the relationship for isotropic turbulence:

$$\varepsilon = 7.5\mu\overline{\left(\frac{\partial u}{\partial z}\right)^2} \qquad (3)$$

where μ is the dynamic viscosity of seawater. The mean square shear is calculated by first deriving the power spectrum for each section of the record (depth interval = 1.5m). This allows the elimination of high frequency noise and the application of a spectral correction for the roll-off of the shear probe response. The latter is based on the fitting of a Kolmogorov spectrum (see fig 1) at wave numbers higher than k_1=494 m^{-1} (f ~55 Hz) at which point the sensor response is reduced by 50%. This spectrum is also used to correct for dissipation at wave numbers lower than k_2=18 m^{-1} (f=2 Hz) where the signal may be is contaminated by low frequency wobble of the profiler body. These spectral corrections generally represent a small percentage of the observed dissipation and exceeded 20% only at high dissipations (>10^{-2} Wm^{-3}) in the near-bed region.

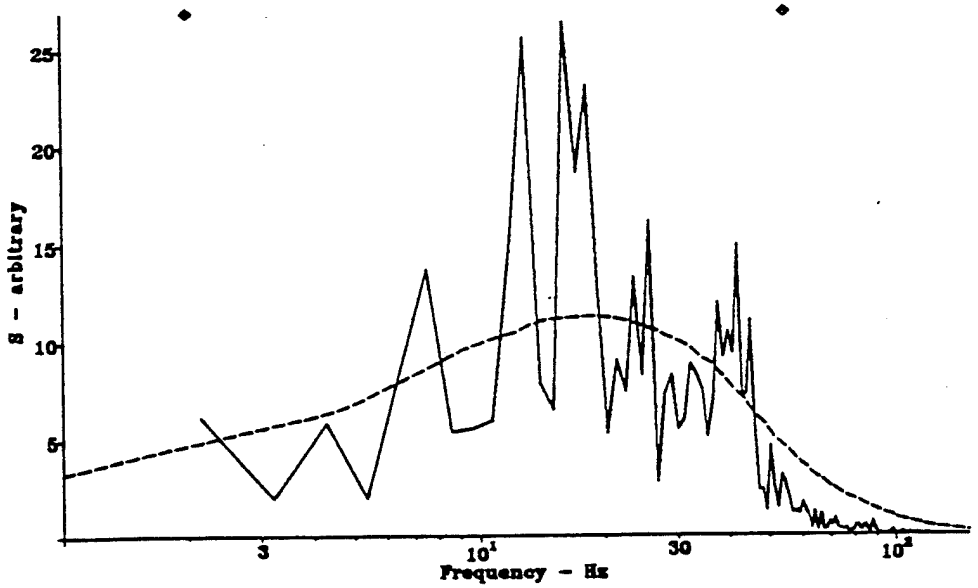

Figure 2. Spectrum of dissipation: observed (continuous) and fitted (dashed) Diamonds represent limits of directly measured contributions to ε.

The sensors at the nose of the profiler are protected by a guard ring which allows the measurement to continue to within a few centimetres of the bottom. After impact with the bottom, the profiler is hauled back to the surface by a light kevlar tether which also acts as a transmission cable for the data stream. The profiler is operated in a yoyo mode cycling between surface and bottom while the ship moves ahead at ~ 0.5 knots. During descent the tether line is fed out by a spooler winch to ensure that the fall of the profiler is unconstrained. A sequence of up to ten profiles were taken between hourly CTD profiles

over one or two semi-diurnal tidal cycles.

Results

The estimates of dissipation from each sequence of profiles were combined to produce ensemble averages of dissipation profile through the water column. The integral of the dissipation over depth should correspond to the total energy loss from the tide which is known to first order from large scale models of the tide as:

$$D = C_d \rho U^3 \tag{4}$$

where U is the tidal current speed and the drag coefficient C_d has a value of ~2.5 x 10^{-3}

Fig. 2 shows a comparison of the depth integral of the local dissipation ε with D based on the current speed at 3m above the bed for measurements in a tidally energetic well-mixed flow with little surface heat exchange. The two quantities are of similar magnitude and exhibit a comparable semi-diurnal cycle.

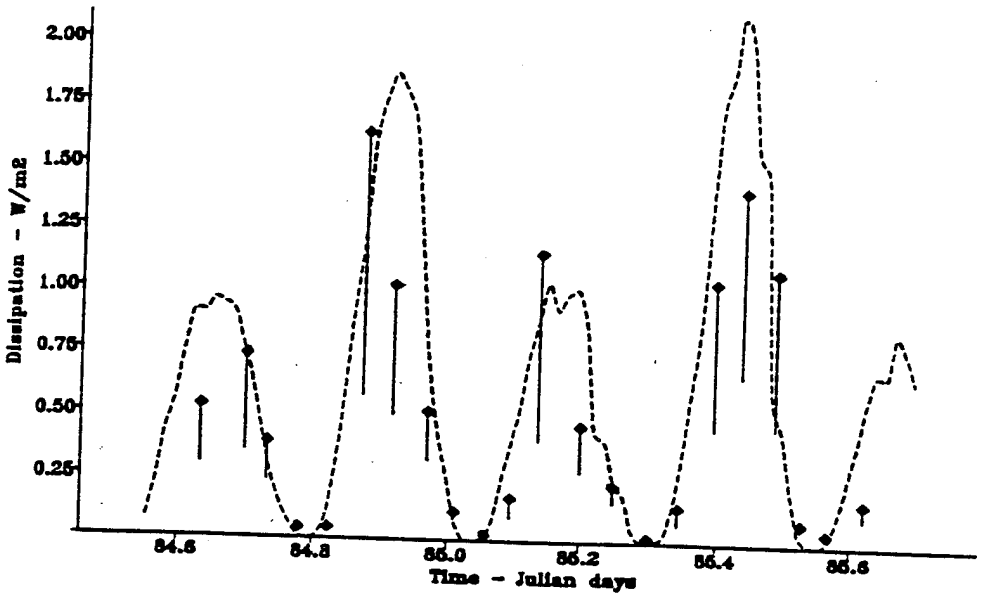

Figure 3. Total water column dissipation estimates based on integration of ε (diamonds) and on the tidal current using equation 2 (dashed).

The ability of the MY2 and MY2.1 models to simulate such data sets under mixed and stratified conditions will be considered in some detail. It is also hoped to include results from a POL model employing a higher level closure scheme which utilizes a differential equation for q^2l (MY2.5)

References

Dewey, R.K., Crawford, W.R., Gargett, A.E. and Oakey, N.S., 1987. A microstructure instrument for profiling oceanic turbulence in coastal bottom boundary layers. *Journal of Atmospheric and Oceanic Technology*, 4(2):288-297.

Simpson, J.H. and Sharples, J., 1992. Dynamically active models in the prediction of estuarine stratification. In *Dynamics and Exchanges in Estuaries and the Coastal Zone*, D. Prandle (ed.), *AGU*, p. 101-113.

Abstracts
for
Poster Sessions

THE ROLE OF THERMAL STRATIFICATION IN TIDAL EXCHANGE AT THE MOUTH OF SAN DIEGO BAY

D.B. Chadwick[1], J.L. Largier [1]and R.T. Cheng[2]
[1]Scripps Institution of Oceanography
La Jolla, CA 92093
[2]US Geological Survey
Menlo Park, CA 94025

Abstract

Introduction:

We have recently examined some aspects of the tidal exchange process at the mouth of San Diego Bay, CA. The horizontal and vertical evolution of the exchange were studied to gain insight into the predominant mechanisms controlling the migration of water-borne contaminants out of the bay. Petroleum hydrocarbons from chronic sources within the bay present a significant environmental concern, and also provide a useful tracer for distinguishing bay water from oceanic water. Previous studies of the tidal exchange process have focused on two general mechanisms. In a coastal embayment, with negligible freshwater inflow, horizontal asymmetries between the ebb and flood tides lead to net tidal exchange through the tidal pumping mechanism (Stommel and Farmer, 1953, Signell and Butman, 1992). In estuaries with significant freshwater inflow, vertical density driven exchange can be expected to provide a significant portion of the net tidal transport (Dyer, 1974).

At the mouth of San Diego Bay, we found that both horizontal and vertical exchange processes appear to be active. This is somewhat surprising in view of the lack of freshwater inflow to the bay during most of the year. The vertical exchange in this case is apparently due to the influence of temperature variations between the bay water and ocean water. The resulting temperature-driven density gradient leads to two related effects which interact with and influence the bay-ocean exchange including, (1) a period of stratified exchange between the outer bay and the ocean primarily during the ebb-flood transition, and (2) the liftoff of the ebb flow as it exists the mouth of the bay. Both of these processes influence the net exchange of bay water to the ocean and visa versa. In this paper, we set out to provide a description of this tidal exchange process at the mouth of San Diego Bay, and investigate the role of thermal stratification in modifying the exchange.

Description of the Study Site

San Diego Bay is relatively long and narrow, 25 km in length and 1-3 km wide, forming a crescent shape between the City of San Diego on the north, and Coronado Island/Silver Strand on the south. Exchange with the ocean is limited to a single passage at the mouth, where the bay forms a north-south channel about 1.2 km wide bounded by Point Loma on the west and Zuniga jetty on the east, with depths between 5-15 meters. The bay hydrograph is characterized by small annual freshwater inflow (mean = 26 cm/year), and zero inflow during most summers. The flow and transport within the bay is generally dominated by a mixed diurnal-semidiurnal tidal forcing with a dominant semidiurnal component(Peeling, 1974). The tidal range from MLLW to MHHW is about 1.7 meters with extreme tidal amplitudes close to 3 meters. Recent bottom mounted ADCP measurements at the mouth indicate current velocities ranging from 20-80 cm/s (Cheng and

Gartner, 1993). Near the mouth, historical observations (Hammond, 1976, Navy, 1950, Smith, 1970), and the ADCP data suggest a net inflow at the bottom, with the bottom velocities leading the surface on the flood tide from between 30 to 90 minutes. Hammond (1976) attributed this inflow to a net northward bottom transport in the ambient flow outside the bay, based on seabed drifter trajectories. However, the ADCP records indicate net landward flow near the bottom is enhanced during periods of neap tide, suggesting that baroclinic circulation may be significant during these episodes.

Surface and bottom water temperatures in San Diego Bay have a seasonal cycle of about 8-9°C (Smith, 1972). During the summer period net heat flux to the bay and limited exchange with the ocean lead to the development of both vertical and longitudinal density gradients in the bay. Smith (1972) found maximum vertical temperature gradients of about 0.5°C/m during the summer. Typical longitudinal temperature gradients of about 7°C over the length (~0.3°C/km) of the bay have been reported (Federal Water Pollution Control Administration, 1973) during the summer months. Spectral analysis of a year-long time series of surface and bottom temperature showed significant peaks at the diurnal and semidiurnal tidal periods, as well as at periods of 8.2, 5.1, and 4.2 (surface only) hours (Smith, 1972). The 8.2 hour response was explained as an interaction between the diurnal and semidiurnal tidal constituents, while the 5.1 and 4.2 hour periods were attributed to a possible seich.

Field Measurements

A series of observations were undertaken during 1993-94 to examine the dynamics which regulate the exchange of bay water with ocean water in the region of the mouth. The observations included bottom-moored ADCP and thermistor records, ADCP/CTD surveys across the mouth of the bay and in the region of the outflowing jet, and axial CTD surveys of the entire bay. In conjunction with the CTD measurements, a flow-through fluorometer was used to measure hydrocarbon concentrations using an ultra-violet fluorometric (UVF) technique as described by Katz and Chadwick (1991).

During the period June 22 to July 23, 1993, a broadband 1.2 MHz ADCP was deployed upward-looking at a bottom depth of about 15 meters just inside the mouth. Data were recorded continuously at a 10 minute interval, providing a temporal record of the vertical flow structure at resolution of 1 meter. Self-recording thermistors were deployed at buoy stations along the axis of the bay at 9 locations and recorded temperatures at 9.6 minute intervals during the period 29 July to 22 August, 1993. Transects across the mouth of the bay were performed through a ~12 hour, symmetrical tidal cycle on 18 May, 1994 using a 1.2 MHz shipboard ADCP and towed CTD/UVF. The CTD/UVF system was profiled while underway to obtain a continuous series of 14 profiles across the mouth. A series of nine transects in the region off the mouth were performed on 19 May, 1994 during tidal conditions similar to the day of the cross-mouth transects. The transects consisted of a series of transverse and axial runs in the region extending from ~1 km inside the mouth to ~5 km offshore from the mouth. Current meters and thermistors were deployed on sub-surface moorings at three locations off the mouth during the period 17-19 May, 1994. A series of CTD/UVF vertical profiles were obtained along the axis of the entire bay on 17 May, 1994.

Results & Discussion

Typical summer conditions for the axial temperature, salinity, density, and UVF tracer distributions are developed from the vertical profiles of 17 May, 1994. The plots show several interesting points. The density field is dominated by the effects of temperature except at the head of the bay where hypersaline conditions have begun to develop. The

overall longitudinal temperature difference in the bay is about 4-5°C, with a local gradient near the mouth of about 0.5°C/km. The temperature/density field progresses from well mixed in the inner bay, to a partially mixed condition in the outer bay where the effect of the cooler ocean water is evident in the enhanced stratification. The vertical gradient in the mid to inner bay is generally less than 0.05°C/m, while near the mouth, the gradient increases to about 0.3°C/m. The UVF distribution clearly indicates the primary source of hydrocarbons in the inner bay, and also illustrates the influence of stratification in the outer bay on the tracer distribution. Surface water conditions off the mouth are examined with a series of near-synoptic contour maps developed from the transects of 19 May, 1994. The tracer and velocity fields indicate that the outflow initiates as a radial source from the mouth, and develops into a jet-like structure which is subsequently "pinched off" during the ensuing flood tide.

A more detailed description of the exchange process and thermal effects is obtained from the transverse and axial sections performed near the mouth where the stratification is strongest. A tidal sequence of the transverse sections for velocity, temperature, and UVF is developed from a subset of the cross-sectional transects from the 18 May, 1994 survey. The sequence begins at the slack flood and progresses through the ebb/flood cycle to the subsequent slack flood. We find that the ebb flow velocities are significantly stronger at the surface with U_Z =O(10-15 cm/s) during much of the ebb period. The transition from ebb to flood is characterized by a period of vertical exchange flow lasting about 1-2 hours during which the surface water continues to ebb while the bottom water has reversed to flood. The flood tide velocities are significantly more uniform in the vertical, and the flood-ebb transition of the surface and bottom velocities occurs approximately in phase. From the density profiles, we find the pycnocline at a slack flood depth of about 6 meters. The vertical temperature difference is about 3°C, leading to a density difference of about 0.5 kg/m^3. The UVF sections show the bay water concentrated in the surface layer during the ebb, the lateral dilution from the channel sides associated with the "pumping" process, and the subsequent return flow of bay water at depth. A qualitative comparison of vertical and horizontal exchange is made on the basis of a T-UVF mixing diagram.

The temporal variation in velocity and density is extracted from the sectional data by looking at mean properties (u,) above and below the average level of the pycnocline at about 6 meters. Plotting this confirms that the bottom velocities are significantly lower than the surface velocities during the ebb flow, while the velocity difference during the flood becomes negligible as the tide approaches peak flow. We find also that the bottom flow reverses approximately 1-1.5 hours ahead of the surface flow during the ebb-flood transition, resulting in a significant period of exchange flow during which the surface and bottom flow are of opposite sign. The internal hydraulic balance of the thermal-driven buoyancy forces and the barotropic tidal forcing is characterized by the barotropic Froude number (Armi and Farmer, 1986) as $F_O = \frac{U_o}{\sqrt{g' h}}$ where U_o is the barotropic component of the velocity, g' is the reduced gravity, and his the water depth. Neglecting frictional effects and mixing, Armi and Farmer showed that strong tidal forcing of a simple two-layer system through a topographic expansion leads to a progression of flow conditions. The cycle begins with a two-layer, baroclinic exchange flow during the slacktide, progresses to an arrested wedge condition as the barotropic forcing increases, and finally to a fully flooded condition in which both layers are driven by the barotropic component. In this progression, the transition from two-layer exchange flow, to the arrested conditions occurs when F_o 0.54, and the transition from arrested flow to a completely flooded section occurs when F_o 1. For the San Diego Bay mouth region, the topographic expansion is replaced by the hydrodynamic expansion of the outflowing tidal jet. Examining the progression of the Froude number and velocity based on the cross-sectional observations, we find

qualitative agreement with this model during the ebb-flood transition, but not during that of the flood to ebb. The tidal asymmetry in the surface and bottom flow is consistent with the tidal straining model suggested by Simpson et al. (1991), however, it is shown that the observed tidal cycle of stratification is inconsistent with this explanation.

To examine the generality of this process, the one-month time series from the bottom mounted ADCP is evaluated. We find that the vertical structure and response of the flow at this station to thermal buoyancy and tidal barotropic forcing is similar to that suggested by the transverse sections at the mouth. In addition, variations during the spring-neap cycle show enhanced effects of the baroclinic terms during the neap tides, giving support to the hypothesis that buoyancy forcing supplied by thermal stratification is important in modulating the tidal exchange process. Analysis of the tidal variation of stratification during a similar time period indicates that the stratification generally builds during the transition from ebb to flood flow, remains stable during the flood, and breaks down during the ebb. This is in contrast to the recent results of Nunes Vaz and Simpson (1994) where the effects of straining of the longitudinal density gradient by the vertical shear lead to the build up of stratification during the ebb and a breakdown during the flood. Since the straining component is negative during the flood flow, the enhanced stratification in our case is explained by an alternative process due to advection of the non-zero longitudinal stratification gradient. The absence of significant strain-induced stratification during the ebb is explained on the basis of vertical mixing (low Rif) due to enhanced vertical shear during the ebb.

References

Armi, L. and D. Farmer, 1986. Maximal two-layer exchange through a contraction with barotropic net flow. *J. Fluid Mech.*, 164:27-51.

Dyer, K.R., 1974. The salt balance in stratified estuaries. *Estuarine Coastal Marine Science*, 2:275-281.

Gartner, J.W., R.T. Cheng, and K.R. Richter, 1994. Hydrodynamic characteristics of San Diego Bay, California - Part II, recent hydrodynamic data collection. *EOS, Transactions, American Geophysical Union*, 75(3):60.

Hammond, R.R., 1976. Seabed drifter movement in San Diego Bay and adjacent waters. Naval Undersea Research and Development Center, San Diego, CA, Technical Report No. TP507.

Katz, C.N. and D.B. Chadwick, 1991. Real-time fluorescence measurements intercalibrated with GC-MS. *Proceedings, Oceans 1991*, 1:351-358.

Nunes Vaz, R.A. and J.H. Simpson, 1994. Turbulence closure modeling of estuarine stratification. *J. Geophys. Res.*, 99(C8):16143-16160.

Peeling, T., 1974. A proximate biological survey of San Diego Bay, California. Naval Undersea Research and Development Center, San Diego, CA, Technical Report No. TP389.

Signell, R.P. and B. Butman, 1992. Modeling tidal exchange and dispersion in Boston Harbor. *J. Geophys. Res.*, 97(C10):15591-15606.

Simpson, J.H., J. Sharples, and T.P. Rippeth, 1991. A prescriptive model of stratification induced by freshwater run-off. *Estuarine Coastal Shelf Sci.*, 33:23-35.

Smith, E.L., 1972. Temperature fluctuations at a fixed position in San Diego Bay. Naval Undersea Research and Development Center, San Diego, CA, Technical Report No. TP298.

Stommel, H. and H.G. Farmer, 1952. On the nature of estuarine circulation. Part II. Woods Hole Oceanogr. Inst. Tech. Rep. WHOI-52-51, Woods Hole, Mass.

FORMATION OF THE COLUMBIA RIVER PLUME - HYDRAULIC CONTROL IN ACTION?

Cynthia N. Cudaback and David A. Jay
Geophysics Program
University of Washington
Seattle, WA, 98115

Abstract

The Columbia River Plume is a large dynamic feature with a significant effect on Northeast Pacific shelf and slope circulation and on local cross-shelf transport of nutrients, pollutants and sediments. The plume is formed on the Oregon-Washington border by outflow from the Columbia River, which carries 3/4 of the fresh water entering the Pacific Ocean between San Francisco and the Canadian border. The surface freshening of the plume, as delineated by the 32.5 psu isopleth, is visible north to the Alaskan coast, where it is augmented by other large rivers (Barnes et al., 1972). Essential characteristics of this plume are determined at its origin, in the constricted entrance to the river. This area is subject to strong river currents and semi diurnal tides with a substantial diurnal inequality. The meeting of salt and fresh water creates a highly stratified flow and large vertical shear. The channel is tightly curved, changing direction by 90 degrees over 10 km. It is constricted laterally by stone jetties in two locations and vertically by a shallow sill. The question at hand is whether these constrictions constitute hydraulic controls.

The sill and lateral constrictions have a significant effect on both the relatively fresh outgoing surface layer and the incoming salt wedge, suggesting a physical interpretation in terms of two-layer hydraulic control theory. Classical steady-state theory, however, is unable to explain crucial aspects of the circulation in the Columbia River entrance. First, the barotropic forcing (riverine and tidal) is strong and time-dependent. Evidence of this time dependence is found in the plume itself, which is formed as a series of distinct fresh water pulses on successive ebbs rather than as a steady outflow. Second, bottom friction and turbulent mixing at the interface have a significant effect on both water masses. Turbulent mixing due to interfacial shear thickens the interface between the upper and lower layer, forming a new interfacial layer of thickness between 1/3 and 3/4 of the water depth. Bottom friction reduces near-bed flows, so the maximum flood current is usually seen in the interfacial layer. Finally, cross-channel depth variations and channel curvature induce lateral circulation and lateral variation in internal Froude number. These effects will be discussed in another paper.

Recent modeling work by Helfrich (1993) expands hydraulic control theory to include strong barotropic forcing which varies sinusoidally in time and suggests parameters to estimate the strength and time dependence of barotropic forcing. Barotropic forcing strength is measured by the ratio of barotropic current speed to the scaling speed (g'H)^1/2, where g' is reduced gravity and H is the total water depth. This ratio is 1-1.5, indicating strong forcing, which can force reversal of the opposing layer and cause alternation of one and two layer flows. The time for an internal wave to propagate across the sill is compared with the tidal period to estimate the amount of time dependence (Largier 1992). For this 8 km long entrance area, the internal adjustment time is about two hours. This is about one sixth of a tidal period, so changing currents may invalidate the quasi-steady-state approximation.

The effects of time dependent forcing at the Columbia River entrance have been examined based on measured salinity and velocity fields, both as time series and along channel sections. All measurements were made with a CTD and a boat-mounted 1.2 MHz ADCP. The time series was taken in May of 1992 and the along channel sections in September and October of 1993. Measurement stations were chosen according to the following topographic influences. The channel curves from northeast to southeast on the landward approach, with a 6 km radius of curvature and a nominal flow width of about 3 km. Lateral and vertical constrictions include: the seaward ends of the North and South Entrance Jetties (km 0) and the crest of the sill (km 1), where there is also a mild lateral constriction. Finally, an intruding jetty (Jetty A, km 4) forms the strongest lateral constriction, and faster currents have scoured out a deep hole. These features have consistent effects on the flood and ebb current and salinity fields.

Velocity and density 18-hour time series measured near the crest of the sill are in reasonable agreement with the predictions of hydraulic control theory incorporating time varying barotropic forcing. Time series measurements of along-channel velocity indicate an alternation of one and two layer flows, consistent with Helfrich's (1993) model for strongly forced systems. However, two layer flows are seen only at the start of flood, not at the start of ebb. This asymmetry is due to the strong river currents, which enhance the ebb and oppose the flow. A steady flow could probably be incorporated into a time-dependent hydraulic control model. The salinity distribution is consistently two-layer, with an interface moving up and down with the tides. The depth of maximum stability was chosen as a layer interface for calculation of a time series of internal Froude number, which shows a clear pattern of long supercritical periods during ebb and flood, interspersed with brief subcritical periods at slack water. This pattern closely resembles model results of Helfrich (1993) for a strongly forced system.

Along channel sections of measured salinity and velocity, taken both an hour after low water and at peak flood (Figures 1 & 2) are in general agreement with the precepts of hydraulic control. Both salinity sections show salt and fresh layers separated by an S-shaped interface as predicted in hydraulic control theory. On early ebb (Figure 1), the topographic uplift at the sill and hydraulic control at Jetty A combine to force plume liftoff just landward of the sill. The internal Froude number at this time is critical seaward of the sill, and strongly supercritical over the sill. On flood (Figure 2), the current is intensified over the sill and reaches its maximum velocity in the constriction at Jetty A. Comparison of the two velocity sections (Figures 1b and 2b) shows the alternation of two-layer and unidirectional flow consistent with time varying barotropic forcing.

The most important differences between observation and theory are due to interfacial mixing and bottom friction. There is a persistent stable layer (high gradient Richardson number, Ri_g) at mid depth due to turbulent mixing caused by interfacial shear. This stable layer moves up and down with the tides and thickens to fill the water column at slack water. This combination of semi and quarter diurnal signals in Ri_g indicates internal tidal asymmetry and is not predicted by hydraulic control theory. The same stable layer shows in the along channel sections. The layer thins over the sill, indicating topographically enhanced mixing. The current at peak flood (Figure 2b) also shows the limitation of two-layer hydraulic control theory. The flood current starts at the river bottom, but is opposed by bottom friction, so the maximum flood velocity is found in the pycnocline. This three layer velocity field cannot be predicted from hydraulic theory. The same figure also shows, as noted above, the enhancing effect of the sill and lateral constriction.

This leads us to the main question of this paper - is this hydraulic control in action? The answer is 'sort of'. The basic importance of sills and constrictions is clear. The salinity

fields show two well behaved layers, with an interface following the predicted trend. Velocity measurements, however, refuse to be confined to a simple two layer pattern. The effects of interfacial mixing and bottom friction, combined with complicated time dependent forcing, show that this area cannot be modeled adequately with hydraulic control theory alone.

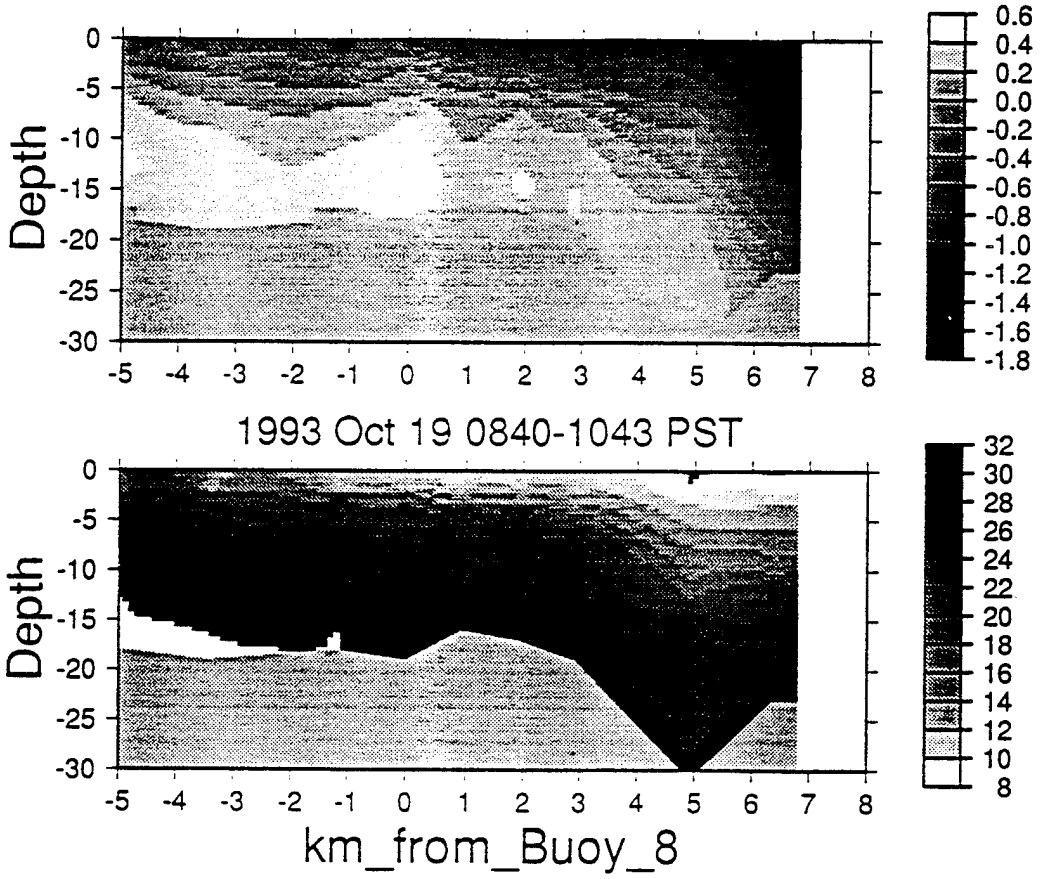

Figure 1) along channel sections 1 hour after low water. a] along channel velocity; b] salinity.

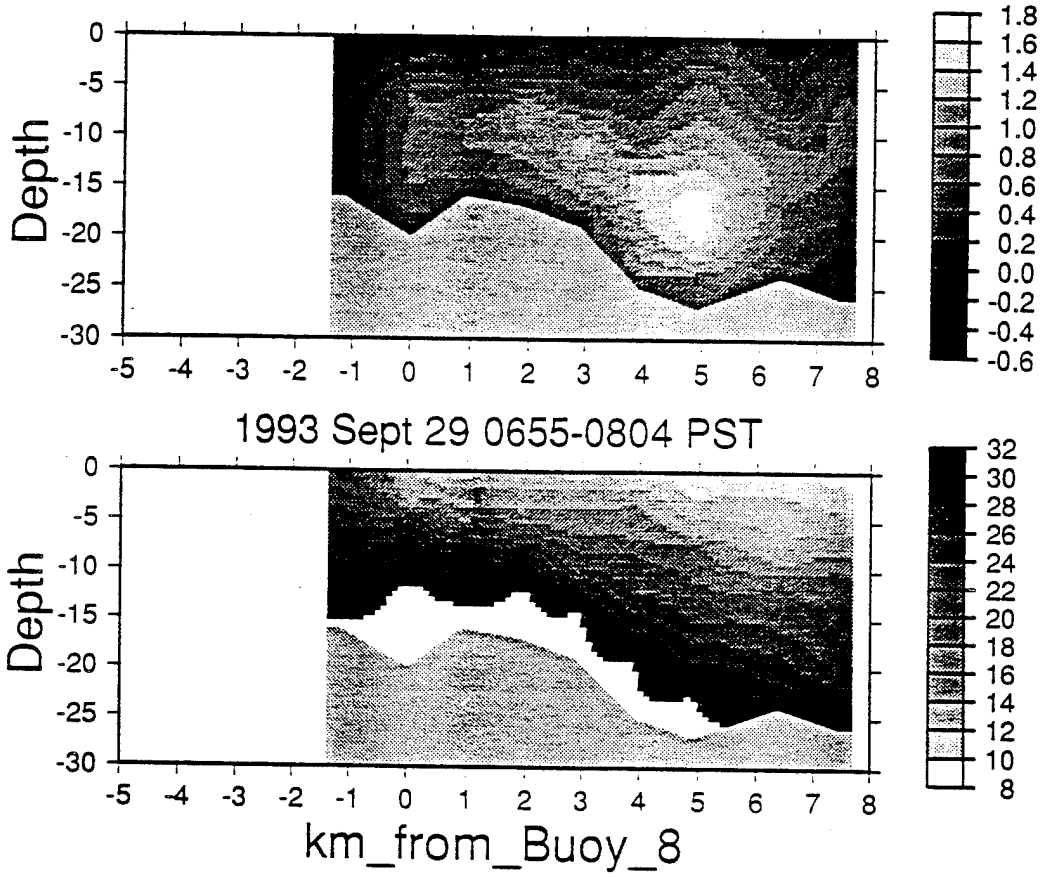

Figure 2) along channel sections near peak flood. a] along channel velocity; b] salinity.

References

Barnes, C. A., A. C. Duxbury, and B. Morse, 1972. Circulation and selected properties of the Columbia River effluent at sea, in The Columbia River Estuary and Adjacent Ocean Waters. A. T. Pruter and D. L. Alverson (eds.), University of Washington Press.

Helfrich, K. R., 1993. Time Dependent Two Layer Hydraulic Exchange Flows, submitted to *Journal of Physical Oceanography*.

Largier, J. L., 1992. Tidal Intrusion Fronts, Estuaries.

THE EFFECT OF RIVER FLOW ON TIDAL CONSTITUENT AMPLITUDES: AN APPLICATION OF WAVELETS

Edward P. Flinchem and David A Jay
Geophysics Program, AK-50
University of Washington
Seattle, WA 98195 USA

Abstract

We apply the recently developed mathematical apparatus of the wavelet transform to the analysis of riverine tides which deviate markedly from the assumption of exact periodicity inherent in the traditional method of harmonic analysis. The wavelet transform (also known as a perfect reconstruction filter bank or a multiresolution analysis) has in the last decade undergone rapid development and seen application in such diverse fields as applied mathematics, quantum mechanics, signal analysis, image processing, turbulence, acoustics, and data compression. We summarize the elementary notions of the wavelet transform and contrast them with those of harmonic analysis. We construct a wavelet basis specially adapted to tidal problems and use it to analyze the modulation of the external tide in a river by variations in stream flow. Assuming upstream tidal propagation in a linear channel of constant cross section with quadratic friction, one may deduce that the amplitude of the semidiurnal wave should vary linearly with the negative square root of the river discharge. The wavelet analysis reveals the predicted relationship which harmonic analysis would have obscured.

Tidal analysis in nearly the same form as it is used today was formulated in the latter half of the 19th century to address the need to predict the tides at coastal seaports. In that role it has proved enormously successful, reducing perhaps 95% of the variance to a table of a few dozen numbers. Success is made possible by the generally valid assumption that tides are a statistically stationary phenomenon, being as they are almost literally an earthly reflection of the music of the celestial spheres.

While the simple form of the prediction problem has long been solved, many less predictable phenomena of significant interest remain which are not amenable to study by the old method. As Munk and Cartwright (1965) observed, "...predicting and learning are in a sense orthogonal, and the most interesting effects are those that cause the most trouble with forecasting...". Precisely the feature of harmonic analysis that enables it to have nearly unlimited predictive scope in certain circumstances, i.e. the infinite extent of the trigonometric basis functions, implies, conversely, that the method is also inherently ill-suited to the description of situations where an aperiodic input modulates the response of an aquatic system to otherwise purely tidal forcing. A fine example are river tides, which can exhibit exceptionally non-stationary behavior on seasonal and shorter time scales due to fluctuations in river flow.

While non-stationary tides can be investigated by the harmonic analysis of a series of short segments of a longer total record, such an approach is inflexible, poorly resolves transient events, and excludes periods greater than the segment length. The newly emerging theory of wavelets provides a very general, flexible, and powerful tool to elucidate the time evolution of the frequency content of data in a self-consistent manner at all time scales. Developed only in the last decade or so, wavelets represent a remarkable synthesis of

developments in mathematics, physics, electrical engineering, and computer science. Rioul and Vetterlie (1991) present a broad overview of the main concepts in wavelet analysis with a minimum of mathematical detail. The simple physics of a frictionally damped, landward propagating tidal wave (Parker, 1991) provides a clean framework in which to explore the potential advantages of a wavelet approach to analyzing time series of oceanographic data. The Columbia River, with its five fold annual variation in flow and tidal influence extending 150 km upstream, illustrates the physics well.

Adopting the viewpoint of the continuous wavelet transform [CWT], we design and construct a prototype wavelet optimized for the problem at hand. The resulting function is symmetrical in time and phase linear. In CWT formalism, the prototype wavelet, $\psi_0(t)$, is a kind of bandpass filter which is continuously scalable in frequency. Unlike the trigonometric basis functions of harmonic analysis which have only a single parameter, frequency, wavelets are parameterized by both position and frequency scale, $\psi_{a,b}(t) = a^{-1/2} \psi_0(at + b)$). Given a time series, x(t), the transform is:

$$\tilde{x}_{a,b} = \int x(t)\psi^*_{a,b}(t)dt$$

Thus, the one dimensional input is transformed into a two dimensional field showing the energy content of the input as a function of both time and frequency scale. The CWT achieves great flexibility in time and frequency resolution at the cost of a greater or lesser degree of overcompleteness or redundancy in the sense of being a basis for $L^2(R)$, the class of all square integrable functions of a real variable. Over-completeness is in no sense a disadvantage for the purposes of data analysis. Exploiting the property of being continuously scalable in frequency, we chose time dilations so as to neatly divide frequency space into ranges isolating the tidal bands of interest: diurnal, semidiurnal, terdiurnal, and quarter diurnal. Extension of the method to include higher overtides and tidal monthly variability is straightforward. In practice, measuring instruments return values at discrete intervals, not continuously, so appropriately scaled versions of the prototype wavelet are discretely sampled and convolved with hourly tidal height data to generate new time series of amplitude and phase for each tidal band.

Year long, hourly tide gauge records from stations at km-28 (river kilometer 28), km-66, and km-133 are analyzed and compared to flow estimates calculated from Bonneville dam data. Theoretical analysis of tidal propagation upstream in a linear channel of constant cross section in the presence of strong friction leads to a diffusive wave equation. Assuming quadratic friction, the amplitude of a semidiurnal tidal constituent should vary as the square root of the river flow. Wavelet analysis of the Columbia River data clearly reveals the expected relationship. An earlier study (Jay, 1984) using harmonic analysis on month long records found a three fold suppression of the amplitude of the semidiurnal tide during the period of peak flow at km-133. The present study reveals an eight fold diminution and shows that the effect is visible on time scales as short as two days. Damping of the tide by river flow decreases from km-133 to km-66, where the reduction is five fold, becoming almost imperceptible at km-28. The effect of flow on the amplitude of the quarterdiurnal wave is dramatically greater with reductions by factors of 24 and 17 at km-133 and km-66, respectively, on days of peak flow.

We expect wavelet techniques to prove invaluable to future studies of the nonlinear, time dependent dynamics of estuaries and coastal seas. Likely applications include analysis of internal tides, the effects of atmospheric forcing, and internal tidal asymmetry. We have focused our attention on tidal problems because they have a structure beautifully suited to showcasing the strengths of the wavelet transform. We foresee, however, a time in the not too distant future when wavelet methods will be applied routinely to a wide variety of

wavelike and unsteady oceanographic processes, regardless of whether they are dynamical, chemical, or even biological in nature.

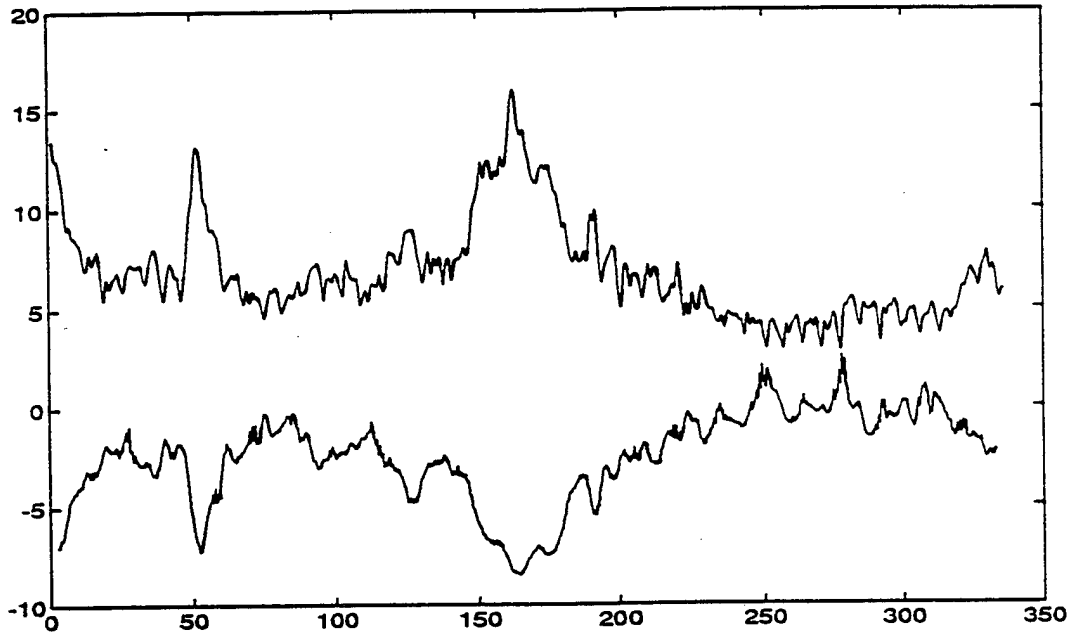

Figure 1. Daily river flow ($10^3 m^3 s^{-1}$, upper line) and 30 times the ratio of M_2 amplitude at km-133 to M_2 amplitude at km-28 (offset by -10, lower curve). At km-28 the tides are essentially unaffected by river flow variations. Tidal amplitude at the upriver station decreases with the square root of the river flow.

References

Jay, D.A., 1984. Circulatory Processes in the Columbia River Estuary. CREST, Astoria, OR.

Munk, W.H. and D.E. Cartwright, 1965. Tidal spectroscopy and prediction. *Philosophical Transactions of the Royal Society of London,* A259:533-581.

Parker, B.B., 1991. The relative importance of the various nonlinear mechanisms in a wide range of tidal interactions. *Tidal Hydrodynamics,* Wiley, New York, p. 237-268.

Rioul, O. and M. Vetterli, 1991. Wavelets and signal processing. *IEEE Signal Processing Magazine,* 8 (4):14-38.

SEASONAL VARIATION IN THE CIRCULATION AND HYDROGRAPHY OF THE TAY REGION OF FRESHWATER INFLUENCE

M. Lyons
The Marine Laboratory
PO Box 101, Victoria Road,
Aberdeen AB9 8DB, Scotland.

Abstract

The Scottish North Sea Coastal Zone (SNSCZ) can be regarded geographically as approximating to the strip of water between the coast and the 50m depth contour extending the length of the Scottish east coast. Probably the most important area within the SNSCZ is that defined by the region influenced by the freshwater output of the Firth of Tay which with a annual mean discharge of 210 cumecs is the largest source of freshwater to the British coast and also one of the largest exporters of dissolved nutrient to the SNSCZ (Lyons et al, 1993).

During 1993 the Marine Laboratory, Aberdeen deployed an array of six moorings within the St. Andrews Bay area, off the mouth of the Firth of Tay, for the duration of the year. A series of nine hydrographic cruises collected data along sections across the study area during the deployment. Data obtained by a selection of moored instruments was subjected to low pass filtering and divided into a set of seven periods which formed the basic data set of the study.

The resolution of the components of a complex circulatory regime such as exists within the St. Andrews Bay area presents a considerable challenge. An obvious first stage in such a resolution is the identification of the major forcing factors associated with the barotropic mode of the circulation. On average 70% of the variance across the area was associated with this mode with somewhat less at the inshore sites (in the vicinity of the plume) and somewhat more offshore. Seasonal variations were apparent with a slight increase in the depth dependence over the summer months. EOF analysis of the low-passed current records revealed the dominant orthogonal mode to be barotropic and topographically steered at all sites over the winter months. During summer however the barotropic mode was split into two oppositely directed modes corresponding to apparently independent motion at the inner and outer moorings (at depths of 15 - 30m and 50 m respectively).

An analysis of correlation between the depth-mean low-passed currents and local wind stress revealed a high degree of coherence at each site with the maximum correlation at both sites typically being with the longshore wind. At the outer moorings however the correlation was inverted suggesting the inner barotropic to be driven directly by the longshore component of the wind while at the deeper outer sites the longshore pressure gradient may be the forcing factor. This was investigated by an analysis of the pressure field along the SNSCZ.

Coastal sea level was obtained at three sites spanning the SNSCZ and converted to coastal pressure via the hydrostatic relation. Coherence between these records and those obtained from moored water level recorders was in excess of 99% demonstrating the large scale of coastal pressure variations in relation to the length scale of the SNSCZ. EOF analysis revealed approximately 85% of the variance in the pressure field to be associated

with simultaneous raising and lowering of the pressure field while the remainder was associated with longshore pivoting. An analysis of the correlation between coastal pressures and the local longshore wind showed little evidence of the "classical" relationship often described in the literature (e.g., Csanady, 1981). Many of these accounts however deal with the North American oceanic coastal boundary where the offshore length scale is large compared to the scale of weather systems and deep water beyond the shelf edge lies relatively close to shore. Neither of these is the case in the shallow and enclosed North Sea. Coastal sea level within the North Sea is dominated by large scale set-up/down associated with storm surges generated at the shelf edge (Heaps, 1969) and so is not necessarily correlated to local winds.

Longshore pressure gradients were calculated for the entire length of the SNSCZ and along the NE coast on which the study area is situated. Variability was found to be highly correlated in all cases (four slopes were calculated) however the amplitude of slopes on the NE coast was approximately twice that of events along the entire SNSCZ. This effect appears to be due to the presence of the Moray Firth, a large embayment, which changes the orientation of the coastline from SW/NE along the NE coast to E/W and changes the mean SW wind from longshore to cross-shore therefore reducing its forcing effect. The longshore pressure gradient was found to be highly correlated with the longshore wind throughout the year. A regression analysis revealed the response of the water column to longshore wind stress to be seasonally invariant with a wind stress of 0.1 Nm^{-2} generating a slope of 8×10^{-7}. This value is comparable to that found by other researchers, for instance Cragg et al. (1983) found a value of 7.5×10^{-7} for the West Florida coast while Marmorino (1983) calculated values twice this for the same region. It appears that the pressure gradient along the coast of NE Scotland is generated directly on sub-tidal scales by the local wind, the effect of the wind modifying slopes associated with storm surges.

The terms of the linear depth integrated longshore momentum equation were calculated for each mooring position and period throughout the year, terms were submitted to an EOF analysis to assess their importance to the momentum balance. The local acceleration was found to be everywhere the smallest term throughout the year with a typically low contribution to the first empirical mode. This suggests that the momentum balance of the study area can be regarded as quasi-steady with acceleration effects due to the traveling wave aspect of storm surges having a small effect on sub-tidal time scales. The Coriolis term was of significant size in all cases ($1\text{-}3 \times 10^{-6}$ ms^{-2}) but was largely uncorrelated to other terms. This is in line with findings of several other studies (Allen and Smith, 1981, Lentz and Winant, 1986) and is likely to be due to the poor vertical resolution afforded by a two-RCM mooring within a baroclinic region.

The bottom stress term was derived using a linear parameterization suitable for tidally dominated regions (e.g., Heaps, 1978) giving a friction coefficient of 10^{-3} ms^{-1}. This value was verified using linear regressions between wind stress and near-bed currents. The term was found to be significant in all cases with an S.D. of $0.5\text{-}3 \times 10^{-6}$ ms^{-2}.

The first EOF mode (using the correlation matrix) was dominated by a balance between the wind stress and longshore pressure gradient terms with 75% of the variance of each term explained by the first mode. The pressure gradient was in all cases the dominant term with a S.D. of $2\text{-}6 \times 10^{-6}$ ms^{-2}, however the amplitude of the wind stress term amounted to only half of this even at the inner sites where wind stress obviously drove the flow at all depths. Plots of the terms of the momentum equation show clearly the inverse correlation between the wind stress term and the pressure gradient. They also

show the wind stress to be balanced by the bottom stress at the inner sites and the pressure gradient to be balanced by bottom stress in deeper (50m) water with typically strong correlations apparent throughout the year. It is also clear however that the wind stress term as calculated is insufficient to fulfill its role at the inner moorings, being dominated by the pressure gradient, resulting in a poor fit to the bottom stress when summed as required by the momentum equation. Regression analysis showed a high degree of correlation with the bottom stress term (proportional to the depth mean flow) could be achieved at the inner sites if the wind stress term was increased by a factor of three prior to summing with the pressure gradient term. The physical reason for this imbalance is unclear at present, it appears likely however that rather than the wind stress term being in error the topography of the bay acts to reduce the local pressure gradient inshore. This is difficult to verify in practice as small scale localized pressure variations give rise to noise of the same order as the signal we need to detect. Further work is currently underway to resolve both this imbalance and the circulation of the region, both barotropic and baroclinic, in greater detail.

In conclusion it is apparent from data and EOF analyses that barotropic flow along the Scottish NE coast is largely determined by the frictionally balanced wind stress and pressure gradient in the manner described by Csanady (1981) as a "shelf circulation cell" with wind stress directly dominant inshore and the longshore pressure gradient acting to produce a current reversal in deeper water. A momentum balance has not yet been achieved for inshore waters and is the subject of work in progress.

References

Allen, J.S. and R.L. Smith, 1981. On the dynamics of wind-driven shelf currents. *Phil. Trans. R. Soc. Lond. A302,* p. 617-634.

Cragg, J., G. Mitchum and W. Sturges, 1983. Wind-induced sea-surface slopes on the West Florida shelf. *J.P.O.,* 13:2201-2212.

Csanady, G.T., 1981. Shelf circulation cells. *Phil. Trans. R. Soc. Lond., A302,* p. 515-530.

Heaps, N.S., 1969. A two-dimensional numerical sea model. *Phil. Trans. R. Soc. Lond. A265,* p. 93-137.

Heaps, N.S., 1978. Linearised vertically integrated equations for residual circulation in coastal seas. *Deut. Hydrogr. Z.,* 31:147-169.

Lentz, S.J. and C.D. Winant, 1986. Subinertial currents on the southern Californian shelf. *J. P. O.,* 16:1737-1750.

Lyons, M.G., P.W. Balls and W.R. Turrell, 1993. A preliminary study of the relative importance of riverine nutrient inputs to the Scottish North Sea Coastal Zone. *Mar. Poll. Bull.,* 26:620-628.

Marmorino, G.O., 1983. Small-scale variations of the wind-driven coastal sea-level response in the West Florida Bight. *J.P.O.,* 13:93-102.

LABORATORY SIMULATIONS OF COASTAL CURRENTS

Timothy P. Mavor and Pablo Huq
College of Marine Studies
University of Delaware
Newark, DE 19716

Abstract

The presence of a density-driven coastal current is of great importance to near-shore physical and environmental processes. As a transport system for pollutants and waste, the current could threaten coastal environments by depositing the contaminants along-shore. Conversely, it could provide off-shore transport and across-shelf mixing for these same hazards. The coastal current also transports nutrients upon which ecosystems depend. Often, a well-defined boundary between the different water masses is observed. Such fronts exhibit steep salinity and temperature gradients, yet the characteristics and dynamics of the frontal boundary are still largely unresolved. Hence, laboratory experiments on a rotating turntable have been conducted to further the understanding of such buoyant flows.

The experimental configuration consists of a buoyant outflow leaving a bay and moving onto a continental shelf. Experimental results show that several parameters characterize the outflow dynamics. The ratio of the buoyant layer depth to that of the total depth of the water, the momentum and buoyancy fluxes of the discharge, as well as varied Coriolis parameters, are of particular significance. The establishment and stability of coastal currents is also considered. On the shelf, meanders and eddy-like instabilities grow to length scales much larger than the internal Rossby deformation radius (R_d), with timescales of ft of θ (100). Cross-shelf eddy diffusivities are found to depend on scales of these instabilities.

Experiments were conducted with various configurations, with particular interest on bay-shelf interaction. The angle of the bay to the coastline was set to be either 90°, 60°, or 45°. Also, a headland was extended up to 4 R_d across the mouth of the bay at upstream baymouth corner. The water depth in the bay-shelf system was also varied between experiments. The salinity difference between the buoyant outflow and the basin water was 1%, with an outflow velocity such that the Froude Number $F < 1$ in all cases, with some experiments having $F \ll 1$. Changes in the buoyant outflow were expected as the experimental configuration was varied. Observed downstream changes in the coastal current itself were slight, with most notable changes occurring near the bay mouth. Additionally, the presence of an inflow was noted along the upstream side of the baymouth. When the headland was present, this inflow generated an anticyclonic gyre approximately the width of the headland. Similar eddies are found due to tidal forcing by Signell and Geyer (1990). The velocities and trajectories of particles in both the inflow and buoyant outflow are documented. The inflow velocity near the baymouth was typically $\frac{1}{4}$ that of the outflow.

Another set of experiments was carried out to more closely examine the coastal current itself. One area of interest is the effect of flow separation and eddy generation by a current around a corner, as found by Klinger (1994). The bay-shelf experiments did not show large flow separation near the corner for the small velocities used in these experiments. To resolve aspects of flow separation, experiments were conducted with the

buoyant source 0.5 R_d away from the straight coastline. These were then compared to similar experiments except that the source was positioned at the coastline. The most notable difference was the time of occurrence of the instabilities. The width and the speed of the current did not change appreciably.

Instability data for experiments, similar to that of Chabert D'Hieres et al. (1991), has been gathered. In addition, we find that the change in the ratio of the top layer depth to the bottom layer depth has an effect on the time of occurrence of the first instability. There is a consistent trend of faster occurrence of the first instability when the top layer of buoyant fluid is closer to the bottom. Griffiths and Linden (1981) also found that the ratio of the top layer depth to the bottom layer depth was an important parameter in their experiments. They determined that when this ratio is small, the instabilities were probably primarily barotropic; when the ratio was of $O(1)$, the instabilities were predominantly baroclinic.

References

Chabert D'Hieres, G., H. Diddle, and D. Obaton, 1991. A laboratory study of surface boundary currents: application to the Algerian Current. *J. Geophys. Res.*, 96:12539-12548.

Griffiths, R.W., and P.F. Linden, 1981. The stability of buoyancy-driven coastal currents. *Dyn. Atmos. Oceans*, 5:281-306.

Klinger, B.A., 1994. Eddy generation at a sharp corner. *J. Geophys. Res.*, 99:12515-12531.

Signell, R.P. and W.R. Geyer, 1990. Numerical simulation of tidal dispersion around a coastal headland. In *Residual currents and long-term transport, Coastal and Estuarine Studies*, 38:210-222.

AN AIRBORNE AND GROUND TRUTH INVESTIGATION OF A BUOYANT PLUME IN A STRATIFIED ENGLISH BAY

Toby J. Sherwin and Peter C. Jonas†*
*Unit for Coastal and Estuarine Studies
UCNW Marine Science Laboratories
Menai Bridge, Anglesey, LL59 5EY, UK
†NRA (South West Region)
Manley House,
Kestrel Way,
Exeter, Devon, EX2 7LQ, UK

Abstract

Introduction

A common perception in the UK water industry is that the British Isles are surrounded by a large tide which generates strong tidal currents which in turn provide significant turbulence to effectively disperse any marine effluent. Whilst there may be some general truth in this idea, there are nevertheless important areas where this is not true and where the tidal currents are weak so that the surface waters become stratified in summer. It is not generally recognized that such regions can exist very close inshore and that it is possible for British marine outfalls to discharge into waters where tidal dynamics do not dominate. An effluent can then become trapped in the surface waters and pollutant dispersion is then determined by other factors such as solar radiation, wind stress and horizontal salinity gradients. In the past it has not been the policy of UK pollution agencies to assess the impact of a new outfall once it has been constructed, so it has been difficult to assess the value of pre-construction site surveys. In this presentation we address some of these points by looking at the performance of a new marine outfall that is located in a small English bay.

Background Oceanography

St Austell Bay on the south coast of Cornwall is unusual (although not unique) for British waters in that although the tidal range is over 3 m, it experiences very weak tidal currents close inshore. The amplitude of M2 (2.4 cm s^{-1}) is much smaller than the mean residual flow (6 cm s^{-1}, see Fig. 1). As a result the water column can become significantly stratified in summer, in particular when wind speeds are less than about 4 m s^{-1} (Sherwin and Jonas, 1994, *Mar. Poll. Bull.*, **28**, 9, 527-533).

The difference in the dynamics of the bay between calm and windy days in summer is very pronounced. On windy days the top 5 to 8 m become mixed, the longitudinal diffusion coefficient (K_x) reduces to about 0.5 m^2 s^{-1} and the surface waters tend to follow the mean circulation, eastward through the bay at about 6 cm s^{-1}. However, when winds are weak the surface waters stratify and the top 2 m becomes decoupled from the flow below. This surface layer is then susceptible to wind forcing and surface shears can result in much higher values of K_x existing in the downwind direction (up to 2 m^2 s^{-1}). In these circumstances onshore sea breezes can result in surface wind driven flows being advected towards the shore at the centre of the bay.

Observations of the Marine Discharge

The dispersion of the discharge from a new marine outfall in the centre of the bay in this latter situation was examined by the National Rivers Authority on 13th August 1993, when a stratified sea breeze event occurred during neap tides. Rhodamine B and *B. globigii* spores were introduced into the flow at the sewage treatment works and their distribution, along with that of faecal coliforms (which always occur in domestic discharges), were measured during the day. This was done using a Chelsea Instruments Aquatracker to measure fluorescence and taking water bottle samples of the bacteria. In addition a Compact Airborne Spectral Imager (CASI), provided by Southampton University, was flown over the bay on several occasions during the experiment. The background oceanography was determined by tracking drogue/floats and obtaining temperature and salinity profiles.

The CASI images show that, as expected, the outflow (which was trapped in the surface waters) was transported northwards and onshore during the morning, at between 5-9 cm s^{-1}; later in the day the flow turned towards the north-east. At all times the centre of the plume was clearly identified, but in addition the images reveal a fine structure which may be wind induced. It is estimated that faecal coliform T_{90} (decay time) values were sufficiently fast (order 1 hour) that the risk to water contact users near the beach was very small, even though the flow was onshore.

Conclusions

A complete analysis of the data is still being conducted, but it should allow estimates of the lateral diffusion coefficient to be made and tie in variability of the *in situ* fluorescence measurements with the CASI images. Even before this work has been done, it would appear that the site surveys conducted before the construction of the outfall have provided a reasonably accurate insight into the behaviour of the discharge into St Austell Bay. The data collected in the post-construction survey should help to improve future survey techniques of measurement and data analysis and, in particular, provide pointers to how such surveys should be conducted in stratified bays around Britain. In addition, the work points to the importance of having accurate estimates of the decay times in the sea of bacteria and viruses that are potentially hazardous to health.

Note

The views expressed in this paper are those of the authors and should not be construed to represent those of the National Rivers Authority.

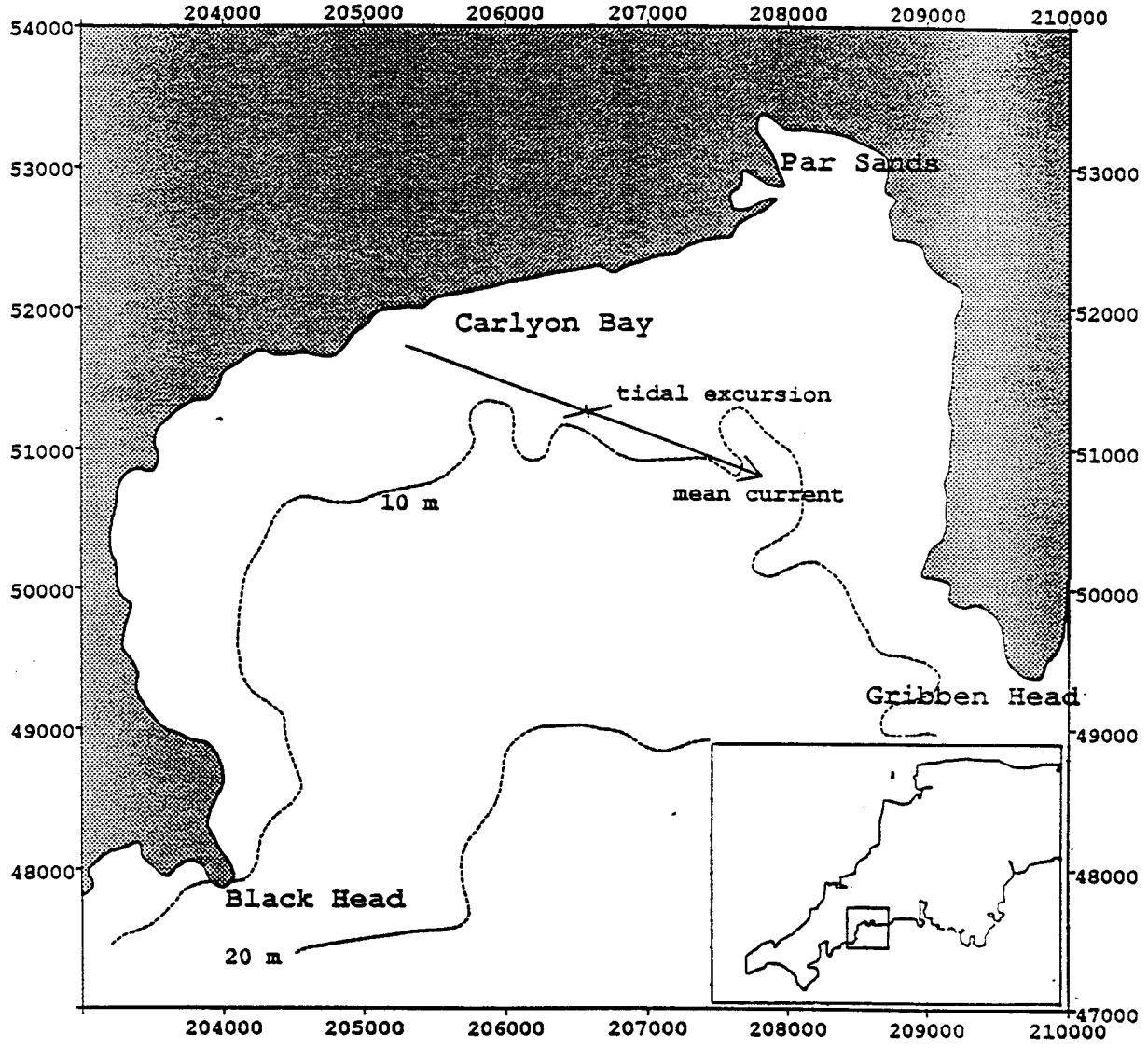

Figure 1. St Austell Bay, showing the longshore and onshore M2 tidal excursions and the distance traveled by the mean current in 12.42 h at the outfall site. The axes are annotated with National Grid co-ordinates. The inset shows the location of the bay in SW England.

BUOYANCY, TURBULENCE AND FRONTS IN THE COASTAL ZONE AND IN ESTUARIES: NUMERICAL MODELS AND OBSERVATIONS

Baumert, H., Burchard, H. and J. Suendermann
Universitaet Hamburg
Germany

Abstract

The paper compares the results of numerical models of buoyancy-driven problems with observations. The following phenomenae are considered: (i) the interplay of buoyancy and turbulence during the evolution of the upper mixed layer in the northern North Sea (FLEX'76); (ii) the role of buoyancy in the cold-spot formation around Heligoland island in a stratified German bight as the result of the island-stirring effect; (iii) the role of buoyancy in the control of the salt wedge position in the Elbe estuary, in relation to freshwater inflow and seaward salinity. The above phenomenae are simulated numerically by 1D, 3D and coupled 3D high-resolution models using turbulence closure schemes. The results presented correspond highly with observations and measurements.

(i) The first part studies the interplay of buoyancy and turbulence in an upper mixed layer. As study object the Fladenground in the northern North Sea is chosen, with a water depth of 145 m. In this open-sea region advective influences are small and allow the application of a one-dimensional model with high vertical resolution to investigate the processes in detail. The study covers a period of 61 days in spring during the Fladenground experiment in 1976 (FLEX'76) the results of which have been condensed by SOETJE & HUBER in a reference data set (Meteor-Forsch.-Erg. Reihe A, 1980, 69 - 77).

The model study of the FLEX'76 mixed-layer evolution is based on the vertically one-dimensional, stratified and rotating Reynolds equations in boundary layer approximation, supplemented by a turbulent transport equation for heat and by different optional turbulence models. The partial differential equations were treated numerically in a unified way by application of a fully implicit four-point, two-layer finite-difference scheme on a staggered grid. The vertical step size was 1.45 m, the time step 150 s.

The turbulent fluxes were calculated by means of two versions of the k-epsilon model described by RODI (Int. Ass. for Hydraulic Research, Delft, 1980) and modified by us: a standard and an advanced model. The latter computes the different elements of the Reynolds stress tensor based on the assumption that a pure transport process alone does not alter the ratio of a tensor element to the turbulent kinetic energy (non-linear algebraic stress relations). In the stratified case both k-epsilon models use an empirical parameter, C3, the exact value of which is still a matter of debate in the literature (see below; the values of the remaining k-epsilon parameters are widely accepted as "universally" valid). The models were forced by the meteorological observations of the FLEX'76 data set. Generally, the correspondence between simulated and measured vertical temperature profiles as well as SST time series was good. This is demonstrated by several figures.

To evaluate the performance of the k-epsilon models, two mixed-layer models from the literature were programmed and forced by the same data. The comparison revealed that the predictive accuracy and the qualitative behavior (smoothness of the solutions and robustness with respect to large time steps) of the k-epsilon models were significantly the best. Their r.m.s. residual errors were of the same small size as the heat disbalance due to

advection. Both k-epsilon models simulated the evolution of a multiple thermocline due to some storm events with high realism. The advanced model performed slightly but not essentially better than the standard model. Taking the higher computational expenses of the advanced model into account, the standard model can highly be recommended for many oceanographic problems.

It is interesting to note that the mixed-layer evolution during FLEX'76 could be simulated with high accuracy although effects like Langmuir circulation, turbulence generation by breaking surface waves, internal waves and fossilization of turbulence were not taken into account.

The numerical simulations were supplemented by an analytical investigation of the idealized case of a diffusion-free, time-dependent k-epsilon system. This simplification allows for a better physical understanding and interpretation of the different empirical parameters within the k-epsilon models and of the buoyancy-turbulence interaction, the latter being the major control element in the mixed-layer evolution. As one result of this approach we could show that k-epsilon models can be rewritten in terms of two critical flux Richardson numbers: the limiting Richardson number describing the limit to the onset of convection, and the steady-state Richardson number labeling the collapse of turbulence due to stratification. Both numbers could be shown to be algebraically related to each other and to the above-mentioned k-epsilon parameter C3 (and other k-epsilon parameters). Based on the FLEX'76 data we estimated these critical numbers as -0.146 and +0.122, respectively, with C3=-1.4. Other consequences of this idealized analysis could be confirmed by the numerical simulations.

(ii) The second part of the paper investigates the complex hydrodynamics of the front formation around Heligoland island in the German Bight/North Sea. Heligoland island consists of the island proper separated by a narrow shipping channel from a flat smaller dune. Together they form a flow obstacle of about 5 x 4 square kilometers. The surrounding sea is characterized by a mean depth of 27 m, a mean tidal elevation of 2.4 m and a nearly circular tidal excursion figure with a radius of about 6 km (semi-diurnal tide). In summer the surrounding sea is usually stratified.

Because the front formation around obstacles is a fully 3D problem, it was computed on a 3D Cartesian grid (80x55x5) with a uniform horizontal mesh-size of 400 m and a vertical mesh size of about 10 m, corresponding to about 10,000 wet points. The time step was between 1 to 2 minutes. The study used the finite-difference code HMT (BAUMERT et al. - Syst. Anal. Model. Simul. 1989, No. 7, 503 - 506) with a semi-implicit time-stepping procedure, an advanced k-epsilon closure with linear, quasi-steady algebraic stress approximation close to that used in the FLEX'76 model study above, and an FCT algorithm to minimize numerical diffusion in the buoyancy transport computation. The problem is characterized by four open (wet) horizontal boundaries, at the four corners of which the water level was prescribed by results of a North-Sea model operated routinely at the Federal Hydrographic Agency of Germany (BSH Hamburg).

To study the island's effect on the flow systematically, different scenarios were simulated, including artificial situations: While hypothetical steady flows revealed large wakes behind the island (in good quantitative correspence to the classical wake theory), the realistic circular tide did not. This is explained by a new analytical theory based on the island Reynolds number discussed by WOLANSKI et al. (J. Geophys. Res. 89, 1984, C6, 10553 - 10569) and the tidal Strouhal number introduced by SIMPSON & TETT (Lect. Notes on Coastal and Estuarine Studies 17, Springer 1986, 42 - 76). A sensitivity analysis of realistic barotropic scenarios shows the macroscopic flow field to be mainly governed by pressure gradients, topography and inertia including the Coriolis force, but

less by wind and friction, while the effect of the wind on the turbulence is strong. Finally, for stratified summer conditions at the horizontal boundaries of the considered domain the island-stirring mechanism discussed by SIMPSON et al. (Cont. Shelf Res. 1, 1982, 15 - 31) is shown to generate a significant "cold spot" around the island on the simulated SST maps. The presented air and satellite photographs (thermal IR) strongly support the simulation results.

(iii) In the third part of the paper the role of buoyancy in the formation and dynamic movement of the salt wedge in the tidal Elbe estuary/Germany is investigated by means of 3D high-resolution numerical models. The Elbe estuary with a length of about 150 km flows into the German Bight/North Sea and is bounded by the limnic Elbe at a weir near the town Geesthacht. It is dominated by the semi-diurnal tide with a tidal elevation of about 3 m. Its topography is highly difficult due to the presence of the docks of the Hamburg harbor.

In this part of the paper the position of the salt wedge is considered in the average over a double tide (a characteristic time unit for this estuary), its dependence upon the headwater discharge and upon the salinity at the seaward boundary. This task is solved by coupling two 3D numerical models: (1) Without consideration of the tidal flats, the first one covers the German Bight and the lowest part of the Elbe estuary by a grid with a horizontal size of 2.5 km, to compute the seaward salinity boundary condition for the second model (SCHRUMM, IfM Hamburg, personal communication, 1994); (2) using the results of (1) as seaward salinity boundary values, the second model resolves the Elbe estuary with full consideration of the large tidal flats using an advanced flooding-drying algorith and a FCT algorithm for the salinity transport computation, on a grid with a horizontal size of 250 m and a variable vertical step size of about 3 m. The freshwater discharge of the Elbe is fed into both models.

The graphical presentation of the results exhibits a monotone seaward shift of the wedge position with increasing headwater in Geesthacht. These results are compared with corresponding empirical curves by KAPPENBERG & GRABEMANN (Int. Symp. on Particulate Matter in Rivers and Estuaries, Reinbek/Germany, March 1994) derived from observations in the Elbe and Weser estuaries/Germany and with an analogous curve derived by UNCLES & STEVENS (Estuaries, March 1993) from observations in the Tamar estuary/UK.

RUNNING ON EMPTY: THE DISTORTION OF COASTAL ECOSYSTEMS

Michael A. Rozengurt
County Sanitation Districts of Orange County, California

Abstract

Among numerous coastal embayments estuaries occupy special places whose immense influence on the adjacent marine environment and fisheries has been recognized by mankind since time immemorial. By definition, **estuaries are intermediate, dynamic, and cumulative links within the river-delta (estuary)-sea ecosystems where continual variable confluence, interaction, and mixing between river and sea takes place.** These processes result in development of four, specific zones of mixed water masses. In accord with the Venice International classification of 1958, they are typified by a strictly defined range of salinity, and other chemicals, and biological characteristics. As is known, the average salinity concentration of 5 g/L is a natural barrier for strictly estuarine species at early stages of their development within the avant-delta zone, the latter confined by 0.1 to 0.5 g/L salinity from the deltaic side.

These and other natural combinations of regime characteristics, developed under an umbrella of unimpaired runoff, have provided for the unique diversity and highest biological productivity of organisms directly or indirectly through food webs related to estuarine systems. But when the impoundment of watersheds has become fully operational, the river-coastal continuum has been mortally wounded, and fisheries have started to fade away since that time (Rozengurt, 1971, 74, et al., 1985).

For over the past two decades, the public perception has been that discharges treated wastewater into estuarine-marine environment was the major cause of their progressive impoverishment. Although some pollutants might have had measurable, progressive effects on the health and reproduction of living resources, the lack of sound scientific information on the more serious effect of the river impoundment on coastal systems has led many to mistakenly believe that more treatment or even "distilled" or "zero" discharges will restore the fishery. As a result, about $200- out of $541 billion were expended over the last two-three decades on pollution control to supposedly remedy the obvious depletion of fish and shellfish stocks. Despite this enormous cost and drastic improvement of treatment processes and the implementation of stringent water quality and fishery regulations (Clean Water and Magnuson Acts), the despoliation of coastal resources and economic losses has continued to persist.

It appears that the systemic depletion of river runoff over the same decades by numerous dams, water storage and the network of water conveyance facilities have had many times higher direct impacts on the aggravation of the regime and biota of the ecosystems in question than effluents (Rozengurt and Haydock 1981, 1993, 94). Ironically, in the Southern California Bight, the submerged ocean outfalls discharging at a distance of three to seven miles from the shore, at a depth of 60 meters are the closest to being a fresh water source, as over 150 rivers and streams of the Bight's watershed have ceased to exist due to impoundment. As a result of the latter, sport fishery has been rendered insignificant, kelp bed have declined, and over hundreds of miles of beaches have experienced inexorable erosion. This combined with other examples of ecological

deprivation of the Nation's coastal embayments (Columbia River Estuary, San Francisco Bay, Colorado River Estuary, Gulf of Mexico, Chesapeake Bay, etc.) provide strong support to the statement that river runoff was, is and will continue to be the ultimate, intrinsic guarantee of estuary-coastal systems survival. The pragmatic manifestation of this statement is based on the universality of the Laws of Thermodynamics, which govern the paths and control the runoff energy distribution and dissipation along the river course (Fig. 1). Note that the basic principles of river hydraulics and estuarine hydrodynamics are derivatives of the laws of conservation of mass and energy. The three major equations: (1) motion of water, (2) continuity of volumes of water exchanged between an estuary and sea, and (3) continuity of salt balance describe how these principles control the estuarine regime. Their solutions together with the results of a statistical analysis of stochastic, seasonal and perennial behavior of unimpaired runoff characteristics provides ample evidence that the lesser the runoff, the greater is the salt intrusion, and higher the salinization of an estuary (Fig. 2).

Simultaneously, the diminishing runoff adversely effects circulation, mixing and the entrainment phenomenon of runoff energy to repulse salt intrusion to maintain quasi-equilibrium dynamics of the estuarine ecosystems. The failure to recognize these and other universal regime features of coastal embayments by watershed development have contributed to: (1) alarming depletion of runoff to 60 to 90% of normal spring or annual values (note that the author had found that unimpaired intra-annual and perennial runoff fluctuations rarely exceed more then plus/minus 25 to 30% of their norms, Rozengurt 1971, 74, 85); (2) deprivation of the entire Central, South Atlantic and Western Pacific coastal zones from thousands of millions of acre-feet freshwater; (3) the current remnants of "regulated" flow, spring in particular, correspond to atypical chronic drought conditions regardless of wetness of the year (a seldom measured phenomenon for a unimpaired regime), their volumes no longer capable of absorbing even natural pollutants, or maintain adequate environment for migration and spawning, and (4) loss of millions of tons of oxygen, organic and inorganic matter and sediments so vital to coastal ecosystem survival. Concurrently, deltas and coastal erosion, subsidence of levees, oxygen deficit, hypoxia, eutrophication and agricultural discharges laden with chemicals have further aggravated the precipitous decline of habitat. The curtailment of 90% of migration routes and spawning grounds by thousands of dams together with the conversion of deltas into plumbing conduit have inflicted the final mortal blow to the Nation's and world fishery. Accordingly, an escalating entropy has become a new, highly negative property of a formerly healthy and rich coastal ecosystems. Subsequently, the new surrogates have only one thing in common with their natural, lustrous past - the same geographic locations and names on the maps. The reason why many prognostic contemporary models have provided erroneous results may be attributed to their inability to integrate the cumulative role of environmental losses (discussed earlier) on coastal systems. Thereby rendering their results nothing more than whistles in the dark. Arguably, the Nation's estuary is in peril.

Application of Laws of Thermodynamics to River-Delta-Estuary-Sea Ecosystems

THE FIRST LAW ⟵ ENERGY CONSTANT ⟶ THE SECOND LAW

(Energy Is Conserved)

- Fluctuation runoff energy within natural range
- Energy dissipation at minimum; Entropy insignificant
- Excess of free energy maintains quasi-equilibrium of ecosystems

(Transformation of Energy Is Accompanied by Entropy)

- Runoff energy transformed by the impoundment and diversions
- Anomalous redirection (alteration) of runoff energy
- Perturbation and cumulative aggravation of the regime of ecosystems
- Entropy and despoliation of ecosystems tend to attain maximum

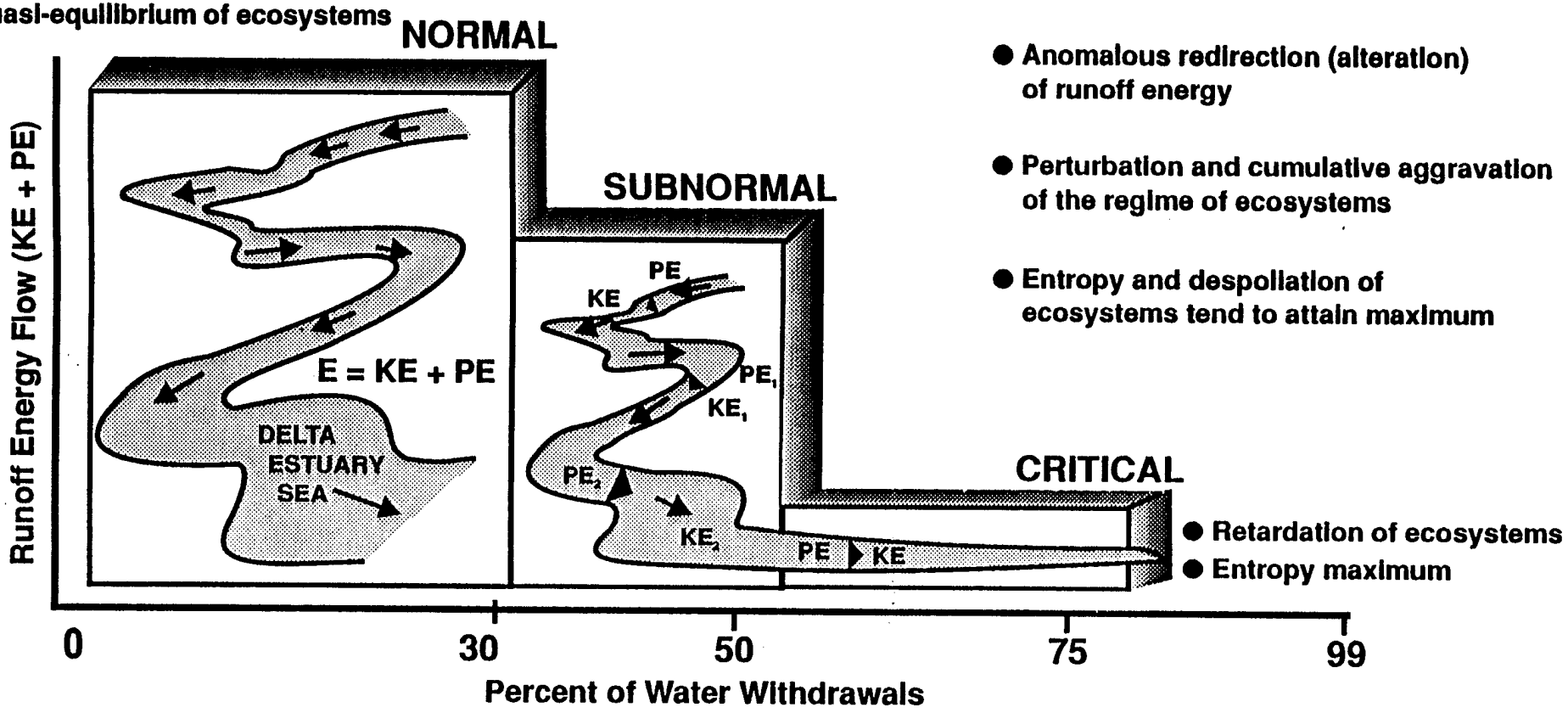

- Retardation of ecosystems
- Entropy maximum

Conceptual Model of Estuarine Water and Salt Balance

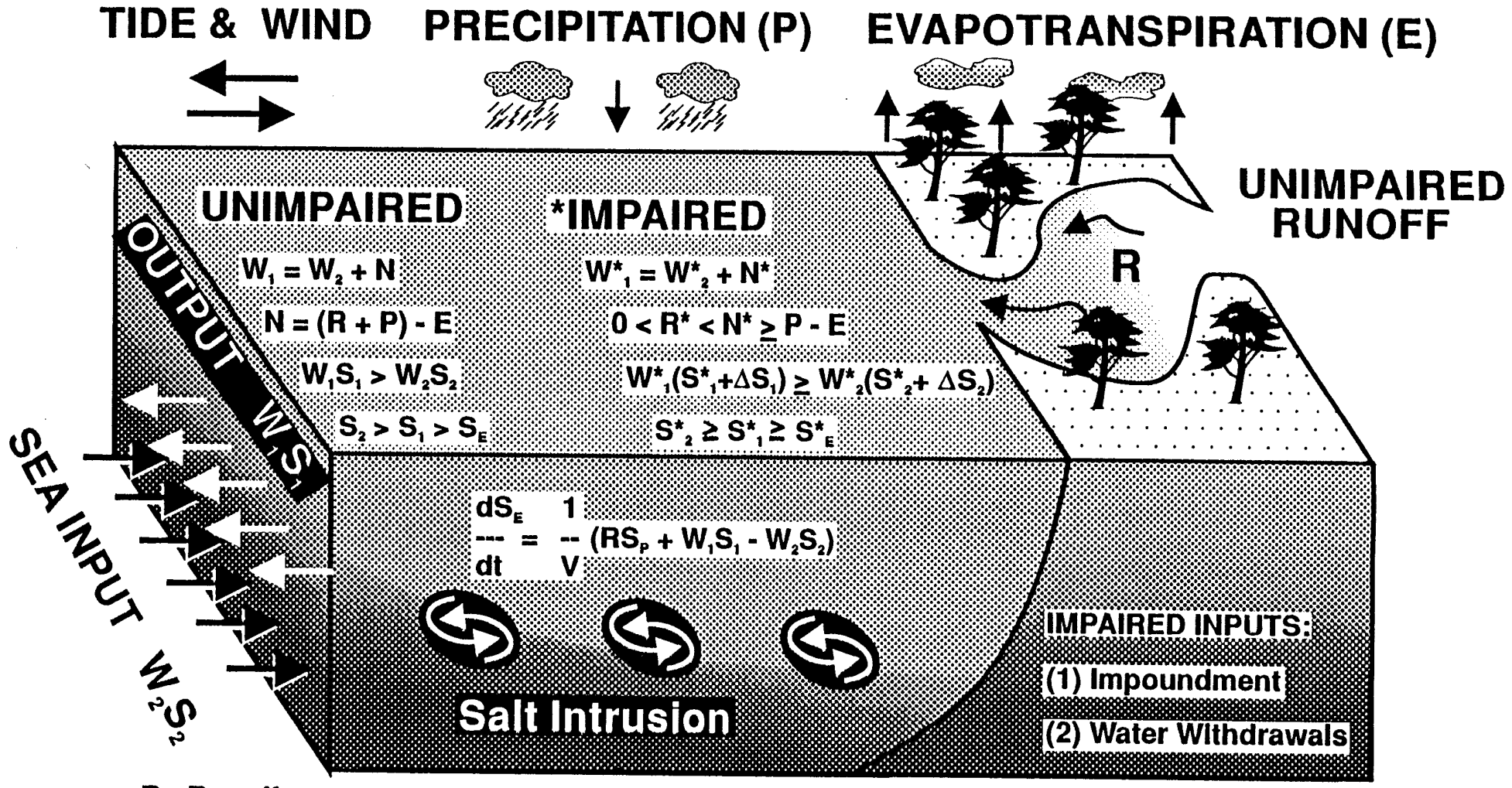

R - Runoff

W_2, W^*_2 - Sea Inflow

W_1, W^*_1 - Estuarine Outflow

V - Estuarine Volume

N, N* - Fresh Water Balance

S_1, S^*_1, S_2, S^*_2 - Salinity Fluxes

S_E, S^*_E - Estuarine Weighted Average Salinities

LOW-FREQUENCY SALINITY VARIABILITY IN A BROAD, SHALLOW ESTUARY

William W. Schroeder[1], William J. Wiseman[2], Jr., Jonathan R. Pennock[1] and Marlene Noble[3]

[1]Marine Science Program, The University of Alabama
Dauphin Island, AL 36528

[2]Coastal Studies Institute, Louisiana State University
Baton Rouge, LA 70803

[3]U.S. Geological Survey
Menlo Park, CA 94025

Abstract

Mobile Bay (Figure 1), on the northern coast of the Gulf of Mexico, is a broad, shallow estuary with depths on the order of 3 m, except for 13 to 15 m depths within a narrow, longitudinal ship channel. The bay is the estuary of the Mobile River system which on average discharges approximately 1850 m^3s^{-1} of fresh water. River input is highly seasonal, flooding normally occurring in late winter and spring while low flow conditions can prevail from mid summer to early winter and the annual discharge varies considerably from year to year (Schroeder and Wiseman, 1986). Winds are also highly seasonal with predominantly gentle breezes from the south during the summer in contrast to strong prefrontal flow from the south and post-frontal flow from the north associated the cold-air outbreaks during the winter (Schroeder and Wiseman, 1985). Previous work (Schroeder et al., 1990) on the salinity stratification-destratification cycle within the bay indicates that river flow appears to be the dominant control, the winds being important only in the absence of large freshwater discharge.

Two years (April, 1990 to April, 1992) of near-surface and near-bottom salinity and temperature, and bottom pressure measurements were collected at mid-bay and lower-bay mooring sites (Figure 1). Over this period low flow river conditions conformed to the long term trend of the Mobile River system for July through mid December, 1990 but were shortened in 1991 to August through mid November. On the other hand flooding conditions ranged from well above average just prior to the beginning of the deployment, to above average and very spiky between February and May, 1991, to well below average during late winter and spring of 1992. Extensive breaks occur in the data records, particularly early in the mooring program. Otherwise, though, the records are of high quality. The data sets indicate the presence of significant longitudinal and vertical salinity gradients. These appear to be characteristic of the salinity regime throughout the bay. This is supported by sixteen extensive bay-wide fair-weather hydrographic surveys performed during the period of the mooring deployments.

The variability of the system within the weather band and its response to external forcing have been discussed elsewhere (Schroeder et al., 1993; Noble et al., 1994). The lower-frequency variability is approached using the techniques of Thompson (1971) and Sturges (1992). Twenty-day low-pass filtered current meter records produced a red spectrum with a break in slope at periods of approximately 3-4 months. Salinity records treated in the same fashion produced spectra with distinct annual signals and, again, a change in spectrum character near periods of 3-4 months. The salinity records clearly reflect the interannual variability in runoff referred to above.

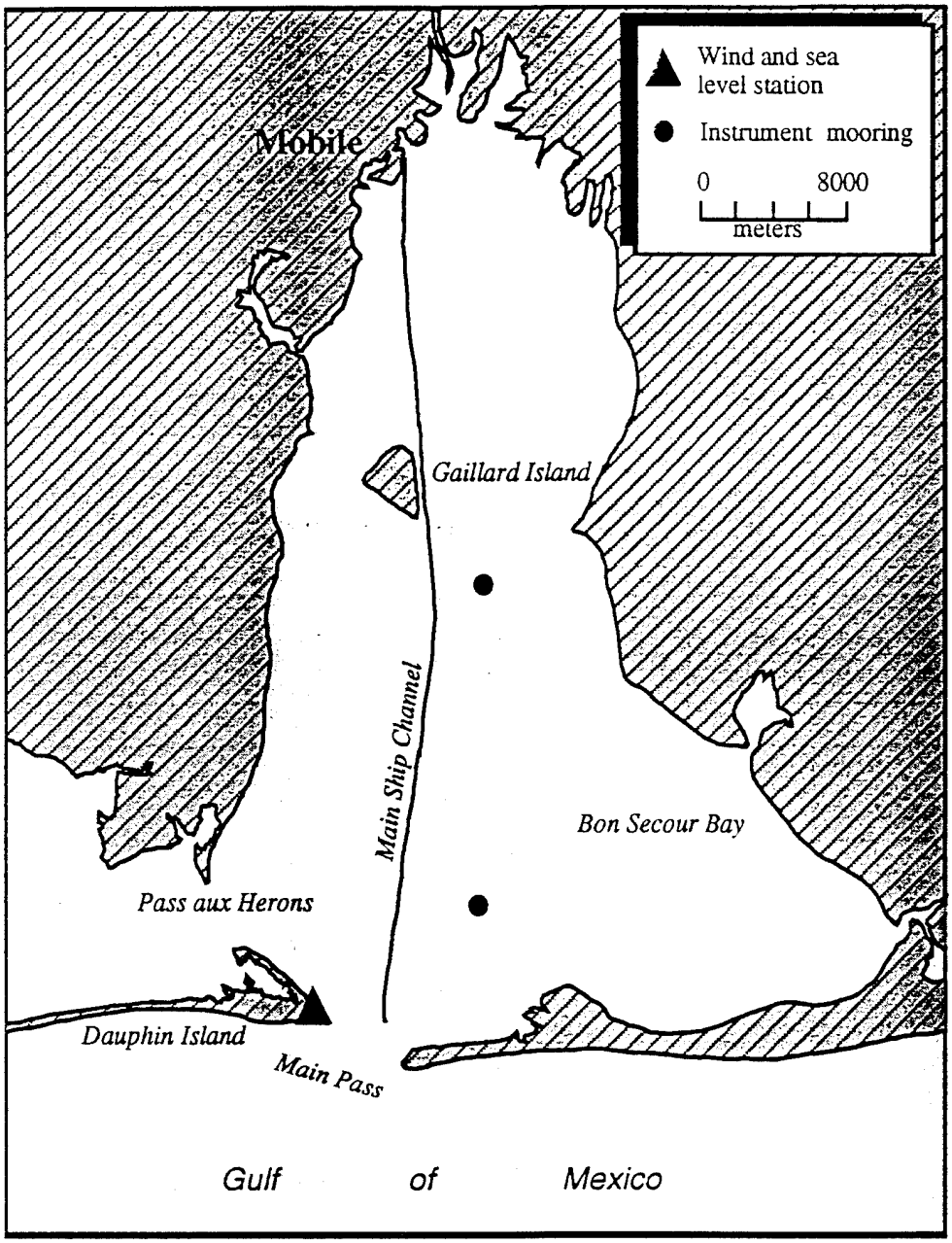

Figure 1. Mobile Bay, Alabama, northern Gulf of Mexico.

References

Noble, M., W.W. Schroeder and Wm. J. Wiseman, Jr. 1994. Sheared subtidal circulation patterns in a shallow highly-stratified estuary. *EOS, Transact. Amer. Geophys. Union,* 75(3):81-82.

Schroeder, W. W. and Wm. J. Wiseman, Jr. 1985. An analysis of the winds (1974-1984) and sea level elevations (1973-1983) in coastal Alabama. Mississippi-Alabama Sea Grant Consortium Publ. No. MASGP-84-024, 106 p.

Schroeder, W. W. and Wm. J. Wiseman, Jr. 1986. Low-frequency shelf estuarine exchange processes in Mobile Bay and other estuarine systems on the northern Gulf of Mexico, p. 355-367. In D. A. Wolfe (ed.), *Estuarine Variability,* Academic Press, New York.

Schroeder, W. W., S. P. Dinnel and Wm. J. Wiseman, Jr. 1990. Salinity stratification in a river-dominated estuary. *Estuaries,* 13:145-154.

Schroeder, W. W., M. A. Noble, G. A. Gelfenbaum and Wm. J. Wiseman, Jr. 1993. The role stratification in controlling circulation in a broad, shallow estuary. *12th Biennial International Estuarine Research Federation Conference,* Hilton Head Island, South Carolina, 14-18 November, 1993.

Sturges, W. 1992. The spectrum of Loop Current variability from gappy data. *J. Phys. Oceanogr,* 22(11):1245-1256.

Thompson, R. O. R. Y. 1971. Spectral estimation from irregularly spaced data. *IEEE Trans. Geosci. Electron,* GE-9:107-110.

THE EFFECT OF TIDAL MOTION ON THE SALINITY DISTRIBUTION IN LOWER DELAWARE BAY

Kuo-Chuin Wong
College of Marine Studies
University of Delaware

Abstract

Delaware Bay is a weakly stratified estuary located on the east coast of the United States. The effect of tidal motion on the salinity distribution across the mouth of Delaware Bay was examined based on a combination of CTD, ADCP, thermosalinograph, and current meter observations. During June 1990 and April 1992, intensive shipboard hydrographic surveys were conducted across the bay mouth. CTD profiles, at roughly 1.8 km intervals, were repeatedly taken as the R/V Cape Henlopen traversed the bay mouth (between Cape Henlopen, Delaware and Cape May, New Jersey) back and forth at about 75-minute intervals. The CTD transects were maintained for one to two tidal cycles so both the tidally averaged distribution and the intratidal variability could be resolved. In addition, a thermosalinograph was used to measure the near surface (0.5 m) salinity and temperature distributions along the shiptrack with a spatial resolution of about 150 m. Furthermore, a RD Instrument ADCP (307 kHz) was used to measure the currents flowing across the transect.

The tidally averaged salinity distribution across the mouth of the bay exhibits considerable transverse structure. Relatively high salinity water resides in the deep channel and domes toward the surface in the central portion of the bay mouth to the right of the channel as one looks upbay. This high salinity water separates two branches of low salinity water, one along the Delaware shore and the other along the New Jersey shore.

The present study indicates the existence of large intratidal variability at the bay mouth. At any particular phase of the tidal cycle the instantaneous distribution may be quite different from the tidally averaged distribution. The intratidal variations depend strongly on both the phase of the tide and the position across the bay. The bay mouth transect can be roughly divided into four regions based on hydrographic variability. Above the depth of 15 m, the Delaware branch of the low salinity water occupies region I between Cape Henlopen and a point about 8 km offshore. Relatively high salinity water occupies region II in the central portion of the bay mouth between 8 km to 12 km offshore from Cape Henlopen, and the New Jersey branch of the low salinity water occupies region III near Cape May. The deep channel at depth greater than 15 m represents region IV, and the salinity there is characterized by a near uniform distribution with minimum intratidal variability.

In region I where the Delaware branch of the low salinity water resides, the surface salinity may vary by 3-4 psu over the tidal cycle. Furthermore, the vertical salinity structure shows highly asymmetrical variation over the period. In general, a well-established vertical structure with a surface to bottom salinity difference of 3-4 psu is maintained over most of the tidal cycle except for a period of about 3 hours when the water column becomes well mixed. Generally speaking this occurs when the overall salinity reaches a maximum around the time of slack water after flood.

Region II is occupied by relatively high salinity water which separates the two branches of low salinity water along the shores. The weakly stratified water there, with surface to bottom salinity difference less than 1 psu, exhibits little intratidal variability over the tidal cycle.

In region III where the New Jersey branch of the low salinity water resides, the surface salinity varies by more than 5 psu over the tidal cycle. The vertical salinity structure also exhibits highly asymmetrical variation over time, but the water column is well mixed over much of the tidal cycle except during a period of about 3 hours when the water column becomes more stratified with a surface to bottom salinity difference in excess of 4 psu. The time of minimum salinity and maximum stratification coincides with slack water after ebb, suggesting that the effects of tidal stirring and tidal straining (Simpson et al., 1990; Simpson, Sharples and Rippeth, 1991) may play an important role in determining the salinity structure there.

The high resolution thermosalinograph data indicate that the high and low salinity water across the bay may be separated by sharp frontal boundaries. Depending on the phase of the tide, salinity may vary by 3 psu over a distance of 150 m across the front. Both the intensity and the position of the fronts change significantly with the phase of the tidal cycle. Bowman and Iverson (1978) postulated that both the lateral shear and lateral salinity gradient in an estuary may be intensified during the ebbing phase of the tide, resulting in the formation of longitudinal fronts which mark sharp transitions in salinity over short distances. Simpson and Nunes (1981) and Simpson and Turrell (1986) showed that the interaction of tidal flow with fresh water buoyancy input could produce tidal intrusion fronts during the flood tide in the estuary of the river Seiont at Caernarfon and the Conway estuary. Huzzey (1988) and Huzzey and Brubaker (1988) demonstrated that the differential tidal advection (between the deep channel and the shoals) acting upon a longitudinal density gradient could produce longitudinal fronts in the York River estuary. All of these mechanisms may be involved in producing the transient fronts in Delaware Bay, as sharp frontal boundaries were observed at both flood and ebb tides at different positions across the bay mouth. The present study further indicates that there is a linear correlation between surface salinity and temperature, with lower salinity corresponding to higher temperature, and vice versa. This correlation is caused by the fact that the brackish estuarine water from inland areas tends to warm up sooner than the saline water on the inner continental shelf during the spring. As a result of this T-S correlation, the temperature may vary by 2°C across the salinity fronts. The sea surface temperature (SST) fields derived from remote sensing techniques may thus be useful in detecting these fronts.

The characteristics of the salinity variation across the bay mouth were further examined based on a set of 30-day current meter observations conducted in April, 1984. The results show that the intratidal salinity variation across the bay may be strongly influenced by the fortnightly spring-neap tidal modulation. Furthermore, the evidence suggests that the atmospherically induced subtidal motion may interact with the tidal motion to modify the intratidal salinity variability across the bay.

FORCING AND RESPONSE IN A SHALLOW MICROTIDAL ESTUARY

Gary A. Zarillo, Clement R. Surak and Adele Militello
Oceanography Program, Division of Marine Systems
Florida Institute of Technology
Melbourne, FL 32901

Abstract

Introduction, Goals and Objectives

The Indian River Lagoon (IRL) is one of the most productive estuarine ecosystems along the east coast of the U.S. and the single most important system in the State of Florida. The IRL, a system consisting of three shallow inter-connected coastal lagoons extending 160 miles along the east coast of Florida, is characterized by transient wind-driven currents and is influenced by episodic freshwater flows from natural creeks, groundwater, and from a series of man-made drainage canals that have added to drainage from the natural watershed of the lagoon.

As a result of its location and importance to the human infrastructure the Indian River Lagoon has been impacted to varying degrees by loading of nutrients, toxins, pathogens, and other materials; by destruction of habitat, by alteration of natural sedimentation and circulation patterns, and by alteration of sediment and freshwater input from upland erosion and land-use practices.

Proper salinity ranges in the lagoon must be maintained to preserve and enhance benthic habitats, maintain larval stages of fish and bivalves, as well as enhance the overall water quality of the estuary. There is concern that the relatively large volumes of freshwater released to the estuary from a watershed artificially expanded by the Florida canal system, may be reducing salinities to critically low levels. To address this problem monitoring of the hydrodynamic and salinity regime was coupled with a numerical modeling scheme to develop a tool for managing freshwater loading to the estuary. Ultimately this tools model will be used to test the effects of, and optimize the options for releasing freshwater to the IRL.

Data Collection and Modeling

Long term and continuous data sets were collected to characterize the estuary and provide data for model calibration and simulations. Data were collected from six fixed locations within the project area. Sampling locations were selected to provide both boundary conditions and points for calibration and validation of the model. Data collection continued for 18 months and included several major freshwater releases to the estuary during both the wet season (June through October) and the dry season. Parameters measured at the Monitoring stations included current speed and direction, water temperature, conductivity, and meteorological parameters which, were logged at 15-minute intervals for the duration of the observation period. Freshwater discharge measurements to the central IRL were provided from gauging data collected the U.S. Geological Survey. The data collection began in February 1992 and continued through November of 1993. The data set adequately accounts for seasonal variability and extremes in marine and meteorological processes and freshwater loadings that influence the central IRL.

The model selected for to simulate hydrodynamics and salt transport in the central of the IRL is the Environmental Fluid Dynamics Computer (EFDC) Code developed by Hamrick, 1990. The hydrodynamic/salinity model simulates water surface elevation,

velocity, flow, and salinity structure resulting from wind stress, fresh-water inflows, influence of the coastal ocean, and storm events. It includes secondary circulation and the response of salinity to combinations of discharges from tributaries in various locations. The major features of the model include:

- Three-dimensional, vertically hydrostatic with a free surface, equations of motion in the so called "primitive" form.
- Transport equations for turbulence intensity and macro-scale, salinity, temperature, dye concentration, and suspended sediment concentration.
- Dependent variables are: three velocity components (u, v, and w), free surface elevation, density as a function of salinity, temperature, and sediment concentration.
- Vertically stretched (sigma) and horizontally curvilinear-orthogonal grid system.

Data Analysis

Long-term observations of physical processes and water quality in the IRL have been analyzed to resolve the various forcing and boundary conditions that control episodic salt intrusion, stratification, mixing, and advection of fresh and salt water in this estuary. Overall, the data show that the hydrodynamics and salinity regime of the IRL are dominated by low frequency processes operating at periods of a few days (meteorological frequency band) to a few months (climatic frequency band). Most of the tidal signal is filtered out by a constricted inlet (Sebastian Inlet) at the ocean boundary.

The forcing and response processes in the Indian River Lagoon varies throughout the year. On an annual basis, dominant weather patterns change from the dry season to the wet season. These seasonal changes in weather systems influence the lagoon both directly through wind stress, and indirectly through discharge and fluctuations in the water elevation of the coastal ocean. During periods of low discharge, the circulation in the estuary is primarily driven by wind forcing. Ultra-low frequency trends in water elevations of the estuary are linked to water level fluctuations in the coastal ocean. The effect of increased discharge during the wet season is obvious in records of salinity and currents in the areas adjacent to fresh water sources.

Processes in the IRL were also found to vary spatially. Monitoring stations located in close proximity to freshwater sources were greatly effected by discharge, not only in terms of salinity structure, but also circulation patterns. The southern monitoring sites were more influenced by the coastal ocean due to the proximity of a tidal inlet. The salinity at these stations recovered more rapidly from fresh water releases than the salinities recorded at stations more distal from the tidal inlet.

Spectral analysis of data records showed that the estuary is dominated by low frequency energy. Most of the spectral density of the hydrographic parameters lies in broad low frequency peaks. This indicates that the majority of the changes in the estuary are not sinusoidal in nature and may be forced by non-periodic and stochastic processes, such as frontal passages and fresh water discharges. Tidal amplitudes were found to be small, but forcing at tidal frequencies, especially diurnal forcing, contributed up to 19% of the total variance of water elevation and current magnitudes recorded closer to the inlet. Salinity fluctuations at tidal frequencies were found to be less than 6% of the total salinity variance at any station, indicating that direct tidal flushing is almost nonexistent in this section of the estuary.

Freshwater discharge had a major impact on salinities, circulation, and water elevations in the central IRL. The major decreases in salinity seen at monitoring stations

coincided with fresh water releases. Relatively small discharge events during the dry season had a large impact on the salinity structure in the estuary since evaporation, which increases salinity values, was low. The response time of salinity to fresh water releases was on the order of a few hours, but minimum salinities may lag maximum discharge values by days. The recording stations first effected by fresh water releases were not always the ones nearest to the discharge source. Fresh water plume movement and the duration of the effect of the fresh water at a station was related to wind stress and direction. Recovery times during the dry seasons were relatively shorter compared with the wet season.

Wind stress is a major direct forcing for currents in the central IRL. Spectral analysis showed that wind forcing on a diurnal basis was as important as lower frequency wind fluctuations. The local land and sea breeze system can have a large impact on circulation and water elevations. Daily increases in water elevation of up to 30 cm were found in certain areas coincided with an intensification of the land and sea breeze system during the fall. These processes, occurring on a daily cycle, were found to influence tidal constituents, which have a period close to 24.0 hours, such as the K1 constituent.

Results of Model Simulations

The circulation and salinity model, calibrated and validated with monitoring data, can be used to quantify salinity distributions resulting from specified sets of independent conditions and releases of freshwater. A series of production runs of the final calibrated model have been used to illustrate impacts on salinity of a wide range of possible freshwater inflow conditions. The simulated discharge data used in the model production runs covers the period from July 1956 through the end of June 1957, which includes an extreme event in mid-October, 1956 when freshwater discharge from a major canal into the central IRL was predicted to have reached more than 100 m^3/sec (3600 cfs).

In the year-long simulation, the lowest predicted salinities and the most stratified conditions occurred in response to freshwater discharge during the October 1956 event. Strong vertical stratification was also predicted near the beginning of the simulation, in response to a minor freshwater release that occurred during this period.

Predictions for the dry conditions that occurred in the first half of 1957 indicate relatively well mixed conditions. A large low frequency variation in mean salinity during the latter part of the simulation caused salinities in the central IRL to exceeded 30 psu in response to dry conditions during the spring and early summer of 1957

Conclusions

The results of data analysis and model predictions clearly show that a shallow estuary of relatively small tidal influence frequently becomes stratified and can be strongly influenced by even minor fresh water inflows. Furthermore, wind forcing and remote forcing of water level changes from the coastal ocean result in strong and persistent flows. Such flows, usually referred to as residual currents, are more obvious in restricted estuaries like the Indian River Lagoon where they are not masked by tidal influence. In this case flushing, salinity regime, and the overall water quality of the estuary are determined by processes that operate on an episodic basis and at subtidal frequencies.

THE RELATION BETWEEN HYDRODYNAMICS AND SUSPENDED MATTER DISTRIBUTION DURING PERIODIC STRATIFICATION IN THE RHINE PLUME IN THE NORTH SEA

J.C.A. Joordens[1], *A.J. Souza*[2], *A. Visser*[3]
[1] National Institute for Coastal and Marine Management
P.O. Box 20907
2500 EX Den Haag The Netherlands
[2] UCNW School of Ocean Sciences
Menai Bridge
Anglesey LL59 5EY UK
[3] Institute for Marine and Atmospheric Research
P.O. Box 80005
3508 TA Utrecht The Netherlands

Abstract

The changes in physical characteristics and suspended matter distribution were observed in a series of high resolution measurements in the Rhine plume near the Dutch coast. During a two week experiment in spring 1994 a shipboard survey was carried out with the SEAROVER undulating CTD, which contained also a transmissometer and a fluorometer. The survey consisted of a repeated 20 km transect in cross-shore direction, covering the width of the Rhine plume. In addition, complementary time series observations were obtained with two moorings on the transect, instrumented with temperature and salinity sensors, Acoustic Doppler Current Profilers (ADCP),, fluorometers and irradiance meters. The experiment covered both a calm weather neap tide period and a spring tide coinciding with strong winds from the North.

This paper presents SEAROVER time series of salinity, temperature, density; chlorophyll-a concentration, transmittance and suspended sediment concentration. Vertical profiles of residual current velocity and direction are given for two positions on the transect, along with profiles of temperature and salinity. Wind speed and direction, irradiance and wave data measured at one position on the transect are plotted as well.

During the neaps period (Julian day 96-98) short-term switching between stratified and mixed conditions occurred within several hours. A frontal region with strong horizontal salinity gradients was generally found between 5 and 20 km offshore. The suspended matter distribution, revealed by transmittance and chlorophyll-a concentration, closely followed the salinity distribution: haline stratification corresponded with stratification in suspended matter distribution. Highest chlorophyll-a concentrations were found near the bottom where the overlying water was stratified. It was observed that concentration of chlorophyll-a in the less haline water from the river plume was relatively low, about the same as in the more haline water at the seaward side of the frontal area.

The springs period (Julian day 101-105) showed to be different from the neaps period in several ways. Mixing by strong tidal stirring and increasingly strong Northerly winds (Bft 6-8) during this part of the experiment caused the suspended matter to be more evenly distributed over the water column, even though weak haline stratification still occurred on day 101. Peak concentrations of chlorophyll-a were higher than in the first period (19 compared to 15 $\mu g.l^{-1}$), and extended to the surface of the water column. After two days in this period the water column was completely mixed, and the experiment had to be interrupted due to the weather. As soon as the wind and sea state allowed, the experiment was resumed. Horizontal gradients in both salinity and suspended matter distribution was observed, despite the still strong stirring action of tide, wind and swell.

The present study confirms the occurrence of the very large semi-diurnal variability in stratification noted by Simpson et al (1993) in this area. The transitions between mixed and stratified conditions have been shown to take place even on time-scales of several hours. The use of the undulating SEAROVER, with a footprint of about 150 m, has revealed a microstructure of salinity, temperature, transmission and fluorescence that has not been recorded before in the Rhine plume region. Covering the same transect over and over again, in combination with data from moored instruments on that transect, allows an estimate of the relative contribution of the different mechanisms responsible for mixing, stratification and suspended matter distribution in the buoyant Rhine plume. Especially the current profiles contribute to an understanding of buoyancy effects on suspended matter in the water column. It seems that high Rhine discharge of fresh water causes haline gradients even when stirring by wind, tide and wave action is high. Chlorophyll-a concentrations can be considered as a relatively conservative tracer in an experiment like this, since time-scales of hours rather than weeks are regarded.

THE INFLUENCE OF A STABLE TIDAL INLET ON THE DISTRIBUTIONS OF SHOREFACE GRAIN SIZES UNDER LOW WAVE ENERGY CONDITIONS

James T. Liu[a], Randall W. Parkinson[b], Phillip F. Venanzi[b], and Li-hua Hou[a]
[a]Institute of Marine Geology, National Sun Yat-sen University
Kaohsiung, Taiwan 80424, ROC
[b]Department of Oceanography, Ocean Engineering, and Environmental Science
Florida Institute of Technology, Melbourne, Florida 32901, USA

Abstract

Introduction

Tidal inlets interrupt wave-induced longshore sediment transport, influencing both the supply of sand to downdrift shorelines and erosional-depositional patterns on adjacent beaches and shoals (FitzGerald, 1988; Oertel, 1988). At present, how exactly inlets affect the pathways of shoreface sediments is still unclear.

Liu and Zarillo (1990) showed signatures of tidal inlet processes in the surficial sediments on the shoreface at locations corresponding to two active but stabilized tidal inlets. These signatures also extend beyond the seaward limit of the average shoaling wave influence, indicating that inlet-related processes interrupt the wave-related processes beyond the shoreface.

The present study is an extension of the work of Liu and Zarillo (1989, 1990), the purpose of which is to examine different ways that tide-related processes affect the distributions of natural grain sizes on the shoreface adjacent to a stable tidal inlet. An improved sampling plan was used to increase the sampling density in both longshore directions from the inlet, whereby, generating data sets that have better longshore resolution than that of Liu and Zarillo's.

Study Area

Sebastian Inlet is one of the three tidal inlets that interrupt the continuity of a narrow barrier island complex that separates the microtidal Indian River Lagoon from the Atlantic Ocean. Most parts of the banks of the inlet channel are armored by structures, and the channel floor is lined by bed rocks of the Anastasia Formation. Due to the constrictive nature of the channel cross-section, the currents going through the inlet are strong, exceeding 2 m/sec on the flood, and 1.5 m/sec on the ebb (Liu, 1990). It is because of the bed rock, the cross-sectional area of the channel is approximately one-half what would have been expected if the inlet channel were free to enlarge, while admitting the existing tidal prism. The estimated tidal prism of the inlet is approximately 9.9×10^6 m^3.

The prevailing winds are northeasterly during the winter and easterly to southeasterly during the summer. The net southerly littoral drift into the northern boundary of the study area averages 175,500 m^3/yr, of which 0.6% is removed from the budget via the accretion of updrift beaches. Approximately 39.1% accumulates within the flood shoal complex, and 3.0% is added to the sediment budget from the erosion of downdrift beaches. Therefore, approximately 125,843 m^3/yr or nearly 71.1% of the initial drift exits through the southern boundary of the study area by natural sand bypassing processes. On average approximately 26.2% of sand is removed from the sand trap located on the landward side of the inlet channel and mechanically transferred to a downdrift feeder beach. Thus, on

average, there is net sediment loss of approximately 7,268 m^3/yr (4.1% of the initial drift) in the vicinity of Sebastian Inlet. From this estimates, clearly that the area around the inlet can be divided into the updrift, inlet proper, and downdrift regions, each having distinctive sedimentation characteristics. These characteristics are likely to be reflected in the surficial distributions of grain sizes in these regions.

Field Work and the Raw Data

In the fall of 1992, 27 shore-normal transects were established within a longshore distance of 16 km on each side of the inlet. On each transect, 10 sediment samples were taken at the average high water line and lower water line on the beach, and at the base of the beach face, and seaward at the depths of 2, 4, 6, 8, 10, 12, and 14 m. All the sediment samples were analyzed for the grain-size frequency distribution within the sand fraction by using a Rapid Sediment Analyzer (RSA). The grain-size frequency distribution in the sand fraction was recorded at quarter-phi intervals between 2 mm (0 phi) and 0.063 mm (4 phi). In total, 21 grain-sizes classes were recorded.

The spatial distribution patterns of the grain sizes indicate that except the two most abundant sizes (0.125 and 0.15 mm), Sebastian Inlet has left distinguishable signals in the distributions. These signals exist as depleted trough-like features for the four finest sizes across the shoreface, and concentrated tongue-like features protruding seaward from the intertidal beach and the respective zones of dynamic equilibrium for sizes between 0.18 and 1.41 mm.

Another way to visualize the spatial variability of the raw data is through the plot of the grain-size frequency distributions at all the sampling depths along four arbitrarily chosen transects that presumably represent the influence of wave-related and tide-related processes. The depth-dependent variations of these signals suggest that wave-related transport and deposition processes of grain sizes have great longshore variability on the upper shoreface.

The signals of the inlet are generally distinguishable from the wave signals at all depths except at 18 ft (6 m), 12 ft (4 m), the surf zone, and the high tide line. Rough comparisons between the two types of signals clearly show that there are different processes that are responsible for the distinctive differences in grain-size frequency distributions along the four arbitrarily chosen transects. All these indicate that the distributions of individual grain sizes are sensitive natural tracers to reveal the effects of different hydrodynamic processes on the substrate of the sea floor near a tidal inlet.

Preliminary Analysis and the Digital Filter Analogy

Based on the result of a preliminary EOF examination of the raw data, the signal of Sebastian Inlet corresponds to an area consisting of four transects nearest to the inlet mouth (two on each side). Subsequently, the study area was empirically divided into three regions. The north region consisted of 12 transects, the inlet region consisted of 4 transects, and the south region consisted of 11 transects.

Hypothetically, the system under study is analogous to a digital filter having its own frequency response characteristics. The multi-grained longshore sediment transport on the updrift side of the inlet is equivalent to the multi-frequency input signal to the filter (the inlet). Through the filtering process the spectral characteristics (the grain-size distribution patterns) of the output (downdrift side of the inlet) were subsequently altered. Following the this analogy, hypothetical sediment movements in both the northward and a southward directions were assumed. In the case of a hypothetical northward sediment transport, the characteristic sediment distribution pattern (the mean cross-shore distribution) in the south region would be equivalent to the input for the inlet filter, and the characteristic

distribution patterns (the mean cross-shore distribution) in the north region would represent the output of the filter, and vice versa for a hypothetical southward sediment transport.

EOF Analysis

Two deviation matrices of the original data matrix R were created by subtracting the mean cross-shore distribution of each grain size for the north and south regions respectively at each transect. Physically, the subtraction represents a minimization process by which the input signal was minimized, and subsequently, the signals of the filter and the output would be enhanced in the resulting data matrix. This technique was used by Liu and Zarillo (1990) to separate the influence of various hypothetical sediment sources from the influence of wave reworking process on the surficial sediments of a barred shoreface. A third deviation data matrix D_i was also created by subtracting the signals of the inlet from the original data matrix as a comparison to the other two direction-oriented deviation matrices. All the matrices D_s, D_n and D_i have the same exact dimensions as R, and were standardized before performing the EOF analysis, so that the resulting eigenweightings would not be dominated by grain sizes that have large values in the deviation matrices.

Results, Discussion and Conclusions

The first three eigen modes of all the three deviation fields are similar in grain-size groupings and their spatial characteristics. The first eigen mode is interpreted as the general trapping mode of the inlet. The second mode is interpreted as the seaward diversion mode, which describes a particular form of sediment bypass of the inlet. The third eigen mode is interpreted as the shoreface mode in which the signal of the inlet no longer dominates the spatial eigen characteristics. In general, the inlet-related processes are responsible for more than 60% of the variance in all the three deviation fields accounted for by the first two eigen modes. Yet, the effects of the inlet on the shoreface is restricted to the region within 600 m on either side of the inlet mouth.

An empirical relationship $r = \Omega/M_{tot}$ for the stability of tidal inlets has been widely used to quantify the relative dominance of the tidal energy versus wave energy at tidal inlets (Bruun, 1978), where Ω is the tidal prism and M_{tot} is the net littoral drift. The value for r at Sebastian Inlet is about 56, whose stability condition according to Bruun (1986), belongs to the category between fair an'd poor. This number suggests that the tidal power at Sebastian Inlet is relatively a weak factor in the determination of the sediment processes. Yet, processes related to the flow of ebbing tide are responsible for the accumulations of sediments seaward of the inlet mouth (Walton and Adams, 1976), and these accumulations are manifested by the inlet signals in the spatial distribution patterns of all but the finest four grain sizes in the study area.

At Sebastian Inlet, the imprint of ebb flow fields in the substrate can easily be identified by all the tongue-like features in the distributions of grain sizes from 0.18 to 1.41 mm according to Oertel's (1988) flow field model for ebb jets. But, there are no grain sizes patterns that would correspond to the areas of flood dominance on both sides of the zone of ebb dominance. Therefore, at Sebastian Inlet the flow fields of the ebbing tide are probably responsible for trapping and diverting most of the grain sizes on the shoreface. Since the velocity decreases at the distal end of the near field resulting in deposition of sediments carried seaward by the flow, the lengths of all the tongues at the inlet are probably equivalent to the lengths of 'effective near fields' of grain sizes. In fact, the length of the sediment tongue becomes shorter (ends at shallower depths) when the grain size becomes coarser. The winnowing of the finest four grain sizes from the substrate in the near field and far field suggests that the mode of sediment transport in the ebb jet for these grain sizes is in suspension (non-deposition), and as bed load for the rest of grain sizes.

The other effect of the near field is to divert grain sizes seaward from longshore transport within their respective zones of dynamic equilibrium. The diversion of longshore currents by inlet jet is called 'dynamic diversion' by Todd (1966), the result of which is to produce a hydrodynamic barrier to the longshore current and prevent the sediment to bypass the inlet. Consequently, sediments are retained on the updrift side of the inlet. The effect of the dynamic diversion can be seen in the differences in abundance between the north and south regions of all grain sizes. Theoretically the abundance of grain sizes would be greater on the updrift side than on the downdrift side. However, the complexity of our data set suggests that at the same depth, different grain sizes might be moving in opposite directions; and for the same grain size, it might be moving in opposite directions at different depths. Nevertheless, the depth-dependent grain-size difference patterns across the inlet do indicate that grain sizes are moving in their perspective zones of dynamic equilibrium.

Although the near field of the ebb jet and its dynamic diversion can explain the observed troughs and tongues in the grain-size distributions, they can not adequately explain the depth-dependent selective sediment bypass across the inlet. It is speculated that these differences are caused by the different ways of inlet bypass of grain sizes in the stable inlet processes (FitzGerald, 1988), which involve the formation, landward migration, and welding of large bar complexes to the downdrift shoreline.

The findings of this study suggest that tidal inlets are active geological agents that affect the spatial sorting of sediment grain sizes on the shoreface near the inlet. The sediment trapping and filtering characteristics of tidal inlets are determined by the unique responses of grain sizes to inlet flow fields. In the future, more studies need to be done in this area so that one can have better understanding of the interrelationships between inlet hydrodynamics and sediment dynamics.

References

Bruun, P., 1978. Stability of Tidal Inlets. Elsevier Scientific Publishing Co., New York, 510p.

Bruun, P., 1986. Morphological and navigational aspects of tidal inlets on littoral drift shores. *Journal of Coastal Research,* 2(2):123-145.

FitzGerald, D.M., 1988. Shoreline erosional-depositional processes associated with tidal inlets. In Hydrodynamics and Sediment Dynamics of Tidal Inlets, Aubrey, D.G. and Weishar, L., eds., *Lecture Notes on Coastal and Estuarine Studies,* vol. 29, Springer-Verlag, New York, pp. 186-225.

Liu, J.T., 1992. The influence of episodic weather events on tidal residual currents: A case study at Sebastian Inlet, Florida. *Estuaries,* 15(2):109-121.

Liu, J.T. and Zarillo, G.A., 1989. Distribution of grain sizes across a transgressive shoreface. *Marine Geology,* 87:121-136.

Liu, J.T., and Zarillo, 1990. Shoreface dynamics: Evidence from bathymetry and surficial sediments. *Marine Geology,* 94:37-53.

Oertel, G.F., 1988. Processes of sediment exchange between tidal inlets, ebb deltas and barrier islands. In Hydrodynamics and Sediment Dynamics of Tidal Inlets, Aubrey, D.G. and Weishar, L., eds., *Lecture Notes on Coastal and Estuarine Studies,* vol. 29, Springer-Verlag, New York, pp. 297-318.

Todd, T.W., 1968. Dynamic diversion-Influence of longshore current-tidal flow interaction on chenier and barrier island plains. *J. Sed. Pet.,* 38:734-746.

Walton, T.L. and Adams, W.D., 1976. Capacity of inlet outer bars to store sand. Proc. 15th. Conf. Coastal Eng., A.S.C.E., pp. 1919-1937.

VARIATION OF SEDIMENT RESUSPENSION CHARACTERISTICS: EXPERIENCE FROM THE LOWER CHESAPEAKE BAY

Jerome P.-Y. Maa[1] and C.-H. Lee[2]
[1]Assoc. Prof., [2]Graduate Student
School of Marine Science
Virginia Institute of Marine Science
College of William and Mary
Gloucester Point, VA 23062.

Abstract

Using the VIMS Sea Carousel to conduct in-situ experiments in the lower Chesapeake Bay, we found significant spatial and temporal variations of sediment characteristics. At the Wolftrap site, we identified the critical bed shear stress for sediment resuspension, τ_{cr}, and a typical "Type I" behavior of sediment resuspension, which shows the resuspension rate decreases with time for a given constant bed shear stress, τ_b, that is larger than τ_{cr}. The sediment behaves like a cohesive sediment because of the biochemical processes. This process also affect the resuspension rates significantly. In a laboratory experiment using Wolftrap sediment sample, without the bio-chemical process, the resuspension rate is about 10 times higher than that obtained from the in-situ experiment. At this site, we found that τ_{cr} varies from 1.1 to 1.9 Pascal before and after Summer. This seasonal variation may also be resulted from the changing of biochemical processes.

On a Winter deployment (Feb. 94) at the Cherrystone site (near bed water temperature is around 2°C), we identified a consolidating layer of fluff at the water-sediment interface. Because of the weak shear resistance, sediment in this layer was slowly redispersed into water column under small τ_b's. After about 70 minutes, while τ_b increases to 0.12 Pa, this fluffy layer seems totally redispersed and the concentration remains constant for $\tau_b = 0.12$ Pa, see Fig. 1. If we count the fluffy layer, then the τ_{cr} is either too small to be detected or not existed at all. If we ignore this fluffy layer, we may say that $\tau_{cr} \approx 0.12$ Pa.

Another experiment conducted at the same site on late Spring (May 1994) also indicated the existence of a consolidating layer of sediment. This time, however, the thickness of this fluffy layer is relatively thin compared with the Winter deployment, so the redispersion stopped relatively fast.

Most of our resuspension tests show the concentration of suspended matter increases with time for a short period, 5 to 9 minutes. The concentration then decreases with time. Fig. 2 is an example showing the results of resuspension tests conducted at the Cherrystone site. After extensive study using a laboratory carousel to scrutinize the possible reasons, we may conclude that the major cause of the decreasing concentration is leakage. Assuming the leakage rate of water is a constant for a given ring speed (i.e., bed shear stress), we may use the following equation to describe the change of suspended matter in the VIMS Sea Carousel.

$$Ah\frac{dC}{dt} = AE_o e^{-\lambda t} - Q_L C$$

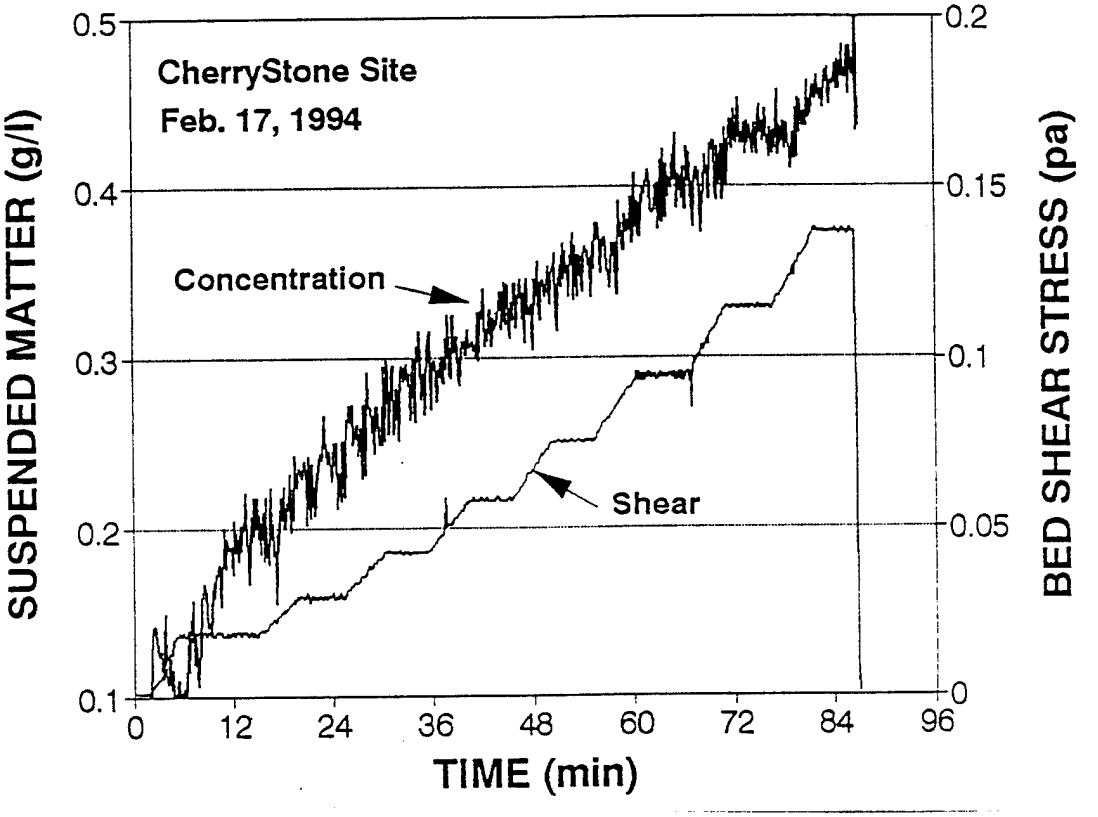

Fig. 1. A Test Conducted at the Cherrystone Site to Find τ_{cr}.

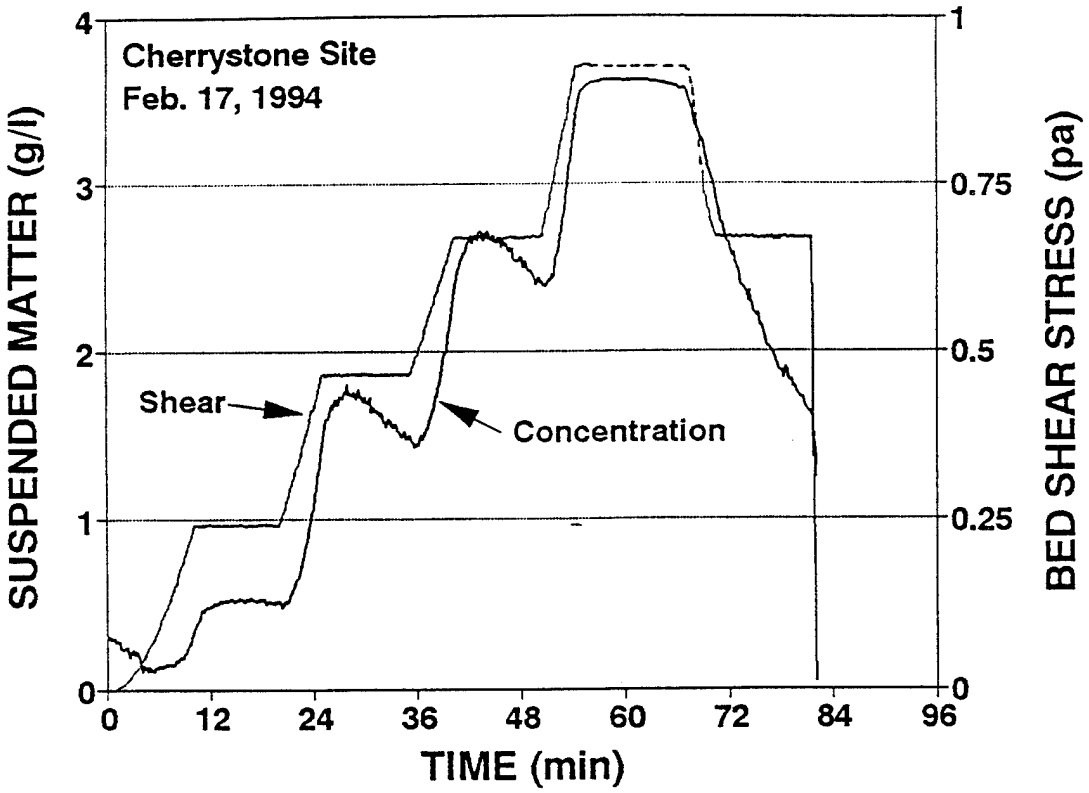

Fig. 2. The results of a Resuspension Test Conducted at the Cherrystone Site.

where E_o is a constant initial erosion rate per unit area (in unit of $g/cm^2/s$), Q_L is the water leakage rate (cm^3/s), A is the flume area (10132 cm^2), h is the channel depth (10 - 12 cm), C is the concentration of suspended sediment (g/cm^3), t is time, and λ is a rate coefficient (s^{-1}). This equation can be solved analytically for the concentration with three unknown coefficients: E_o, Q_L, and λ. Using the resulted equation, the measured concentration data, and a least square technique, we can find these three unknown coefficients to best fit the data. Fig. 3 shows the relationship between E_o and τ_b. Notice that E_o from these two Cherrystone experiments are roughly parallel to each other. The one conducted on May indicates a higher E_o, which may be because of more biological activities at a warmer water temperature (15°C).

At the Burry Bay site in the James River, although the bed is too soft (mainly clay and silt) to anchor our research vessel to against the changing tide, we still can clearly see the τ_{cr}. There may be pockets of fluff that is enclosed by the Carousel, but in general, a well established water-sediment interface is there. The τ_{cr} is small compare with other site mainly because of the high content of fine-grained sediments and the loose sediment structure.

All the three sites show the type I resuspension behavior. This means there is a vertical variation of sediment erosion resistance as well as the bulk density.

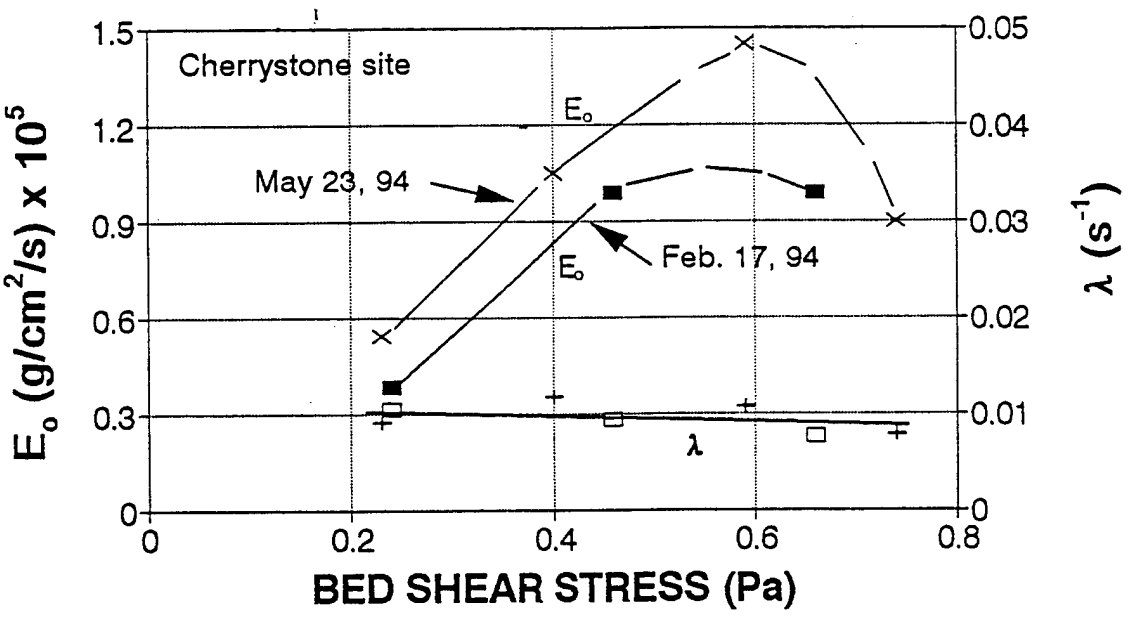

Fig. 3. The relationship between E_o and τ_b for the Cherrystone Sediment.

THE EFFECT OF TIDAL ASYMMETRIES ON THE NET TRANSPORT OF SUSPENDED SEDIMENTS IN THE EMS DOLLARD ESTUARY

Herman Ridderinkhof
Netherlands Institute for Sea Research
P.O. Box 59
AB Texel, the Netherlands

Abstract

The Ems Dollard estuary is a more or less funnel-shaped tidal basin in the Dutch Wadden Sea. The estuary, which consists of a channel surrounded by tidal flats, is some 50 km long and the depth of the main channel varies between 5 and 20 m. The amplitude of the dominant semidiurnal vertical tide is about 1 m at the mouth and 1.25 m at the landward end. Tidal currents in the main channel have an amplitude of some 1 m/s. On average fresh water inputs into the estuary are relatively small and, in first approximation, gravitational circulation can be ignored.

In the past many observations have been done on the horizontal distribution of suspended matter in the estuary (e.g. de Jonge, 1992). In all of these studies an increase of the suspended sediment concentration in a landward direction is found. Such a gradient implies that there must be an inward flow of suspended matter to counterbalance the outward flow by tidal exchange processes since the main source of suspended sediment is the adjacent North Sea. This inward flow is assumed to be the result of the interaction between the sedimentation/erosion cycle of the sediments and the advection by the tidal currents.

A characteristic feature of the sedimentation/erosion cycle of fine-grained sediments in tidal flows is that it results in an hysteresis in the concentration vs. velocity curve between accelerating and decelerating stages of the current. This hysteresis is caused by the settling and scour lag of the sediments. Combining this hysteresis with an asymmetrical tidal current results in a net flow of suspended sediments. (Postma, 1967, Groen 1967).

In this study the importance of this mechanism for net fluxes of fine-grained suspended sediments in the Ems Dollard is examined. For the tidal current field results of a realistic 2D hydrodynamical model of the area are used. This model is forced with the M_2, M_4 and M_6 tide at the open boundaries in the adjacent North Sea. At representative positions along the main channel of the estuary the amplitude and phase of the M_2-tidal current and it's higher harmonics (M_4, M_6, etc.) are determined. Subsequently the residual displacement of a particle at these positions is calculated by coupling these velocity fields to a very simple particle model for the behavior of fine-grained sediments. In this model the hysteresis effect is simulated by assuming that the velocity at which a particle starts moving in an accelerating current, i.e. the critical erosion velocity, is higher than the velocity at which the particle stops moving in a decelerating current, i.e. the critical deposition velocity.

Firstly the residual displacement of a particle is calculated for each position on basis of the local, Eulerian, expressions for the velocity field. Thus it is assumed that the current field does not change during the excursion of the particles. At most positions this results in a small landward directed residual displacement. Analyzing the relative importance of the different harmonic components shows that the inclusion of M_6 and M_8, if compared with

the residual displacement if only M_2 and M_4 are taken into account, influences the results significantly in that not only the magnitude of the residual displacement changes but also it's direction.

Secondly the effect of changes in the current field during the excursion of a particle is examined by taking into account the longitudinal gradient in the amplitude of the harmonic components of the tidal current in representative longitudinal sections of the estuary. This addition to the current field appears to result in a much larger (more than 10 fold increase) residual displacements of the particles. The gradient in the amplitude of the M_2 component appears to form the most important contribution to the residual displacement.

Thus large differences occur if the residual displacement of particles is calculated on basis of the Eulerian current field as compared with a calculation on basis of the Lagrangian current field. For the net flux of fine-grained sediments asymmetries in the Lagrangian velocity field appear to be far more important than asymmetries in the Eulerian current field. These differences between the Eulerian and Lagrangian current fields are further illustrated by comparing the magnitude of the generated higher harmonic components in both current fields which shows that the amplitude of the higher harmonics in the Lagrangian current field is much larger than the amplitude of these components in the Eulerian current field.

Observations on the longitudinal gradient of suspended sediments in the Ems Dollard estuary support this conclusion in that a large gradient in the concentration of suspended sediments is found in the area with a strong decrease in amplitude of the tidal currents.

References

De Jonge, V.N., 1992. Physical processes and dynamics of microphytobenthos in the Ems estuary (The Netherlands). Ph.D.-Thesis, Groningen University, 176 pp.

Groen, P., 1967. On the residual transport of suspended matter by an alternating tidal current. *Neth. J. Sea Res.*, 3:564-575.

Postma, H., 1967. Sediment transport and sedimentation in the estuarine environment. *Amer. Ass. Adv. Sci. Pub.*, 83:158-179.

SEDIMENT TRANSPORT STUDIES IN RIVER MOUTHS WITH THE USE OF NATURAL RADIOACTIVITY

Boris Shteinman
Israel Oceanographic & Limnological Research
Kinneret Limnological Laboratory
P.O.B. 345, Tiberias, Israel 14102.

Abstract

Sediment transport phenomena are important in coastal engineering and marine ecology. Bottom relief develops under various flow regimes and wave energetics, and is affected by many factors. It is desirable to follow sediment trajectories on a regular basis and especially after storms and during persistent winds. A simple and reliable way of monitoring sediments of fixed origin would be helpful in predicting many important effects, such as coastal erosion.

The aim of this paper is to present a method using natural radioactivity of sediments to follow their movements in a river-lake system. Sediments of different origin differ in their isotopic composition and may be classified by specific gamma spectra signatures. The use of passive gamma spectra for sediment transport studies has been successfully applied in several rivers and seas. Many radiometric investigations have been made using sediments made radioactive, artificially. However, a great number of radioactive isotopes of radium, strontium, rubidium kalium and others occur naturally in sediments.

Radiometric investigations were made for solving some questions about sediment movement at the Kura River mouth (Caspian Sea) and at the Jordan River mouth (Israel). The distribution of river sediments at the river mouth (Figs. 1A & 1B) were determined by means of a submarine radiometric survey (Kura River mouth) utilizing gamma spectra measurements. Gamma spectra of the probes were obtained with a 3" x 3" NaI well type detector and measuring system, developed in the Van De-Graaff Accelerator Laboratory at the Department of Physics of the Technion (Israel). Typical spectra are presented in Figs. 1C and 1D. Two spectral ranges suitable for tracing purposes can be seen: 1.46 MeV line of K-40 and the lower energy range of the U-Th family. The spectral resolution appears sufficient for our proposed goals, but it can be improved by mathematical means.

Regions of the sediments of different facies and different ages are well outlined by isolines of gamma-radiation intensity (Fig. 2). The results obtained from the submarine radiometric survey are in the form of records of characteristic radiation spectra. As the gamma-radiation intensity of the sea bottom sediments are small (2.5-6.0 microroentgen an hour), the occurrence of anomalous values above this background permits exact mapping of the river fans of the river alluvium.

Figures 2A and 2B show the chart of gamma activity for the bed of the Kura River mouth obtained during a calm period and after winds, respectively. The results of investigations showed that river diluted silts with dimensions of less than 0.01 mm correspond to the area of maximum intensity, equal to 6.0 or more relative units. Sandy silt of 0.01-0.05 mm diameter, corresponds to the area of a high intensity of 4.5-6.0 units. The area of moderate intensity (3.0-4.5 units) demarcates the area of the fine fractions of river origin. The grounds of marine origin, are characterized by the intensity of gamma-radiation (<3.0 units).

Figure 2 contains results of a survey made under conditions of relatively calm weather and large river discharge (A, C). Therefore, the cartogram of gamma activity reflects the sedimentation character of the river mouth area under the influence of discharge currents, due to the river flow in general.

The survey in Fig. 2B was made following a period of prevailing NE and SW winds. These conditions caused displacement of river silts offshore, to a great depth. Displacement of the area of the greatest gamma activity of the grounds is explained by the fact that during stormy periods with high waves muddy bed sedimentation takes place, and wind currents transfer the alluvium.

Because there is a close interrelation between natural gamma radioactivity and the percent of silt fraction content (analytically written as a logarithmic function), radiometric surveys allow determination not only of the area of river sediment accretion, but also the predominant fraction in the sediments.

The advantage of the radioactive method consists in that other methods (i.e. sediment sampling) require more effort and are less representative of long term conditions. The distribution of river alluvium at the discharge depends on hydrometeorological conditions that frequently change during hours. It is clear that the data obtained at any specific time are not representative, as they are not connected to equal hydrometeorological conditions. A submarine radiometric survey made by towing a radiometer and recording gamma activity lasts for some hours. This allows the connection of data on sediment migration with concrete hydrometeorological conditions.

A recent study carried out on sediment transport from the River Jordan into Lake Kinneret showed that probes taken before and after certain hydrometeorological events could elucidate the effect of those events. However, in my opinion, use of devices capable of measuring gamma radiation from sediments *in situ* would provide much more information. The use of natural radioactivity in studies of sediment transport in river mouths may be unique in providing the following information:

- sediment composition of large built-up forms, such as sand bars and spits, under different conditions;

- location of zones of maximal sediment accumulation;

- location of zones of erosion;

- change in littoral zone relief due to sediment transport and decomposition under varying conditions.

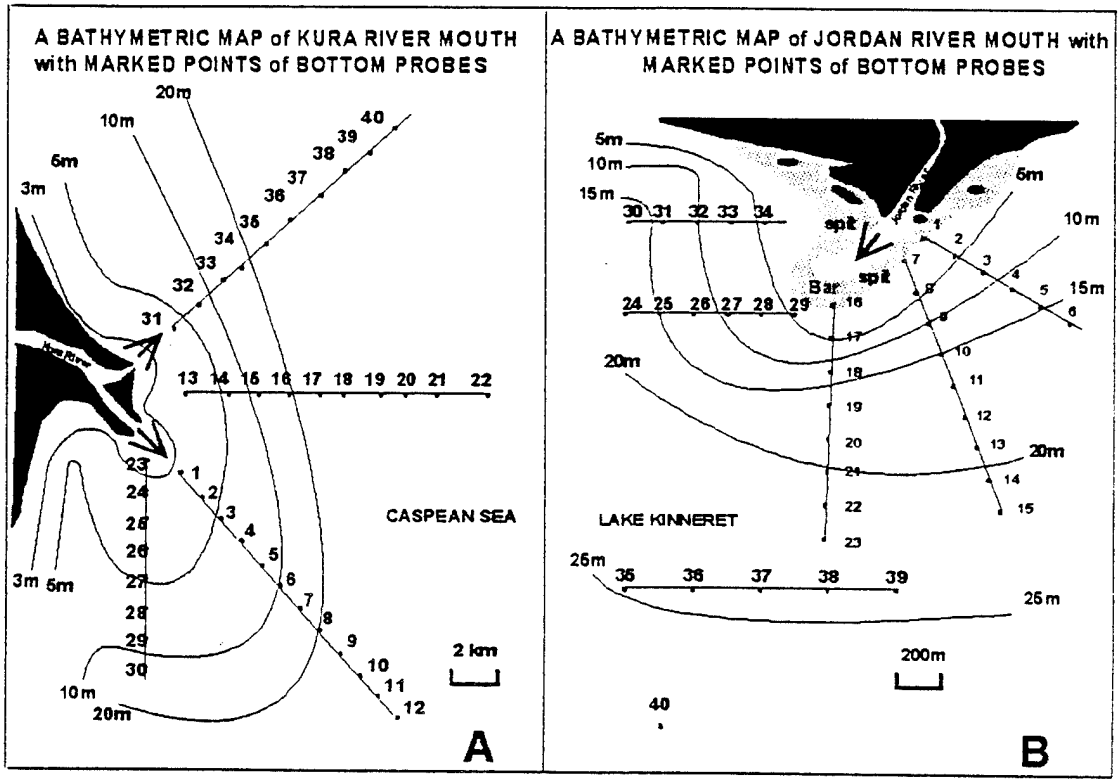
A BATHYMETRIC MAP of KURA RIVER MOUTH with MARKED POINTS of BOTTOM PROBES
20m
10m
6m
3m
40
39
38
37
36
35
34
33
32
31
13 14 15 16 17 18 19 20 21 22
23
24
25
26
27
28
29
30
1
2
3
4
5
6
7
8
9
10
11
12
CASPEAN SEA
3m
5m
10m
20m
2 km
A
A BATHYMETRIC MAP of JORDAN RIVER MOUTH with MARKED POINTS of BOTTOM PROBES
5m
10m
15m
30 31 32 33 34
spit
Bar
spit
5m
10m
15m
24 25 26 27 28 29
20m
20m
LAKE KINNERET
25m
35 36 37 38 39
25m
200m
40
B

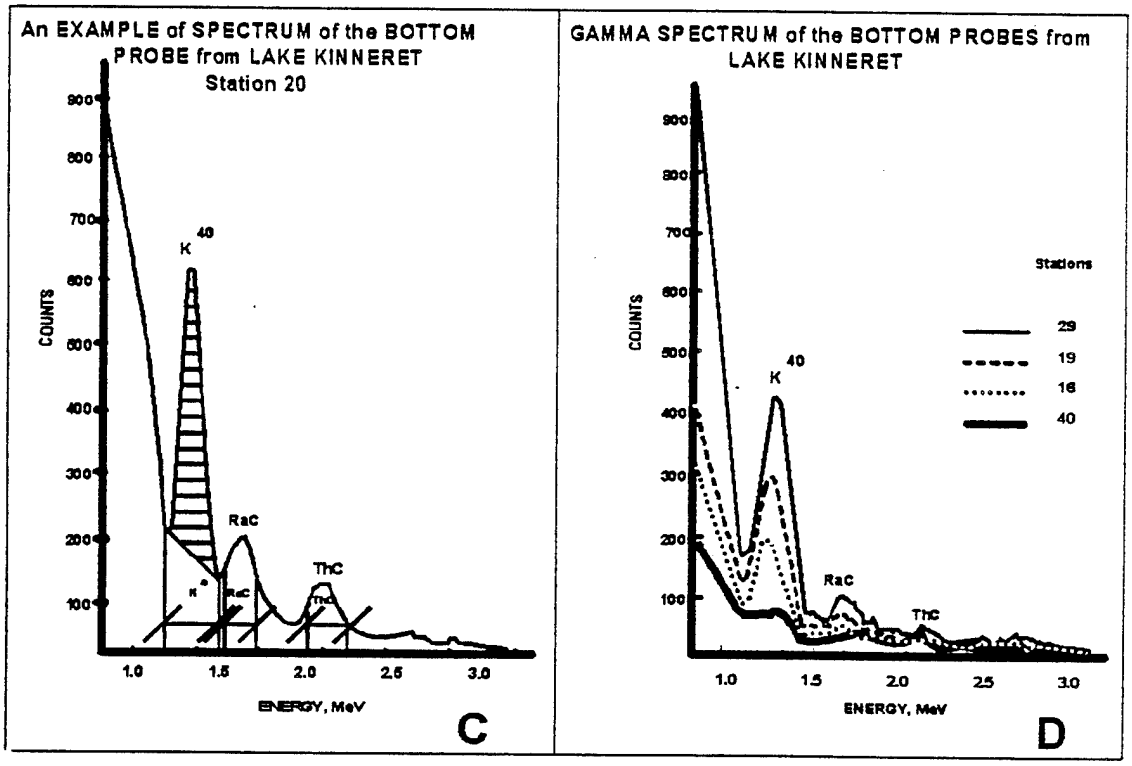
An EXAMPLE of SPECTRUM of the BOTTOM PROBE from LAKE KINNERET
Station 20
COUNTS
900
800
700
600
500
400
300
200
100
K 40
RaC
ThC
1.0
1.5
2.0
2.5
3.0
ENERGY, MeV
C
GAMMA SPECTRUM of the BOTTOM PROBES from LAKE KINNERET
COUNTS
Stations
29
19
16
40
K 40
RaC
ThC
1.0
1.5
2.0
2.5
3.0
ENERGY, MeV
D

Fig.1

INTENSITY of NATURAL GAMMA-RADIATION from the BOTTOM

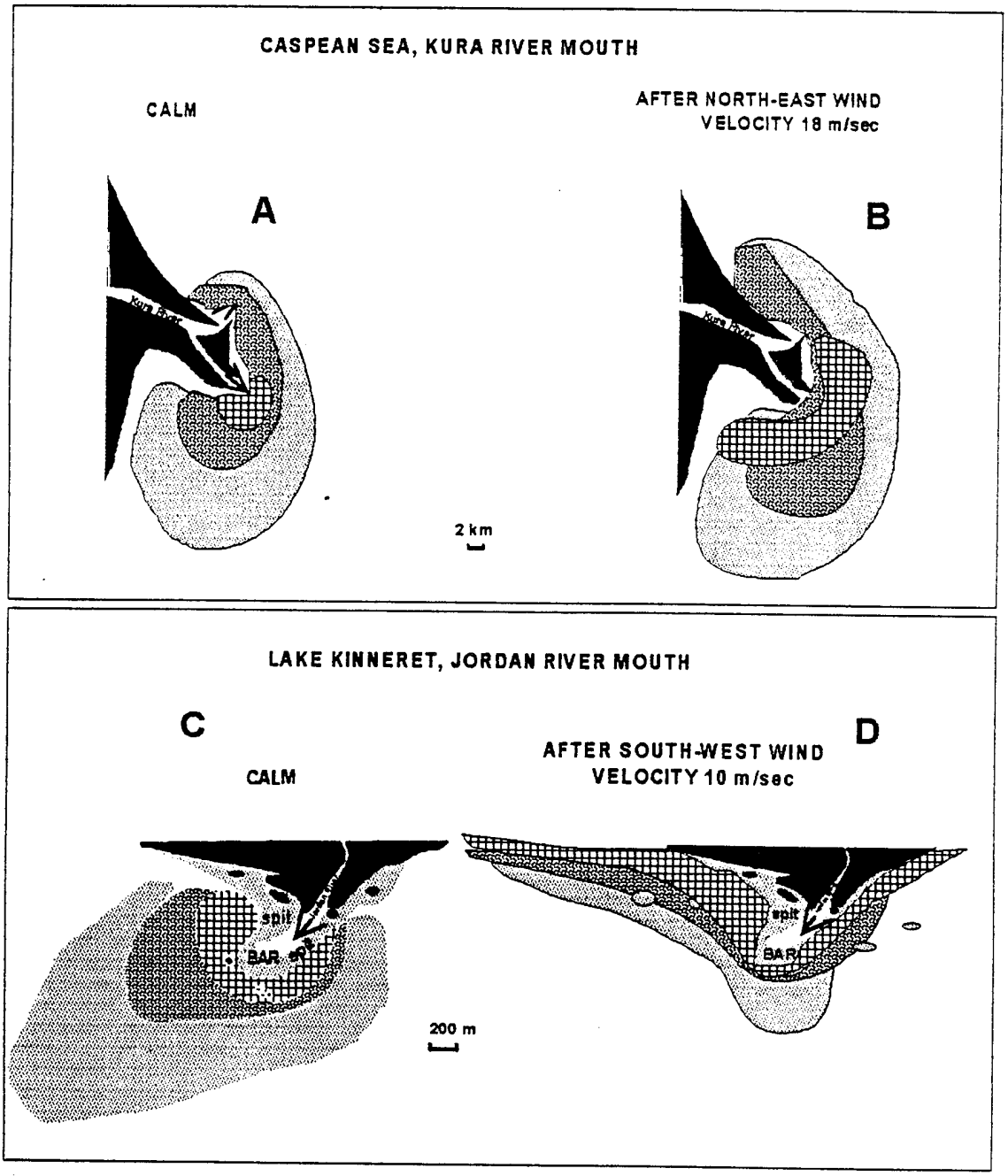

Fig.2

STORM-INDUCED SEDIMENT TRANSPORT IN MASSACHUSETTS BAY

Richard P. Signell, Bradford Butman, and Michael Bothner
U.S. Geological Survey, Quissett Campus, Woods Hole, MA 02543

Abstract

Massachusetts and Cape Cod Bays form a roughly 100 x 50 km semi-enclosed embayment in the western Gulf of Maine. They are bounded on the east by Stellwagen Bank, which rises to within 20 m of the sea surface. The average depth of the bays is 35 m with the deepest water of 80-100 m found in Stellwagen Basin, located just west of Stellwagen Bank. Boston Harbor empties into Western Massachusetts Bay, providing a major source of contaminated sediment in the region.

Sediment traps and light transmission measurements show that storm-generated surface waves are the major cause of sediment resuspension. The largest waves are typically associated with northeasterly wind events in excess of 5 dynes/cm2, which generate significant wave heights in excess of 4 m. Observations during these storms suggest a quasi-equilibrium response dominated by wind-stress, bottom-stress and pressure gradient, with strong downwind flow in the shallow sections of the bays, and broad return flow against the wind in the deeper sections of the bays.

Despite the simplicity of the momemtum balance during winter storms, the resulting flow field is strongly three-dimensional due to the topography of the bay. The Blumberg-Mellor three-dimensional numerical model was therefore used to simulate the trajectories of suspended sediment particles in Western Massachusetts Bay during selected major storms when wind, wave, current, light transmission and suspended sediment observations were available. The modeled flow fields are consistent with the observed circulation patterns, and the complexity of the resulting particle trajectories confirms that three-dimensional modeling is essentially required to predict particulate transport.

REINFORCEMENT OF GRAVITATIONAL CIRCULATION BY WIND

Jack Blanton
Skidaway Institute of Oceanography
Savannah, GA USA

Abstract

Introduction

The cross-shelf density structure of many coastal regions resembles that of a partially mixed to well mixed estuary. The density deficit of the low-salinity water causes it to override ambient shelf water of higher density to form a coastal frontal zone (CFZ) that usually extends 20 - 30 km offshore. The pressure gradient from low-density water at the coast drives a cross-shelf gravitational estuarine-like circulation that is offshore in surface layers and onshore near bottom. The strength of the gravitational component is proportional to the horizontal density gradient, which, in turn, is proportional to the magnitude of riverine discharge. Model studies (Werner et al., 1993) and observations (Blanton, 1981; 1986) have shown that the strength of this cross-shelf flow component is on the order of 10 cm/s.

This paper focuses on the reinforcement of the gravitational circulation component in CFZs on shallow continental shelves. Riverine and estuarine discharges along continental margins can form zones of low salinity water that extend along the coast. The southeastern US continental shelf (SAB) has a multi-inlet coast line connecting low-lying coastal marshes to the ocean. Several rivers, five each discharging freshwater at rates exceeding 100 m^3/s, form plumes of low-salinity (low-density) water at the coast. Subsequent tidal and wind mixing blends the plumes into a band of low salinity that extends along the coast over a distance greater than 400 km. While we customarily define the inner shelf in the SAB to depths between 0 - 20 m, the seaward extent of the low-density band varies temporally and spatially and defines, in a dynamic sense, the inner shelf.

Background

The low-salinity band formed by estuarine discharges contains the main buoyancy source for the CFZ. Vertical density gradients exhibit a high degree of spatial and temporal variation due to (1) vertical mixing provided by tidal current friction at the sea bed, (2) surface friction provided by wind stress, and (3) the source strength of freshwater discharge and its spatial distribution.

The source strength is defined by the buoyancy flux, N(o), a quantity directly proportional to freshwater discharge. While buoyancy inputs due to solar radiation can be important in many coastal regions, significantly more power is required to mix the freshwater-induced buoyancy along the South Carolina and Georgia coast (Blanton and Atkinson, 1983). Approximately 10^{-4} to 10^{-3} W m^{-2} is required to mix observed ranges of total river discharges varying between 1000 m^3 s^{-1} in autumn to 8000 m^3 s^{-1} in spring.

Blanton and Atkinson (1983) estimated that tidal power dissipation at the bottom ranges from 0.3 to 2 x 10^{-4} W m^{-2} in water depths less than 20 m off the Georgia coast. This is sufficient to vertically mix buoyancy due to heat additions but is too weak to

vertically mix the buoyancy normally provided by freshwater discharge. However, wind-induced surface stress can provide a significant increment of power over that of tidal currents. Mixing power due to strong wind events can range between 1 and 3 x 10^{-3} W m^{-2} (Atkinson and Blanton, 1986), or an order of magnitude greater than that provided by tidal power.

Wind Effect on Coastal Gravitational Circulation

Alongshelf wind stress produces an Ekman-induced cross-shelf flow that combines with the gravitational circulation component. Upwelling favorable wind stress spreads the front seaward, and there is an offshore component of flow above and within a strong pycnocline. Currents are onshore below the pycnocline. Thus, upwelling reinforces the estuarine circulation component, and the cross-shelf flow structure resembles the along-axis flow of a partially mixed estuary.

Downwelling-favorable wind (southward stress) advects the frontal zone shoreward and steepens the front. In contrast to the upwelling-favorable case, the downwelling-induced cross-shelf flow opposes the gravitational component.

Examples of CFZs Under Contrasting Coastal Discharges

Discharges during summer 1992 and spring 1993 varied by a factor of four. The low buoyancy flux in summer 1992 resulted in a relatively well-mixed CFZ out to 40 km from the coast. Contrast this with spring 1993 when the quadrupled freshwater discharge stretched the CFZ seaward with vertically stratified water out to 40 km. Wind stress was upwelling favorable but stronger than in summer 1992.

We have summarized the mixing energy requirements for these two seasons (Table 1). In order to completely mix this buoyancy supply for water depth H = 10-m, mixing power must also increase by a factor of four. This is a lower estimate because the upwelling circulation reinforces the gravitational circulation and advects the low-density water over even deeper water. For H = 20 m, the required power $\left(\frac{dV}{dt}\right)$ is double that given in Table 1.

Cross-shelf Advection of Buoyancy Under Upwelling CWonditions

By reinforcing the ambient gravitational circulation, upwelling winds efficiently transport surface low-density water seaward. This process was explored for the CFZ off the Georgia coast (Blanton et al., 1989) using a 2-D numerical model, which shows that the continuous application of alongshore upwelling favorable wind stress stretched the CFZ seaward. While wind and tidal currents efficiently mix the shallow portions of the water column near the coast, the transport of buoyancy by the reinforced gravitational circulation increases vertical stratification farther offshore. Eventually, low-density water at the coast mixes with mid-shelf water coming shoreward underneath the stratified waters farther offshore. This mixture is advected seaward in the form of shallow lenses having a cross-shelf scale of about 20 km. When winds reverse, the simulation shows that the gravitational circulation is essentially shut-down by onshore Ekman transport and vertical stratification is destroyed within a day or so.

Table 1. Energy required $\left(\frac{dV}{dt}\right)$ to vertically mix a given amount of buoyancy for a water depth of 10 m.

	Q	F	N(o)	$\left(\frac{dV}{dt}\right)$	Pt	Pw
	(m^3 /s)	($kg/m^2/s$) ($F \times 10^4$)	(m^2/s^3) ($N \times 10^6$)	(mw/m^2) buoy	(mw/m^2) tidal	(mw/m^2) wind
Low	1500	1.9	1.8	0.2	0.1	< 0.1 breeze
High	6000	7.5	7.4	0.9	0.6	3 stormy

Q = Freshwater discharge between Charleston SC and Jacksonville FL
F = Buoyancy source strength
N(o) = Equivalent buoyancy flux at surface
H = Water depth = 10 m
ρ' = Density deficit of low-density source = 25 kg/m^3
$\left(\frac{dV}{dt}\right) = \left(\frac{H}{2t}\right)\rho' N(o)$

A series of 6 cross-sections off South Carolina confirmed many of the aspects discussed above. These data were obtained during the high runoff season in spring 1993. The first three sections were completed under upwelling-favorable winds lasting over a period of 5 days.

The first section showed a CFZ that tilted upward and offshore with 33 PSU water intersecting the bottom at a depth of about 8 m. Shoreward of relatively strong vertical stratification, there was a shallow lens of low salinity and relatively warm water.

Winds strengthened one day later. The density structure was more flattened, and the shallow lens had disappeared. Four days after this, upwelling favorable winds began to relax even as vertical stratification increased even more farther offshore. High salinity water from the mid-shelf was apparently advected closer to shore where the 34-PSU isohaline almost intersected the surface within 10 km of the coast. Instead of well-mixed water closer in, however, the shallow coastal water was strongly stratified with what appeared to be the alongshore advection directly downwind of a low-salinity water source located farther south.

Twelve hours later, weak downwelling winds had set in. The highly stratified water within 10 km of the coast was mixed to a weakly stratified frontal zone tilting upward and offshore to a distance of about 13 km. The disappearance of strong stratification at the coastal boundary was probably due to decreased wind-driven advection into the section from the location of the low-salinity coastal source. Farther offshore, the strongly stratified water seen 24 km offshore 12 hours earlier actually extended at least 40 km offshore by the time the prolonged upwelling winds finally relaxed.

The final two sections were done during an interval of weak but downwelling favorable winds. Stratified low-salinity water reappeared at the offshore edge of the section reminiscent of the highly stratified water seen in earlier sections. Even though upwelling winds set in for an additional 3 days, the shallow stratified lens never reappeared in subsequent sections, suggesting that the lens-like feature had a finite alongshelf extent.

Conclusion

Cross-sections of hydrographic structure through a CFZ off the southeastern US continental shelf revealed that upwelling- favorable winds reinforce an estuarine-like circulation component that enhances the cross-shelf transport of coastal water. Coastal water is apparently lost in the form of shallow low- density lenses with a cross-shelf scale width of about 20 km. These results conform to results of numerical simulations published previously.

The rate of decrease of buoyancy in the inner shelf region of the SAB during seasonally high spring runoff appears to be related to the strength of seasonally averaged upwelling- favorable wind strength (Blanton and Atkinson, 1983). This relationship is consistent with a process that reinforces the gravitationally-driven circulation of the inner shelf.

References

Atkinson, L.P. and J.O. Blanton, 1986. Processes that affect stratification in shelf waters. In: *Baroclinic Processes on Continental Shelves (Coastal and Estuarine Sciences 3).* C.N.K. Mooers (ed.), p. 117-130. *American Geophysical Union,* Washington, D.C.

Blanton, J.O., 1981. Ocean currents along a nearshore frontal zone on the continental shelf of the southeastern U.S. *J. Phys. Oceanogr.,* 11:1627-1637.

Blanton, J.O., 1986. Coastal frontal zones as barriers to offshore fluxes of contaminants. *Rapp. P. -v. Reun. Cons. int. Explor. Mer,* 186:18-30.

Blanton, J.O. and L.P. Atkinson, 1983. Transport and fate of river discharge on the continental shelf of the southeastern United States. *J. Geophys. Res.,* 88:4730-4738.

Blanton, J.O., L.-Y. Oey, J. Amft and T.N. Lee, 1989. Advection of momentum and buoyancy in a coastal frontal zone. *J. Phys. Oceanogr.,* 19:98-115.

Werner, F.E., J.O. Blanton, D.R. Lynch and D.K. Savidge, 1993. A numerical study of the continental shelf circulation of the U.S. South Atlantic Bight during autumn of 1987. *Continental Shelf Res.,* 13:971-997.

Acknowledgments

I wish to express my appreciation to the several individuals without whose help this project would have not been possible. First my thanks go to Julie Amft who coordinated and implemented many aspects of the field work and data analyses. The able support of the captain and crew aboard the R/V BLUE FIN, Jay Fripp (Capt), Raymond Sweatte and Chris Knight and Captain Paul Tucker of the R/V ANITA is also appreciated. I also gratefully acknowledge the help of my colleagues at South Carolina Marine Resource Research Institute: Charlie Barans, Betty Wenner, Bruce Stender and David Knott. Graphics for this poster were designed and carried out by Anna Boyette. I also thank Leo Oey, Francisco Werner, and Peter Verity who provided many stimulating discussions on coastal and estuarine processes.

This work was sponsored by joint grants from the Georgia Sea Grant Program (Grant No. R/EA-15) to the Skidaway Institute of Oceanography and the South Carolina Sea Grant Consortium (Grant No. 93277) to the SC Marine Resource Research Institute.

SIMULATIONS OF BAROCLINIC FLOW IN DIXON ENTRANCE, BRITISH COLUMBIA

V. A. Ballantyne, M. G. G. Foreman, W. R. Crawford, K. S. Lee
Institute of Ocean Sciences, Fisheries and Oceans Canada
P.O. Box 6000
Sidney, B.C. Canada V8L 4B2

Abstract

Introduction

This paper describes the development and validation of a diagnostic baroclinic model of flow in Dixon Entrance, British Columbia. Simulated currents are compared with observed currents measured by moored current meters, and 8 weeks of observations using surface drifting buoys.

This work is part of a project funded by the Panel for Energy Research and Development (henceforth PERD) to study surface currents in waters surrounding the Queen Charlotte Islands. This project aims to establish a basic understanding of surface flows for use in the event of an oil spill. The PERD field program includes current meter and tide gauge deployments, ship-mounted acoustic Doppler current profiler measurements, CTD surveys and the deployment and tracking of drifters. Current meter and tide gauge observations were used to validate a three-dimensional tidal model, whose bottom velocities were applied to bottom friction in the three-dimensional baroclinic model described here. Current meter, CTD, and drifter observations will be discussed here as they are also used in validating the model.

Geographical Area

We focus on near-surface currents in Dixon Entrance, an east-west strait off the west coast of Canada. It lies north of Graham Island, the northernmost of the Queen Charlotte Islands, and south of Clarence Strait and the southernmost islands of Alaska (Figure 1). During the summer of 1991 two vessels measured the density structure of the ocean using CTD measurements while also monitoring the movement of Loran-C drifting buoys, over a period of 8 weeks.

There are several current patterns of interest in this strait: the Rose Spit Eddy and an eddy around Learmonth Bank. Bowman et al. (1992) reviewed the observed evidence for the existence of a these two gyres. They concluded that although the Learmouth Bank eddy could be attributed to tidal rectification, only part of the Rose Spit eddy could be simulated by tidal factors. The Rose Spit Eddy has been observed throughout the year, and appears to be a major factor in the retention of water in Dixon Entrance.

Numerical Technique

The numerical method is similar to that employed by Walters (1992) and Lynch et al. (1992). The governing equations are the three-dimensional, shallow-water equations with conventional hydrostatic and Boussinesq assumptions, and viscosity closure in the vertical. The Coriolis parameter was given the value for 54N. The vertical eddy viscosity was set to 0.01 m^2/s while the linear bottom stress coefficient was set to 0.01 in MKS units. The

bottom friction is quadratic and uses bottom tidal velocities calculated by a three-dimensional barotropic tidal model, sharing the same grid, and developed by the authors for this program.

Sea water density in Dixon Entrance is affected by runoff from the Nass and Skeena Rivers, by solar heating and by precipitation and evaporation. Ideally we would like to use seasonally averaged values and compute seasonal buoyancy flows as was done on Georges Bank by Naimie et al (1994). However, our data sets, like so many others, are too sparse and cover too few years to make this possible. This paper shows that interesting and useful results can still be achieved with less than ideal data sets.

The Dixon Entrance model grid (Figure 1) is simply a subset of the grid for the whole of the north coast of British Columbia used in Foreman, Walters, Henry and Ballantyne (1993). It has 1306 nodes and 2106 elements. Flow is restricted to be normal to the open boundary.

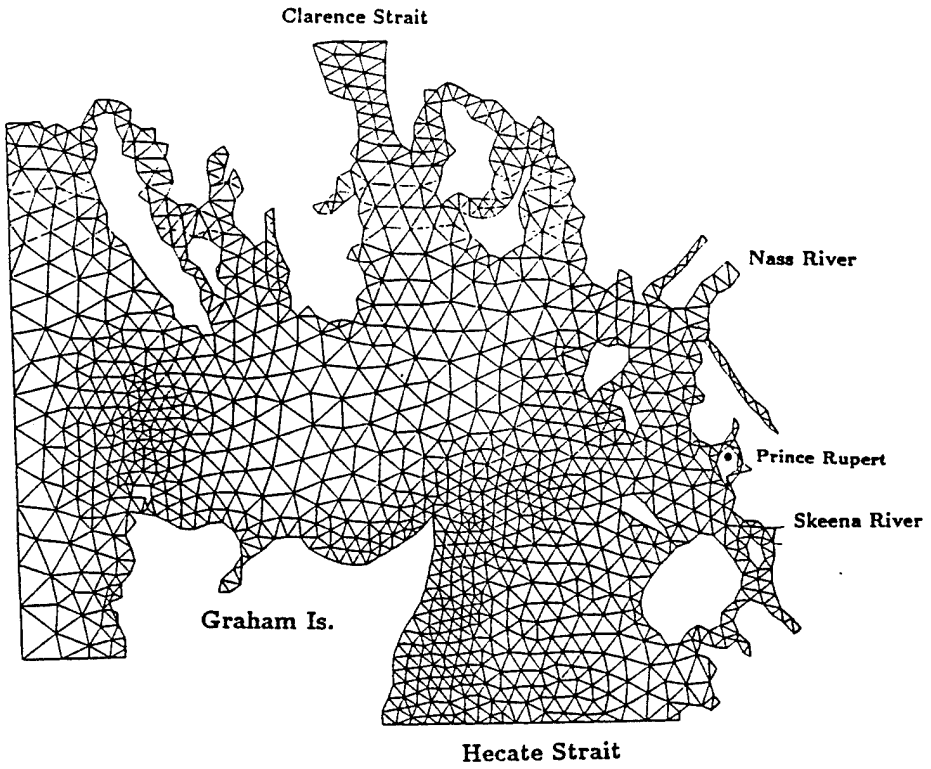

Figure 1. Actual triangular grid used for horizontal discretization in the tridimensional finite element model (with the courtesy of M.G.G. Foreman, 1993).

The observed sigma-t values were processed for model use by initially interpolating them to a regular grid, with approximately 4.5 km separation. This was done with an objective analysis algorithm similar to that described by Denman and Freeland (1985). Due to the complicated nature of the model region, with Dixon Entrance meeting Hecate Strait at a right angle, the correlation ellipse was chosen to be a circle, since no single ellipse would be appropriate. The radius of this circle varies between 30 km and 25 km depending on the formation of the CTD study lines. The size of the radius was chosen by contouring the values on the regular grid produced by various radii. For each CTD study the chosen radius was the one that produced the most fine detail of the sigma-t values without creating

details where the CTD data were sparse. The horizontal interpolation was done at specific depths in the water column (0, 10, 20, 30, 40, 50, 75, 100, 125, 150, 175, 200, 225, 250, 300, 400, and sometimes 500 m). Once these interpolations were done, horizontal gradients were calculated. These gradients were then interpolated horizontally to the nodes of the triangular model grid and vertically to the sigma surfaces.

Observed currents

We illustrate here the results for the summer of 1991, the period with the most observations. Although there were current meters moored in Dixon Entrance and in the channels to the east through all of July and August, the moorings in western Dixon Entrance were damaged by draggers and no data are available in the upper 50 m. It was the intense fishing by draggers in these waters, and expected damage to moored instruments, which caused us to shift our observational effort to surface drifters.

Figure 2 shows the averaged currents for the model area determined from the tracks of Loran-C surface drifters. Drifters were drogued at 3m depth. To average out the tidal velocities, vectors of velocities were calculated from the drifter positions at 25-hour intervals. The mid-point of each vector is assigned to the centroid of the 25-hour drifter track. Once all the drifter tracks in the region were processed, all the vectors from tracks with centroids within rectangles of 0.1 degrees of latitude and 0.1667 degree of longitude

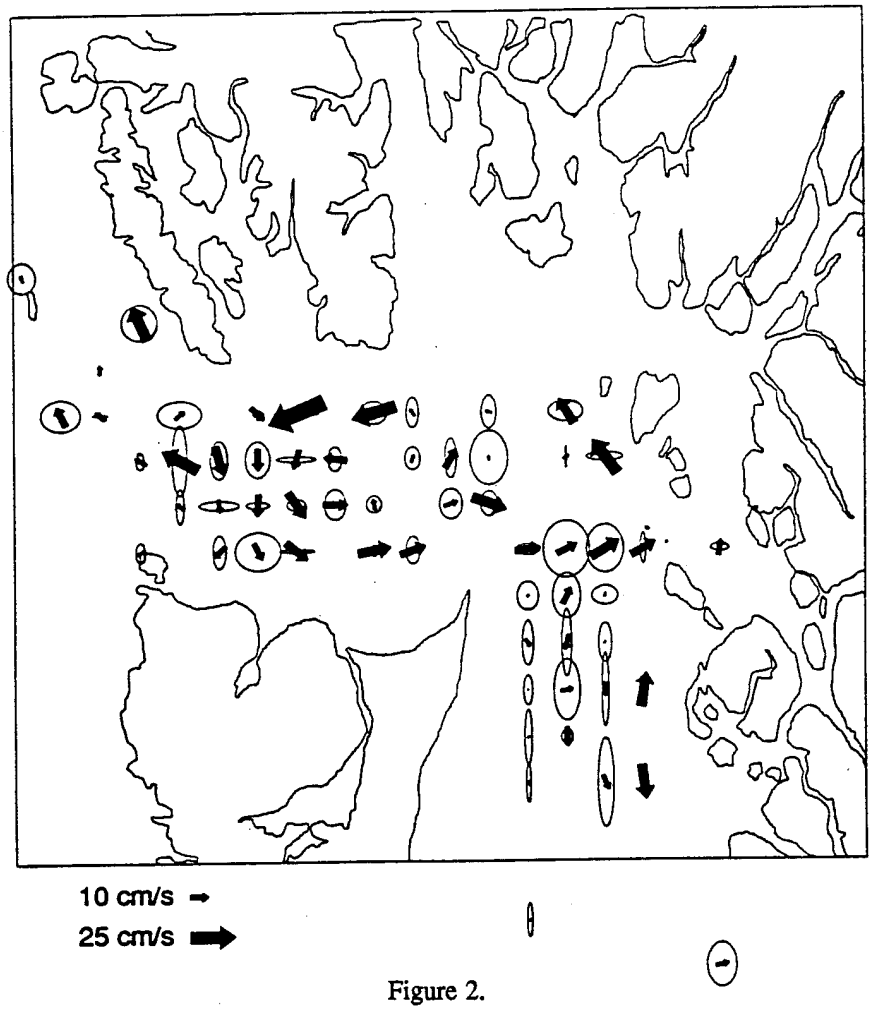

Figure 2.

were averaged. Vectors representing these averaged velocities are positioned in the middle of the rectangles. The standard deviations of the eastward and northward speeds are represented by an ellipse in Figure 2.

Comparison of Simulated and Observed Currents

Figures 3 and 4 show the model results at 3 m and 50 m depths for July and August, 1991. Note that both the model-simulated and drifter-observed vectors reveal the presence of the gyre in eastern Dixon Entrance. During these months the eddy extended to the west almost to the western end of the strait. Strongest flows are observed in the southwest portion of Dixon Entrance in the simulations of currents at 3 m depth, but the strongest currents observed in drifter tracks lie in the north-central portion of the strait.

The body of water in the southeast part of the region in Figures 2 and 3 is northern Hecate Strait, a shallow channel along the eastern side of the Queen Charlotte Islands, separating these islands from the mainland of British Columbia. The simulated currents here are weak, and the currents observed by the drifting buoys are irregular, with strong standard deviation. Actual currents here are wind driven, and the winds here alternate between north and south. Once we binned the currents measured by drifting buoys into three periods: weak winds, strong northward winds, and strong southward winds, a clear pattern of wind-driven currents emerged. This pattern also emerged in a two-dimensional wind-driven model of the region developed by Hannah et al. (1991).

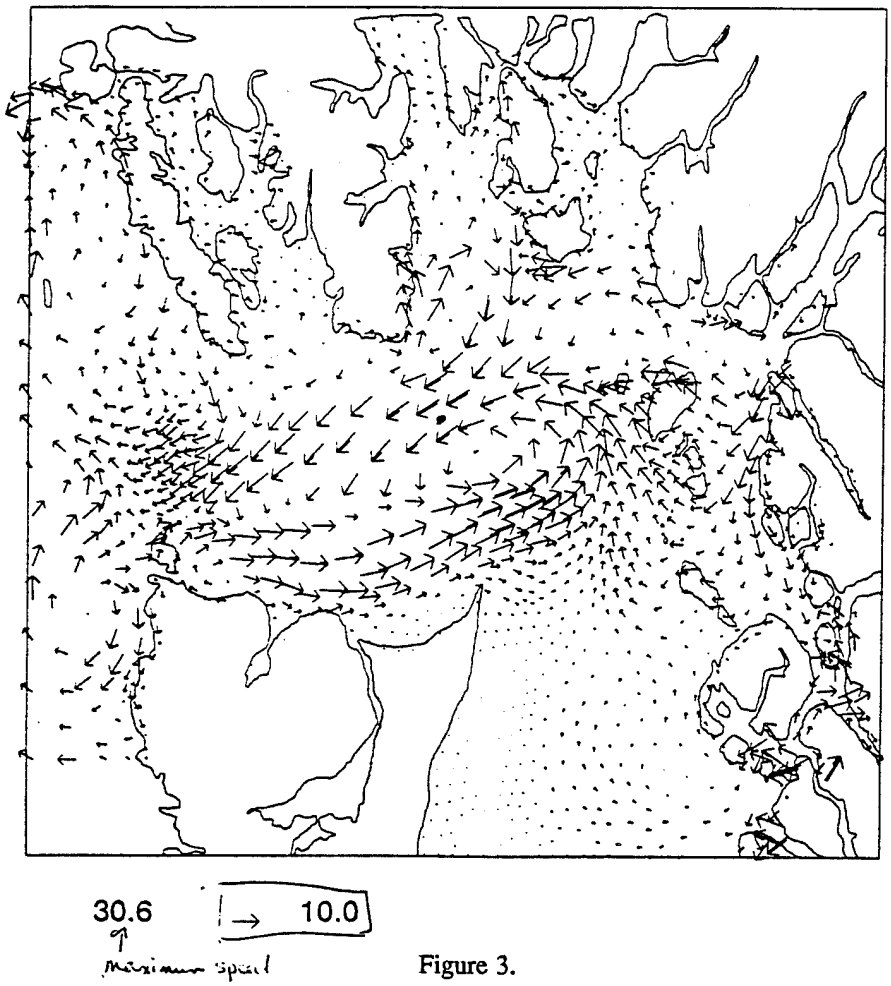

Figure 3.

We have computed similar comparisons for observations of water structure and currents over the previous decade. Where current meter observations permit comparisons in regions of strong currents, the favourable comparisons lead us to believe that this diagnostic baroclinic model is a valuable tool for simulating currents through the water column.

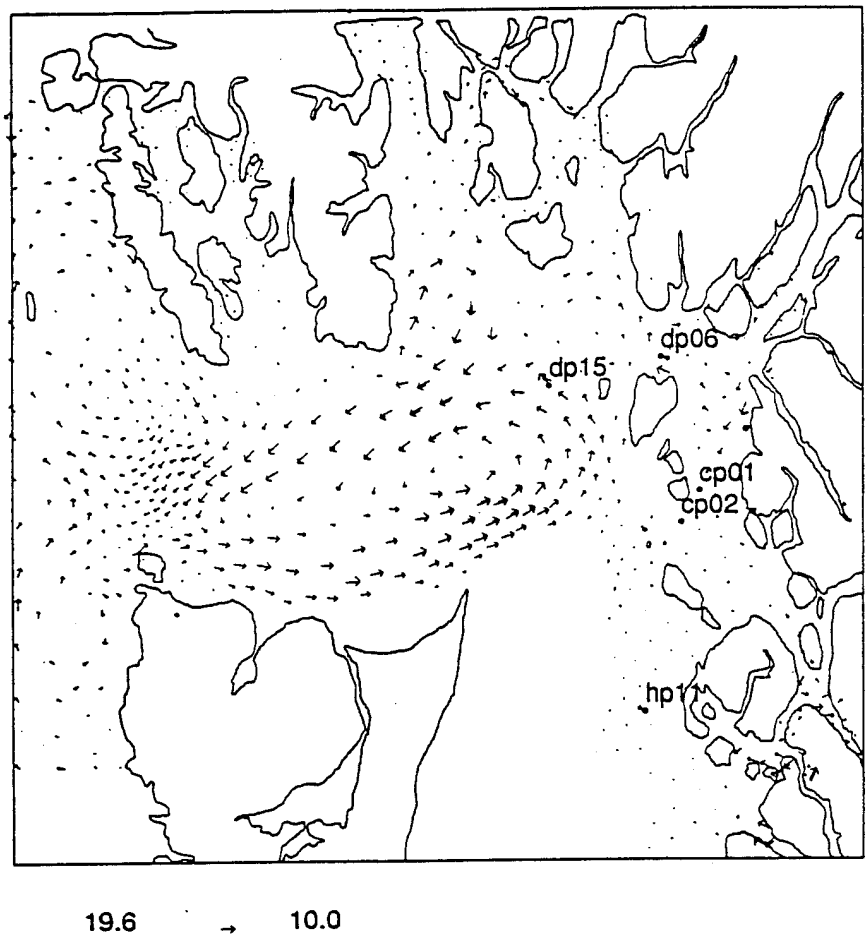

Figure 4.

References

Bowman, M.J., A.W. Vissar, and W.R. Crawford, 1992, The Rose Spit Eddy in Dixon Entrance: Evidence for its existence and underlying dynamics. *Atmospher-Ocean,*, 30(1):70-93

Denman, K.L. and H.J. Freeland, 1985. Correlation scales, objective mapping and a statistical test of geostrophy over the continental shelf. *Journal of Marine Research,*, 43:517-539

Foreman, M.G.G., R.F. Henry, R.A. Walters, V.A. Ballantyne, 1993. A finite element model and resonance along the north coast of British Columbia. *J. Geophys. Res.*, 98, C2: 2509-2531.

Hannah, C.G., P.H. LeBlond, W.R. Crawford, W.P. Budgell, 1991. Wind-driven depth-averaged circulation in Queen Charlotte Sound and Hecate Strait. , *Atmospher-Ocean,* 29(4):712-736.

Naime, C.E., J.W. Loder, D.R. Lynch, 1994. Seasonal variation of the three-dimensional residual circulation on Georges Bank. submitted to *J. Geophys. Res.*

SEASONAL VARIATION OF THE BAROCLINIC CIRCULATION IN THE SCOTIA-MAINE REGION

C. G. Hannah and J. W. Loder
Department of Fisheries and Oceans
Bedford Institute of Oceanography
Dartmouth, Nova Scotia, B2Y 4A2

Abstract

Introduction

Seasonal circulation in the Scotian Shelf-Gulf of Maine (henceforth Scotia-Maine) region is generally dominated by the along-shelf (equatorward) flow of relatively cold and fresh water, with strong seasonality and topographic steering by submarine banks and basins. At depth, denser Slope Water moves on-shelf via several deep channels, providing an `estuarine' nature to the large-scale shelf circulation regime. Most of this circulation has been attributed to density forcing, and corroborative investigations of the baroclinic flow component have been carried out in some areas. However, the large-scale baroclinic circulation is not well described and it is poorly understood. Suggestions for important baroclinic dynamics have included a large-scale buoyancy-driven coastal current (Chapman and Beardsley 1989), buoyancy forcing from coastal freshwater discharge such as the Gulf of St. Lawrence outflow (Drinkwater et al.\ 1979), geostrophic adjustment to Slope Water intrusions (Brooks 1985, Brown and Irish 1992), transport amplification through the Joint Effect of Baroclinicity and Relief (e.g. Lazier and Wright 1993), and seasonal intensification of bank-scale gyres by tidal-mixing fronts (Loder and Wright 1985).

Here we present some initial results from a diagnostic investigation of seasonal baroclinic circulation in the Scotia-Maine region. Our long-term goals are to obtain 3-d climatological fields for the seasonal-mean circulation in the region, and to elucidate the underlying dynamics of the baroclinic flow component so that sensitivities to forcing variations can be assessed. Our investigation is based on the large historical temperature-salinity database for the region and uses the diagnostic finite-element circulation model of Lynch et al. (1992) and various circulation and vorticity diagnostics for interpretation.

Methodology

The database used in the present study is comprised of approximately 57,000 CTD and bottle (with reversing thermometer) stations in the greater Scotia-Maine region, with coincident temperature and salinity observations. Climatological mean temperature, salinity and density fields for selected seasons are estimated using 4-d optimal linear interpolation with various choices of correlation scales. The optimal linear interpolation procedure provides estimates of the mean scalar fields at specified grid points in 4-d (x,y,z,t) space from its nearest-neighbour data points based on separation distances scaled by the correlation scales.

The model domain extends from Cabot Strait to Long Island and has variable grid size allowing increased resolution in target areas. Two meshes are considered, the first is focussed on Georges Bank (g2s mesh) and the second has increased resolution over the shelf-break and on the Scotian Shelf (gb3 mesh).

Two sets of density fields are considered. The first set resolves the seasonal variation using 6 bi-monthly fields on the g2s mesh with time correlation scales of 30-45 days. The horizontal correlation scales are taken as isotropic over the shelf, except on the sides of Georges Bank where larger scales are used in the along-bank directions. These density fields were used by Naimie et al. (1994) in a model study of the seasonal variation of circulation over Georges Bank driven by tides, wind and density.

The second set of density fields, for winter and summer seasons on the gb3 mesh, is used to explore the importance of the time correlation scales and anisotropic horizontal correlation scales. The latter are specified parametrically from the bathymetric gradient vector, with larger scales in the along-isobath direction proportional to the bottom slope. Particular attention is given to the effectiveness of such a specification in minimizing artificial along-isobath density gradients (and resulting flow features) associated with aliased temporal variability and sparsity of the density database.

The 3-d linear harmonic circulation model computes elevation and velocity fields for baroclinic pressure gradient fields specified from the fixed density fields. Bottom friction coefficients and vertical eddy viscosity coefficients are taken from nonlinear solutions including the M2 tide and vary with horizontal position (Lynch and Naimie 1993, Naimie et al. 1994). Elevations at the upstream (cross-shelf) and offshore boundaries are specified to yield zero normal geostrophic velocity at the seafloor, and a geostrophic-flow condition is used on the downstream (cross-shelf) boundary.

Results

The bi-monthly fields show the spatial structure of the strong seasonal variation in upper-ocean temperature and the persistent cross-shelf salinity gradient in the Scotia-Maine region. Seasonal influences from the Gulf of St. Lawrence outflow and coastal run- off in the Gulf of Maine are also apparent in the salinity fields. Dynamic height fields referenced to 1200 m and computed following the approximation method of Sheng and Thompson (1994, unpublished manuscript) illustrate important features of the baroclinic circulation, such as the seasonally-varying flow on the western side of Cabot Strait which supplies the Nova Scotia Current off Halifax and the seasonal flow into the Gulf of Maine off southwestern Nova Scotia. Strong topographic steering is also apparent, with anticyclonic baroclinic flow around the Banquereau-Sable-Emerald Bank complex and Georges Bank, and cyclonic flow around Emerald Basin and basins in the Gulf of Maine.

Examination of the domain-wide velocity and transport streamfunction fields in the Naimie et al. (1994) model solutions (with the bi-monthly density fields) provides initial indications of both the associated circulation and the adequacy of the density fields for diagnostic computations. Many circulation features consistent with observational information are apparent, particularly on large scales, but there are also closed streamlines and large velocities in some areas whose reliability for the climatological mean is questionable. Vorticity diagnostic computations on the density fields reveal that the term representing vortex stretching by geostrophic flow across isobaths has large fluctuations on small scales in some areas, suggesting that density data noise and the Joint Effect of Baroclinicity and Relief result in some spurious circulation features. The variation of density along selected isobaths through the domain shows both systematic large-scale variations of probable importance to the large-scale circulation and smaller-scale fluctuations of dubious reliability. In particular, the vertically-averaged density generally increases with distance downstream, consistent with on-shelf supply of Slope Water.

To investigate whether alternative choices of time and horizontal correlation scales in the optimal interpolation procedure can reduce the density data `noise' and sparsity

problems, attention is focussed on winter and summer seasons using the second set of density fields (gb3 mesh and updated density database). A modified optimal linear interpolation procedure (I. He, R. Hendry and G. Boudreau, 1994) which allows different correlation scales at each grid point is used to estimate density fields with various forms of anisotropic horizontal correlation scales over the entire model domain. Initial model results are encouraging; the solutions are similar to the bi-monthly model solutions in the Georges Bank region and some small-scale features are eliminated elsewhere in the domain. The sensitivity to alternative choices of season mid-time and larger time correlation scales in order to offset data sparsity is also investigated.

The study results are being used in conjunction with those from collaborators to formulate future collaborative research strategies for baroclinic circulation on the northwestern Atlantic shelf, involving extended model domains, additional temperature (e.g. bathythermograph) data, more sophisticated circulation (e.g. prognostic) models, and decadal-scale hydrographic and circulation variability.

References

Brooks, D.A., 1985. Vernal circulation in the Gulf of Maine. *J. Geophysical Research,* 90:4687--4705.

Brown, W.S., and J.D. Irish, 1992. The annual evolution of geostrophic flow in the Gulf of Maine. *J. Physical Oceanography,* 22:445--473.

Chapman, D.C., and R.C. Beardsley, 1989. On the origin of shelf water in the Middle Atlantic Bight. *J. Physical Oceanography,* 19:384--391.

Drinkwater, K.F., B. Petrie, and W.H. Sutcliffe, 1979. Seasonal geostrophic volume transport along the Scotian Shelf. *Estuarine and Coastal Marine Science,* 9:17--27.

Lynch, D.R., F.E. Werner, D.A. Greenberg, and J.W. Loder, 1992. Diagnostic model for the baroclinic, wind-driven and tidal circulation in shallow seas. *Continental Shelf Research,* 12:37--64.

Naimie, C.E., J.W. Loder and D.R. Lynch, 1994: Seasonal variation of the three-dimensional residual circulation on Georges Bank. *J. Geophysical Research,* 99:15,967.

UPWELLING ON TWO WIDE SHELVES DOMINATED BY LARGE LATERAL BUOYANCY FLUXES

Andreas Munchow
Center for Coastal Studies
Scripps Institution of Oceanorgaphy
La Jolla, CA 92093-0209
Co-authors (not of the abstract):
Eddy C. Carmack, IOS Sidney, British Columbia, Canada
Richard W. Garvine, University of Delaware, U.S.A.
Roby W. Macdonald, IOS Sidney, British Columbia, Canada

Abstract

Introduction

Continental shelves along passive margins are generally wide, gently sloping, and receive large amounts of freshwater from rivers and estuaries. The local winds are fairly uniform over the coastal plains and adjacent continental shelves. Typical topographical scales are about 500 km and 50 km in the along- and across-shelf directions, respectively. We here compare the interaction of wind and buoyancy forced motions on two such shelves by analyzing data from the Beaufort Sea in the Canadian Arctic and the Mid-Atlantic Bight on the eastern seaboard of the U.S.A. The two shelves have similar topographic scales, receive similar amounts of freshwater, and are forced by similar winds. An important difference between the two shelves, however, is the location of their respective buoyancy source. The Beaufort shelf receives all its freshwater (10,000 m^3/s) from the Mackenzie delta which discharges almost undiluted freshwater directly onto the shelf. No estuary is present. In contrast, the Mid-Atlantic Bight receives its freshwater (5,000 m^3/s) from three estuaries which discharge a brackish mixture onto the shelf. We here study the response of the buoyant waters on both shelves to upwelling favorable winds. Strong similarities between the two shelves emerge.

Specifically, we find that the upstream source of buoyancy substantially alters the classical two-dimensional concept of up-welling, i.e., the Ekman flux divergence in the surface layer is not always compensated by a vertical flow component. On the Beaufort shelf as well as in the Mid-Atlantic Bight the Ekman flux divergence can instead be balanced by an enhanced outflow from the delta or the estuary, respectively. The response to up-welling favorable winds is then three-dimensional, includes a strong across-shelf circulation, and results in an enhanced along-shelf flow against the local winds below the pycnocline. It appears that the vertical stratification on the inner shelf is enhanced rather than reduced by the upwelling. Cold, dense, and nutrient rich waters are advected onshore more than 50 km from the middle and outer shelf. The three-dimensional baroclinic circulation, however, is inherently unsteady and little is known about its detailed velocity structure and the balance of forces in time and space.

Sea level Oscillations

A first measure of the potential importance of wind driven motions is the correlation of the local winds with the local sea level. For the Mackenzie shelf a 40 day long record from the summer of 1987 represents conditions during a period when the shelf is largely ice-free. We find moderately strong winds with speeds of about 5 m/s whose direction varies with time. Periods of persistent upwelling and downwelling favorable winds correspond to

periods of low and high sea level, respectively. The range of the sea level oscillations exceeds 60 cm. The frequency domain correlation of the along-shore winds with sea level for the Mackenzie shelf reveal that about 70% of the sea level variance is explained by a linear correlation at 5 days. The winds lead the sea level oscillations by about 12 hours at 5 days. Similar fluctuations occur in the Mid-Atlantic Bight. We thus find significant linear correlation between wind and sea level oscillations on both shelves. We interpret the wind forced sea level oscillation as the integrated effect of across- and along-shelf transports. The dynamics of these transports, however, are largely unknown because, as we discuss next, the water on both shelves is only a few Ekman layers deep and strongly stratified in the vertical.

Hydrography

Vertical and lateral buoyancy fluxes result in characteristic hydrographic conditions on continental shelves. In the Mid-Atlantic Bight solar insulation causes the formation of a seasonal thermocline in summer. On Arctic shelves solar insulation melts ice first before it warms the surface layer of the coastal ocean. The vertical buoyancy flux is thus due to the release of melt water, which is fresh, and the subsequent warming of these waters. Lateral buoyancy fluxes on both shelves originate from the fresh water that is discharged by rivers and estuaries. Within a few internal deformation radii off the coasts density gradients are dominantly due to salinity gradients. We thus discuss the hydrography mostly in terms of salinity.

Torrential rains 10 days prior and strong downwelling favorable winds off the coasts of New Jersey, Delaware, and Maryland resulted in a complex salinity pattern on the inner shelf of the Mid-Atlantic Bight in the summer of 1989. We discern a circular pool of light water off New Jersey, a front at the mouth of the Delaware Estuary, the onset of a banded structure along the coast downstream of the estuary, and several smaller eddies near the off-shore zone of large salinity gradients. We believe that all these features are the direct result of the estuarine discharges from the Hudson and the Delaware estuaries. The vertical distribution of salinity during this event is stratified off New Jersey, but partially mixed off Delaware and Maryland. Downstream of Delaware Bay the buoyant waters extend to the bottom and represent waters of the Delaware Coastal Current (Munchow and Garvine, 1993). The large circular pool or eddy upstream of Delaware Bay is only 5 m deep and presumably originates from an unstable coastal current fed by Hudson River discharges.

The horizontal salinity distribution on the Mackenzie shelf between the 10 m and the 60 m isobath is equally convoluted. We find a band of low salinity water about 60 to 80 km from the coast which appears to originate from the Mackenzie Delta to the west. The across- and along-shore salinity gradients are large and reach several psu/km, i.e., strong surface fronts occur throughout the entire region, however, these are not always resolved by the survey grid. This is especially true for a particular front near the 10 m isobath. The interpretation of the map is further complicated by a strong upwelling favorable wind event on day 243 (Aug. 30, 1986) when the local sea level first decreased and then increased by more 50 cm/day. The vertical salinity distribution as well as the water mass characteristics reflect this event. Prior to day 243 we surveyed a transect about 100 km from the Mackenzie Delta. We observe two haloclines with a large (moderate) vertical salinity gradient 8 m (15m) below the surface. The temperature-salinity diagram for the data of this section indicates three different water types. These are fresh and warm estuarine surface waters, salty and warm ambient shelf waters, and finally cold and very salty ambient bottom shelf waters. No mixing between ambient shelf and estuarine waters is apparent prior to the wind event. About 60 hours later and 50 km upstream we find a 15 m thick halocline and only a single mixing line between estuarine and bottom shelf waters. The

transect intermediate in both time and space between these two extremes is almost centered on the upwelling favorable wind event. We find a strong halocline at about 8 m, however, at depths between 8 m and 20 m we now find almost continuously stratified water. Mixing now takes place between all three water types. Hydrographic observations taken a week after this event both up- and downstream of the location of these three transects suggest that the vertical structure of the water column is indeed a temporal, not a spatial phenomena. Some overlap of spatial and temporal processes, however, always occurs.

Velocity

Off New Jersey in the summer, buoyant waters are generally found only within about 20 km off the coast. Southward surges of a buoyancy driven coastal current supported by downwelling favorable winds, however, appear more than 150 km from the buoyancy source which is the mouth of the Hudson Estuary. The current width scales with the internal deformation radius. ADCP and CTD observations in the summer of 1989 reveal a three dimensional evolution of such a surge as the winds shift from upwelling to downwelling and back to upwelling favorable. The downwelling favorable winds bring buoyant waters from the Hudson Estuary into the study area. The buoyant waters extend about 10 km from the coast; isopycnals intersect both the surface and the bottom; and the vertical stratification is weak inshore of a region of enhanced lateral density gradients. Upwelling favorable winds, however, induce across-shelf fluxes that move buoyant waters offshore near the surface and dense bottom waters onshore. Drifters drogued 2 m below the surface indicate a swift movement offshore and upstream with the winds. Removing the tidal signals from the ADCP measurements, we find onshore velocities of about 6 cm/s within 5 m of the bottom.

No velocity data is available from the Mackenzie shelf, however, an extensive field study is currently underway. We will present preliminary results from the Beaufort Arctic Storms Experiment (BASE). BASE is a multi-disciplinary effort to understand the movement of the atmosphere, the ice, and the coastal ocean. Frequent atmospheric storms (polar lows) at the end of summer set the early stage for the formation of ice, however, our intention is to study the interaction of buoyancy and wind forced motions in the absence of ice. We will deploy 15 surface drifters, profile the shelf with two ADCPs, survey the density field, and service several current meter moorings. Concurrent NCAR aircraft overflights will map the spatial distribution of sea surface temperature, winds, and ice.

INLET CONTROL OF TIDES AND SALINITY IN A SHALLOW BAY

Daniel C. Conley
Marine Sciences Research Center, State University
of New York, Stony Brook, NY 11794-5000

Abstract

Introduction

The northeaster which initially struck Long Island on 11 December 1992 caused a breach in the barrier island at Westhampton Beach which came to be known as Little Pike's Inlet. This breach eventually developed into an inlet providing a second direct pathway for ocean-bay exchange. A subsequent engineered closing of this inlet provided a unique opportunity for observation of inlet effects in this shallow estuary system. This work describes a set of observations intended to identify the various physical effects associated with the short life of this inlet.

Moriches Bay is a shallow, narrow, east-west trending bay which is bounded by Westhampton Beach and Fire Island barrier islands to the south and the south shore of Long Island to the north. The bay has a surface area of approximately 41.8 million m^2 with a mean depth of 1.2 m, which results in a total volume of $51m^3$ (Redfield, 1952). The bay is approximately 20 km long and varies in width from about 1.4 to 4 km. The western end of Moriches Bay is connected to Great South Bay through the narrows at Smith Point, where the channel is about 300 m wide with a cross sectional area of 625 m^2. The eastern end communicates with Shinnecock Bay through the long and narrow Quantuck Canal, which has a minimum cross sectional area of $75m^2$. Moriches inlet is located near the middle of Moriches Bay and separates Fire Island and Westhampton Beach . This inlet, which provided the sole direct passage to ocean prior to December 1992, has a cross sectional area of approximately $110m^2$ and a mean depth of 4.8 m (USACOE, 1982).

Following the initial breaching in the December 1992 northeaster, the Westhampton Beach opening grew to an approximate width of 600 m over an 8 month period. Following this period, it was decided to refill and close the breach, a process which was completed in late September 1993. None the less, for this 10 month period, this inlet provided a second direct ocean opening which came to be know as Little Pikes Inlet. This event provided a unique opportunity to monitor the effects of multiple and single inlet geometries on water quality in estuarine bodies. While no monitoring program was in place when the breach occurred, a series of sensors was deployed well before the closing of the new inlet. These included a tide gauge mounted directly landward of the breach and several salinometers distributed over the length of the bay. As these sensors were maintained throughout the remainder of the life of Pikes Inlet and several months after its closure, this data set provides an excellent measurement of "before and after" estuarine conditions.

Tide Measurements

Water surface elevation measurements were made almost due north of Little Pike's Inlet across the bay at Speonk Point. A self recording Fisher Porter model 35-1550 float type tide gauge was mounted on a jetty wall in about 1 m of water. Sea surface elevation was measured four times hourly, and recorded on a punched paper tape which was removed and saved in digital format on a monthly basis. The instrument was in place from 1 April

1993 until 5 January 1994 and a complete record of over 26,000 points was obtained during this period. In order to accurately determine tidal transmission, simultaneous determination of local ocean tides is required. These were collected using an Endeco model 1032 auto recording absolute pressure sensor which was bottom mounted approximate one kilometer from shore in 8.8m of water at Westhampton Beach. These measurements were corrected for atmospheric pressure by subtracting the Islip, NY sea surface atmospheric pressure from the total pressure. The only successful deployment of this instrument occurred from 19 April until 20 May during which a full 31 days of data, recorded at a data rate of 6 samples per hour, were obtained. Additional tide data was obtained from National Oceanographic and Atmospheric Administration (NOAA) measurements at Sandy Hook, NJ and Montauk Point, NY. For calculations of mean tidal conditions, a transfer function between Westhampton Beach and each of the NOAA stations was derived. The transfer function was based on the amplitude and phase of 25 tidal constituents with residual sea surface elevations assumed to be long period effects which would be felt synoptically by all three locations [Wang, 1979]. A calculated tide was then computed at Westhampton Beach using the Sandy Hook tidal data and a sliding 31 day window centered about the day being calculated. Similar calculations were performed using the Montauk Point data which indicated a difference in mean tidal range between the two sets of data on the order of 1% of the range. This calculated tide was utilized to determine local mean tidal levels while calculations using tidal constituents were based on the original NOAA data.

Salinity Measurements

The salinity measurements were collected using Aandera model RCM4 current thermosalinigraphs with the current measurement component disabled. These sensors were shore mounted in approximately one meter of water with the sensing elements approximately 0.35 m above the bottom. The instrument housings were attached either to pilings or instrument mounts which remained in the measurement location for the duration of the observations. The sensors recorded temperature and conductivity 6 times per hour. In order to ensure reliable measurements, it was found necessary to clean the instruments weekly at which time water samples, as well as a second set of salinity measurements, were collected as controls. Each instrument was replaced approximately every five weeks when the old instrument was retrieved for data recovery and sensor servicing.

In order to investigate the character of the salinity response in Moriches Bay, two sensors were deployed within Moriches Bay. One instrument was adjacent to the tide gauge near the breach in the eastern half of Moriches Bay and a second was located in the western half of Moriches Bay near the junction with Great South Bay. These two instruments can therefore provide information about what kind of variation in salinity was experienced over the extent of Moriches Bay. In order to determine which changes were due to inlet effects and which were from other regional causes, a third sensor was placed in a near shore location at the western end of Shinnecock Bay. This location was chosen because it represents a shallow estuarine environment similar to the Moriches Bay locations, yet the only contact between Shinnecock and Moriches Bay is through the long and narrow Quantuck Canal, which could be expected to minimize the transmission of any effects from Little Pike's Inlet. This station therefore represents the control for the system and any changes in Moriches Bay can be contrasted against changes at this location.

Data Analyses

The computed tides at Westhampton Beach were used to calculate a daily time series of tidal range, defined as the difference between mean high and low water as determined on a time centered 28 day sliding average. This tidal range was compared against a time series of Moriches Bay tides which was similarly derived from the measurements of bay tides.

Mean water levels, calculated as a necessary mid-step in this process, were used to explain how observed differences in tidal transmission were distributed among high and low waters.

Salinity measurements were processed by calculating and cleaning temperature and conductivity records, at which time any detected sensor drift was corrected. Salinity values were then determined. Data recovery was not as complete as the tide data with data loss occurring for two major reasons. The first was the water temperature drifting above or below the temperature range of the instrument and the second was instrument malfunction. While daily high and low temperatures drifted out of range at the start of winter and summer, at no time did this prevent collection of reasonable data during some part of every day. Instrument failure, on the other hand, resulted in the total loss of data during the period of failure. The largest such loss occurred at the control site in Shinnecock Bay from 29 June through 31 August 1993. A smaller loss occurred at this site in late October, while no such losses were experienced at the other two sites. Linear interpolation was used to fill in small gaps (O(1 day)) but larger gaps were left open. Fortunately, the data return from all instruments at all locations was adequate to detect any significant trends in the salinity following the breach closure on 25 September 1993. Short-period daily fluctuations in the salinity signal have been removed by forming daily averages at each station.

Discussion

Much as expected the tidal transmission record shows a strong correlation to the life history of Pikes Inlet. The tidal transmission demonstrate quite clearly the effects of a multiple inlet geometry, dropping from a pre-closure high of about 73% to a post-closure mean of about 55%. The change in the transmission appears to mirror quite closely the life history of the inlet, exhibiting slight increase in the months prior to the start of infilling after which it flattens out during the period of shore line stabilization and initial filling and finally drops rapidly during the final period which corresponds to rapid inlet filling. While the associated 0.6m change in tidal range initially appeared to be distributed predominantly among an increase in mean high water, comparisons to mean water level in the ocean suggest that the new range was evenly distributed among a decreased mean low water as well as an increased mean high.

Simple arguments for the circulation and mixing in shallow estuaries would predict that the enhanced mixing associated with the increased tidal range would lead to elevated salinity levels within the bay. Such a prediction is supported by the observations at the eastern end of Moriches Bay near the new inlet. At this location the mean salinity decreased 1.4 ‰ in the four months following the inlet closure. This is in contrast to a small but statistically insignificant salinity increase at the control station in Shinnecock Bay. Thus these observations suggest that the reduced mixing due to the reduced tidal range in Moriches Bay does lead to a decrease in the bay salinity and the magnitude is of in relative agreement to what might be predicted by a simple water quality inlet model (Isaji & Spaulding, 1981).

The observations at the western end of the bay indicate the inadequacies of such models when applied to locations of greater complexity. The measurements in this portion of the bay indicate absolutely no change in mean salinity following the closure of the breach. The measurements demonstrate the presence of an eastward increasing gradient in salinity during the life of Pikes Inlet. The drop in salinity in the eastern end following inlet closure tended to drive the salinity there to a level which was closer to the constant western values. This scenario suggests that the effects of Little Pikes Inlet were constrained to the eastern portion of the bay and raises the question as to what role is played by the exchange between Moriches and Great South Bay.

These measurements have successfully identified some of the physical effects of Little Pikes Inlet. A definite increase in tidal transmission can be attributed to the presence of the inlet. Additionally, a local increase in bay salinity also appears to be due to the inlet but this effect does not span the bay indicating a spatial distribution in the bay response. Other details to be investigated include the behavior of individual tidal components as well as an examination of the role of the exchange with Great South Bay.

References

Isaji, T and M.L. Spaulding, 1981. A simplified model for assessing the impact of breachway modifications on coastal pond circulation and flushing dynamics. *Proc. Oceans 81*, Boston Ma., p. 824-828.

Redfield, A.C., 1952. Report to the Towns of Brookhaven and Islip N. Y., on the Hydrography of Great South Bay and Moriches Bay. *Reference #52-26*, Woods Hole Oceanographic Institution, Woods Hole Ma., 80 pp.

US Army Corps of Engineers, 1982. *General Design Memorandum Moriches Inlet Project, Long Island, NY*, USACOE New York District.

Wang, D-P, 1979. Low frequency sea level variability on the Middle Atlantic Bight. *Jour. Marine Research*, 37(4):683-697.

TURBULENT FEATURE ON BUOYANT CURRENT TOWARD INLET IN MAN-MADE LAKE

Yuichi Kitakura and Sotoaki Onishi
Electric Power Development co. Ltd. (EPDC)
8-15-1. Ginza, Tokyo, Japan
Civil Engineering Department
Science University of Tokyo
Noda, Chiba

Abstract

Introduction

Buoyant current toward an intake in water have been studied in laboratory by many researchers. In these studies Froude's similarity is applied in general, neglecting turbulent or diffusive nature of the stratified reservoir. In practical reservoir, however, the flow is disturbed by many causes such as inflow, outflow, wind and other. In the present paper, the in-field observation has been done to get data rates of inflow and outflow, wind, current velocity, water temperature, concentration of suspended soil particle and chlorophylin at the Kazaya dam reservoir. With the obtained data the authors discuss some aspects of turbulent characteristics of stratified current in the reservoir.

Description of the Kazaya Reservoir

The Kazaya dam, which completed in 1960 along the Shingu River running north to south almost in the center of Kii peninsula in Japan. The reservoir is exclusively for power generation. The annual water exchange rate of the reservoir are 5 to 10, and stable theremocline are formed in the reservoir in summer. From November major circulation period of the reservoir begins and mixing occurs. The intake is planned to withdrawal the water of middle layer in the reservoir.

Physical Parameters Relating to Stratified Current in Reservoir

Current toward intake and spillway in the reservoir are generally of nature of stratified current except in winter, and its dynamic feature may vary with many physical parameters such as Reynolds number and Froude number or Richardson number, intake condition, wind stress at water surface, stratification and others. Effects of these concerning parameters on the dynamic feature of the currents in the reservoir are discussed through the observations in field.

Method of In-Field Observation

To see turbulent feature in the Kazaya reservoir, we have been measuring current velocity, water temperature, water turbidity and chlorophyllin at four stations at the reservoir through a year since October of 1992. Wind velocity was measured at the stations as well. The measurements are done from the reservoir surface to the bottom with an ordered depth intervals. At each measuring points, it is planned with a two minute stoppage. After a stoppage measurements except velocity elements begin to be collected. For the velocity, the observation has five patterns of measurement depth pitch of z = 2.5, 5.0, 7.5, 10.0 and 20.0m.

Observation Results

Change of stratification through one year

The observations of water temperature and turbidity from the beginning of October of 1992 to September of 1993 show that in the beginning of April stratification in the reservoir and distinguished interface is produced. The stratification descents gradually with passing time to reach nearly the elevation of the intake opening at the beginning of June. After the mid of May a thin surface layer begins to appear. Under such condition as there exist the upper and lower interfaces, the current in the reservoir can be modeled with the three layered stratification flow. From the beginning of November the stratification begin to lack stability and the water in the reservoir turn over down. The turning over is not finished in a straight way, but is shall progress periodically with a period of approximately half a month in the early stage.

Mixing length and eddy viscosity coefficient

In practical field, Reynolds number of flow is generally large and the flow becomes turbulent and the shear stress (τ) in a flow is represented by the following equation,

$$\tau/\rho = \upsilon\, \partial u/\partial z = u'w' = (\upsilon + \varepsilon)\partial u/\partial z \qquad (1)$$

where ρ = water density, (u, w)= horizontal and vertical velocity components of velocity, υ = kinematic viscosity coefficient of water, ε = eddy viscosity coefficient, z = water depth.

Eddy viscosity coefficient is represented by

$$\varepsilon = l'\sqrt{W'} = l^2|\partial u / \partial z| \qquad (2)$$

in which l,l' = mixing length. The mixing lengths of momentum, water temperature and mass may differ each other and are described by theø following equations.

$$l = l_0 + kz, \quad l_H = l_{\sigma lH} + k_{\ H}z, \quad lr = l_{\sigma\rho} + k_\rho z \qquad (3)$$

in which $l_{\sigma l}$ $l_{\sigma lH}$, $l_{\sigma l\rho}$ = mixing length at interface, k, k_H, k_ρ = Karman constants for momentum, water temperature and mass. Referring to Egashira and Ashida's study suggesting that the mixing lengths are in inverse proportional to third power of velocity factor, we define the mixing length of momentum normalized with water depth of middle layer (d_2) as follows;

$$\beta = l_{\sigma l}/d_2 = \gamma_1(U/u*)^{-3} \qquad (4)$$

a) Mixing length

Observed relations between the normalized mixing length and the velocity factor at the interface, together with those obtained by Lofquist and Egashira are shown in Figure 1. One can see that the coefficient γ_1 in equation (4) distribute in a range of 1.25×10^3 to 1.25×10^4 in the Kazaya reservoir, which are considerably large as compared with those of 120 through 300 obtained by the laboratory tests of previous researchers. Actually in the Kazaya reservoir the thickness of the interface is around 5 to 10m, which are much thicker

than those in the laboratory tests. It is considered that the currents in the kazaya reservoir involve turbulence of the time and scale scales larger than those observed in the laboratory tests.

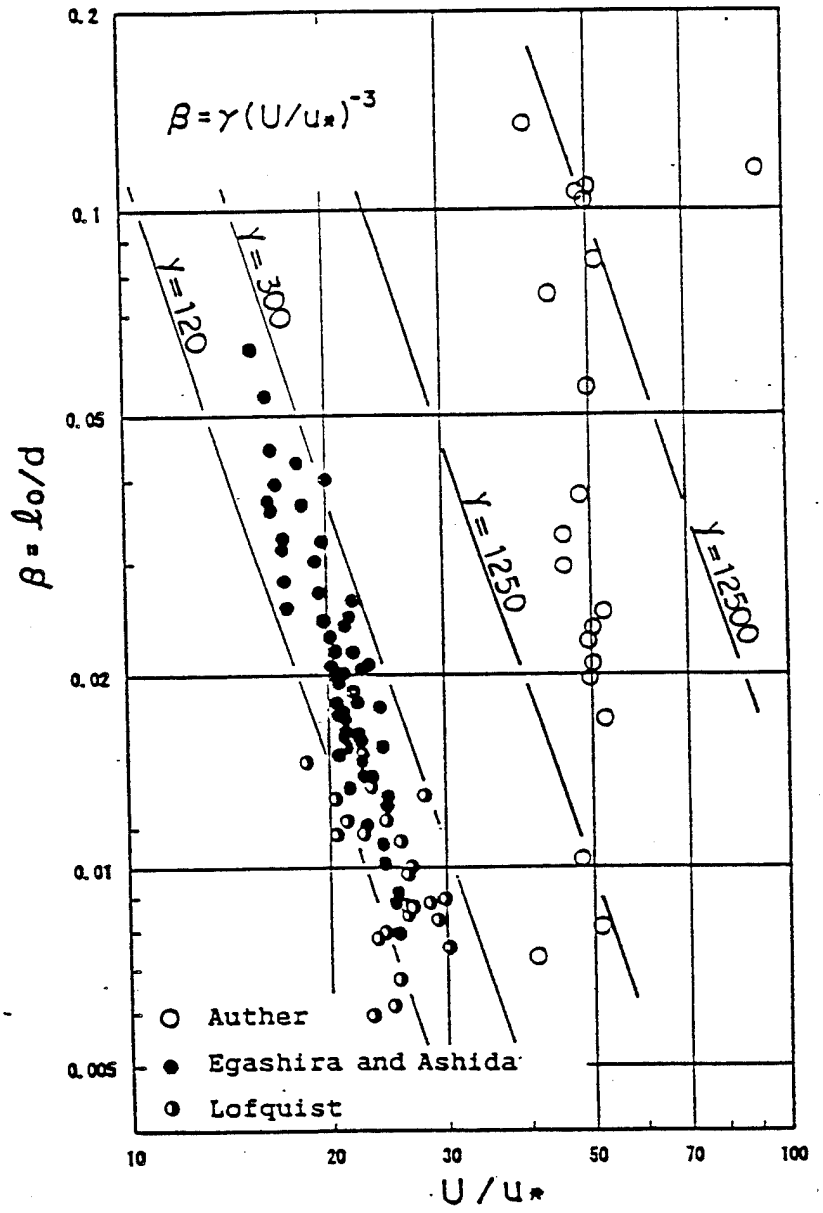

Figure 1. Relations between mixing length and velocity factor.

b) Eddy viscosity coefficient

Vertical distribution of the eddy viscosity coefficient are estimated with the data obtained in different seasons. In January the estimated eddy viscosity coefficient ε are widely dispersed in a range of 10 to 10^3 cm^2/sec and the values of ε become maximum around the center of the middle layer. In May the dispersed range of ε is same as winter's. But the eddy viscosity coefficients have tendency to increase toward the water surface. At the

beginning of summer, the value of ε are same range as other seasons but its dispersing range is wider near the surface. During flood the coefficients become smaller toward the upper and lower interfaces and its maximum value is appeared at mid of the middle layer. As mentioned above, the estimated eddy coefficients are rather in disorder from the values from laboratory tests. We consider that such dispersion comes from the existence of turbulence with various scales in the practical reservoir as well as errors in the data collecting process. We investigated also relationship between the eddy viscosity coefficient and Richardson number (Ri) as well as buoyant frequency (N) defined as follows;

$$R_i = -g(d\rho/dz)/\rho(du/dz)^2 \quad (5)$$

$$N = \left\{(g/\rho 0)\left|\partial\rho/\partial z\right|\right\}^2 \quad (6)$$

Figure 2 is an example of the obtained results, indicating relationship between Richardson number and eddy viscosity coefficient. We can see that the eddy viscosity has tendency to increase with Richardson number. Estimation results of the buoyant frequency indicate that the eddy

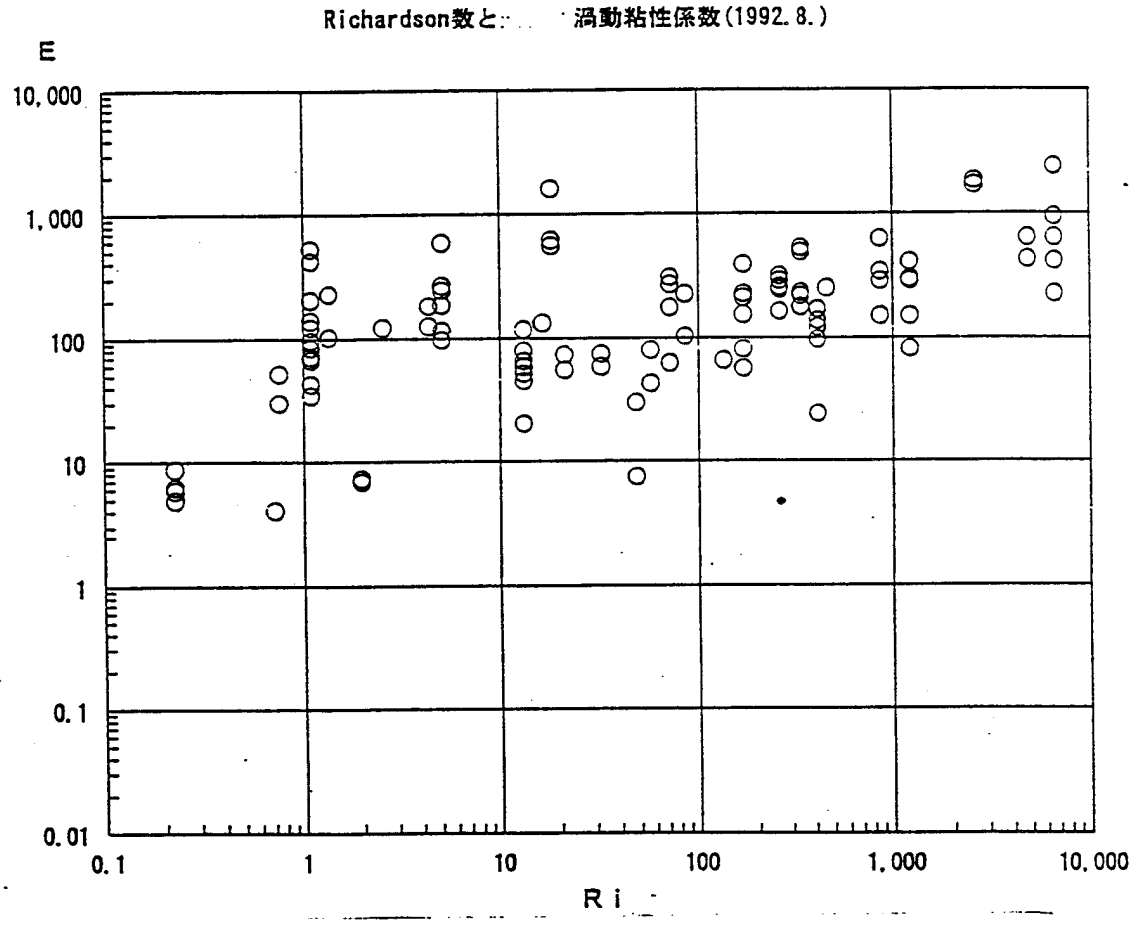

Figure 2. Relation between buoyant frequency and eddy viscosity coefficient.

INTERACTION BETWEEN MEAN WATER COLUMN STABILITY AND TIDAL SHEAR IN THE PRODUCTION OF SEMI-DIURNAL SWITCHING OF STRATIFICATION IN THE RHINE ROFI

A.J. Souza and J.H. Simpson
School of Ocean Sciences,
University of Wales Bangor,
Menai Bridge, Gwynedd LL59 5EY, U.K.

Abstract

Introduction

The discharge of an average of 2,200 m^3s^{-1} of freshwater into the North Sea by the Rhine represents a major source of buoyancy which has important implication for water column structure and dynamics over a large area of the eastern North Sea.

The basic competition between the stratifying effect of the buoyancy input and the mixing influence of stirring by the tidal flow, winds and waves leads to an alternation between periods of strong stratification and complete vertical mixing in the Rhine ROFI in much the same way as has been observed in other ROFIs. The periodic variation in the intensity of tidal stirring tends to impose a fortnightly cycle on the system with stratification breaking down at, or soon after, spring tides. At the same time, variations in wind and wave conditions as well as fluctuations in river discharge introduce more random components of variability. The competition between stabilising and stirring forces is well visualised in the laboratory experiments of Linden and Simpson (1988) with the important addition in the real world of the effects of the earth's rotation acting to limit the spreading of the density current which gets deflected parallel to the coast forming a baroclinic contribution to the north-flowing current along the Dutch coast. A further complication apparent in the observed time history of stratification was that, even during "stratified" periods, the structure was observed to oscillate with a semi-diurnal frequency between a highly stable structure and conditions of near or full vertical mixing.

The work described here make use of new observations from instrumented moorings and survey by undulating CTD (SEAROVER) to clarify the role of straining and allow some conclusions about the origin of the important component of shear in the tidal flow.

Single Point Observations of Stratification

The evolution of stratification $\Delta\rho$ appears to be related to the levels of stirring, calculated from observations of tidal velocity at the moorings and from wind measurements at the Noordwijk tower. Strong bursts of wind stirring with energy inputs of up to 0.2 mWm^{-3} are seen to dominate at times over the tidal contribution. The influence of the combined stirring power inputs is reflected in the mean level of the stratification; low stratification at the start of density record follows a bout of strong wind mixing after which lower winds and neap tides allows the development of strong stratification at the moorings with values of the mean bottom to surface density difference $\Delta\rho$ ~2 kg m^{-3}. Immediately following this the combination of an episode of strong wind stirring augmented by the tidal stirring induces an almost complete vertical mixing.

Superimposed on the these changes in the average level of stratification is a very prominent semi-diurnal variation the amplitude of which is large in relation to the daily mean so that, at the time of minimum stratification,the system approaches complete homogeneity. This semi-diurnal signal is apparent at both moorings and shows similar phase and amplitude in both cases.

Space-Time Evolution of Stratification

It is clear from the observations that in the vicinity of the moorings there is a significant evolution of the density field on short time scales due to the marked semi-diurnal variation in column structure. If this pattern of variation is a general characteristic of the stratified region, it would seem that time-dependent changes will be interpreted as spatial structures in mapping exercises. In order to test the notion that there is a general semidiurnal oscillation under stratified conditions, we have combined the data from a SEAROVER survey with the mooring data for the same period. Surface to bottom density differences observed by the SEAROVER system when inside the ROFI (i.e. within 15 km of the coast) generate a time series which exhibits a significant coherence with $\Delta\rho$ from mooring A. This suggests that the semi-diurnal oscillation is a general characteristic of the ROFI. Some differences in the phase of the data from fixed and moving sensors may be expected due to the change in the phase in tidal processes over the area.

Interaction Between Mean Water Column Stability and Tidal Shear in the Production of Semi-Diurnal Switching of Stratification in the Rhine ROFI

Semi-diurnal variations in water-column stability of this kind have been previously identified in other ROFI and estuarine regimes and attributed to the influence of tidal straining (Simpson et al. 1990). The amplitude of semi-diurnal variation in the Rhine ROFI is, however, considerably greater in relation to the mean amplitude than in previously observed cases. Reference to the 1990 observations show similar behaviour with even larger oscillations of salinity stratification (amplitude ~4 salinity units) than we observe in the 1992 measurements.

The question then arises as to the role of tidal straining in the present case and whether or not other mechanisms are involved. As a first step in answering these questions we have investigated the relation between the density stratification and the relative cross-shore tidal displacement (the cross-shore "straining"). This straining has been computed in two different ways. The first uses a predicted shear displacement is obtained from tidal velocity constituents derived from harmonic analysis over the full duration of the record and shows that the straining signal has an amplitude of 1.5 km and is somewhat advanced in phase relative to the two large oscillations of $\Delta\rho$ on days 254-255. The second has been calculated by high pass filtering the ADCP data for the 4 day period. Prior to midday on day 255, there was a strong enhancement of the straining with a relative displacement of 7 km between current meters at depths of 4m and 16m. Following the onset of intense wind mixing on day 255, the tidal shear signal was greatly reduced. These changes in the straining signal are clearly reflected in the $\Delta\rho$ variation suggesting that straining is the primary process driving the semi-diurnal stratification cycle.

Point Model

In order to combine all these mechanisms and test the above hypothesis for the generation of the semi-diurnal oscillations in stability, we have utilised the 1-d turbulence closure model of Simpson and Sharples(1992) to achieve a synthesis of the various processes operating in the ROFI regime. The model uses an explicit scheme to integrate the equations of motion and a level 2 turbulence closure.

We have run this model with simplified forcing by surface slopes obtained from tide gauge observations at the mooring positions, the (predominant) cross-shore gradient derived from temperature and salinity measurements at moorings A and D and meteorological data provided by KMNI, from the Noordwijk tower (wind speed, air temperature, humidity) and Valkenburg (solar radiation).

Comparisons between the observations and the model suggest a good degree of correspondence between the two with the model exhibiting the main features of the observations notably the two strong maxima in $\Delta\rho$ on days 254-255 which are simulated with satisfactory

timing and magnitude. The model also confirms the operation of the cross-shore straining mechanism in driving the semi-diurnal oscillations of stability.

Discussion

A striking feature of the observations is the relatively large cross-shore straining which evidently operates during periods of stratification and which provides the primary drive for the semi-diurnal oscillation. This straining with a relative displacement of surface and bottom waters of ~7 km is large in relation to the average amplitude of the cross-shore tidal flow. It appears to be associated with the change in the shape of the tidal ellipse which is brought about by the development of mean stratification.

It should be noted that the phase of the tidal straining in relation to the elevation is quite different in this case from that observed in Liverpool Bay (Simpson and Sharples 1992) where the tidal motion is almost a pure standing wave and minimum stratification tends to occur close to high water. In the present case, the tide is better described by a Kelvin wave travelling to the north east along the Dutch coast and the maximum alongshore current occurs near local HW. The phase of the cross-shore shear during times of stratification is such that minimum stability occurs near low water.

On basis of the above results we hypothesise that the mechanism responsible for the strong semi-diurnal variability in stratification involves the sequence of interactions illustrated in figure 1. Following a period of complete vertical mixing, when the isopycnals are vertical (fig. 1a) the density gradients start to relax under gravity as the laboratory experiments of Linden and Simpson (1988), but limited by the effect of the Earth's rotation, generating a coast parallel flow (fig. 1b). The stratification will then induce changes in the tidal ellipses by de-coupling the surface and bottom layers, generating a strong cross-shore component of tidal shear (fig. 1c). The resulting off-shore tidal straining initiates oscillations in stability which combine with the mean stratification give the observed pattern of stability variation with the system coming close to complete mixing in each tidal cycle. When the added effect of wind and tidal stirring increases again (fig. 1d), vertical exchange is enhanced and the off-shore tidal shear is suppressed as the ellipses revert to near degenerate form and the stratification is broken down.

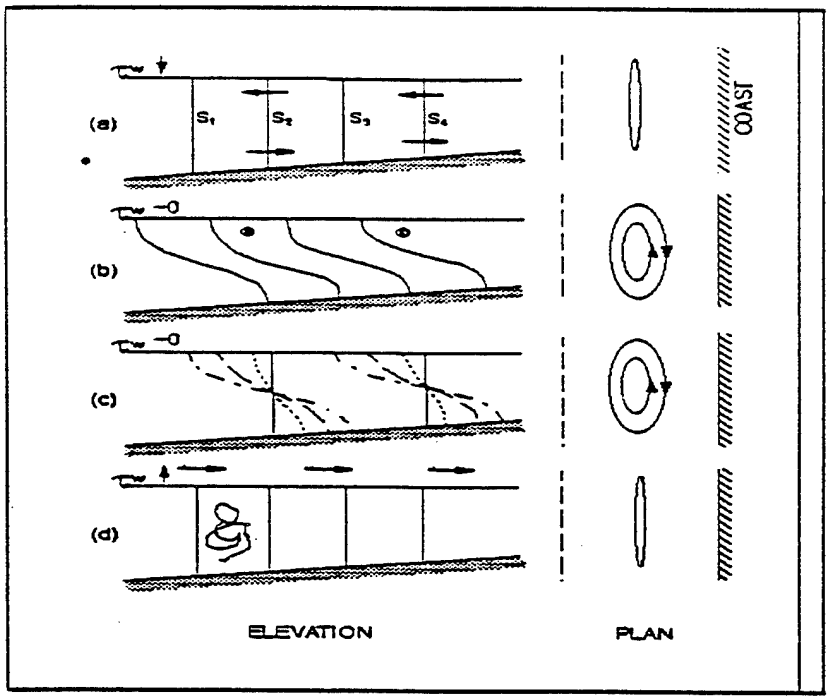

Figure 1. Process summary schematic showing the changes in ellipse characteristics due to the onset of stratification and the resulting semi-diurnal oscillations in stability driven by tidal straining

References

Linden, P.F. and J.E. Simpson, 1988. Modulated mixing and frontogenesis in shallow seas and estuaries. *Continent. Shelf. Res.*, 8:1107-1127.

Simpson, J.H., J. Brown, J. Matthews and G. Allen, 1990. Tidal straining, density currents and stirring control of estuarine stratification. *Estuaries*, 13(2):125-132.

Simpson, J.H. and J. Sharples, 1992. Dynamically-active models in prediction of estuarine stratification, in: Dynamics and exchange in estuaries and coastal zone. In D. Prandle (ed.), *Coastal and Estuarine Studies*, 40, AGU, Washington, D.C., 1992.